Shrinkage Behaviour of One and Two Part Alkali-Activated Mortars: Factors and Mitigation Techniques

Ahmad Alhamdan

A Thesis

in

The Department

of

Building, Civil and Environmental Engineering

Presented in Partial Fulfillment of the Requirements

for the Degree of Master of Applied Science (Civil Engineering) at

Concordia University

Montréal, Quebec, Canada

April 2018

© Ahmad Alhamdan, 2018

CONCORDIA UNIVERSITY

School of Graduate Studies

This is to certify that this thesis prepared
by: Ahmad Alhamdan

Entitled: **Shrinkage Behaviour of One and Two Parts Alkali-Activated Mortars: Factors and Mitigation Techniques**

and submitted in partial fulfillment the requirements for the degree of

Master of Applied Science (Civil Engineering)

complies with the regulations of the University and meets the acceptable standards with respect to originality and quality.

Signed by the final examining Committee:

_____	Chair
_____	Supervisor
Dr. A. Soliman	
_____	Examiner
Dr. M. Nokken	
_____	Examiner External (to program)
Dr. X. Wang	
_____	Examiner
Dr. B. Li	

Approved by

Dr. F. Haghighat, GPD
Department of Building, Civil and Environmental Engineering

Dr. Amir Asif, Dean
Faculty of Engineering and Computer Science

Date

ABSTRACT

Shrinkage Behaviour of One and Two Part Alkali-Activated Mortars: Factors and Mitigation Techniques

Alkali-Activated Binders (AABs) are promoted as sustainable alternatives to ordinary Portland cement (OPC) due to their promising characteristics and ability to reduce the global greenhouse emissions of construction materials. Despite many years of research, volumetric stability (i.e. shrinkage) of AABs, which has been scarcely investigated, is hindering their wider implementation in the construction sector. Hence, the initial attempt of the current study is to fully characterize and understand the shrinkage behaviour of AABs considering different factors. These factors included precursor materials, activator types and concentrations, and curing temperatures. Moreover, the effectiveness of shrinkage reducing admixtures (SRA) as a shrinkage mitigation technique and its interaction with AABs were evaluated. Two preparation methods for AABs, namely one-part (i.e. powder binder-powder activator) and two-part (i.e. powder binder-liquid activator), were also tested for comparison. Fresh properties including workability, setting behaviour, and heat evolution along with hardened properties (i.e. compressive strength) were explored. Results revealed that shrinkage for fly ash-based alkali-activated mortars was the lowest followed by blended fly ash/ slag, while alkali-activated slag-based mortars exhibited the highest values. Regardless of the preparation method, the higher the activator concentration, the higher the shrinkage. There is a strong link between AAB's matrix rigidity and shrinkage behaviour. For both preparation methods, SRA was more effective in reducing shrinkage strains for slag-based alkali-activated mortars at different temperatures. Similar to OPC, SRA addition had induced a reduction in the compressive strength for all tested ABBs mixtures. However, the reduction in AABs mixtures strength was significantly lower than that for OPC mixtures.

ACKNOWLEDGEMENT

First and foremost, praises and thanks to God, the Almighty, for the showers of blessings throughout my research work which without nothing would have been accomplished.

This master's thesis is the result of hard work in which many people have supported me. I am happy to express my sincere gratitude to all of them now.

I would like to sincerely thank my advisor Dr. Ahmed Soliman, without whom I would not have earned the opportunity to further my education at Concordia University. His integral view on research, keen enthusiasm, and timely help led to the successful completion of this work. His advice, dedication and patience are truly appreciated.

I would also love to thank all my colleagues and friends that have supported me along the way. Special thanks go to my friend and colleague, Sameh Diab, for his inexhaustible patience, friendliness, help, and support in the material lab.

I'm extending my thanks to Lafarge Canada for supplying some of the materials used in this research.

Finally, special thanks go to my father, mother, sisters, and brother for their prayers, love, support, and motivation which contributed directly to the accomplishment of this work.

Table of Contents

List of Figures

List of Tables

List of Abbreviations

AA	Alkali-Activated
AAB	Alkali-Activated Binder
AAC	Alkali-Activated Concrete
AAF	Alkali-Activated Fly Ash
AAFS	Alkali-Activated Fly Ash/Slag
AAM	Alkali-Activated Mortars
AAS	Alkali-Activated Ground Blast Furnace Slag
C-A-S-H	Calcium Aluminate Silicate Hydrate
C-S-H	Calcium Silicate Hydrate
EDX	Energy Dispersive X-Ray
FA	Fly Ash
GGBFS	Ground Granulated Blast Furnace Slag
LWA	Lightweight Aggregate
N-A-S-H	Sodium Aluminate Silicate Hydrate
OPC	Ordinary Portland Cement
PC	Portland Cement
SEM	Scanning Electron Microscopy
SRA	Shrinkage Reducing Admixture
UTM	Universal Testing Machine

1

CHAPTER

Introduction

1.1 Background

Global concrete production has grown widely over the recent decades parallel with the population growth and the need for more infrastructure. The high demand for concrete in the construction industry increases ordinary Portland cement (OPC) production. The depletion of natural resources and the significant environmental pollution associated with carbon dioxide (CO_2) emissions generated during the cement manufacturing process are of significant concern. AABs have been gaining popularity as a promising alternative to OPC binders in many construction applications (Yang *et al.*, 2013).

AABs rely on alumina-silicate precursors, found naturally occurring (e.g., metakaolin) or formed as industrial by-products (e.g., fly ash, slag), leading to a significant reduction in carbon dioxide emissions. AAB production requires an alkaline medium (e.g., sodium silicate Na_2SiO_3) and water to chemically activate the precursor forming the cementitious material (Khale and Chaudhary, 2007). This process (so-called "geopolymerisation") initiates with the dissolution of silicon and aluminum ions from the precursors into the alkaline medium. The dissolved ions react with sufficient alkalinity to produce silicate and aluminate compounds which are converted to a poly (alumina-silicate) structure with interconnected silicate oxide (SiO_4) and aluminate oxide

(AlO_4) tetrahedral. Thereafter, the hardening stage is achieved through the poly-condensation of those hydrolyzed species (Provis and Bernal, 2014). This process requires cations like Na+, or K+ to reduce the charge variation which may be due to the coordination of aluminum in the whole structure (Duxson *et al.*, 2007).

Despite various advantages of utilizing AABs in the construction industry, their widespread use has been hindered due to several challenges. One of the main challenges is shrinkage. Shrinkage mechanism of AABs is still not well understood. Shrinkage can significantly affect AAB's performance by inducing cracks under restraining conditions. Previous studies showed that the drying shrinkage of heat-cured alkali-activated fly ash (AAF) mortar was much lower than that of OPC mortar, while under ambient conditions it was significantly higher (Fernández-Jimenez *et al.*, 2006). Other studies showed that alkali-activated ground blast furnace slag (AAS) products undergo significant higher autogenous and drying shrinkage than OPC products (Collins and Sanjayan, 2000; Neto *et al*., 2008). On the other hand, activator species and dosage along with particle size of slag (Pacheco-Torgal *et al.*, 2008) and curing conditions (Bakharev *et al.*, 1999) had great influence on the shrinkage of AAS products. These findings indicate that the shrinkage behaviour of AABs is sensitive to many factors.

For cement-based materials, shrinkage is closely related to the chemical reactions, self-desiccation, loss of capillary water, microstructure development, and moisture conditions of the material. Given the utterly different reaction mechanism and microstructure between AABs and OPC binders, the shrinkage mechanism of AABs is expected to be very different from that of OPC binders (Duxson *et al.*, 2007). These uncertainties about the shrinkage of AAB hamper the broader acceptance and application of this material in the construction industry.

Moreover, in the two-part AABs, which is the conventional production process, liquid activators are used, and elevated curing temperatures are applied. This production method limits AAB production to precast applications. However, in one-part AABs, the use of dry ingredients and ambient curing makes the utilization of these binders more convenient in field practices. The activation of AABs with the aid of solid activators under ambient curing conditions was found to influence the properties of the resulting binder products (Van Deventer *et al.*, 2012; Nath and Sarker, 2014). Moreover, the shrinkage behaviour of one-part AABs has been scarcely investigated.

Nevertheless, suitable admixtures to control the shrinkage behaviour, and early age rheology in AABs has not been developed so far (Heidrich *et al.*, 2015). Several researchers showed that the use of shrinkage reducing admixture (SRA), and water reducing admixture in AABs showed only limited success (Palacios and Puertas, 2007; Provis and Bernal, 2014). Therefore, further investigations are required to check the effectiveness and identify the limits of those admixtures in AABs.

1.2 Objectives and Scope

To address the aforementioned research needs, the fundamental theme of this research is improving the current level of knowledge on the shrinkage behaviour of AABs and evaluating the efficiency of shrinkage mitigation methods. The specific objectives of the research are multi-fold:

- Introducing fundamental knowledge on the relationship between different types of shrinkage of AABs under different exposure conditions.
- Investigating the effect of preparation method on the shrinkage behaviour of AABs (i.e., one-part vs. two-part)

- Evaluating the influence of exposure conditions on the efficiency and mechanisms of the applied shrinkage mitigation techniques.

To achieve the above objectives, the scope of this research includes:

- Different types of precursors including fly ash (FA) and ground granulated blast furnace slag (GGBFS) were used to prepare alkali-activated mortars (AAMs). Mixtures were divided into two levels: single (FA or GGBFS) and binary (FA and GGBFS with a ratio of 1:1).
- Liquid activators with different concentrations were prepared and used to form two-part AABs. Sodium hydroxide solution with concentrations of 3M, 6M, and 12M was combined with sodium silicate and used as a liquid activator.
- Three types of powder activators including sodium hydroxide (NaOH), sodium bicarbonate ($NaHCO_3$), and calcium hydroxide ($Ca(OH)_2$) were used to form one-part AABs. The three activators were added at three different percentages (5, 10, and 15%) of precursor mass to form one-part AABs.
- SRA was added at 0, 1, and 2% of precursor mass to evaluate its efficiency in reducing shrinkage of both one-part and two-part AABs.
- All samples were cured under the ambient condition (23°C) or inside an oven at 60°C to evaluate the effect of curing conditions on shrinkage behaviour of AABs.

1.3 Structure of Thesis

This thesis has been prepared according to the guidelines of the Faculty of Graduate Studies at Concordia University. It comprises five chapters organized according to the following: Chapter 2 contains a state-of-the-art review of the current most relative knowledge on AAM composition

and properties, their relationships, factors affecting their shrinkage behaviour and influences of shrinkage mitigation techniques.

Chapter 3 was devoted to the introduction and experimental program of the three main experimental phases. Staring by phase 1, which focused on enhancing the fundamental knowledge about shrinkage for the conventional two-part AABs, moving to phase 2, where one-part AABs are introduced and followed by phase 3, where the use of SRA's as a shrinkage mitigation technique is proposed.

Chapter 4 focused on the experimental results and evaluation discussion of each phase beginning with phase 1, where the mechanisms of different types of shrinkage experienced by two-part AABs exposed to different curing regimes are evaluated and discussed, moving to phase 2, where the influence of different activators on different types of shrinkage experienced by one-part AABs exposed to different curing regimes is discussed, followed by phase 3, where the role of SRAs as a shrinkage mitigation technique and their performance under different curing regimes is evaluated and discussed.

Finally, general and specific conclusions drawn from the research study along with recommendations for future research are included in chapter 5.

1.4 Original Contributions

This research introduces a series of fundamental investigations related to the shrinkage of AABs and the role of SRAs under different curing conditions. It explores the influence of a wide range of AAM compositions and the efficiency of the most common shrinkage mitigation strategy. Moreover, it highlights the effect of AAM preparation method on achieving lower shrinkage and risk of cracking, yet with a smaller environmental impact. Specific original contributions of this dissertation include:

- Developing a broad and comprehensive database on the shrinkage of AAM exposed to different curing conditions.
- Identifying the mechanisms for different types of AAMs shrinkage exposed to different curing conditions. Explicitly, it was revealed that: (i) the calcium content in the precursors has a significant effect on shrinkage, (ii) the rapid development of AAM's microstructure controls the amount of shrinkage.
- Evaluating the performance and efficiency of SRA and their interaction with the surrounding environment. Specifically, it was found that: (i) the efficiency of SRAs is profoundly affected by the ambient relative humidity and temperature, (ii) The efficiency of SRAs is strongly correlated to the AAM composition including precursors and activator types.

2

CHAPTER

Literature Review

This chapter presents a brief review of the terminology and the chemistry of alkali-activated (AA) materials. It also illustrates the needs for AA materials to enhance sustainability in the construction sector. The available published data on AA materials technology is also briefly reviewed.

2.1 Environmental Issues

Construction is one of the fast-growing industries worldwide. As the demand for concrete as a construction material increases, so also the demand for Portland cement (PC). According to the 2017 world statistics, the annual global production of Ordinary Portland Cement (OPC) is around 3.39 billion metric tons (US Geological Survey, 2017). The quantity is forecasted to increase by almost 20 % within the next ten years.

OPC production is a very energy-intensive activity, and many production power plants rely upon coal to provide this energy (Farris, 2017). The manufacturing process of cement in coal-burning power stations generates large amounts of carbon dioxide (CO_2) which significantly increases the global warming and atmospheric landfill pollution (Malhotra, 2002).

Global warming is caused by the emission of greenhouse gases, such as CO_2, to the atmosphere by human activities. The cement industry is hence held responsible for a significant portion of the carbon dioxide (CO_2) emissions. The production of one ton of PC releases

approximately one ton of CO_2 into the atmosphere (Malhotra, 2002). Moreover, the disposal of coal burning by-product materials produced during cement production is also increasing the landfill pollution. Consequently, there is an urgent need for further investigation to find alternative cementitious products with lower environmental impacts and higher economic benefits.

Many studies have been conducted to find alternative binder materials to replace cement; particularly by-product materials such as fly ash, and granulated blast furnace slag (Duxson *et al.*, 2007; Jiang *et al.*, 2005; Khale *et al.*, 2007; Li *et al.*, 2010; Pacheco-Torgal *et al.*, 2008). Most studies estimate a reduction of 40% in CO_2 emissions associated with OPC production by the utilization of fly ash, and slag as a replacement of OPC (Habert *et al.*, 2011; Duxson *et al.*, 2007; Van Deventer *et al.*, 2012; Yang *et al.*, 2013; Mellado *et al.*, 2014; McLellan *et al.*, 2011). Furthermore, the gainful utilization of these by-product materials as cement replacement materials is increased and lower by-product disposal related problems are pronounced. The impact of OPC production on the environment should be considered seriously hence, finding solutions to reduce this impact is crucial. From this point of view, the utilization of by-product materials shows considerable promise for application in the construction industry as an alternative binder to the Portland cement (Duxson *et al.*, 2007).

2.2 Alkali-Activated Binders

AABs are polymeric binding materials developed by Joseph Davidovits in the 1970s. Davidovits proposed that an alkaline activating liquid could be used to react with the silicon (Si) and the aluminate (Al) content in precursor materials of earth origin such as metakaolin, or in by-product materials such as fly ash and slag, to produce AABs (Geopolymer Institute, 2010). The chemical reaction that takes place, in this case, is a polymerization process. AABs are inorganic polymers produced from various alumina-silicate material reacted by alkaline solution (Davidovits, 1994).

The chemical composition of AAMs is similar to natural zeolitic materials, but the microstructure is indeterminate. The polymerization process involves a chemical reaction between solid aluminosilicate oxides and alkali metal silicate solutions under a highly alkaline condition yielding amorphous to semi-crystalline three-dimensional polymeric structures, which consist of Si-O-Al-O bonds (Davidovits, 1994). The schematic formation of AAB is shown in **Eqs. 2.1** and **2.2** (Davidovits, 1994). These formations indicate that all materials containing mostly Silicon (Si) and Aluminium (Al) can be used to produce AABs.

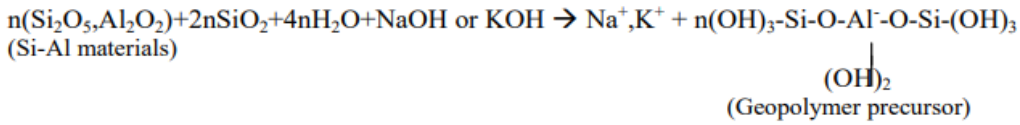

Eq. 2.1

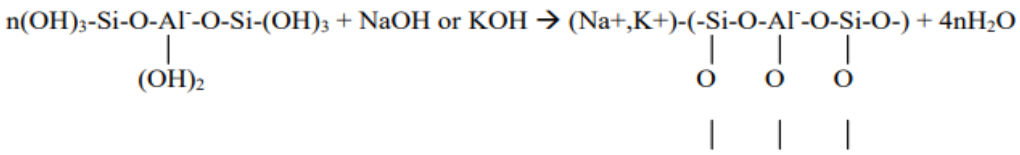

Eq. 2.2

From **Eq. 2.2**, it can be noticed that the last term represents the released free water during the chemical reaction that occurs in AABs. The single key to activating these materials is the use of alkaline solutions; hence, this expelled water seems to play no role in the chemical reaction taking place. It merely provides the workability to the mixture during handling.

AABs have a wide range of applications in the field of industries such as in the automobile and aerospace, civil engineering and plastic industries (Davidovits, 1994). The suitable material for the specific application is determined by the Silica-to-Alumina (Si: Al) atomic ratio of that material. **Table 2.1** shows the classification of the application based on the Si: Al atomic ratio (Davidovits, 1994). Typically, binders with low Si: Al atomic ratio of 1-3 create a highly ridge 3-D network matrix. On the other hand, binders with Si: Al atomic ratio higher than 15, provide a

polymeric character to the AA material (Davidovits, 1994). According to **Table 2.1,** binders with low Si: Al atomic ratio of 1-3 are suitable for many applications in civil engineering.

Table 2.1 Alkali-activated material applications (Davidovits, 1994).

Si: Al ratio	Applications
1	▪ Bricks ▪ Ceramics ▪ Fire protection
2	▪ Low CO_2 cements and concretes ▪ Radioactive and toxic waste encapsulation
3	▪ Fire protection fiberglass composite ▪ Foundry equipment - Heat resistant composites, 200°C to 1000°C ▪ Tooling for aeronautics titanium process
>3	▪ Sealants for construction industry, 200°C to 600°C ▪ Tooling for aeronautics SPF aluminum
20-35	▪ Fire-resistant and heat resistant fiber composites

2.3 Precursor Materials

The main constituents of AABs are the precursor material and alkaline activation solution. Generally, any material rich in Silicon (Si) and Aluminum (Al) is a possible precursor material for the production of AABs. Precursor materials could be materials of earth origin such as metakaolin, kaolinite, etc. or by-product materials such as fly ash, slag, etc. The choice of precursor materials for making AA products depends on many factors such as availability, cost, and type of application. In this study, by-product materials (fly ash, and slag) were used as precursor materials. The following sections provide more information about those two precursor materials.

2.3.1 *Fly ash*

Fly ash is a by-product of the combustion of ground coal used as fuel in electric power generation. Fly ash is collected using an electrostatic precipitator system or a dust collection system from boiler chimneys. The process involves removing fly ash as a fine particulate residue from combustion gases before they are discharged into the atmosphere. Coal plants in the United States create around 130 million tons of fly ash annually (Farris, 2017). Consequently, this vast amount of fly ash generated is creating several disposal related problems. Typically, disposal of fly ash at power plants is accomplished by dumping in nearby surface impoundments and landfills. This means that the many toxic heavy metals present in fly ash have the potential to seep into groundwater hence, introducing health effects for humans and wildlife (Van Jaarsveld *et al.*, 1999). Despite initiatives taken by the governmental, non-governmental, and research organizations, only 25% of the total produced fly ash is utilized globally (Farris, 2017). Various technologies have been developed for the safer management of fly ash, but the gainful utilization should be enhanced.

Fly ash is classified in relation to its calcium content. Bituminous coals produce low calcium fly ash which in turn introduces pozzolanic properties due to its high silica content. Lignite or sub-bituminous coals produce high calcium fly ash which is both, a cementitious and pozzolanic material (it has lower silica and alumina content but higher CaO content) (Gourley, 2003). Two classes of fly ash are defined by ASTM C618-17a, (Standard specification for coal fly ash and raw or calcined natural pozzolan for use in concrete): Class F fly ash, and Class C fly ash. The main difference between these classes is the amount of calcium, silica, alumina, and iron content in the ash. Fly ash class F derived from bituminous coals has a low calcium oxide (CaO) content (less than 10%), while fly ash class C derived from sub-bituminous or lignite coals has higher (CaO) content (more than 10%) (Davidovits, 2008). The standard specifies typical fly ash class F and class C to have 4.3%, and 27.4% CaO content, respectively. The color of fly ash is in the range

light to dark grey, depending on its mineral and chemical compositions (Malhotra, 2002). Fly ash particles are spherical with a diameter range of 0.5 μm to 300 μm; they are typically finer than OPC particles. The chemical composition of class F and C fly ash is shown in **Table 2.2**.

Fly ash has also been successfully used as a mineral admixture component of Portland pozzolan blended cement for nearly 60 years (Gourley, 2003). The use of fly ash as a partial cement replacement in concrete has led to substantial cost savings. As a partial cement replacement, fly ash acts as an artificial pozzolan. Silicon dioxide content in fly ash reacts with the $Ca(OH)_2$ (from the cement hydration process to form the binder calcium silicate hydrate (C-S-H) gel, therefore enhancing the overall mechanical properties and durability performance of concrete. Moreover, the unique spherical shape and particle size distribution of fly ash makes it a good mineral filler in asphalt applications. The high consistency of fly ash presents unique opportunities for use in structural fills and other highway applications.

It has been stated that low calcium fly ash (class F) is preferred over high calcium fly ash (class C), as precursor material (Gourley, 2003). High calcium content in source materials may interfere with the polymerization process. The utilization of waste materials such as fly ash contributes to the immobilization of toxic metals into the environment (Van Jaarsveld *et al.*, 1999). Barbosa *et al.* (2000) reported that higher compressive strength values were achieved in AAMs produced with calcined source materials such as fly ash compared to the ones produced with non-calcined as instance kaolin clay, and other naturally occurring minerals.

Table 2.2 Chemical composition of class F, and C fly ash (Christy and Tensing, 2011).

Chemical composition (wt.%)	Class F fly ash	Class C fly ash
SiO_2	20-60	15-45
Al_2O_3	5-35	20-25
Fe_2O_3	6-24	4-15
CaO	1-12	15-40
MgO	0-5	3-10
K_2O	0-3	0-4
Na_2O	0-4	0-6
SO_3	0-4	0-10
LOI	0-15	0-5
TiO_2	1-2	<1

2.3.2 *Ground granulated blast furnace slag (GGBFS)*

Ground granulated blast furnace slag (GGBFS) is another industrial by-product, which forms from the rapid water cooling of molten steel impurities. Slag is known to have advantageous properties for the concrete industry as it is relatively cheap to obtain and achieves high compressive strengths when alkali activated. Furthermore, slag is highly resistant to chemical attack and maintains excellent thermal properties (Li *et al*., 2010). The main components of slag include SiO_2, CaO, MgO, and Al_2O_3 as shown in **Table 2.3**. Its relative reactivity potential derives from its chemical composition, glass phase content, surface morphology, and particle size distribution (Cartwright *et al.*, 2014). GGBFS is a glassy coarse material with a particle size greater than 4.5 mm (Li *et al*., 2010). Since it contains a significant amount of reactive aluminum, silica, and calcium, blending slag with other alumina silicate precursor materials improves the reactivity within the alkali

medium (Xie *et al*., 2009). As a result of higher reactivity, the setting time of AAM is shortened, but higher compressive strength is achieved (Kumar *et al*., 2010). Oh *et al*. (2010) found that calcium content in the slag is more reactive than calcium content in fly ash, in fact, calcium in slag dissolves easier in the alkali activator compared to that in fly ash.

Table 2.3 Chemical composition of GGBFS (Li et al., 2010).

Chemical composition (wt.%)	GGBFS
SiO_2	31-38
Al_2O_3	9-13
CaO	38-44
MgO	7-12

Even though slag has high glass content, no direct correlation between glass content and the reactivity of slag was found (Li *et al*., 2010). The addition of slag to alumina-silicate precursor materials in an AA system results in calcium aluminate silicate hydrate (C-A-S-H) and calcium silicate hydrate (C-S-H) phases apart from the geopolymer gel. Kumar *et al*. (2010) reported the production of C-S-H as the dominant phase in the alkali activation of fly ash and slag blend under ambient (25°C) curing temperature. They also observed that C-S-H gel increased as the slag content was increased. Conversely, no signs of either C-A-S-H or C-S-H products where observed in neat fly ash-based mixtures. Furthermore, authors found that the activation of slag and fly ash blend at 60°C curing temperature can produce C-A-S-H when Si/Al atomic ratio is around 2 and C-S-H when Si/Al, and Ca/Si ratios are 2.5, and 0.8, respectively. Coexistence of the products mentioned above is essential in improving the compactness of AA material microstructure (Kumar *et al*., 2010). Puertas *et al.* (2000) found that the C-S-H products formed in AABs have lower

calcium content compared to that of forming in OPC binders. Li and Liu (2007) conducted X-ray photoelectron spectroscopy (XPS) and found that the binding energy is decreased in the presence of slag. Authors stated that the new binding energy was more favorable to zeolite formation. This implies that amorphous phases in AAMs can transfer into zeolite crystalline phases easier in the presence of slag.

Heidrich (2002) stated that 3.1 million tons of slag were produced in 2001, of which 75% was utilized in various applications. The corresponding figures for fly ash productions were 12 million tons/year, of which only 5.5 million tons were utilized. The above numbers suggest that fly ash is produced in far excess compared to slag hence, suggesting that fly ash would be a better candidate for geopolymer utilization. However, adding slag as partial replacement of fly ash in AA materials production would contribute in enhancing several properties. In this study, three precursor blends were utilized; single fly ash, and slag along with binary fly ash/slag with a ratio of 1:1 to cover a wide range of precursor blends.

2.4 Alkaline Activators

Activation of the selected precursor materials is an essential parameter in producing a mechanically-sound AA product. Alkali activators play a vital role in the initiation of the geopolymerisation process. A robust alkaline medium is necessary to increase the surface hydrolysis of the aluminosilicate particles present in precursor materials (De Vargas *et al.*, 2011). Alkali activators prompt the precipitation and crystallization of the siliceous and aluminous species present in the solution. Hydroxide (OH-) acts as a catalyst for reactivity, and the metal cation serves to form a structural element and balance the negative framework carried by the tetrahedral aluminum (Rangan, 2008).

On the other hand, the dissolution of Si and Al species during the synthesis of AABs is very much dependent on activator concentration, where the amount of Si and Al leaching is mostly controlled by the activator concentration and the leaching time (Panias *et al*., 2007). Khale and Chaudhary (2007) stated that when precursor materials are mixed with alkaline solutions, their glassy component is quickly dissolved, hence, no sufficient time or space is available for the resulting gel to grow into a well-crystallized structure. As a result, a microcrystalline, amorphous or semi-amorphous structure is formed. Sindutha *et al*. (2006) reported that very high soluble silicate content in precursor materials could reduce the reactivity of the AA mixtures as the concentration of cyclic silicate species inhibits the further condensation of aluminum ions.

Common activators include sodium hydroxide (NaOH), sodium or potassium silicate (waterglass), sodium sulfate (Na_2SO_4), sodium bicarbonate ($NaHCO_3$), potassium hydroxide (KOH), potassium carbonate (K_2CO_3), potassium sulfate (K_2SO_4), calcium hydroxide ($Ca(OH)_2$), and cement clinker (Garcia-Lodeiro *et al*., 2015). The mixtures of NaOH and sodium silicate or KOH and potassium silicates in liquid form, are the most commonly used activators in AA systems (Oh *et al*., 2010). Since NaOH is cheaper than KOH, the utilization of NaOH and Na_2SiO_3 mixtures as alkali activators has been favored in most studies.

2.4.1 *Sodium hydroxide (NaOH)*

NaOH is one of the most commonly used alkaline activators in AA material production. Although a Na+ ion does not maintain the high level of activation as a K+ ion, it is smaller in size and can move throughout the paste network with much less effort promoting better zeolitization (Duxson *et al*., 2007). Moreover, Na+ ion bear a higher charge density which promotes additional zeolitic formation energy. The resulting paste properties are dependent on the molarity of the activating solution.

Mishra *et al*. (2008) studied the effect of alkaline liquid concentration and curing time on strength and water absorption of alkali-activated concrete (AAC). Authors reported that higher compressive strength values were achieved when NaOH concentration was increased from 8M to 16M. Moreover, they added that longer curing periods increased the compressive strength values of AAC specimens. Khale and Chaudhary (2007) found that while higher NaOH concentrations tend to accelerate the chemical dissolution, they also retard the ettringite and CH (carbon-hydrogen) formation during the binder formation. Moreover, authors stated that although higher strength at early age is achieved with higher NaOH concentrations, the strength of aged materials might get compromised due to the excessive OH- in the solution causing a non-uniform final product structure.

Garcia-Lodeiro *et al*. (2007) stated that AACs activated with sodium hydroxide develop greater crystallinity thus improving stability in aggressive environments of sulfates and acids. Nevertheless, Chareerat *et al*. (2006) stated that the use of NaOH buffers the pH level of pore fluids and regulates the hydration activity hence, directly affecting the formation of the main C-S-H product in AA pastes.

2.4.2 *Sodium silicate (Na_2SO_3)*

Sodium silicates are manufactured by fusing sand (SiO_2) with sodium carbonate (Na_2CO_3) at temperatures in excess of 1100 °C and dissolving the product with high-pressure steam into a semi-viscous liquid referred to as waterglass (Fernández-Jiménez *et al*., 2005). Sodium silicate solution is commercially available in different grades depending on purity and silicate dioxide (SiO_2) to sodium oxide (Na_2O) ratio. Fernández-Jiménez *et al*. (2005) stated that mass ratio of SiO_2 to Na_2O in sodium silicate solution is a critical parameter in the activation mechanism. Feng *et al*. (2004) found that soluble silicates reduce alkali saturation in pore solution, hence, promoting greater interparticle bonding. Authors' tests revealed that specimens activated with sodium silicate

solution containing highly soluble silicates achieved much higher compressive strength than those activated with a lower soluble silicates solution. However, neat sodium silicate is rarely used as an activating agent, as it may not possess enough activation potential to initiate activation reaction alone (Chindaprasirt *et al*., 2007).

Gebregziabiher *et al*. (2016) found that the early strength development of ambiently cured slag mortar specimens activated with neat sodium silicate was prolonged. Specimens could only be demolded after 72 hours of casting due to the delayed setting and low early strength. Hou *et al*. (2007) suggested that the use of neat NaOH in activating AAC resulted in a weaker bond structure between the paste and aggregates. However, authors found that the addition of sodium silicate (waterglass) combined with NaOH enhanced the bond structure significantly. Currently, a common practice in AAC research involves preparation of the activating solution by combining appropriate amounts of the two activators (e.g., NaOH and waterglass) and allowing them to cool and homogenize for a period before being used in alkali activation. The mixture of NaOH with waterglass enhances the alkalinity in the solution, hence, increasing the reaction rate and the overall specimen strength.

Chindaprasirt *et al*. (2007) recommended the use of sodium silicate solution with a SiO_2 to Na_2O mass ratio of 2.0 mixed with 8–16M NaOH activator to achieve a mechanically sound AA product. Brough and Atkinson, (2002) tested AAS mortars activated with a mixture of sodium silicate and sodium hydroxide or potassium hydroxide. Sodium silicate-NaOH activated mortars exhibited a higher compressive strength and low porosity at the interface, compared to sodium silicate-KOH activated ones.

2.4.3 *Calcium hydroxide ($Ca(OH)_2$) and Sodium bicarbonate ($NaHCO_3$)*

The primary key in alkali activation is to provide the sufficient alkalinity to prompt the precipitation and crystallization of the siliceous and aluminous species present in the source

materials. Hence, any material that can provide alkali cations, raises the pH of the reaction mixture, and facilitates precursor dissolution can be used as an activator (Provis *et al.*, 2014). Moreover, the use of solid alkali activators in AA systems is less hazardous than using liquid activators and leads to "cement-like" mixture, where only water is needed to activate the hydration of the binder. The use of AA products in field application require user-friendly practices, and incorporation of solid activator rather than premixed solutions would be much more advantageous. Moreover, handling large amounts of corrosive and often viscous liquid activators is difficult for commercialization and mass production of AA materials.

It is argued that using dry solid powders tend to retard the geopolymerisation reaction; therefore, strength results may not be high as liquid-based systems (Khale and Chaudhary, 2007). Nematollahi *et al*. (2015) tested one-part, and two-part sodium hydroxide and sodium silicate activated binders. Authors reported successful activation of low calcium (class F) fly ash with the aid of powder activators. Sodium silicate activated binders achieved compressive strength values ranging from 29-37 MPa. However, the achieved compressive strength values were around 30% less than the ones observed in the counterpart two-part AAB. Kovtun *et al.* (2015) published promising results with solid Na_2CO_3 and slaked lime as the activators for blast furnace slag mortars. The authors obtained up to approximately 50 and 85 MPa compressive strength (28 d) at 25 and 85 °C curing temperatures, respectively. Kim *et al.* (2013) found that CaO powder is very efficient in the activation of blast furnace slag although it generated very high heat of hydration. On the other hand, Yang and Song (2008) achieved a maximum compressive strength of 3.5 MPa in NaOH, and Na_2SiO_3 powder activated fly ash mortars after 28 days of curing.

Other researchers attempted dissolving solid activators in water before being mixed with the precursor materials. Ismail *et al.* (2013) used solid alkali activators in their research study, but

the activator was first dissolved in distilled water before mixing it with fly ash and slag blends. Guerrieri *et al.* (2010) also used solid sodium metasilicate as an activator in their study. Again, authors also dissolved the activator to produce an alkaline solution as the activator was not added to the mix in solid form.

The activation of AA products using only solid materials would eliminate most of the practical difficulties associated with mass production. However, the current level of knowledge in one-part AA material behaviours, especially the volumetric stability, requires more attention. Solid dry calcium hydroxide (hydrated lime) and sodium bicarbonate were used as activator agents in this study, in an attempt to verify their activation ability with different source materials.

2.5 Curing Regimes

2.5.1 *Ambient temperature curing*

The use of AA products in the construction industry is linked with the practicality of its production (cast in-situ applications). Hence, the utilization of ambient curing regimes is the only feasible or achievable option. One major challenge for successful AA material production is obtaining adequate mechanical properties at the ambient temperature (i.e., 23 ±3 °C). Studies had shown that the synthesis of fly ash-based AA materials at ambient temperatures is hard to achieve (Fernandez-Jimenez and Puertas, 2002). Shi and Day (1999) stated that the activation reaction of fly ash at room temperature was prolonged. The implementation of elevated temperature curing in precast AA material production seems to be achievable. However, it can be very expensive or impossible to achieve in cast-in-situ production. Studies investigating an AA material mixture design that can undergo proper activation using ambient curing regimes are on the run. However, large-scale ambient cured AA material production in construction industries remains a matter of question.

Rangan (2008) suggested that curing of AA material mixtures could be achieved with temperatures as low as 30°C. Wallah and Ranjan (2006) performed compressive strength test on AAF mortars cured at ambient temperatures ranging from 8-25 °C. Authors concluded that compressive strength was increasing as temperatures increased reaching a maximum value of 35 MPa at 25 °C. Although heat curing might be essential for the setting of pure alumina-silicate (class F fly ash or metakaolin) based AA materials, studies have shown that the curing of calcium-rich alumina-silicate (slag) based AA materials could be achieved under ambient curing temperature. Altan and Erdoğan (2012) found that AAS mortars cured at ambient temperature achieved comparable compressive strength values with AAF mortars cured at elevated temperatures. The authors reported slag mortar specimens achieving 28 days compressive strength of around 55 MPa. However, similar compressive strength values could be achieved much quicker under elevated curing temperature of 80 °C.

2.5.2 *Elevated temperature curing*

The alkali activation reactions in AA products might not proceed at a sufficient rate to produce high strength binder under ambient temperatures. Therefore, elevated curing temperatures might be necessary to achieve the proper geopolymerisation. Prompting the alkaline reactivity using an external heat source would enhance the geopolymerisation reaction degree resulting in a more mechanically sound AA product. Moreover, elevated temperatures tend to catalyze the binder product's formation chemistry in fresh paste (Doleža *et al*., 2006). Palomo *et al*. (1999) studied the curing of AAF mortars at 65°C and 85°C. They indicated that the compressive strength of mortars cured at 85°C after 24 h was much higher than those cured at 65°C. Sindutha *et al*. (2006) disclosed that elevated temperature curing (30-75°C) tend to expand the total pore volume and surface area which in turn accelerates the dissolution of the precursor in AAF mortars. In addition,

at low temperature (below 30°C), the binder formed contained precipitation of dissolved species instead of poly-condensation of silicate and aluminate.

Elevated temperature curing can be accomplished by the aid of dry or steam heat techniques. Studies showed that steam heating methods tend to yield higher compressive strengths compared to dry heating methods (Doleža *et al*., 2006). The effect of dry and steam heat curing techniques on AAF pastes was studied by Kovalchuk *et al*. (2007). Specimens were dry cured at 150 °C or steam cured at 95 °C. At the age of 28 days, specimens dry cured achieved compressive strength of 31.8 MPa, while specimens steam cured achieved 71 MPa. Research showed that elevated heat curing at temperatures in the range of 50–80 °C successfully enhances the strength development of AA materials. However, a temperature threshold exists, beyond which the strength gain rate is negligible (Khale and Chaudhary, 2007). Sumajouw *et al*. (2007) stated that the effect of elevated temperature curing on geopolymerisation is only an enhancement to mechanical properties of AAMs at early ages. Authors noted that as reaction time increases with high curing temperatures, the final compressive strength of AAMs was decreased. They explained this by noting that at early age, the heavy initial formation of reaction products makes the higher alkalinity offered by heat curing useful in the densification of these products. While at later age, the reaction products become exponentially less and increased temperatures only serve to degrade previously created aluminosilicate gels within the matrix. Heah *et al*. (2011) found that the curing of metakaolin-based AAMs at elevated temperature (40, 60, and 80 °C) favored the strength gain after 1–3 days. However, authors noted that curing at a high temperature for a longer period of time caused thermolysis of –Si–O–Al–O– bond in specimens at later age.

Despite the previously mentioned studies, the optimum heat curing temperature and period in AAM production is still not very clear. Generally, the use of heat curing in precast AA products

prior to site delivery could be an effective solution to overcome cast in-situ curing difficulties until proper solutions are developed.

2.6 Fresh Properties of Alkali-activated Mortar

2.6.1 *Workability*

Workability is one of the main parameters influencing the fresh properties of both AA and OPC products. AA materials produced with various precursors, and activators can be very stiff. Consequently, it will not possess adequate workability to facilitate its placement. Research studies had shown that AA products tend to have lower flowability compared to that of OPC products (Fernández-Jimenez *et al*., 2006; Palacios and Puertas, 2005). This was attributed to the different rheological properties of AAB from those found in PC binders (McDonald and Thompson, 2006). Pozzolan-based AA binder products possess higher static and dynamic viscosities compared to PC products, hence, can require additional vibration efforts to minimize entrained air pockets in the fresh paste (McDonald and Thompson, 2006). Moreover, the essential need for an alkaline environment in AA material activation contributes in affecting mixtures workability as most of the liquid activators used tend to have high viscosities (Chindaprasirt *et al*., 2007).

Generally, AA materials produced with fly ash are known to have better workability compared to ones produced with other precursor materials. This is mainly due to the spherical shape and large specific surface area of fly ash particles (Fernández-Jimenez *et al*., 2006). Temuujin *et al*. (2010) reported that AAF mortars prepared with a high precursor to sand weight ratio (3–9) exhibited acceptable flow values, while mortars prepared with a low precursor to sand ratio (1–1.5) were stiff and difficult to pack into the plastic molds. Authors considered a minimum flow of 110 ± 5% as an acceptable limit to have mortars easily placed into the molds. Chindaprasirt *et al*. (2007) studied the workability and strength of high calcium fly ash mortars activated with

different dosages of NaOH and sodium silicate. The flowability of mortar mixtures decreased with the increase in NaOH concentration and sodium silicate solution amount. The higher the NaOH concentrations, the higher the viscosity of the solution. Sodium silicate (waterglass) solution is itself a solution of very high viscosity, hence, any increase in its amount would reduce the flow of mortar mixtures. Higher w/b ratio or superplasticizers are required to achieve proper flow in mixtures containing a high activator dosage.

Generally, superplasticizers are considered a viable solution for stiff mixtures. However, provisions to the mixture design must be made accordingly to identify the optimum dosage. To overcome workability problems, a number of superplasticizers, water reducers, and set retarders have been tested with AA systems to increase the flowability with varying extents of success (Provis *et al*., 2015). Douglas and Brandstetr (1990) reported that the addition of a water reducers such as sodium lignosulphonate and naphthalene sulphonate-based superplasticizers to different AAMs caused a reduction in compressive strength without any improvement in workability. Doležal *et al*. (2006) tested the addition of the same naphthalene sulphonate-based superplasticizer for up to four percent of the fly ash by mass in mortar mixtures. Superplasticizer dosages up to 2% had improved the workability of the fresh mortars without affecting strength. However, at higher dosages (> 2%), a decrease in compressive strength of hardened products was observed.

Palacios and Puertas (2005) studied the addition of polycarboxylate, vinyl copolymers, melamine, and naphthalene-based superplasticizers in AAS mortars. Successful improvement in the workability of NaOH activated slag mortar mixtures was achieved with the addition of the proposed superplasticizers. Naphthalene-based superplasticizer addition achieved the highest flow rate in AAS mortars.

2.6.2 *Setting time*

Previous research studies had shown that AA products tend to show rapid setting compared to ordinary Portland cement products (Palacios and Puertas, 2005*;* Lee *et al*., 2013). AA products should exhibit desirable rheology and setting behaviour in order to allow their transportation and casting. Irreversible mistakes might happen if setting time is very short. Conversely; if the setting time is too long, it will not be economical.

According to the literature, the setting behaviour of AA products is dependent on various parameters including precursor soluble silica and calcium content, activator type, and water content (Nath and Sarker, 2014; Lee *et al*., 2013; Balczár *et al*., 2015). Nath and Sarker (2014) studied the effect of slag addition to sodium hydroxide and sodium silicate activated fly ash mortars. The setting time was reduced significantly when slag content was increased in AAF mortar mixtures. They attributed that behaviour to the higher calcium oxide content in slag which in turn implied a higher geopolymerisation reaction degree resulting in a rapid set. To depict the influence of slag content on setting time, tests were carried out at a controlled temperature of 21–23 °C. Under this condition, AA mortars containing fly ash only as the precursor generally take a longer time to set due to their slow rate of chemical reaction at ambient temperature. Lee *et al.* (2013) studied the setting behaviour of fly ash/slag pastes activated with alkali solutions made with mixtures of different NaOH molarities and sodium silicate to NaOH solution weight ratio. The authors stated that activator concentration, and slag content and can highly affect the strength development and reaction kinetics of AAF binders and may cause rapid setting. Their reported test results showed reductions in both initial and final setting times with the increase in NaOH concentration and sodium silicate to NaOH weight ratio. Moreover, the authors added that rapid set was more pronounced in paste mixtures containing higher slag content.

Balczar *et al*. (2015) tested metakaolinite-based mortars activated with different mix solutions of NaOH and sodium silicate. The authors reported reductions in setting behaviour with the increase in the SiO_2/Al_2O_3 ratio. They explained this by the fact that the increase in SiO_2/Al_2O_3 ratio will simultaneously lower the alkali content in the activating solution. Therefore, slowing the geopolymerisation reaction and reducing the setting time. The authors concluded that the alkali content, rather than the soluble silica content, has a crucial influence on the setting time.

Generally, the use of superplasticizers to control the setting behaviour AABs can be an ideal solution for a rapid set. Jang *et al*. (2014) studied the effect of polycarboxylate-based, and naphthalene-based superplasticizers on setting behaviour of NaOH/sodium silicate activated fly ash/slag blended pastes. The initial and final setting times were unaffected by the addition of the naphthalene-based superplasticizer. However, the setting was retarded by the addition of the polycarboxylate-based superplasticizer. In the case of the polycarboxylate-based superplasticizer at 4% dosage, the initial and final setting times were retarded by around 50 and 70 minutes, respectively. Ravikumar and Neithalath (2012) used sodium hydroxide in powder and liquid form to AAS mortars. The authors observed that fresh slag mixtures activated with solid materials tend to set quicker than mixtures activated with liquid solutions.

2.7 Hardened Properties of Alkali-Activated Mortars

2.7.1 *Compressive strength*

Previous research indicated that AA products could have comparable strength properties to those achieved by OPC products (Khale, and Chaudhary, 2007*)*. However, the strength of AA products is influenced by various factors including precursor chemical composition, alkali activator type and content, liquid/binder ratio, and curing regimes. AA materials produced with a higher alkali content, a higher curing temperature, and a low water content can achieve very high strength values

of 80 MPa or more (Khale and Chaudhary, 2007). However, the production of high strength AA materials requires precursors that boast a high reactive potential. Chindaprasirt *et al*. (2007) reported that class C fly ash-based AAMs achieved 28 day compressive strength of 52 MPa when cured at 70 °C for three days and prepared with sand/binder ratio of 2.75. Authors stated that elevated heat curing for three days was essential in achieving the aforementioned strength.

De Vargas *et al*. (2011) tested AAF mortars activated with sodium silicate solution containing several molar ratios of Na_2O/SiO_2. The authors reported that specimens prepared with low Na_2O/SiO_2 ratios (0.2) did not achieve satisfactory mechanical performance. The 28 day compressive strength was around 2 MPa. This was attributed to the inadequate fly ash solubilization and the insufficient formation of aluminosilicate gel. These findings were supported by scanning electron microscopy (SEM) analysis. The matrix of these specimens contained only aggregated and practically intact fly ash particles after being in contact with the activator for more than 180 days. The highest 28 day compressive strength of 22 MPa was achieved in AAF mortars activated with a high Na_2O/SiO_2 ratio (0.4).

Temuujin *et al*. (2010) studied the effect of sand/precursor ratio in AAF mortars activated with high concentrations (14M) of NaOH and sodium silicate mixture solution and initially cured at 70 °C for 24 hours, followed by ambient curing. The recorded highest 28 day compressive strength value of 60 MPa was achieved in fly ash specimens prepared with sand/precursor ratio of 1.5. This improvement was attributed to the increase in sand/binder ratio in mortar specimens. Increasing the sand/binder ratio for up to 9.0 results in a reduction in the amount of geopolymerisation but does not significantly impact the compressive strength.

Görhan and Kürklü (2013) investigated the influence of the NaOH/sodium silicate solution on the 7 days compressive strength of AAF mortars activated with three different NaOH

concentrations (3, 6, and 9M). The precursor/sand ratio of (1:3) and NaOH/sodium silicate ratio of (1:2) were maintained constant. The 6M activated specimens achieved the highest 7 days compressive strength of 22 MPa. They claimed that an ideal alkaline environment for proper dissolution of fly ash particles was found in 6M NaOH solution. The low NaOH concentration (3M) is not sufficient to stimulate a strong silica dissolution. While, using high NaOH concentration (9M) caused premature coagulation of silica, resulting in a weaker mortar in both cases.

On the other hand, slag-based AA materials are well known to achieve higher strength properties when compared to fly ash-based ones. This was previously attributed to the chemical composition of the former precursor (Altan and Erdoğan, 2012). Slag was hence utilized as a neat precursor in slag-based systems or as a replacement of fly ash in fly ash/slag-based systems. Yang and Song (2009) investigated the strength behaviour of ambient cured AAF and AAS mortars prepared with several sand/precursor ratios and activated with different concentrations of NaOH and sodium silicate. The authors observed that AAF mortars tend to develop insufficient 28 day compressive strength (<3 MPa). However, they found that AAS mortars exhibited much higher 28 day compressive strength (40 MPa) under the same mixing condition. The authors investigated their findings using energy-dispersive X-ray (EDX) analysis combined with scanning electron microscopy (SEM) analysis. Very few hydration products were detected with the presence of unreacted fly ash particles and many voids in AAF mortars. This explains the weak strength achieved by those specimens. The effects of activator concentration and sand/precursor ratio on strength behaviour were not apparent in AAF mortars as the low compressive strength results achieved were meaningless, while the aforementioned effects were evident in AAS mortars. Increasing the Na_2/SiO_2 ratio from 0.038 to 0.089 produced AAS mortar specimens with up to 2.2

times higher compressive strengths. As the sand/precursor ratio increased up to 2.5, the compressive strength also increased, after which it dropped significantly.

Brough and Atkinson (2002) prepared AAS mortars using slag, sand, and activator in a ratio of 1:2.33:0.5. Sodium silicate or KOH were used as alkali activators in their report. AAS mortar specimens activated with sodium silicate gained 28 days compressive strength of 50 MPa, while KOH activated slag-based mortars achieved lower compression strength values. SEM analysis revealed that the porosity at the interfacial zone plays a significant role in the achieved strength, as low porous sodium silicate activated mortars achieved higher compressive strength compared to the highly porous KOH activated ones.

2.7.2 *Isothermal calorimetry*

Understanding the kinetics of AA material formation is very important in tailoring the material for desired applications. The alkali activation reactions of fly ash and slag-based binders act differently than the well-known hydration reaction in cement binders. Hence, utilizing different investigation techniques such as calorimetry to study the reaction kinetics of alkali activation is crucial (Provis and Van Deventer, 2009). It has been reported previously that AAF binders are very sensitive to the reaction temperature, as they require higher curing temperature to initiate full alkali activation (Shi and Day, 1999).

Chithiraputhiran and Neithalath (2013) studied the heat evolution of various blends of slag, and fly ash pastes activated with 6, 9, and 12 M NaOH solution at 20 °C for 48 h. An exothermic peak was appearing immediately when the activator is mixed with the solid material; this peak was designated as the wetting and dissolution of solid material. The observed peak was found similar to the initial (pre-induction) period found in cement hydration process. Moreover, the magnitude of the first heat peak was increased with increasing NaOH concentration. After the initial

dissolution, the heat flow in AAF pastes was very weak, but not zero as the cumulative heat was slowly increasing. The low activation reaction in AAF pastes is responsible for the low heat flow rates observed as mixtures did not harden even after 24 h at 20 °C. On the other hand, the heat flow of AAS pastes was significantly higher compared to that of AAF pastes.

Shi and Day (1995) investigated the heat evolution of AAS pastes activated with various activators. AAS paste activated with disodium phosphate experienced the highest heat flow rates, followed by sodium hydroxide, sodium silicate, and finally, OPC pastes. It can be seen that the total heat of hydration depends on both precursor and activator type.

2.7.3 *Shrinkage of alkali-activated binders*

The acceptance of AA products in the industry has been hindered by concerns related to their shrinkage. Shrinkage is a critical parameter affecting the durability of the AA material and its resistance to cracking. Shrinkage can be defined as a reduction in the volume of the material due to either drying or chemical reactions taking place in the system. These reductions in volume induce stresses in the material matrix causing deformations. As deformations are restrained in the hardened binder, cracking occurs. The formation of cracks allows the ingression of aggressive chemicals into the concrete, therefore, significantly reducing its service life.

2.7.3.1 Types of shrinkage

Shrinkage in concrete may occur due to carbonation, thermal effects, drying, or self-desiccation (Thomas *et al*., 2017). The latter two are of main concern in the present work. Drying shrinkage occurs due to the loss of internal water to the external environment through evaporation. Autogenous shrinkage occurs due to self-desiccation (i.e., water consumption with continued hydration reactions). When specimens are firmly sealed to avoid any moisture loss or carbonation, only autogenous shrinkage occur.

2.7.3.1.1 ***Autogenous shrinkage***

Autogenous shrinkage can be defined as the macroscopic change in volume that occurs when moisture loss and carbonation are nonexistent. It is a result of chemical shrinkage affiliated with the hydration of cement particles (Japan, 1999). Holt (2001) described the autogenous shrinkage occurring in three different stage: liquid, skeleton formation, and hardening stage. At the liquid stage immediately after mixing components, chemical shrinkage occurs because the volume of hydration products is smaller than the volume of reactants. At this stage, autogenous shrinkage is equal to the chemical shrinkage. The relation is shown in **Fig. 2.1**.

The next stage is the skeleton formation stage where the binder paste begins acquiring strength to form its solid skeleton. At this point, chemical shrinkage begins to get more and more restrained and autogenous shrinkage begins diverging from chemical shrinkage. As the paste continues to hydrate and consume water, tiny menisci begin appearing in the pores of the paste. This observation is shown in **Fig. 2.2.** Furthermore, as water is lost from pores, the water meniscus will continue to be pulled into the capillary of smaller pores and will generate more stresses on the capillary pore walls. Consequently, the capillary pressure will start to develop and cause autogenous shrinkage. This phenomenon can be described using the Laplace equation **Eq. 2.3**. Similarly, capillary pressures can then be converted to ultimate shrinkage of the paste using the Mackenzie-Bentz equation **Eq. 2.4** (Bentz *et al*., 1998; Mackenzie, 1950).

$$Pcap = -\frac{2\gamma}{\mathrm{r}} \qquad \textbf{Eq. 2.3}$$

where $Pcap$ = Magnitude of capillary stresses, γ = Surface tension of pore solution, r = Radius of the largest pore emptied. The pores are assumed to be cylindrical with a contact angle of zero degrees.

$$\varepsilon = \frac{S}{3} Pcap \left[\frac{1}{K} - \frac{1}{Ks} \right] \quad \textbf{Eq. 2.4}$$

where $\mathcal{E}$= Ultimate shrinkage, S= Volumetric degree of saturation, K= Bulk elastic modulus of the paste, Ks= Bulk modulus of the solid skeleton (e.g., C-S-H or unreacted solids).

$$ln\theta = -\frac{Pcap\ M}{\rho RT} \quad \textbf{Eq. 2.5}$$

where θ= relative humidity, M= the molecular weight of water (18 kg/kmol), ρ= the density of water (998 kg/m^2), R= gas constant (8,214 J/(kmol°K)), T= temperature in kelvin scale (°K).

Finally, at the hardened stage when the free water is gradually consumed, the binder in search for extra water will attract it from the capillary pores first and then from the gel water for the hydration to proceed. The consumption of capillary water and gel water decreases the relative humidity in the pores. This phenomenon is called "self-desiccation" because of the decrease in the internal humidity without any water egress to the exterior. Self-desiccation induces a negative pressure in the meniscus formed, leading to further autogenous shrinkage. The Laplace and Kelvin equations can be combined to show the relation between relative humidity and negative pressure, as given in **Eq. 2.5** (Janz, 2000) and demonstrated in **Fig. 2.3** (Holt, 2001).

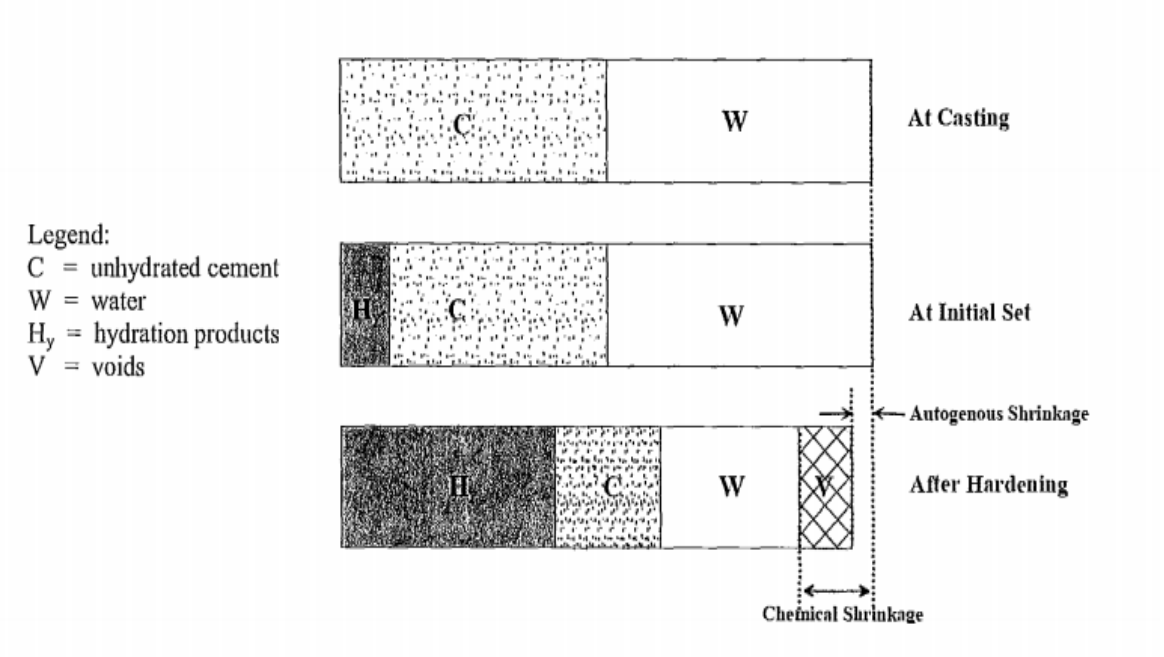

Figure 2.1 Chemical and autogenous shrinkage interaction in the horizontal direction (Japan, 1999).

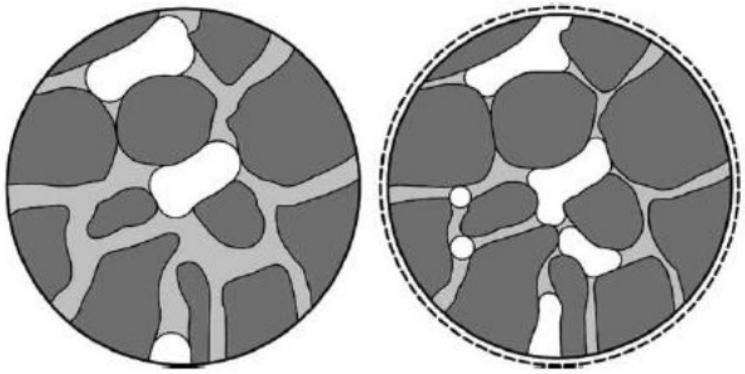

Figure 2.2 Left: Early age binder undergoing hydration, Right: A more mature binder with increased air void formation (Jensen and Hansen, 2001).

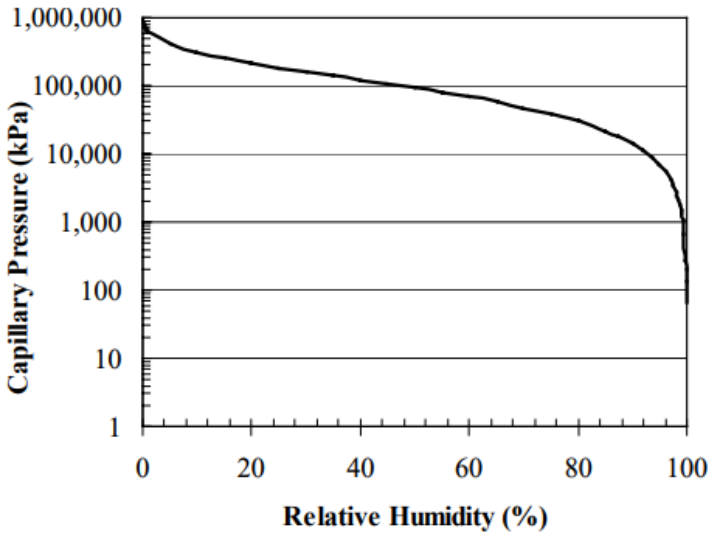

Figure 2.3 Relation of relative humidity and negative suction pressure based on combination of Laplace and Kelvin equations (Holt, 2001).

The study on autogenous shrinkage of ambient cured sodium silicate activated fly ash pastes carried by Ma and Ye (2015) showed that shrinkage strains were increasing with higher Na_2O/SiO_2 ratios. Very high autogenous shrinkage values reaching around 3800 με in fly ash mixtures activated with Na_2O/SiO_2 ratio of 1 were reported. However, this large strain did not necessarily lead to an early age cracking of the samples. Moreover, AAS products autogenous shrinkage strains have been reported to be up to seven times higher than the corresponding OPC products (Bakharev *et al*., 1999; Cincotto *et al.*, 2003; Chen *et al*., 2007; Collins and Sanjayan, 2000).

Figure. 2.4 shows the autogenous shrinkage measurements of various ambient cured AAS mortars activated with different concentrations of sodium silicate solution recorded by Neto *et al*. (2008). It can be clearly seen that autogenous shrinkage strains were generally high approaching more than 2500 με in mixtures with the highest Na_2O/SiO_2 ratio. The autogenous strains were influenced by the activating solution as the shrinkage was increasing with higher Na_2O/SiO_2 ratios.

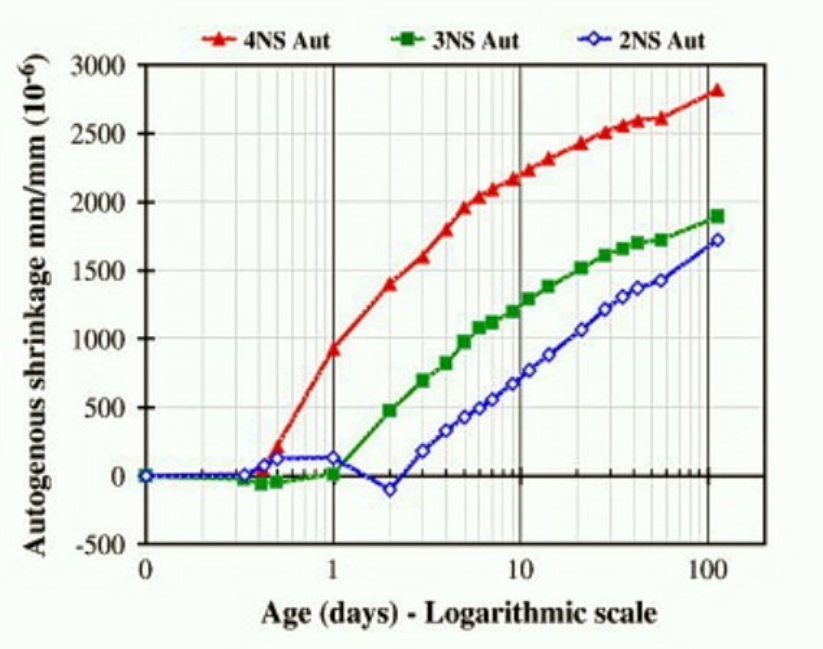

Figure 2.4 Autogenous shrinkage strains of AAS mortars activated with different Na_2O/SiO_2 ratios (Neto et al., 2008).

2.7.3.1.2 ***Drying shrinkage***

Drying shrinkage is similar to the autogenous shrinkage where both occur due to water loss. For drying shrinkage, the water is transferred to the surrounding, whereas for autogenous shrinkage the water is transferred within the pore structure. As the water begins escaping the binder matrix to the exterior environment through evaporation, the binder material shrinks in return. Holt (2001) explained the phenomenon by stating that initially, free water escapes to the binder surface as bleed water. This bleed water can evaporate off the surface to the surrounding environment. Once the bleed water is entirely evaporated, the free surface from which extra water is lost will then migrate into the binder body as evaporation continues. The drying mechanism will begin pulling interior water from the binder mass. The loss of internal water causes suction capillary pore stresses (similar to the ones mentioned in autogenous drying). This suction pressure can also be represented using the Laplace equation **(Eq. 2.3)**, and capillary pressures can then be converted to ultimate

shrinkage using the Mackenzie-Bentz equation **(Eq. 2.5)**. The water suction phenomenon for two binder particles at the paste surface is demonstrated in **Fig. 2.5** below.

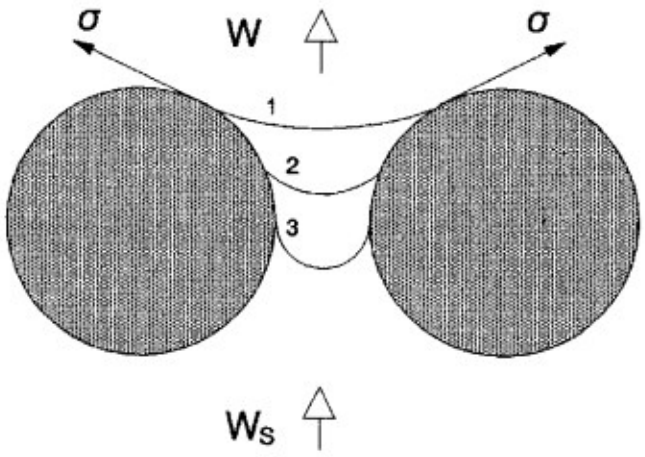

Figure 2.5 Suction stresses pulling the water meniscus between two binder particles due to water loss (Holt, 2001).

Figure 2.5 shows that when the evaporated water (W) exceeds the bleeding water (Ws), the meniscus level begins dropping, therefore, inducing suction capillary stresses (σ) that would result in drying shrinkage. While, if the bleeding rate exceeds the evaporation rate this excess water will act as a curing blanket. In this case, there will be no drying shrinkage since there is enough water on the surface to allow for evaporation without drawing extra water from the internal capillary pores. This shows that the drying shrinkage is very dependent on the rate of evaporation and the total amount of water lost.

Many authors have established investigations on the drying shrinkage of AAF mortars at different curing regimes. Fernández-Jiménez *et al.* (2006) found that AAF mortars ambient cured at 50% relative humidity experienced drying shrinkage strains larger than that found in OPC mortars. While when steam curing at 85 °C for 20 h is adopted, shrinkage was significantly reduced to values below than the ones found in OPC mortars. This approach was also observed by Wallah

and Rangan (2006), as AAF concrete specimens heat cured at 60 °C for 24 h experienced much lower drying shrinkage compared to AAF concrete specimens ambient cured at 25 °C for the same period. Authors stated that heat curing time for 24 h before exposure to ambient conditions was sufficient in dropping the drying shrinkage of AAF concrete.

Previous studies showed that AAS mortars undergo a drying shrinkage 2–4 times higher than that of OPC mortar and the shrinkage value can reach to about 2200 με (Ye *et al.*, 2017*;* Atiş *et al*., 2009; Palacios and Puertas, 2007). Ye and Radlińska (2016) observed that the drying shrinkage of NaOH activated slag paste was 4 times higher than that of OPC paste after 60 days. Moreover, the drying shrinkage of AAS concrete was found to be 3 times higher than that of OPC concrete (Collins and Sanjayan, 2000). Compared to OPC, the more refined pores found in AAS result in higher capillary stress which in turn can significantly increase the drying shrinkage (Cartwright *et al.*, 2014; Ye and Radlińska, 2016).

In addition to the pore structure, the primary hydration product of AAS binders (calcium alumina silicate hydrate gel C-A-S-H) was found to have a significant effect on the measured drying shrinkage (Ye *et al*., 2017*;* Ye and Radlińska, 2016). The structural incorporation of alkali cations in C-A-S-H reduces the stacking regularity of C-A-S-H layers. Therefore, making the C-A-S-H collapse and redistribute easily upon drying. On the other hand, shrinkage performance of alkali-activated fly ash/slag (AAFS) mortars remains poorly understood; with only a few studies reporting the shrinkage of AAFS specimens cured at room temperature (Lee *et al.*, 2013; Gao *et al.*, 2016; Yao *et al.*, 2016). For AAFS mortars, the drying shrinkage has also been found to be larger than that of OPC mortars. It was reported that the drying shrinkage of the blended fly ash/slag binders increased with higher aqueous silica contents in the activator (Gao *et al.*, 2016). There is a disagreement on the effect of slag versus fly ash proportions on shrinkage of the AAFS

binders. Some studies (Lee *et al.*, 2013; Gao *et al.*, 2016) reported that drying shrinkage increased with higher slag contents, another study (Yao *et al.*, 2016) showed that higher slag content led to lower drying shrinkage. Lee *et al*. (2013) showed that higher slag and soluble silica contents led to larger chemical, autogenous, and drying shrinkage. They also highlighted the need for further research to characterize the shrinkage of these blended binders.

2.7.3.2 Shrinkage mitigation techniques

Many researchers have attempted to mitigate shrinkage in AA products. However, it is still unclear which method is effective, mainly due to the lack of knowledge of the actual mechanism governing AA material shrinkage. Palacios and Puertas (2007) attempted to reduce the shrinkage in AAS mortars using shrinkage reducing admixtures (SRAs). SRAs are beneficial because they tend to reduce the surface tension of the pore solution (Radlinska *et al*., 2007). Authors reported reductions in autogenous and drying shrinkage strains, however, the drying shrinkage strains remained significantly higher than those experienced by OPC mortars.

Similarly, Collins and Sanjayan (2000) attempted to use internal curing as a shrinkage mitigation strategy in AAS concrete. Internal curing is a method that counteracts autogenous shrinkage by providing additional water, to reduce self-desiccation and relieve tensile stresses inside pores within the hydrating cementitious paste (Bentz and Weiss, 2011). Lower autogenous shrinkage strain in AAS systems was reported with internal curing. However, the porous system eventually lost all its water content to the surrounding under drying conditions. Therefore, the use of porous coarse aggregates in internal curing reduces the autogenous shrinkage but only delays the drying shrinkage (Radlinska *et al*., 2007).

Other researchers have recently attempted to eliminate autogenous shrinkage in AAS mortars activated with NaOH-sodium silicate or sodium carbonate by the aid of internal curing (Sakulich and Bentz, 2012). A blend of four types of lightweight aggregate (LWA) designated

sands were used in preparing mortar specimens. A properly sized aggregate is crucial to the success of this mitigation strategy due to the low permeability of the AAS pastes (Bentz *et al.*, 2011). Authors reported that the chemical shrinkage associated with autogenous shrinkage was equal in all specimens including the control OPC mortar. Furthermore, internal curing showed only minor drying shrinkage reduction in AAS mortars regardless of activator type. Authors suggested further investigation to clearly identify an effective shrinkage mitigation technique in AA materials.

3

CHAPTER

Evaluating the Shrinkage Behaviour and Effects of the Shrinkage Mitigation Technique of One and Two Part Alkali-Activated Mortars

3.1 Phase 1: Evaluation for Shrinkage Behaviour of Two-Part Alkali-Activated Mortars

3.1.1 *Introduction*

A review of fresh and hardened properties along with shrinkage behaviour of AA materials was provided in the previous chapter (i.e., Chapter 2). According to the literature, shrinkage of AA materials is not yet fully understood. Many factors are affecting the shrinkage behaviour of these materials. This included precursor type, activator type and concentrations, and curing conditions. Even using the same ingredients, the shrinkage behaviour will differ as the physical characteristics, and chemical composition of the used materials will differ from one lab to another. Besides, measuring methods and procedures will have significant effects on the measured shrinkage. For instance, variations in the time for the initial reading will directly affect the total amount of measured shrinkage at early age. As a result, effects of the pre-mentioned factors on shrinkage behaviour of AA materials still needs to be examined. Therefore, in this chapter, a comprehensive data based on shrinkage behaviour of AAMs is generated. This will assist in understanding the effect of each parameter while controlling others.

3.1.2 *Experimental program*

The experimental work in this phase will be divided into two parts. The first part will be conducted at ambient temperature without any heat curing. The second part will focus on heat cured AAMs. For each part, different types of shrinkage will be monitored along with evaluating fresh and hardened properties for different mixtures. The focus of this phase will be devoted to two-part AAMs chemically activated by sodium hydroxide and water glass. FA and GGBFS were used separately and combined as the precursor. The selection of these two binders and alkali activator was based on the literature as these materials are commonly used to produce AA materials.

3.1.2.1 Raw materials

Low-Calcium FA and GGBFS were used as cementing components. The chemical compositions and physical properties of both precursors are listed in **Table 3.1**. In this phase, the activator used was waterglass with a silicate modulus (Ms = SiO_2/Na_2O by mass) of 2. Sodium hydroxide with a purity level of 98% and sodium silicate (SiO_2 (30%), Na_2O (20%), H_2O (50%), specific gravity 1.38 g/mL) were used to prepare the alkali activators. The alkali activator was prepared as the following: distilled water was used to dissolve the NaOH solid at 3M, 6M, and 12M. Sodium silicate solution was then mixed with the NaOH solution to form the alkali activator solution (mass of sodium silicate solution/ NaOH solution = 2). The hot liquid was then left overnight to cool to ambient temperature while covered to prevent carbonation. The fine aggregate used was ASTM C109 river sand with oven dry, saturated surface dry specific gravity, and absorption of 2.54 g/mL, 2.55 g/mL, and, 0.08 %, respectively.

3.1.2.2 Mixture proportions

Single and binary binder levels were tested in this phase. For single binder mixtures, FA or GGBFS was used as a sole cementitious material. For binary mixtures, FA and GGBFS were blended at 1:1 ratio (FS). The mixture proportions of the AA fly ash, slag, and fly ash/slag mortars are shown

in **Table 3.2**. The activator was prepared using a fixed ratio of sodium silicate and a varying molar concentration of NaOH. For each precursor, three AAM mixtures were designed using a three different NaOH concentrations namely (3, 6, and 12M). The mass ratios of sand to precursor and activator solution to precursor were fixed at 2, and 0.4, respectively for all mixtures. Two curing regimes where adopted in the whole study. Samples were cured at 23°C with relative humidity of 60 ± 5% to simulate ambient curing conditions. Other samples were cured at 60°C inside the oven to simulated heat curing procedure. In **Table 3.2**, the first letter of any mixture label represents the precursor type; (i.e., fly ash (F), slag (S), and fly ash/slag 1:1 (FS)) and the number refers to the molarity of the NaOH solution.

Table 3.1 Properties of precursors used.

Chemical composition (%)	**Fly ash (FA)**	**Slag (GGBFS)**
CaO	2.60	56.10
SiO_2	46.00	21.00
Al_2O_3	33.00	17.00
Fe_2O_3	10.50	0.62
SO_3	-	0.77
Physical properties		
Specific gravity (S.S.D)	2.38	2.90
Surface area (m^2/kg)	290 (Blaine)	485 (Blaine)

3.1.2.3 Specimen preparation

Initially, precursors were dry mixed with sand in an electric mixer at a slow speed of (140 ± 5 revs/min) and medium speed (285 ± 5 revs/min) for 2 minutes to ensure homogeneity of the mixture. The prepared alkali activator solution is then added to the mixture and mixed for an additional 2 min. Immediately after mixing, 50 mm cubic molds for compressive strength

evaluation according to ASTM C109 (Standard test method for compressive strength of hydraulic cement mortars), and 25 mm × 25 mm × 285 mm prismatic molds for shrinkage measurements according to ASTM C596 (Standard test method for drying shrinkage of mortar containing hydraulic cement) were cast. All specimens were cured at room temperature of 23 °C and a relative humidity of 60% ± 5% inside the molds for 24 hours. After which, specimens were demolded and moved to the corresponding pre-mentioned curing conditions until the testing age. All reported results represent the average of three replicates.

Table 3.2 Mix proportion of 1 m^3 AAM mixtures.

Mixture	FA (kg)	GGBFS (kg)	NaOH solution molarity (M)	NaOH solution (kg)	Na_2SiO_3 solution (kg)	Sand (kg)
F3	655	0	3	87.33	174.67	1,310
F6	655	0	6	87.33	174.67	1,310
F12	655	0	12	87.33	174.67	1,310
S3	0	627	3	83.6	167.2	1,254
S6	0	627	6	83.6	167.2	1,254
S12	0	627	12	83.6	167.2	1,254
FS3	320.5	320.5	3	85.46	170.94	1,282
FS6	320.5	320.5	6	85.46	170.94	1,282
FS12	320.5	320.5	12	85.46	170.94	1,282

3.1.2.4 *Testing program*

The workability and flow of mortar mixtures was evaluated following the procedure of ASTM C1437-15 (Standard test method for flow of hydraulic cement mortar). After mixing, fresh mortar mixtures were placed in a flow mold on a drop table and stroked for 25 times as shown in **Fig. 3.1**. The diameter of the new shape of the mortar after testing was measured at four locations using a

caliper. The flow was calculated by taking the summation of four reading. Initial and final setting times were measured using a Vicat needle as described in ASTM C807-13 (Standard Test Method for Time of Setting of Hydraulic Cement Mortar by Modified Vicat Needle).

Compressive strength development was evaluated at ages of 1, 7, 14, and 28 days using a 300 kN universal testing machine (UTM) in accordance with ASTM C109 (Standard test method for compressive strength of hydraulic cement mortars). Cubic specimens (50 × 50 × 50 mm) were prepared for compressive strength measurements. The mortar cubes were compacted using a vibrating table and a tamping rod. All mortar specimens were moist cured (100% RH, 23± 0.5°C) until the time of testing. For each mortar and at each age, 3 cubes were tested, and the results were averaged. The hydration progress was investigated by monitoring the heat of hydration reaction using Isothermal Conduction Calorimetry. Dry-mixed binder (fly ash and/or slag), sand, and the pre-mixed alkali activator, prepared earlier, was mixed in the calorimetry cup apparatus at room temperature (23°C) before placing them into the calorimetry device.

The autogenous, and drying shrinkage strains were measured using prism samples (25 × 25× 280 mm) in accordance with ASTM C490 (Standard practice for use of apparatus for the determination of length change of hardened cement paste, mortar, and concrete) as shown in **Fig 3.2**. Change in length was monitored using a length comparator with dial gauge accuracy of 0.001 mm as shown in **Fig. 3.3**. Fresh mortars were cast into prism molds and consolidated using a vibrating table and tamping rod. Prismatic bars were moist cured (95% RH, 23± 0.5°C) for 24 hours before demolding. Immediately after demolding, autogenous shrinkage specimens were wrapped with a first layer of polyethylene film and a second layer of aluminum foil to prevent any moisture loss. Autogenous and drying specimens where then placed in either ambient (60% RH, 23± 0.5°C) or oven (60°C) curing conditions. Autogenous and drying shrinkage measurements

began directly after demolding at age 24 hours Measurements were taken initially at 15 minutes intervals for the first hour, after that at 3 hours , 7 hours , 12 hours , 1 day and daily for up to 8 days, after which readings were taken on day 14, and 28. The mass change was also monitored simultaneously under the same conditions of the tested shrinkage specimens.

Figure 3.1 Flow table test of AAM mixtures.

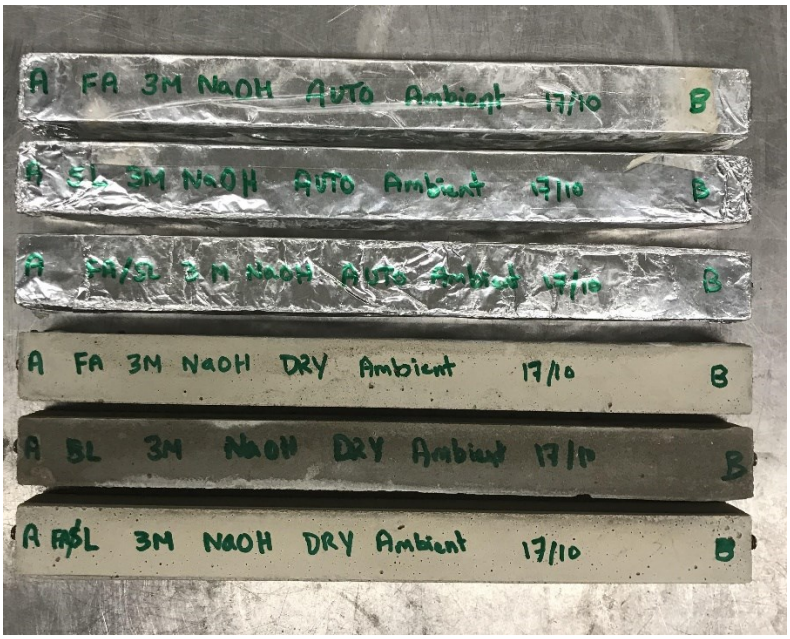

Figure 3.2 AAM shrinkage prismatic mortar bars (autogenous (upper 3) and drying (lower 3)).

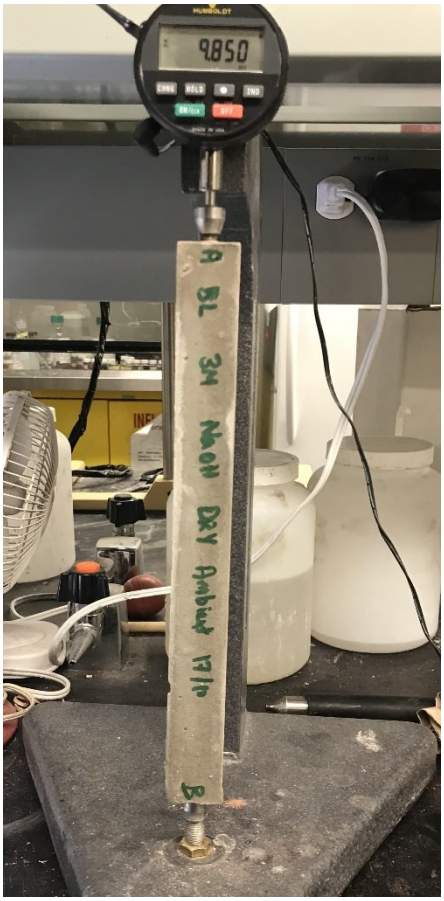

Figure 3.3 Length comparator used to determine shrinkage of mortar bars.

3.2 Phase 2: Evaluation for Shrinkage Behaviour of One-Part Alkali-Activated Mortars

3.2.1 *Introduction*

The Alkali activation process involves the utilization of concentrated aqueous alkali solutions, which are viscous, corrosive, and not user-friendly. Consequently, the development of so-called one-part or "just add water" AA materials may have greater potential than the conventional two-part AA ones, especially in cast-in-situ applications. One-part AA material production involves a dry mixture that consists of a solid aluminosilicate precursor, a solid alkali source, and possible admixtures to which water is added, similar to the preparation of OPC. Several studies pointed out the high autogenous and drying shrinkage strain experienced by the conventional two-part AA materials compared to OPC mortars (Cincotto *et al.*, 2003, Bakharev *et al.*, 1999). However, less attention has been given to the shrinkage behaviour of one-part AA materials. This phase aims to investigate the shrinkage behaviour of FA and GGBFS based mortars activated with solid $Ca(OH)_2$ and $NaHCO_3$ and cured under both ambient and elevated temperatures. Fresh and hardened properties of one-part AAMs were also addressed in this phase.

3.2.2 *Experimental program*

3.2.2.1 Raw materials

In the present phase, Class-F FA and GGBFS were used as precursors similar to phase 1. Chemical and physical properties of the FA and GGBFS were listed previously in phase 1 **(Table 3.1)**. Activators were certified grade calcium hydroxide and sodium bicarbonate with a density of 2.240 g/cm³ and 2.159 g/cm³, respectively. The oven-dry specific gravity, saturated surface dry specific gravity, and absorption of the standard sand used were 2.54 g/cm³, 2.55 g/cm³, and 0.08%, respectively.

3.2.2.2 Mixture proportions

Mixtures proportions of the AAF, AAS, and AAFS mortars are shown in **Table 3.3**. Three precursor blends were utilized in this phase according to the following: single Fly ash (F), Slag (S), and binary fly ash and slag at 1:1 ratio (FS). The ratio of sand to precursor was fixed at 2:1 for all AAM mixtures. Calcium hydroxide and sodium bicarbonate, both in the powder form, were used as activators.

Table 3.3 Mixture proportions of one-part AAMs mixtures.

Mixture	FA (kg)	GGBFS (kg)	$Ca(OH)_2$ (kg)	$NaHCO_3$ (kg)	Activator dose (%)	Sand (kg)	Water (kg)
FL5	655	0	32.75	0	5	1,310	262
FL10	655	0	65.5	0	10	1,310	262
FL15	655	0	98.25	0	15	1,310	262
SL5	0	627	31.35	0	5	1,254	250.8
SL10	0	627	62.7	0	10	1,254	250.8
SL15	0	627	94.05	0	15	1,254	250.8
FSL5	320.5	320.5	32.05	0	5	1,282	256.4
FSL10	320.5	320.5	64.1	0	10	1,282	256.4
FSL15	320.5	320.5	96.15	0	15	1,282	256.4
FN5	655	0	0	32.75	5	1,310	262
FN10	655	0	0	65.5	10	1,310	262
FN15	655	0	0	98.25	15	1,310	262
SN5	0	627	0	31.35	5	1,254	250.8
SN10	0	627	0	62.7	10	1,254	250.8
SN15	0	627	0	94.05	15	1,254	250.8
FSN5	320.5	320.5	0	32.05	5	1,282	256.4
FSN10	320.5	320.5	0	64.1	10	1,282	256.4
FSN15	320.5	320.5	0	96.15	15	1,282	256.4

Three different dosages of calcium hydroxide and sodium bicarbonate (5, 10, and 15%) by mass of binder were chosen to cover a wide activator dosage range. The water to precursor ratio was

fixed at 0.4 for all AAM mixtures. Mixtures were cured under two temperatures, at 23°C with relative humidity of 60 ± 5% (ambient) and at 60°C (oven). It should be mentioned that the first letter of any mixture label represents the binder type; (i.e., fly ash (F), GGBFS (S), and FA/GGBFS 50% (FS)) and the second letter represents the activator (i.e., calcium hydroxide (L) and sodium bicarbonate (N)). While, the number refers to the percentage of the activator used, (i.e., GGBFS activated with 5% lime (SL5)).

3.2.2.3 Specimen preparation

Initially, precursors and powder activators were dry mixed with sand in an electric mixer at a slow speed of (140 ± 5 revs/min) and medium speed (285 ± 5 revs/min) for 2 minutes to ensure homogeneity of the mixture. Tap water is then added to the mixture and mixed for an additional 2 min. Immediately after mixing, 50 mm cubic molds for compressive strength evaluation according to ASTM C109 (Standard test method for compressive strength of hydraulic cement mortars), and 25 mm × 25 mm × 285 mm prismatic molds for shrinkage measurements according to ASTM C596 (Standard test method for drying shrinkage of mortar containing hydraulic cement) were cast. All specimens were cured inside the molds at room temperature of 23 °C and relative humidity of 60% ± 5% for 24 hours. After which, all specimens were demolded and stored in ambient room conditions or in the oven at 60°C until testing age. All reported results represent the average of three replicates.

3.2.2.4 Testing program

The detailed testing program was similar to the one utilized in phase 1 **section (3.2.5)**. It should be mentioned that all shrinkage specimens for fly ash activated mortars were very weak and could not be tested. Hence, the shrinkage discussion will only focus on slag and fly ash/slag activated mixtures.

3.3 Phase 3: Effects of Shrinkage Reducing Admixture on Shrinkage Behaviour of One and Two Part Alkali-Activated Mortars

3.3.1 *Introduction*

Alkali activated materials have received much attention from the academic field owing to significant advantages such as the lower energy demands and CO_2 emissions in comparison with the manufacturing of common PC products. Several studies indicated that AA materials present high mechanical strength and good performance in chemical attack, frost-thaw cycles and high temperatures (Fernández-Jiménez and Puertas, 2002; Bakharev *et al*., 1999). However, other studies had shown that AA materials are subject to substantial autogenous and drying shrinkage (volumetric instabilities), this being one of the main drawbacks to their definitive use as an alternative to traditional PC binders (Cincotto *et al*., 2003; Bakharev *et al*., 1999).

The criteria behind this shrinkage have not yet been fully understood. Authors suggested that the characteristics of the binder product gel and the pore size distribution, have a direct effect on drying shrinkage (Collins and Sanjayan, 2000; Neto *et al*., 2008). Few authors, however, have studied the possible ways to reduce the shrinkage experienced by AA materials (Palacios and Puertas, 2007; Bakharev *et al*., 2000). The effect of SRA has been well documented in PC systems (Berke *et al*., 2003). However, the effect of SRA on shrinkage behavior of one-part and two-part AAMs cured under both ambient and elevated temperatures has not been determined to date to the best of the author's knowledge and constitutes the object of the present phase. Moreover, the effect of SRA addition on the fresh and hardened properties of AAMs was also addressed.

3.3.2 *Experimental Program*

3.3.2.1 Raw materials

In the present phase, class-F FA and GGBFS were used as precursors similar to phase 1 and 2. Chemical and physical properties of the FA and GGBFS were listed previously in phase 1 (**Table 3.1)**. Activators used in one-part AAM were Certified Grade calcium hydroxide and sodium bicarbonate with a density of 2.240, and 2.159 g/mL, respectively. While, the activator used in two-part AAMs was a liquid solution made of sodium hydroxide with a purity level of 98% and sodium silicate (SiO_2 (30%), Na_2O (20%), H_2O (50%), specific gravity 1.38 g/mL). ASTM standard river sand was utilized as the fine aggregate material. The oven-dry, saturated surface dry specific gravity, and absorption of the standard sand used were 2.54 g/mL, 2.55 g/mL, 0.08%, respectively. Sika® Control-75 shrinkage reducing admixture was used in this study. Sika® Control-75 conforms to the requirements of ASTM C494 (Standard Specification for Chemical Admixtures for Concrete), Type S.

3.3.2.2 Mix proportions

Mixtures proportions of one-part and two-part AAF, AAS, and AAFS mortars are shown in **Tables 3.4 and 3.5,** respectively. Three precursor blends were utilized in this phase according to the following: single Fly ash (F), Slag (S), and binary fly ash and slag at 1:1 ratio (FS). The ratio of sand to binder was 2:1 for all mixtures. Three different dosages of powder calcium hydroxide and sodium bicarbonate (5, 10, and 15%) by mass of binder were chosen to cover a wide activator dosage range in one-part AAMs. While, three NaOH concentrations (3, 6, and 12M) mixed with constant sodium silicate content were utilized in two-part AAMs. The liquid to precursor ratio was fixed at 0.4 for all mixtures. Mixtures were cured under two temperatures, at 23°C (ambient) with relative humidity of 60 ± 5% and at 60°C (oven).

Table 3.4 Mix proportions of 1 m^3 one-part AAM mixtures containing SRA.

Mixture	FA (kg)	GGBFS (kg)	$Ca(OH)_2$ (kg)	$NaHCO_3$ (kg)	Activator dose (%)	SRA dose (%)	Sand (kg)	Water (kg)
SL5R1	0	627	31.35	0	5	1	1,254	250.8
SL10R1	0	627	62.7	0	10	1	1,254	250.8
SL15R1	0	627	94.05	0	15	1	1,254	250.8
SL5R2	0	627	31.35	0	5	2	1,254	250.8
SL10R2	0	627	62.7	0	10	2	1,254	250.8
SL15R2	0	627	94.05	0	15	2	1,254	250.8
FSL5R1	320.5	320.5	32.05	0	5	1	1,282	256.4
FSL10R1	320.5	320.5	64.1	0	10	1	1,282	256.4
FSL15R1	320.5	320.5	96.15	0	15	1	1,282	256.4
FSL5R2	320.5	320.5	32.05	0	5	2	1,282	256.4
FSL10R2	320.5	320.5	64.1	0	10	2	1,282	256.4
FSL15R2	320.5	320.5	96.15	0	15	2	1,282	256.4
SN5R1	0	627	0	31.35	5	1	1,254	250.8
SN10R1	0	627	0	62.7	10	1	1,254	250.8
SN15R1	0	627	0	94.05	15	1	1,254	250.8
SN5R2	0	627	0	31.35	5	2	1,254	250.8
SN10R2	0	627	0	62.7	10	2	1,254	250.8
SN15R2	0	627	0	94.05	15	2	1,254	250.8
FSN5R1	320.5	320.5	0	32.05	5	1	1,282	256.4
FSN10R1	320.5	320.5	0	64.1	10	1	1,282	256.4
FSN15R1	320.5	320.5	0	96.15	15	1	1,282	256.4
FSN5R2	320.5	320.5	0	32.05	5	2	1,282	256.4
FSN10R2	320.5	320.5	0	64.1	10	2	1,282	256.4
FSN15R2	320.5	320.5	0	96.15	15	2	1,282	256.4

Table 3.5 Mix proportion of 1 m^3 two-part AAM mixtures containing SRA.

Mixture	FA (kg)	GGBFS (kg)	NaOH solution molarity (M)	NaOH solution (kg)	Na_2SiO_3 solution (kg)	SRA dose (%)	Sand (kg)
F3	655	0	3	87.33	174.67	0	1,310
F6	655	0	6	87.33	174.67	0	1,310
F12	655	0	12	87.33	174.67	0	1,310
F3R1	655	0	3	87.33	174.67	1	1,310
F6R1	655	0	6	87.33	174.67	1	1,310
F12R1	655	0	12	87.33	174.67	1	1,310
F3R2	655	0	3	87.33	174.67	2	1,310
F6R2	655	0	6	87.33	174.67	2	1,310
F12R2	655	0	12	87.33	174.67	2	1,310
S3	0	627	3	83.6	167.2	0	1,254
S6	0	627	6	83.6	167.2	0	1,254
S12	0	627	12	83.6	167.2	0	1,254
S3R1	0	627	3	83.6	167.2	1	1,254
S6R1	0	627	6	83.6	167.2	1	1,254
S12R1	0	627	12	83.6	167.2	1	1,254
S3R2	0	627	3	83.6	167.2	2	1,254
S6R2	0	627	6	83.6	167.2	2	1,254
S12R2	0	627	12	83.6	167.2	2	1,254
FS3	320.5	320.5	3	85.46	170.94	0	1,282
FS6	320.5	320.5	6	85.46	170.94	0	1,282
FS12	320.5	320.5	12	85.46	170.94	0	1,282
FS3R1	320.5	320.5	3	85.46	170.94	1	1,282
FS6R1	320.5	320.5	6	85.46	170.94	1	1,282
FS12R1	320.5	320.5	12	85.46	170.94	1	1,282
FS3R2	320.5	320.5	3	85.46	170.94	2	1,282
FS6R2	320.5	320.5	6	85.46	170.94	2	1,282
FS12R2	320.5	320.5	12	85.46	170.94	2	1,282

3.3.2.3 Specimen preparation

The specimen preparations of one-part and two-part AA mortar mixtures were similar to the ones utilized in **phase 2 section (3.3.4),** and **phase 1 section (3.2.4),** respectively. However, it should be noted that SRA dosage was mixed with tap water in one-part AA mortar mixtures and mixed with activator solution in two-part AA mortar mixtures.

3.3.2.4 Testing program

The testing program was similar to the one utilized in phase 1 **section (3.2.5)**.

4

CHAPTER

Experimental Results

4.1 Phase 1: Evaluation for Shrinkage Behaviour of Two Part Alkali-Activated Mortars

4.1.1 *Flowability*

Variations in workability for different AAM mixtures with respect to NaOH concentrations are shown in **Table 4.1**. In general, the flow of AAMs decreased as the molar concentration of NaOH in the activating solution increased. For instance, reductions in the flow of AAF mortars when NaOH concentrations increased from 3M to 6M and 12M were 5.56%, and 14.81%, respectively. Liquid (waterglass- Na_2SiO_3) is known to have a high viscosity itself. Hence, blending waterglass and NaOH solutions tends to increase the viscosity of the activating solution and thus reduces the flow of AAM (Chindaprasirt *et al*., 2007).

The flowability of AAS mortars was lower than that of the AAF, and AAFS mortars at a similar NaOH concentration. For example, the flowability of 3M NaOH AAS mortar was around 11% and 7% lower than that of 3M NaOH AAF and AAFS mortars, respectively. FA is known to improve the workability of fresh mortar due to its globular shape and large specific area (Fernández-Jimenez *et al*., 2006). On the other hand, the flowability of AAS mortars is dominantly affected by the rapid reaction between GGBFS and the alkali activator (Jang *et al*., 2014).

Binary mortar mixtures incorporating FA and GGBFS with 1:1 ratio (AAFS) exhibited flow values that were in between those reported for AAS and AAF mortars. For instance, the flowability of 3M NaOH AAFS mortars was 8% less than that of AAF mortars and 6.5% more than that of AAS mortars activated with similar NaOH concentration. It should be noted that the effect of activator concentrations on the workability of AAMs was similar regardless of the precursor type. Results clearly showed that activator concentration and precursor type are of main influence on the workability of AAM.

4.1.2 *Setting time*

Setting time tests were performed in order to ascertain the effects of precursor type and NaOH solution molarity on the stiffing of AAMs. Initial and final setting time results of different AAM are shown in **Table 4.1**. Generally, increasing NaOH concentrations accelerated both the initial and final setting of AAM mixtures. For instance, reductions in the initial setting time of AAF mortars when NaOH concentrations increased from 3M to 6M and 12M were 12.5%, and 38.2%, respectively. The corresponding reductions in final setting times were 11.2% and 35%, respectively.

Table 4.1 Setting time and flow values of AAM mixtures.

Mixture	Setting time (min)		Flow (cm)
	Initial	Final	
F3	144	286	108
F6	126	254	102
F12	89	186	100
S3	108	171	94
S6	72	114	87
S12	47	76	76
FS3	120	202	100
FS6	104	184	92
FS12	72	112	84

Increasing activator concentrations tends to accelerate the rate of the hydration reaction. This directly influences the stiffness development of AAMs. AAS mortar mixtures exhibited a faster setting time compared to that of AAF and AAFS mortar mixtures. For example, the initial setting in 3M NaOH AAS mortars was achieved 36 and 12 minutes earlier than that in 3M NaOH AAF and AAFS mortars, respectively. Moreover, the corresponding final setting was achieved 115 and 86 minutes earlier in AAS mortars compared to AAF and AAFS mortars. The shorter setting behaviour observed in AAS mortars can be ascribed to the higher calcium (CaO) content of GGBFS. Increasing CaO content was found to accelerate the hydration reactions, and hardening process of AAS mortars (Yip, 2004). Generally, the use of superplasticizers to control the setting behaviour can be a solution to this rapid setting of AAS mortars.

The initial and final setting times of AAFS mortars was in between those values exhibited by AAF and AAS mortars. For instance, 3M NaOH AAFS mortars achieved the initial setting 24 minutes earlier than AAF mortars and 12 minutes later than AAS mortars activated with a similar NaOH concentration. The corresponding final setting of AAFS mortars occurred 84 minutes earlier than AAF mortars and 32 minutes later than AAS mortars. The replacement of FA with GGBFS shortened the setting of AAFS mortars compared to that of AAF mortars. The effect of activator concentrations on the setting behaviour of AAMs was found to be similar regardless of the precursor type.

4.1.3 *Compressive strength*

4.1.3.1 Effect of activator concentrations

The compressive strength development of AAM specimens activated with different concentrations of NaOH was studied. **Figure 4.1** shows the compressive strength of AAF mortars. Generally, the compressive strength of AAF mortars increased with higher activator concentrations under both curing conditions. For instance, when NaOH concentration increased from 3M to 6M and 12M,

the 28 day compressive strength of ambient-cured AAF mortars increased by 46.2%, and 117.26%, respectively. The increase in the 28 day compressive strength of oven cured AAF mortars due to higher NaOH concentrations was almost equal to the one found in ambient cured ones. **Figure 4.2** shows the compressive strength of AAS mortars. A similar compressive strength increase trend with higher NaOH concentrations was found in AAS mortars. For example, when NaOH concentration increased from 3M to 6M and 12M, the 28 day compressive strength of ambient cured AAS mortars increased by 32.3%, and 66%, respectively. The corresponding increase in oven cured AAS mortars was 11.3%, and 18.2%, respectively. The increase in compressive strength of AAS mortars due to higher activator concentrations was less pronounced in oven cured specimens compared to ambient cured ones.

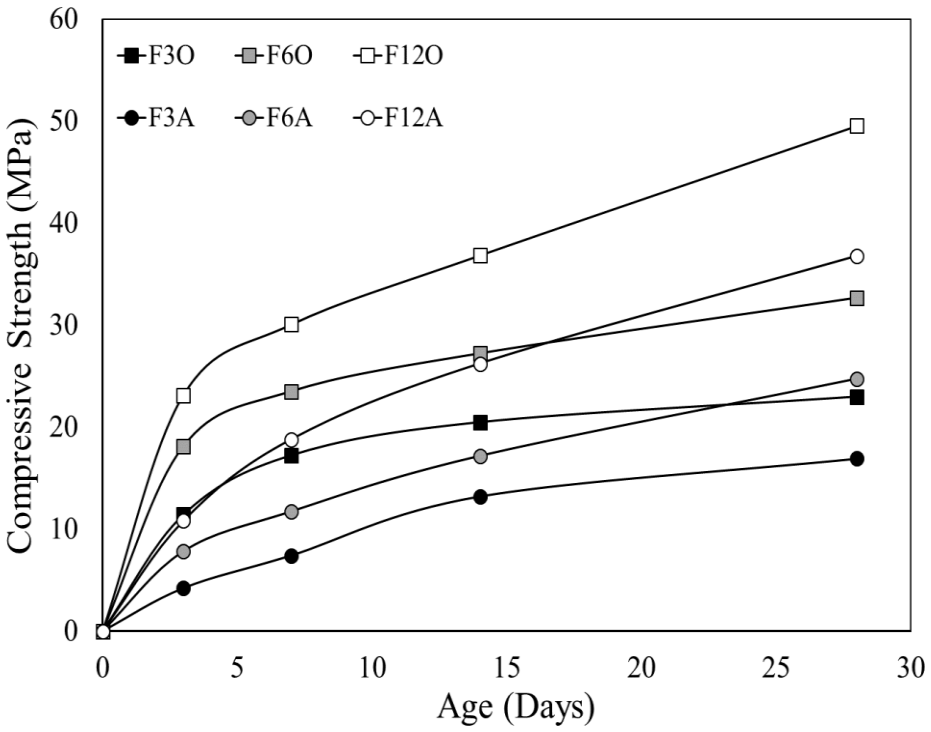

Figure 4.1 Compressive Strength of AAF mortar specimens (ambient (A) and oven (O) cured).

Figure 4.3 shows the compressive strength of AAFS mortars. The compressive strength of AAFS mortars also increased as NaOH concentration increased. For example, increasing NaOH

concentration from 3M to 6M and 12M, increased the 28 day compressive strength of ambient cured AAFS mortars by 17.5%, and 60%, respectively. The corresponding increase in oven cured AAFS mortars was 17%, and 20%, respectively. The increase in compressive strength of AAFS mortars due to higher activator concentrations was significantly decreased in 12M NaOH activated oven cured specimens compared to ambient cured ones.

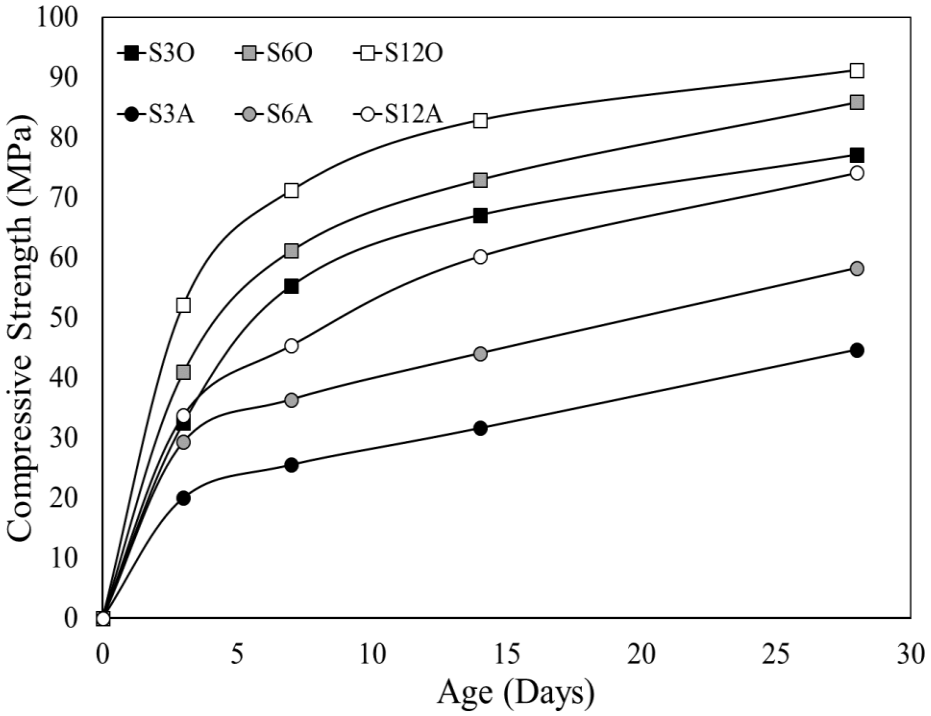

Figure 4.2 Compressive Strength of AAS mortar specimens (ambient and oven cured).

In the alkali activation polymerization process, strong alkalis are required to activate the silicon and aluminum present in precursors to allow the glassy structure to partially or entirely dissolve and then transform into a very compacted composite (Guo *et al*., 2010). High NaOH concentration increases the solubility of amorphous silica and alumina present in precursors (Guo *et al*., 2010). Therefore, the leaching out of Si^{4+} and Al^{3+} ions from FA, and GGBFS particles is expected to increase at higher NaOH concentration. As a result, an increase in the compressive

strength is achieved due to the subsequent formation of sodium aluminosilicate hydrate (N-A-S-H) and calcium aluminosilicate hydrate (C-A-S-H) binder gels (Cho *et al.*, 2017). However, the amounts of dissolved silica and alumina from precursors begin to get limited due to the precipitations of binder gels around the surface of FA and GGBFS particles (Cho *et al.*, 2017). Hence, excessive NaOH concentrations may generate a blocking effect on the acceleration of AAM polymerization (Fernández-Jiménez and Palomo, 2005), which leads to a slower strength development rate.

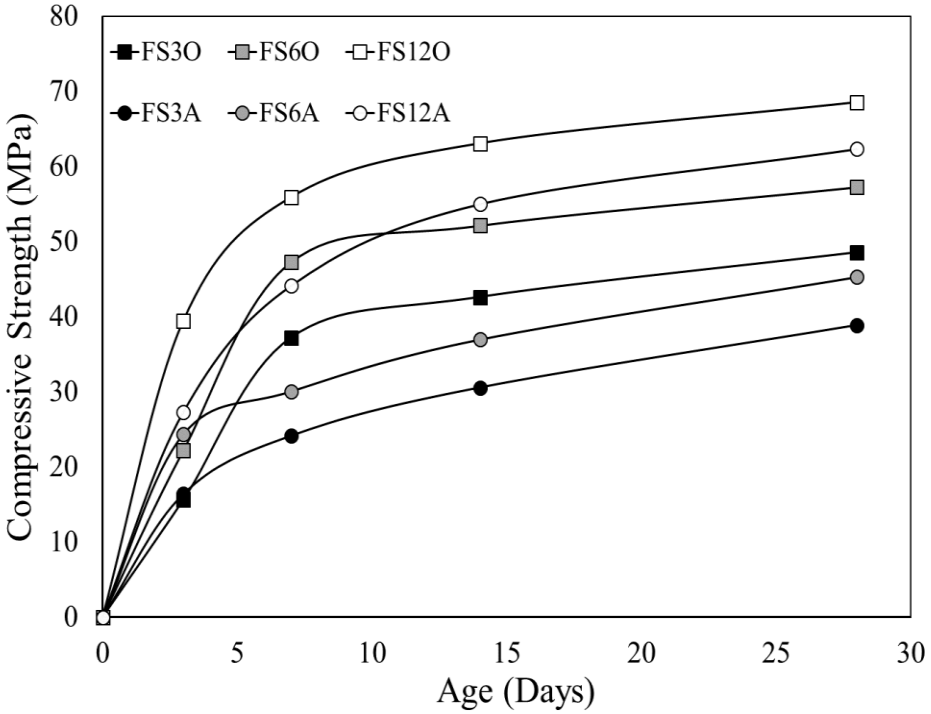

Figure 4.3 Compressive Strength of AAFS mortar specimens (ambient and oven cured).

From the above argument, it could be concluded that the concentration of NaOH activator is a crucial parameter affecting the compressive strength of AAMs. This is in agreement with the previous study done by (Atiş *et al.*, 2009). Successful alkali activation requires a highly concentrated NaOH solution (12M) to achieve better silica and alumina dissolution and therefore

better strength properties. Nevertheless, (Wang *et al.*, 1994) showed that the more Na_2O used, the higher the achieved strength. However, when Na_2O% reaches a particular value (depending on activator type and curing condition), there is no further significant increase in strength and detrimental properties such as efflorescence and brittleness are increased because of the effect of more free alkali in the product. In this case, trying to increase the strength by increasing the alkali dosage is not accomplishable.

4.1.3.2 Effect of precursor type

Compressive strength results for all mortar specimens activated with 3M, 6M, and 12M NaOH concentrations and cured at both ambient and oven conditions are plotted in **Figs. 4.4-4.6**. Generally, AAM specimens exhibited steady strength development between 3 and 28 days. AAS mortar specimens achieved the highest 28 day compressive strength followed by AAFS, and finally, AAF mortars under both curing conditions. For instance, at low activator molarity (3M NaOH), the 28 day compressive strength of ambient cured AAS mortars was 15%, and 160% higher than that of AAFS and AAF mortars, respectively. The corresponding compressive strength of oven cured AAS mortars was 59%, and 263% higher than that of AAFS and AAF mortars, respectively.

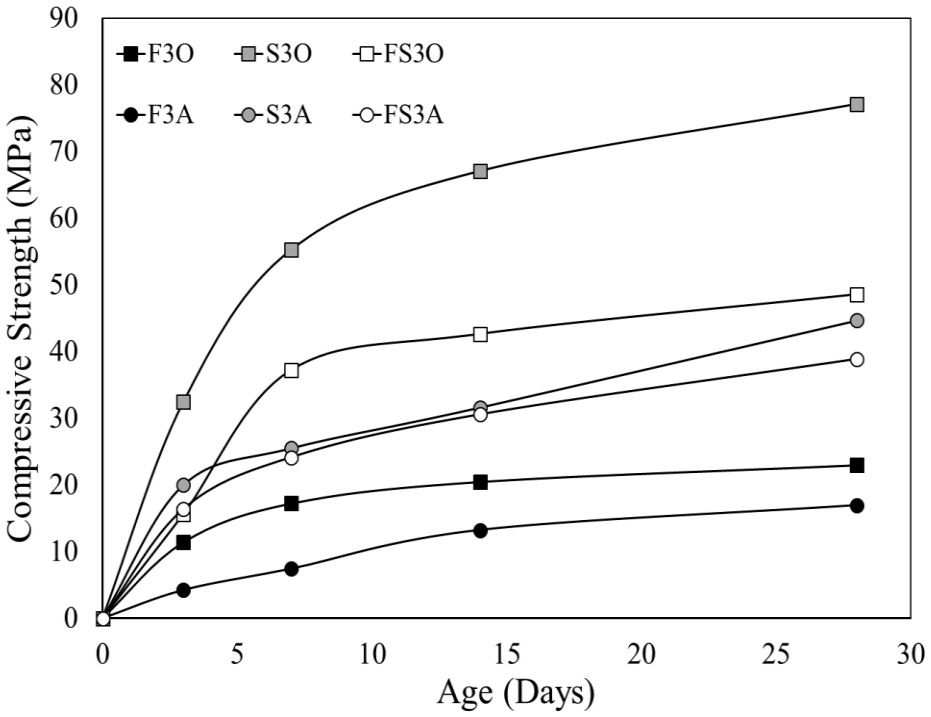

Figure 4.4 Compressive strength of AAMs activated with 3M NaOH (ambient and oven cured).

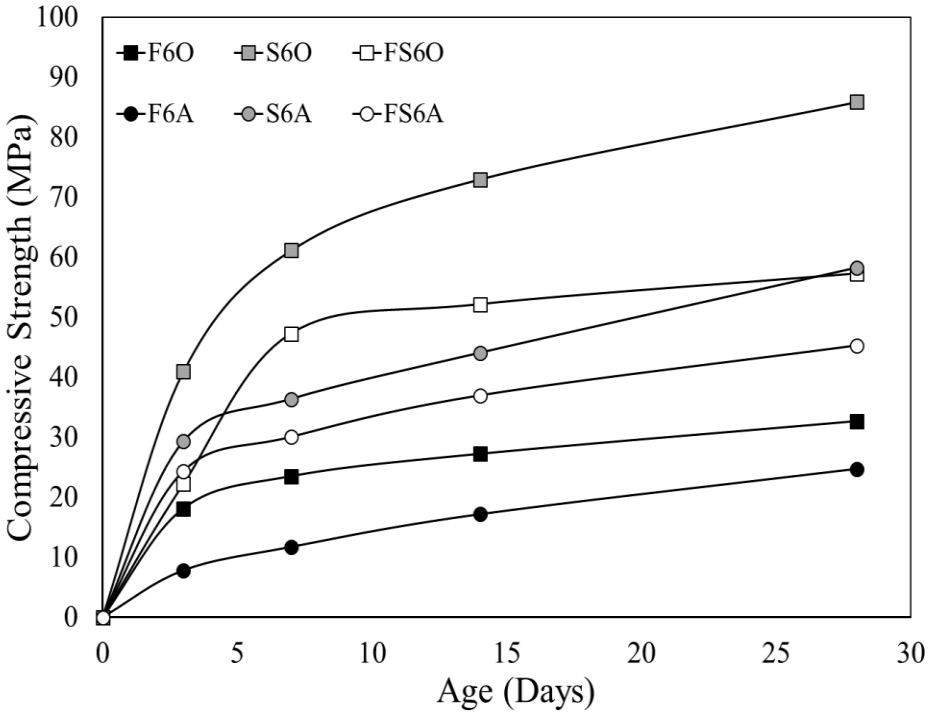

Figure 4.5 Compressive strength of AAMs activated with 6M NaOH (ambient and oven cured).

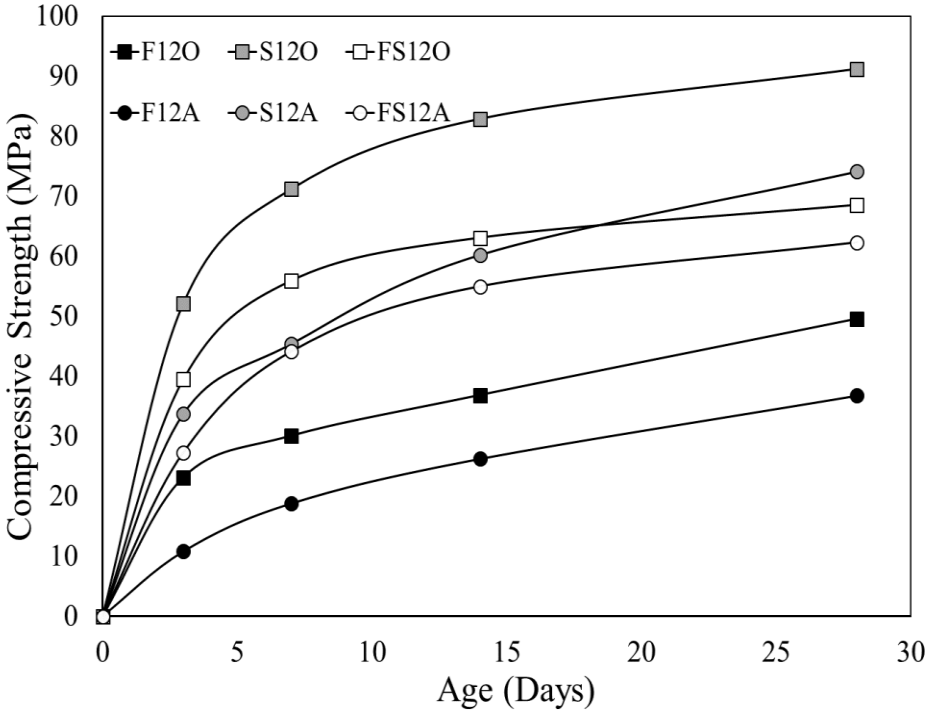

Figure 4.6 Compressive strength of AAMs activated with 12M NaOH (ambient and oven cured).

On the other hand, at a high activator concentration (12M NaOH), the 28 day compressive strength of ambient cured AAS mortars was 19%, and 102% higher than those of AAFS and AAF mortars, respectively. The corresponding compressive strength of oven cured AAS mortars was 33%, and 84% higher than those of AAFS and AAF mortars, respectively. Results suggest clearly that compressive strength is favorable when GGBFS content is higher. It is well known that the main component of GGBFS is calcium oxide. The increase in calcium content significantly accelerated the hardening and development of AAMs microstructure (Pangdaeng *et al.*, 2014). It was also reported by (Lee *et al.*, 2002) that the additional calcium content increases the solidification rate and causes rapid hardening. This is in agreement with previous setting results.

Two different types of binder gel structures form in activated GGBFS and FA: C-A-S-H, which is mainly formed in the AAS products, and N-A-S-H, which is mainly formed in AAF

products (Van Jaarsveld *et al*., 2003); C-A-S-H gel (calcium aluminosilicate hydrate gel) associated with GGBFS is known to give better binding properties compared to the N-A-S-H gel (sodium aluminosilicate hydrate gel) associated with FA (Lee *et al.*, 2002). Therefore, the improvement in strength of AAS mortars compared to AAF and AAFS mortars was due to the increase in the reaction products with the contribution of C–A–S–H gel (Luga *et al.*, 2017). Moreover, the higher the degree of dissolution of GGBFS compared to FA led to the precipitation of higher amount of reaction products than expected under the lower alkaline condition (Song and Jennings, 1999). These results indicate that GGBFS is a higher reactive material than FA and contributes significantly to the final strengths.

On the other hand, the contribution of FA to the compressive strengths of AAM through the produced N–A–S–H gel is influenced by the curing temperature (Luga *et al*., 2017). AAF mortar results indicated a very low level of activation at ambient conditions as the obtained compressive strength of those specimens was very little. However, when oven curing was adopted, a higher level of activation was observed. This shows the dependency of AAF mortars on curing temperatures to achieve sufficient levels of activation and therefore, compressive strength.

4.1.3.3 Effect of curing temperature

Compressive strength results of AAF, AAS, and AAFS mortars activated with different NaOH concentration and cured at ambient and oven conditions are shown **Figs. 4.1-4.3**. Results indicated that all specimens cured in the oven had acquired higher compressive strength than those cured under ambience at the age of 28 days. For instance, the 28 days compressive strength values of ambient cured AAF mortars activated with 3M, 6M, and 12M NaOH concentrations was increased by 36, 32, and 35%, respectively, when cured at the oven. Usually, the activation reaction of FA at room temperature is slow (Shi and Day, 1999). Previous research shows similar results

about AA fly ash class F systems. The activation reactions do not proceed at the rate that is sufficient to produce high strength paste under ambient temperature. Hence, elevated temperatures are necessary to accelerate the reactions of AAF mortars (Xie and Xi, 2001).

On the other hand, previous research showed that GGBFS could be activated efficiently at room temperature (Shi and Day, 1999). Therefore, ambient cured AAS mortars activated with 3M, 6M, and 12M NaOH concentrations achieved 28 days compressive strength results of 44.67, 58.22, and 74.11 MPa, respectively. These values were even increased by 73, 47, and 23%, respectively when specimens were exposed to oven curing condition. Generally, increasing curing temperature accelerates the rate of hydration reactions in AAMs.

The increase in compressive strength values in oven cured AAFS mortars activated with 3M, 6M, and 12M NaOH concentrations were 25, 26, and 10%, respectively compared to ambient cured ones. The compressive strength increase rate due to oven curing was less pronounced in AAFS mortars compared to AAF and AAS mortars. The combination of FA and GGBFS in AAFS mortars seem to be affected by the high curing temperature. The above findings suggest that precursor type and ratio accompanied with activator concentration are all critical values in the strength improvements due to oven (heat) curing.

Van Jaarsveld *et al*. (2003) studied the correlation between the changes in the main oxide percentages present in GGBFS and FA activated mortar due to heat curing and the achieved compressive strength values. They suggested that the strength development for ambient cured mortars is strongly correlated to the CaO, SiO_2, and Al_2O_3 contents. However, such a correlation was not observed in heat cured mortars because of the temperature factor.

4.1.4 *Heat evolution tests*

Precursor type and alkali activator concentration are well known to influence the hydration reactions. Activator concentration is adjusted by varying the solution dosage of specific liquid to

solid ratio. The effect of NaOH concentrations on the cumulative heat of AAF, AAS, and AAFS mortar mixtures was studied at 23°C as shown in **Figs. 4.7 and 4.8.** The test was carried for 26 hours, however only the first 10 hours are shown on the heat flow plots as the rates were almost constant after that. Moreover, the change in the heat flow rates as NaOH concentration increased is illustrated in **Figs. 4.9-4.11.**

Generally, a high short exothermic peak appeared immediately after the activator is mixed with the precursor in all AAMs. This initial peak can be designated as the initial wetting and dissolution of precursor solid materials (Provis, 2017). In cement hydration, a very much similar peak is found during the initial period of cement hydration process, although the chemical reactions occurring in both may be very different (Yao *et al*., 2009).

The beginning of solid material dissolution which resulted in the first high heat flow peak seems to be affected by the activator (NaOH) concentration. As shown in **Figs. 4.9-4.11**, increasing NaOH concentration broadens the heat rate evolution peak in most cases. Following the dissolution peak, the heat flow began to gradually decrease up to a relatively low value after and kept constant until the end of the test period. No other remarkable features can be seen from the heat flow curves. Cumulative heat curves suggest that the heat evolution in all AAM mixtures is also affected by NaOH concentration since the magnitude was increased by increasing the activator concentration.

It is well known that the formation and polymerization of binder gels are responsible for the induced cumulative heat (Yao *et al*., 2009; Chithiraputhiran and Neithalath, 2013). The continuous dissolution and transformation of dissolved particles into gels which accounts for over 98% of the reaction time measured but only 54% of the cumulative heat released, is responsible for the slow cumulative heat increase in AAF mortars (Sun and Vollpracht, 2017). As shown in **Fig. 4.9**, the heat flow curves for AAF mortars were relatively low but did not stop completely.

This can be seen in the corresponding cumulative heat plot **(Fig. 4.8)** as the cumulative heat was still gradually increasing.

Heat flow peak and rates were the highest in AAS mortars followed by AAFS, and finally AAF mortars. In agreement with the compressive strength results, AAF mortars are well known in exhibiting a low hydration reaction rate at room temperature. Conversely, AAS mortars showed an accelerated hydration reaction because of the higher CaO content in GGBFS compared to FA. Polymerization and condensation of binder gels are exothermic and make the main contribution to heat flow and cumulative heat (Yao *et al*., 2009). A higher reaction degree will release a high exothermic heat, hence, higher heat flow rate and eventually higher cumulative heat. The heat flow rate and cumulative heat released by AAFS mortars came in between the values achieved by AAS and AAF mortars. The addition of 50% GGBFS did, in fact, contribute to both the higher heat rate and cumulative heat released by AAFS. It can be concluded that the heat flow and cumulative heat released were significant influenced by both activator concentration and precursor type.

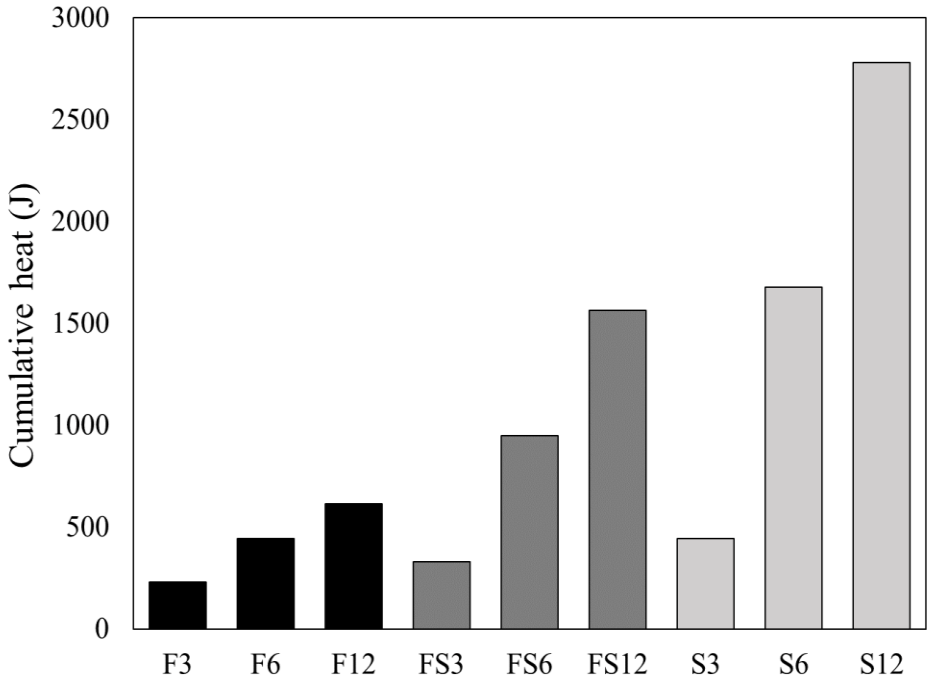

Figure 4.7 Cumulative heat of AAM activated with different NaOH concentrations.

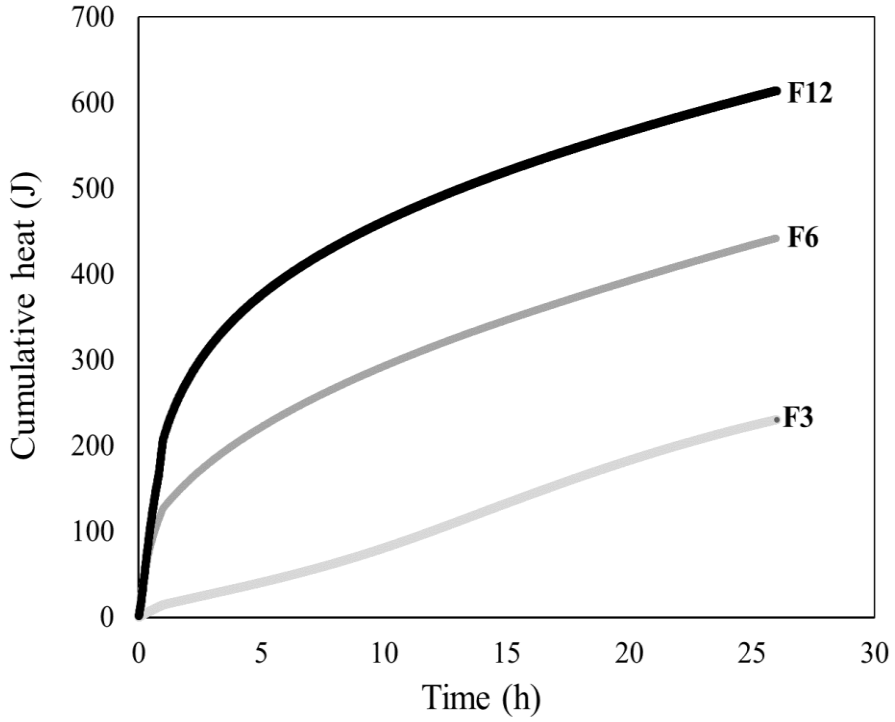

Figure 4.8 Cumulative heat of AAF mortars activated with different NaOH concentrations.

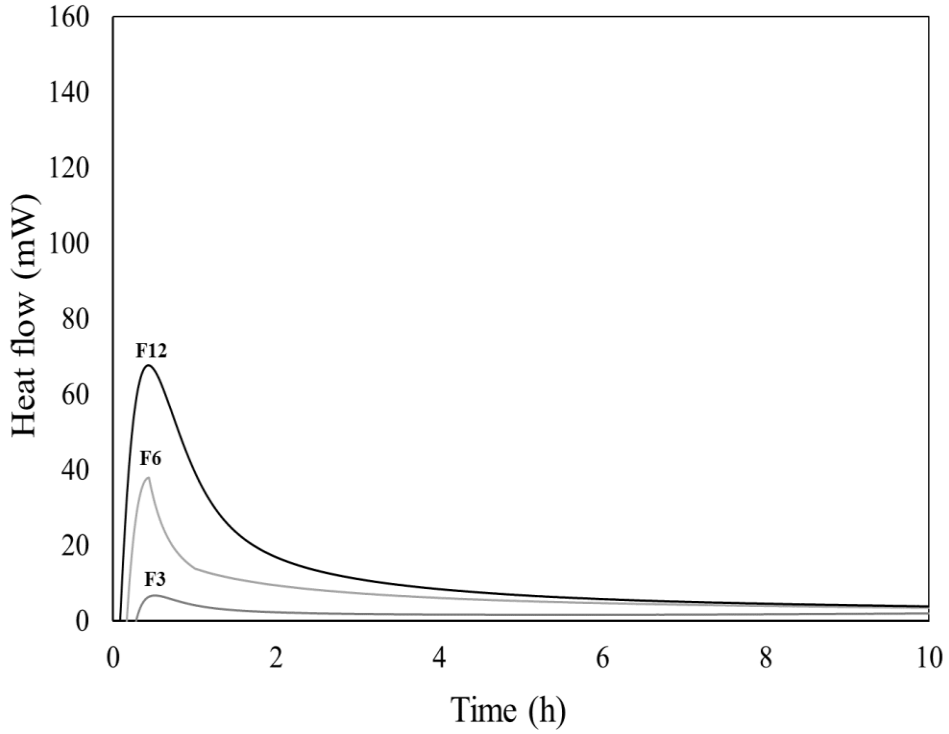

Figure 4.9 Heat flow of AAF mortars activated with different NaOH concentrations.

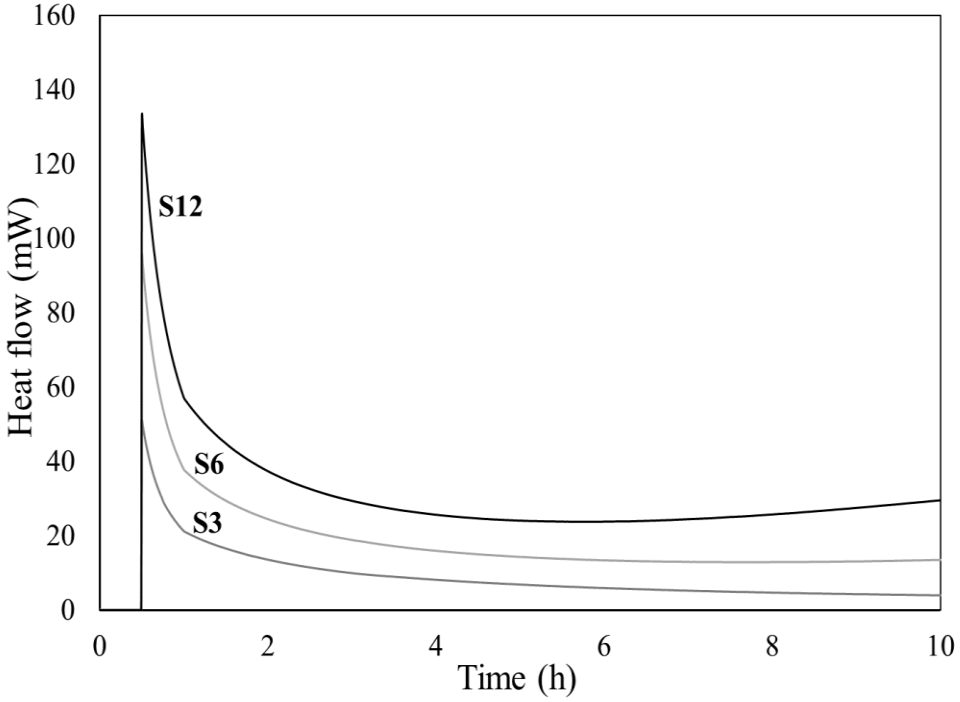

Figure 4.10 Heat flow of AAS mortars activated with different NaOH concentrations.

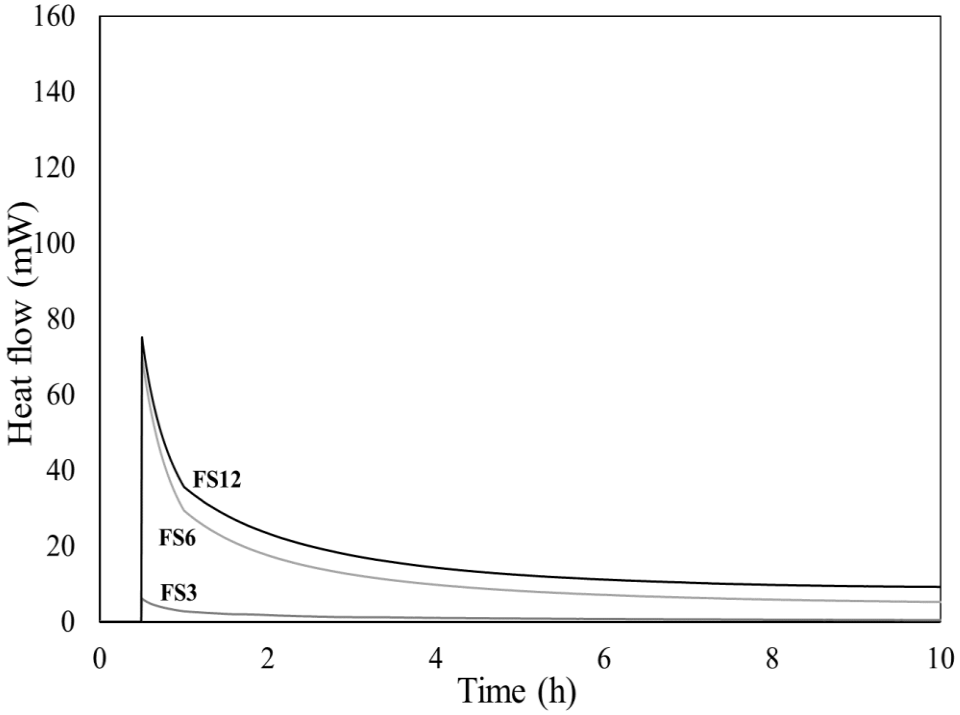

Figure 4.11 Heat flow of AAFS mortars activated with different NaOH concentrations.

4.1.5 *Drying Shrinkage*

4.1.5.1 Effect of activator concentrations

Shrinkage is a critical parameter for long-term serviceability of concrete structures. The drying shrinkage strains of AAM activated with different (NaOH) concentrations and cured at ambient and oven temperatures are plotted in **Figs. 4.13-4.15**. Typically, the magnitude and rate of drying shrinkage in all AAM specimens increased as the NaOH concentrations increased. For instance, the drying shrinkage strain experienced by 12M NaOH activated AAF mortars was 25%, and 34% more than the one experienced by 6M, and 3M NaOH activated mortars, respectively under ambient curing. The corresponding drying shrinkage strains under oven curing were also 18%, and 27% higher, respectively. Around 80-86 % of the total shrinkage was observed within the first 7 days depending on the activator concentration.

For AAS mortars, the increase in drying shrinkage induced by increasing the activator concentrations was less than the one observed in AAF mortars under both curing conditions. For instance, the magnitude of drying shrinkage was 33%, and 14.4% higher in AAF and AAS mortars, respectively under ambient curing when activator concentration increased from 6M to 12M. The corresponding drying shrinkage increase under oven curing was 21% and 3.5%, respectively. It is clear that the increase in drying shrinkage due to higher activator concentrations is less pronounced under oven curing temperature. The increase in drying shrinkage strains of AAFS mortars with higher activator concentrations came in between both AAS and AAF mortars.

NaOH concentration greatly influences the porosity, and degree of hydration in AAMs, which are determining factors for the evolution of drying shrinkage (Neto *et al*., 2008). It was reported that the total porosity decreases as NaOH concentrations in the activator solution increased (Kumarappa *et al*., 2017). Reduction in porosity would cause more shrinkage occurring due to the extra-capillary stress induced. Moreover, as the activator concentration increases, the

degree of hydration reaction increases (Atiş *et al*., 2009). The higher rate of reaction densifies the mixtures leading to finer pore structure (Thomas *et al*., 2017).

Finer pore size distribution along with the higher surface tension of the pore solution dominates the capillary stress formation. Ma and Ye (2015) showed that the drying shrinkage of AAF pastes was strongly affected by the silica and sodium oxide content. Specimens with a higher sodium and silica content exhibited a larger drying shrinkage. Hence, the increased shrinkage in AAMs with higher activator concentrations can be ascribed to the finer pore structure.

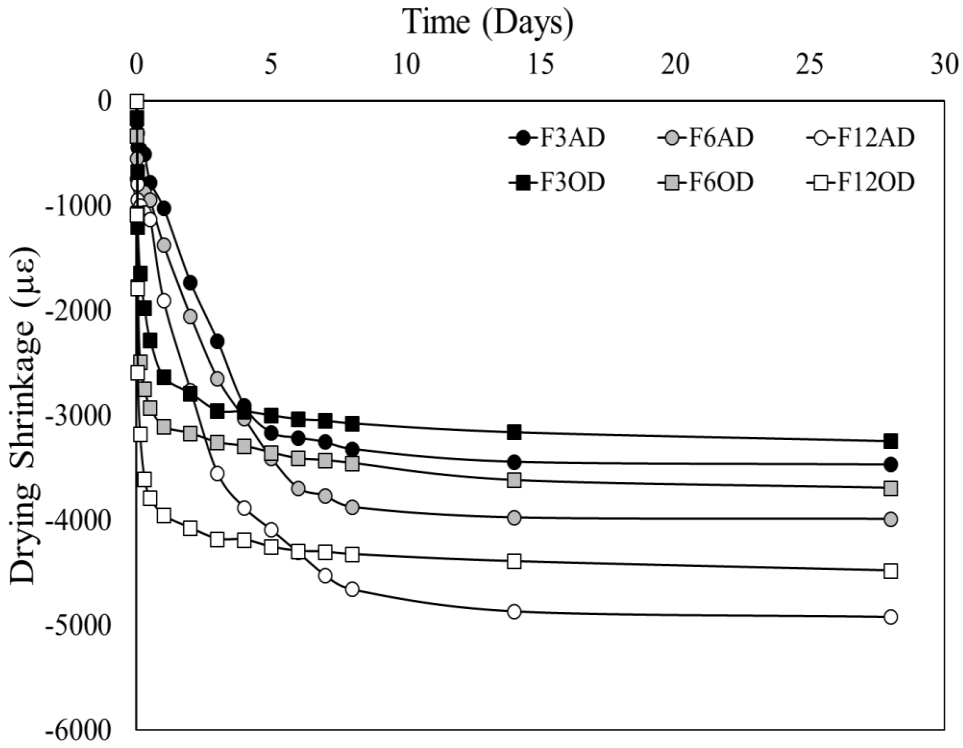

Figure 4.12 Drying shrinkage of AAF mortar specimens (ambient and oven cured).

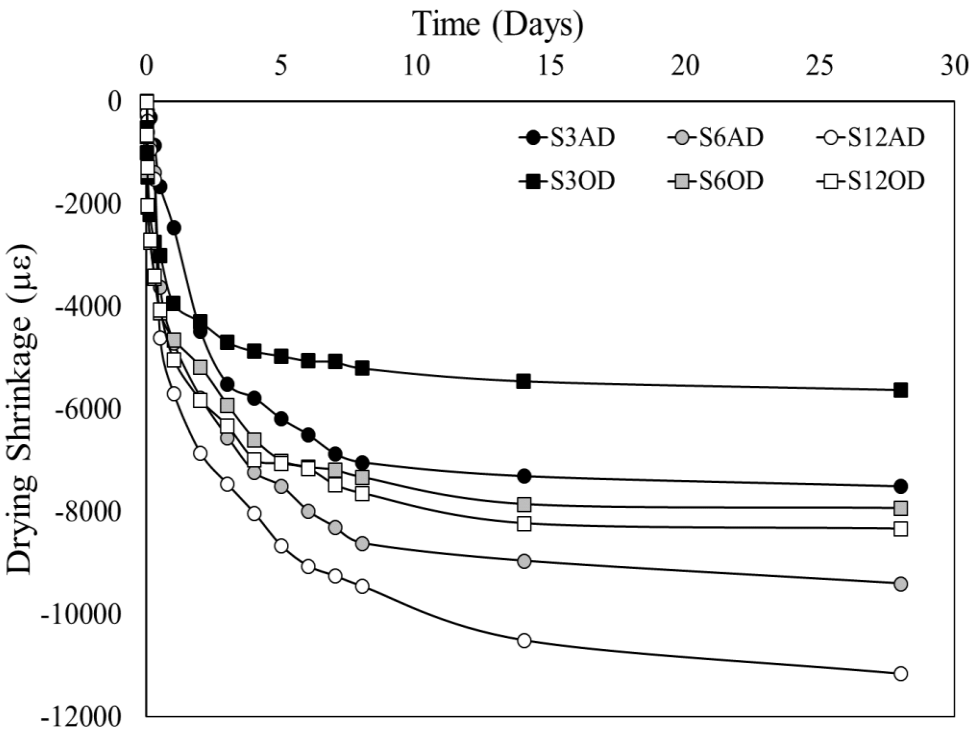

Figure 4.13 Drying shrinkage of AAS mortar specimens (ambient and oven cured).

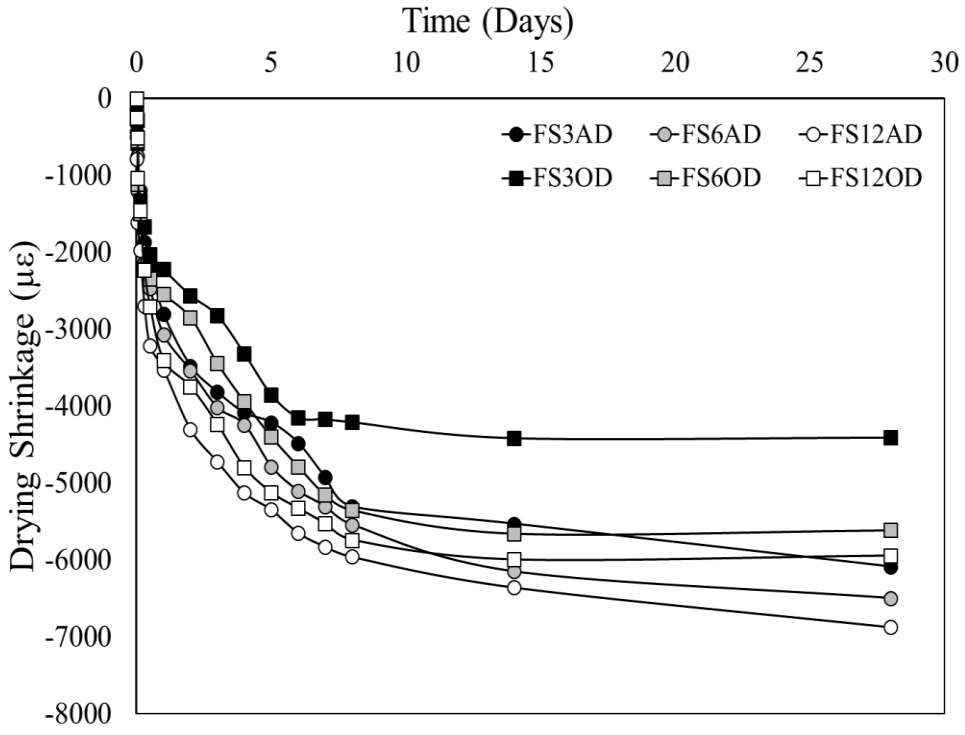

Figure 4.14 Drying shrinkage of AAFS mortar specimens (ambient and oven cured).

4.1.5.2 Effect of precursor type

The effect of precursor type on drying shrinkage of AAMs was investigated. Drying shrinkage strains of different mortar specimens activated with 3M, 6M, and 12M (NaOH) concentrations and cured at ambient temperature are plotted in **Figs. 4.16-4.18**. Results indicated that AAS mortars experienced the highest drying shrinkage values, followed by AAFS and finally, AAF mortars. For instance, at low activator concentration (3M NaOH), the drying shrinkage of ambient cured AAS mortars was 38.5%, and 142% higher than that of AAFS, and AAF mortars, respectively. The corresponding drying shrinkage strains for oven cured AAS was 25.2%, and 71.8% higher than that of AAFS and AAF, respectively. These results are in agreement with the literature (Fernández-Jimenez *et al*., 2006; Chi and Huang, 2013). Around 81-85 % of the total drying shrinkage was observed in the first 7 days. Moreover, a high degree of dimensional stability was achieved in all mortar specimens within around 28 days.

For AAMs activated with high activator concentrations (12M), the drying shrinkage strain of AAS mortar was 61.6%, and 109.3% higher than that experienced by AAFS, and AAF mortars under ambient curing, respectively. The corresponding drying shrinkage for oven cured AAS mortars was 35.8%, and 81.6% higher than that of AAFS and AAF mortars, respectively. These results give an idea of the better dimensional stability of AAF mortar compared to AAS and AAFS mortars. This is due to the spherical shape of FA particles that acted as the micro-aggregate to fill minor voids hence, increasing the volume stability (Rashad, 2013).

Shen *et al.* (2011) activated neat GGBFS blended with FA and activated by waterglass with a SiO_2/Na_2O ratio of 2.4. The addition of FA in replacement ratios of GGBFS lowered the drying shrinkage of AAS paste. These results are in accordance with this study. Other studies had shown the pore structure had a significant effect on the drying shrinkage experienced in AAS concrete (Collins and Sanjayan, 2000).

Moreover, AAS binders are known to have a high percentage of mesopores compared to that of AAF and OPC (Chen and Brouwers, 2007). Consequently, the more refined pores found in AAS resulted in higher capillary stress which in turns significantly increased the drying shrinkage. Moreover, studies had shown that C-A-S-H gel present in AAS binders tend to have a low layer stacking capacity. Therefore, the bond of C-A-S-H can be easily damaged and redistributed upon drying. Hence, the high drying shrinkage of AAS binders can be attributed to the relatively low creep modulus of AAS hydration products (Ye *et al*., 2017; Ye and Radlińska, 2016).

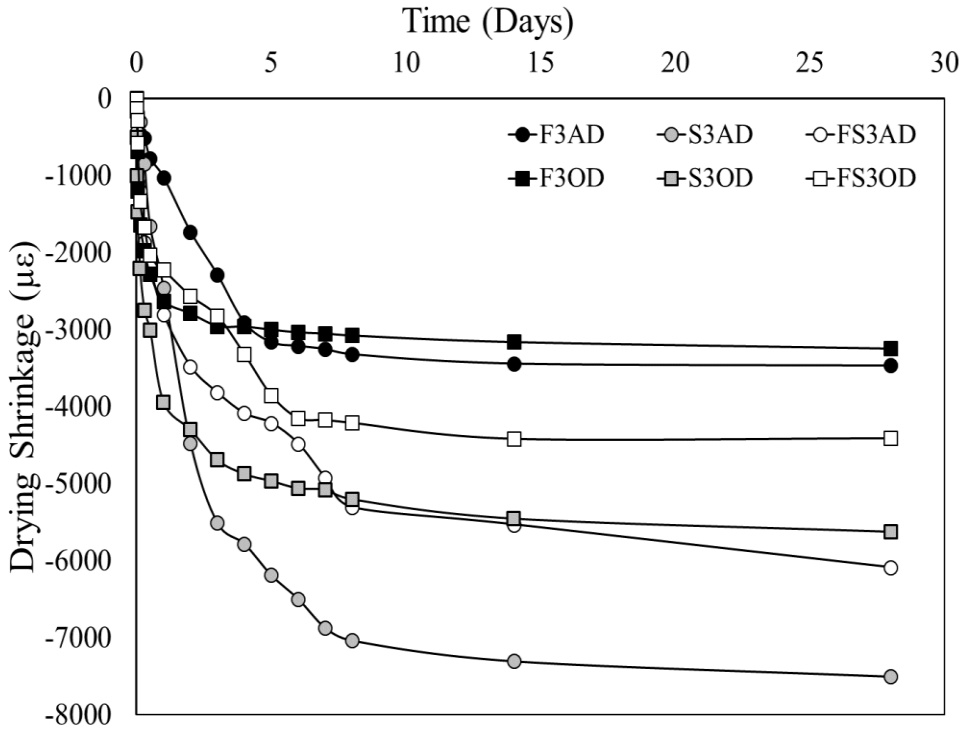

Figure 4.15 Drying shrinkage strains of AAMs activated with 3M NaOH.

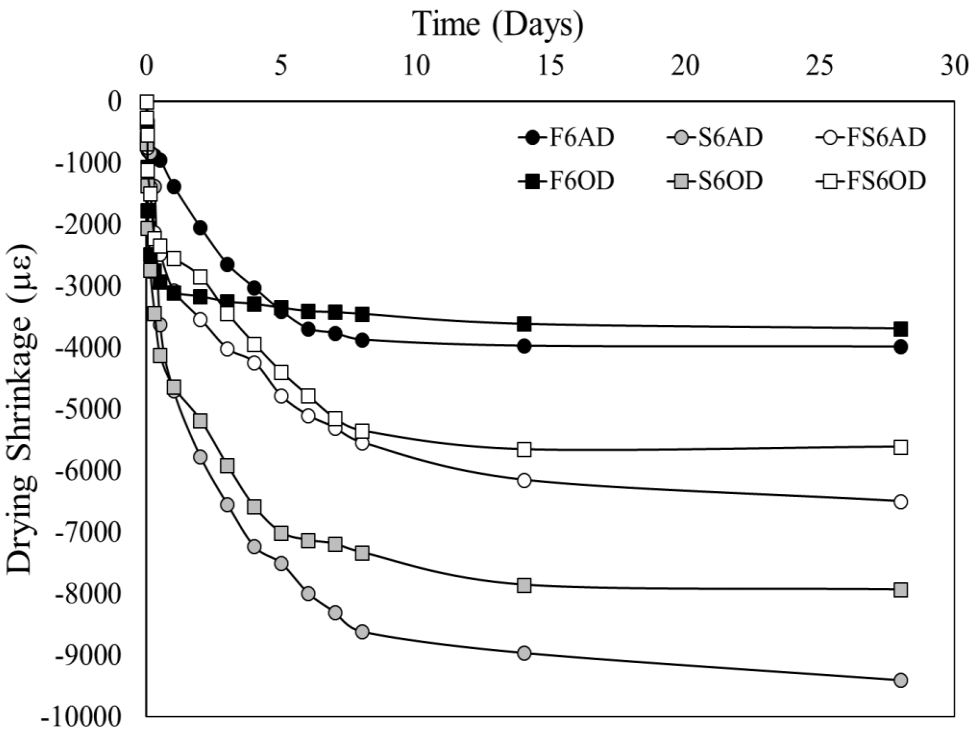

Figure 4.16 Drying shrinkage strains of AAMs activated with 6M NaOH.

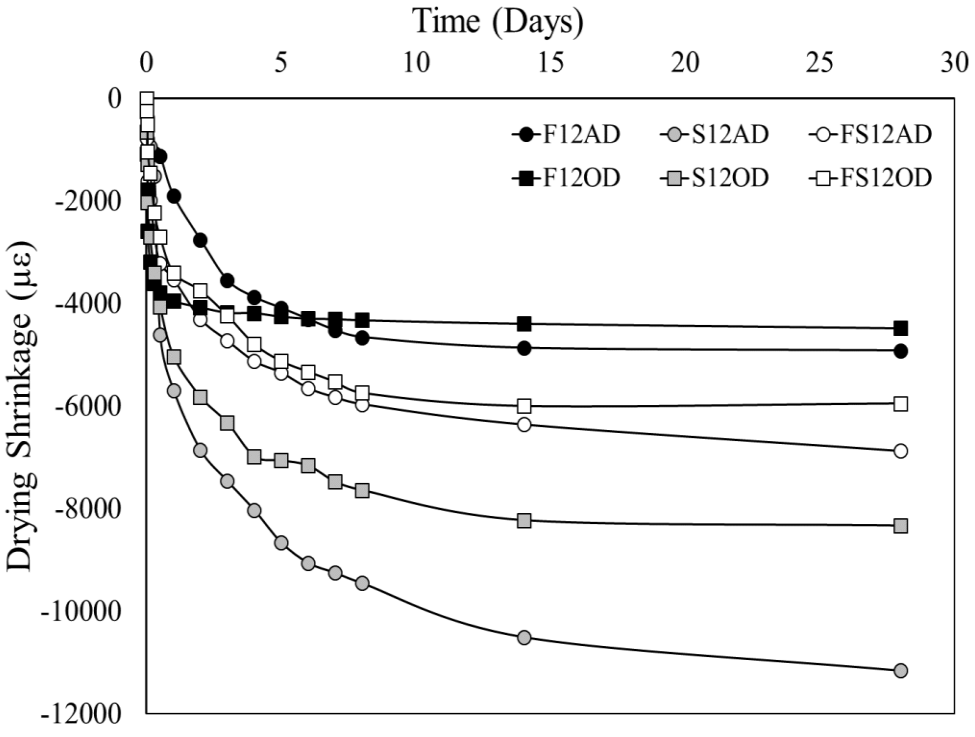

Figure 4.17 Drying shrinkage strains of AAMs activated with 12M NaOH.

4.1.5.3 Effect of curing temperature

One of the major obstacles challenging the implementation of AAMs in the industry is the requirement for a high curing temperature to obtain the expected superior properties over OPC products. Effects of curing conditions on different AAMs at several activator concentrations was studied. Drying shrinkage strains of AAF, AAS, and AAFS mortars cured at both ambient and oven conditions are shown in **Figs. 4.13-4.15**. Generally, the drying shrinkage strains were reduced in all mortar specimens cured in the oven at 60 °C compared to ones cured at ambient temperature (i.e., 23 °C). The amount of reduction in shrinkage had a correlation with both precursor type and activator concentrations. In AAF mortars, the shrinkage of oven cured mortars activated with 3M, 6M, and 12M NaOH concentrations had decreased by around 8.13, 9.10, and 16.83%, compared to that of specimens cured at ambient temperature, respectively. For AAS mortars, the reduction was more pronounced as the final shrinkage strains were reduced by 34.82, 19.56, and 27.47% activated with 3M, 6M, and 12M NaOH concentrations, respectively. AAFS reduction values were in between AAF and AAS mortars achieving 27.93, 9.7, and 12.93% reductions, respectively.

Generally, curing at elevated temperature accelerated hydration making AAMs matrix in much denser and hence increase the rigidity of the solid network (Ma and Ye, 2015). This denser and more rigid matrix exhibits higher resistance to the drying shrinkage. Significant strength development can be expected in AAMs even when heat-cured for shorter durations (Thomas *et al.*, 2017). Furthermore, Bakharev *et al.* (2001) showed that the relatively localized hydration in heat-cured AAS binders resulted in a coarser porosity. Typically, as the porosity increases the resultant capillary pore stresses are reduced. Authors attributed the reduction in drying shrinkage to the change in the pore structure of heat cured AAS binders.

Nevertheless, it is very important to mention that OPC binders are very stable in phase composition and reach that stability fairly early in the curing period. On the other hand, AAMs are

known to change in both compositions and concentrations throughout their curing period (Thomas *et al*., 2017). These changes in phase compositions may also have a significant effect on the final shrinkage. Hence, it is also important to consider the changes in product phase compositions that occur in AAMs with curing and age.

4.1.6 *Mass loss*

4.1.6.1 Effect of mass loss on the drying shrinkage at ambient curing

The effect of mass loss on drying shrinkage is a critical parameter which investigates the reactivity of length change with respect to mass loss due to water loss at ambient curing. **Figure 4.19** shows the mass loss with respect to age of different AAMs activated with 3M, 6M, and 12M NaOH under ambient curing. **Figures 4.20-4.22** show the curves representing the relationship between drying shrinkage and mass loss of AAF, AAS, and AAFS mortars, where the abscissa is mass loss and the ordinate is drying shrinkage. The slope of the curves represents the length change per unit mass loss. Evaluating the length change per unit mass loss provides tips about the mechanism involved in drying shrinkage changes. Capillary tensile stress and the magnitude of shrinkage resulting from a unit mass loss are functions of pore sizes. Hence, a change in the curve slope suggests a change in pore size. An increase in the slope indicates a finer porosity, while a decrease in slope suggests a coarser porosity.

Figure 4.20 shows the relationship between drying shrinkage and mass loss for AAF mortars activated with 3M, 6M, and 12M NaOH. Regardless of activator concentrations, the slope was similar at early-age for all mixtures. This suggests that the porosity was not affected by the activator concentration at the early age. At the later age, 3M and 6M specimens showed a similar increase trend for up to 0.6% mass loss after which the slope decreased significantly indicating an increase in pore size, although the water loss was not affected. After 0.6% mass loss, the drying shrinkage showed a prolonged increase rate with the increasing mass loss. For 12M AAF mortars,

the shrinkage increase trend continued for up to 1.1% mass loss. This suggests that at later age, the drying shrinkage is not affected by the increased mass loss. The very low reduction in mass loss suggests only a minor decrease in porosity. Ma *et al.* (2013) indicated that the porosity of AAF mortars is reduced with age and heat curing. Thomas *et al.* (2017) found that the AAF mortars showed surface micro-cracking, especially when heat cured. Mass loss from micro-cracking would not generate enough capillary stress to increase drying shrinkage. Hence, the reduced slope in AAF mortars at later age may be a result of surface micro-cracks.

Figure 4.21 shows the relationship between drying shrinkage and mass loss of AAS mortars activated with 3M, 6M, and 12M NaOH. Regardless of activator content, the slope changes were similar throughout the test period. At the early age, the shrinkage increase trend was stable up to about 0.5% mass loss. After 0.5% mass loss, the slope increased significantly for up to 1% mass loss suggesting a decrease in pore size. After 1% mass loss, the drying shrinkage increase rate was reduced, hence, gradually reducing the slope. It is well known that the porosity of AAS mortars is normally lower than that of AAF mortars (Thomas *et al.*, 2017). This might be the reason for the observed increase of drying shrinkage per unit mass loss.

Figure 4.22 shows the relationship between drying shrinkage and mass loss for AAFS mortars activated with 3M, 6M, and 12M NaOH. Regardless of activator content, the slope changes were similar throughout the test period. At the early age, specimens showed a very high shrinkage increase trend with a minimal mass loss. The slope was decreased significantly after that indicating a coarser porosity, although the water loss was not affected. At the later age, the slope slightly increased till the end of the test period. The drying shrinkage of AAFS mortars seems to be more sensitive to mass loss than any of the other mortars.

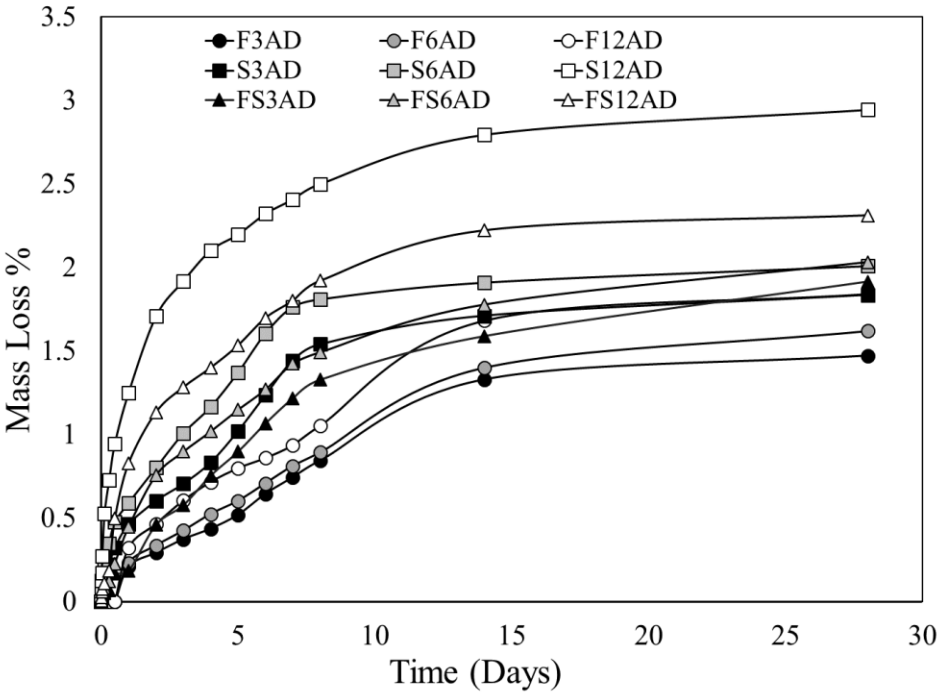

Figure 4.18 Mass loss with age of different AAMs at ambient curing.

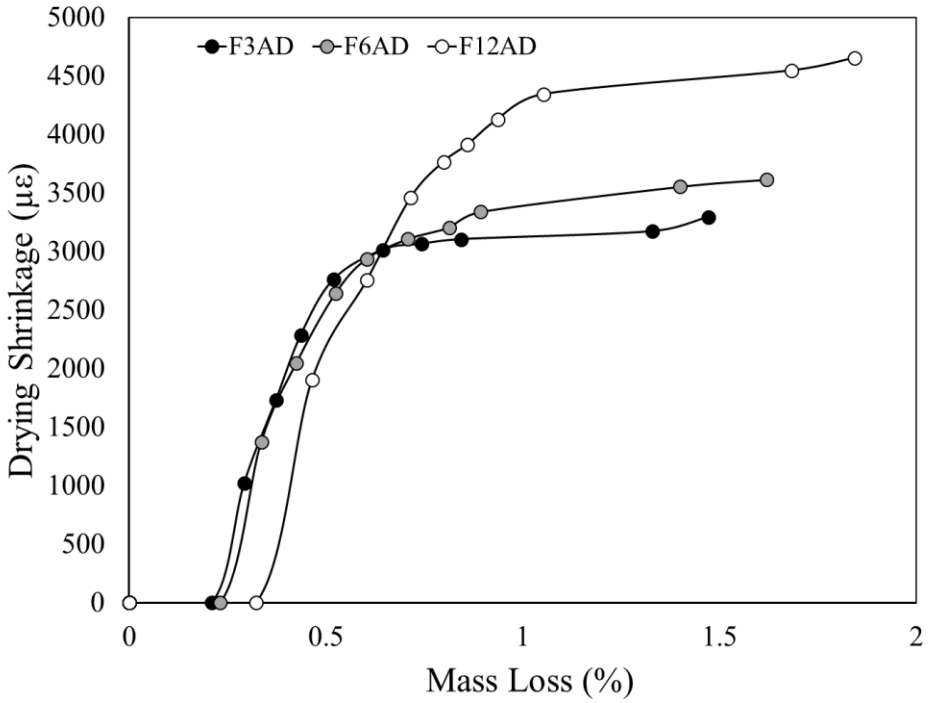

Figure 4.19 Mass loss vs. drying shrinkage of AAF mortars at ambient curing.

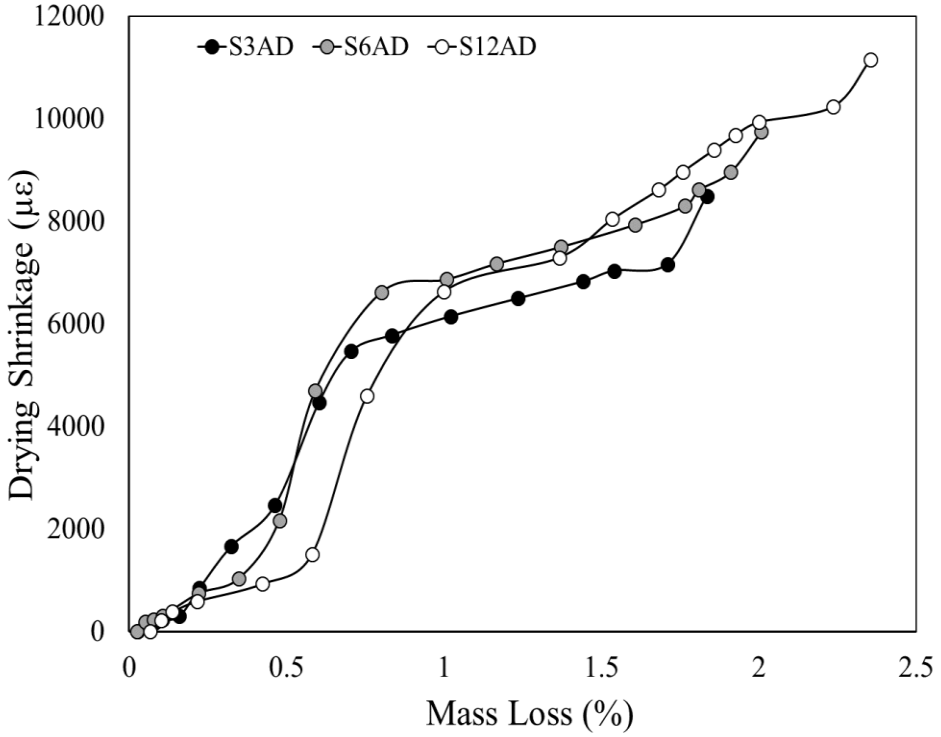

Figure 4.20 Mass loss vs. drying shrinkage of AAS mortars at ambient curing.

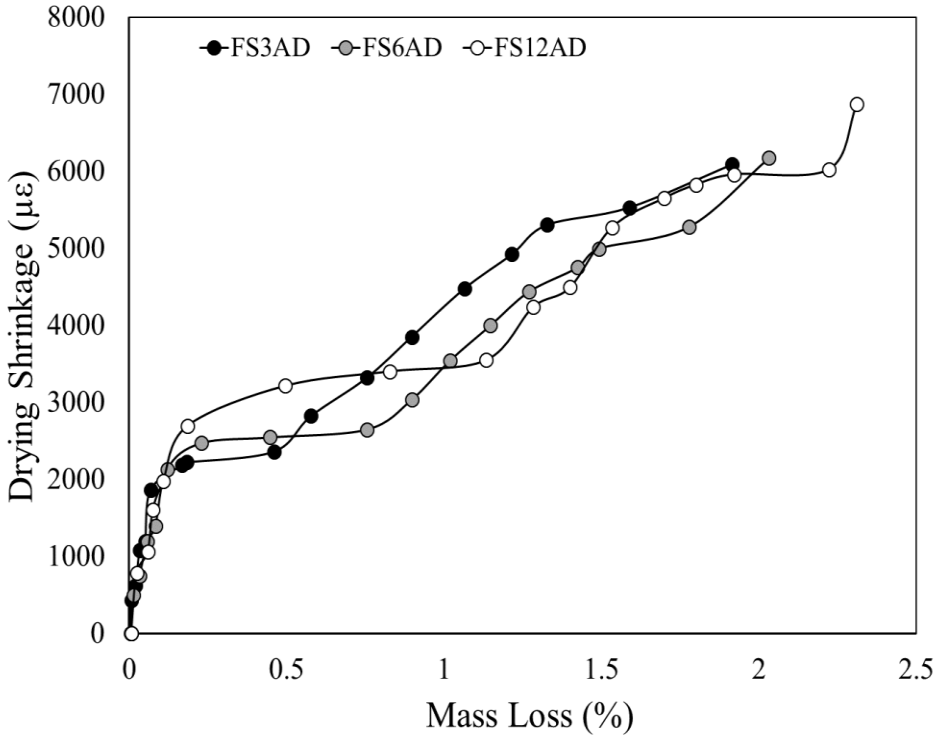

Figure 4.21 Mass loss vs. drying shrinkage of AAFS mortars at ambient curing.

4.1.6.2 Effect of mass loss on the drying shrinkage at oven curing

The effect of mass loss on drying shrinkage of oven cured AAMs was studied. Mass loss occurs more rapidly due to low humidity (lower than 100%) and the higher curing temperatures compared to normal curing temperatures. **Figure 4.23** shows the mass loss with respect to age of different AAMs activated with 3M, 6M, and 12M NaOH under oven curing. **Figure 4.24** represents the relationship between drying shrinkage to mass loss AAF mortars oven cured and activated with 3M, 6M, and 12M NaOH. Generally, the rate of shrinkage at the early age was very high in oven cured specimens compared to ambient cured ones. AAF mortars activated with 6M induced a very steep continuous slope at the early age, suggesting a very fine porosity. The slope was significantly reduced afterward, decreasing the length change per unit mass loss up to the end of the test period. On the other hand, AAF mortars activated with 3M NaOH showed a less steep curve slope compared to 6M activated specimens. However, the slope curve was still relatively high clearly showing the finer porosity. The slope was reduced after around 2% mass loss suggesting an increase in porosity with age and kept steady afterward for up to final test age. AAF mortars activated with 12M showed the lowest slope gradient. The slope was approximately steady and constant throughout the test period indicating minimal changes in porosity and mesoporous volume with age and heat curing.

Figure 4.25 represents the relationship between drying shrinkage to mass loss in AAS mortars oven cured and activated with 3M, 6M, and 12M NaOH. It was observed that AAS mortars followed a steady increase in length change per unit mass loss suggesting a uniform pore size that was barely affected by activator concentration, heat curing, or curing age. The pore size distribution in AAS mortars under oven curing shows that the fine pores were not affected by the increased hydration reaction. This is in contrast with the reported results in AAS mortars ambient

cured. However, 3M specimens showed a minimal slope gradient reduction after 4% mass loss, suggesting a slight increase in porosity.

Figure 4.26 represents the relation of drying shrinkage to mass loss in AAFS mortars oven cured and activated with 3M, 6M, and 12M NaOH. Drying shrinkage per unit mass loss seems to follow a uniform slope similar to the one found in AAFS. The addition of 50% GGBFS in AAFS mortars is clearly dominating the pore size distribution. However, a slight increase in slope gradient can be seen in AAFS mortars activated with 3M NaOH after 1.2% mass loss. This increased slope gradient kept constant up to 3% mass loss and was reduced back after that, suggesting minimal changes in porosity with age and heat curing in 3M NaOH AAFS mortars. At final test age, the shrinkage in all AAFS mortars had almost reached its ultimate values and was not affected by the further minimal increase in mass loss.

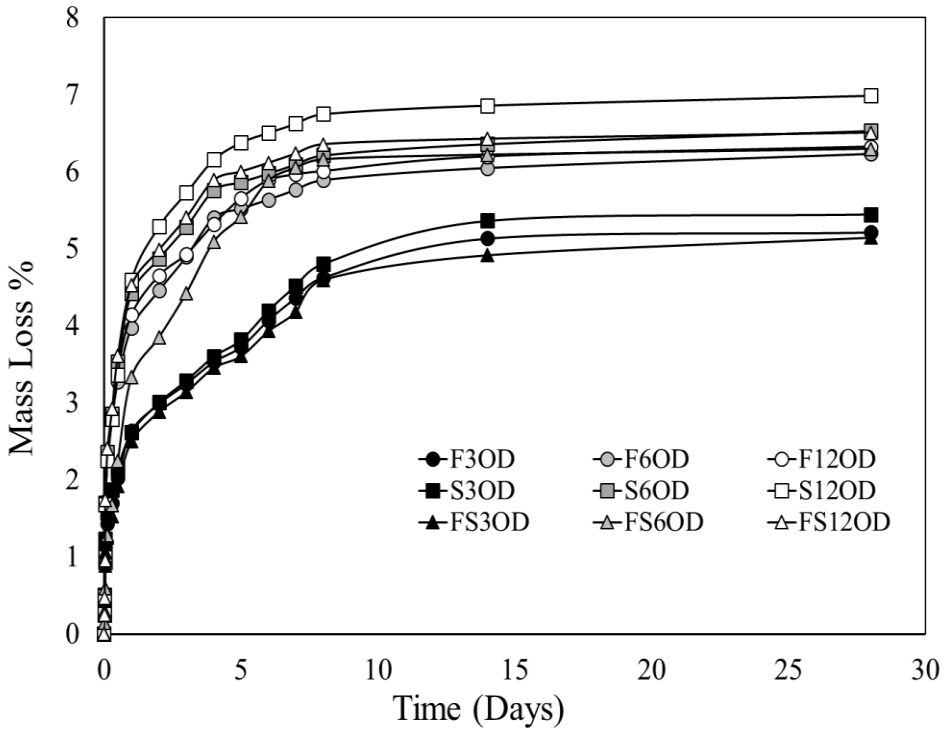

Figure 4.22 Mass loss with age of different AAMs at oven curing.

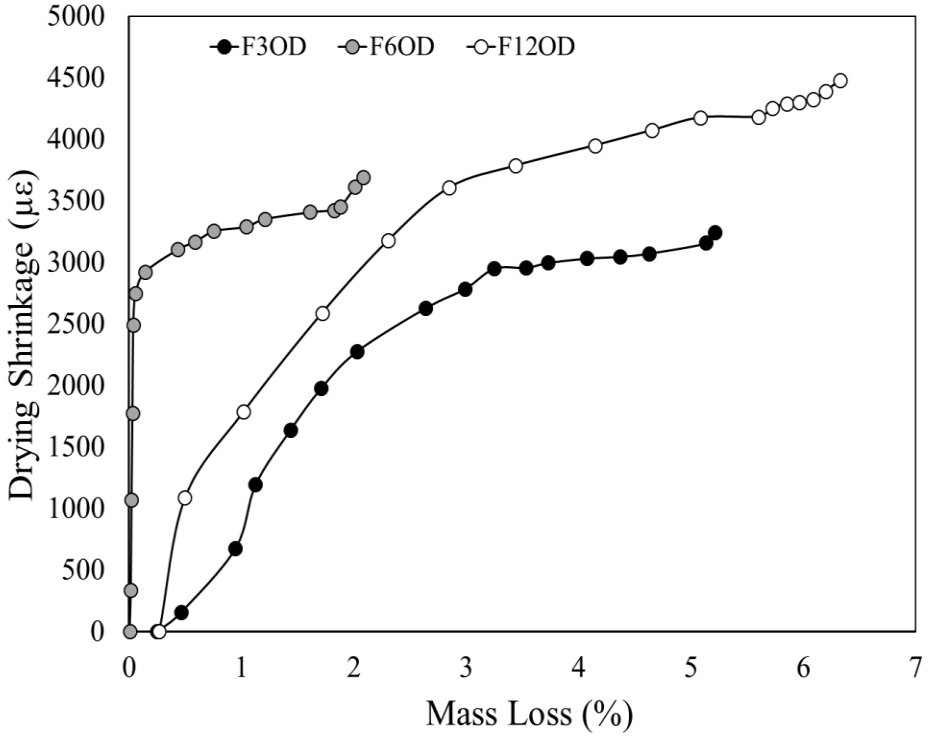

Figure 4.23 Mass loss vs. drying shrinkage of AAF mortars at oven curing.

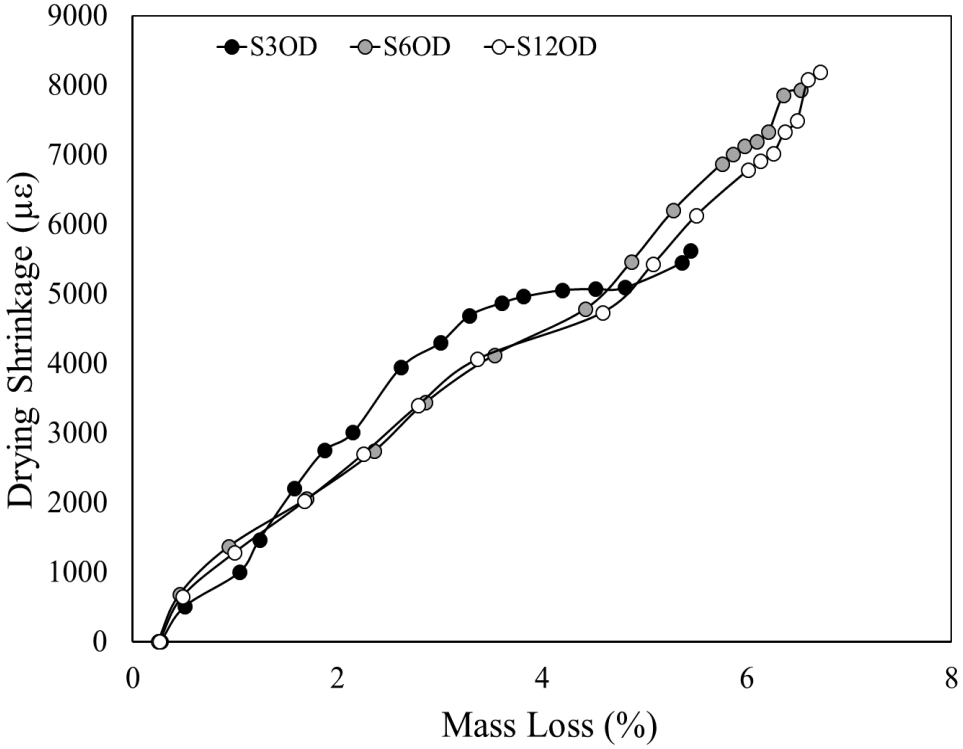

Figure 4.24 Mass loss vs. drying shrinkage of AAS mortars at oven curing.

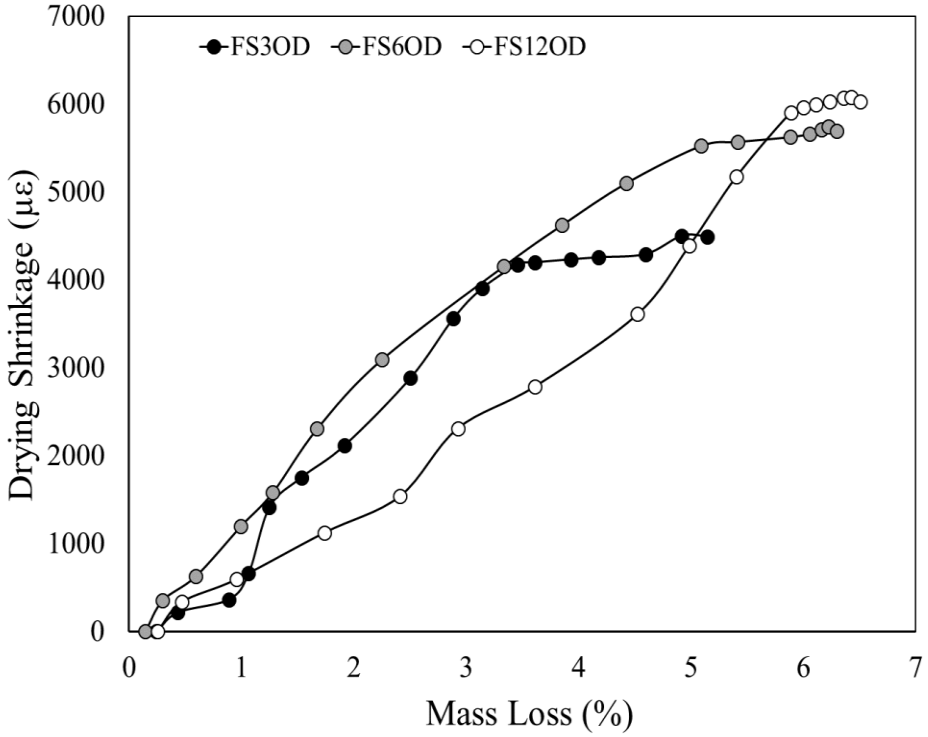

Figure 4.25 Mass loss vs. drying shrinkage of AAFS mortars at oven curing.

4.1.7 *Autogenous Shrinkage*

4.1.7.1 Effect of activator concentration

Autogenous shrinkage is caused by self-desiccation as explained previously. The autogenous shrinkage strains of AAF, AAS, and AAFS mortars activated with different (NaOH) concentrations and cured at ambient and oven temperatures are plotted in **Figs. 4.27-4.29**. Generally, autogenous shrinkage rates and strains of AAM specimens increased as activator concentrations increased. For instance, the autogenous shrinkage strain experienced by 12M NaOH activated AAF mortars was 9.3%, and 19.3% more than that of mortars activated by 6M, and 3M NaOH under ambient curing, respectively. The corresponding autogenous shrinkage strain under oven curing was also 28.5%, and 55.7% higher, respectively. About 85-90 % of the total shrinkage was observed in the first 7 days depending on the activator concentration.

The increase in autogenous shrinkage due to higher activator concentrations was more pronounced in AAS mortars compared to AAF mortars under both curing conditions. For instance, the magnitude of autogenous shrinkage was 9.1%, and 15.5% higher in AAF and AAS mortars under ambient curing, respectively when activator concentration increased from 3M to 6M. At oven curing condition, the increase in autogenous shrinkage strain under oven curing was 10.8% and 21.6%, respectively. The increase in autogenous shrinkage due to higher activator concentrations was relatively higher under oven curing temperature. Autogenous shrinkage strains for AAFS mortars was in between those of AAF and AAS mortars. Shrinkage values of AAFS mortars were theoretically fit because the addition of 50% FA as a replacement of GGBFS binder is expected to decrease the overall autogenous shrinkage of AAS mortars.

Increasing NaOH concentration reduces the total porosity and increases mesoporous volume, which is directly related to self-desiccation. Moreover, a portion of autogenous shrinkage is related to chemical shrinkage (Neto *et al.*, 2008). Hence, the increase in the degree of hydration due to higher NaOH concentrations also contribute to the total measured shrinkage. This was confirmed by the thermogravimetric analysis performed by Neto *et al.* (2008). Considering the aforementioned results, it can be concluded that the higher autogenous shrinkage found in AAMs activated with high NaOH concentrations occurred mainly due to both the increased self-desiccation in the hardened state and the increased volume contractions by chemical shrinkage in the fresh state.

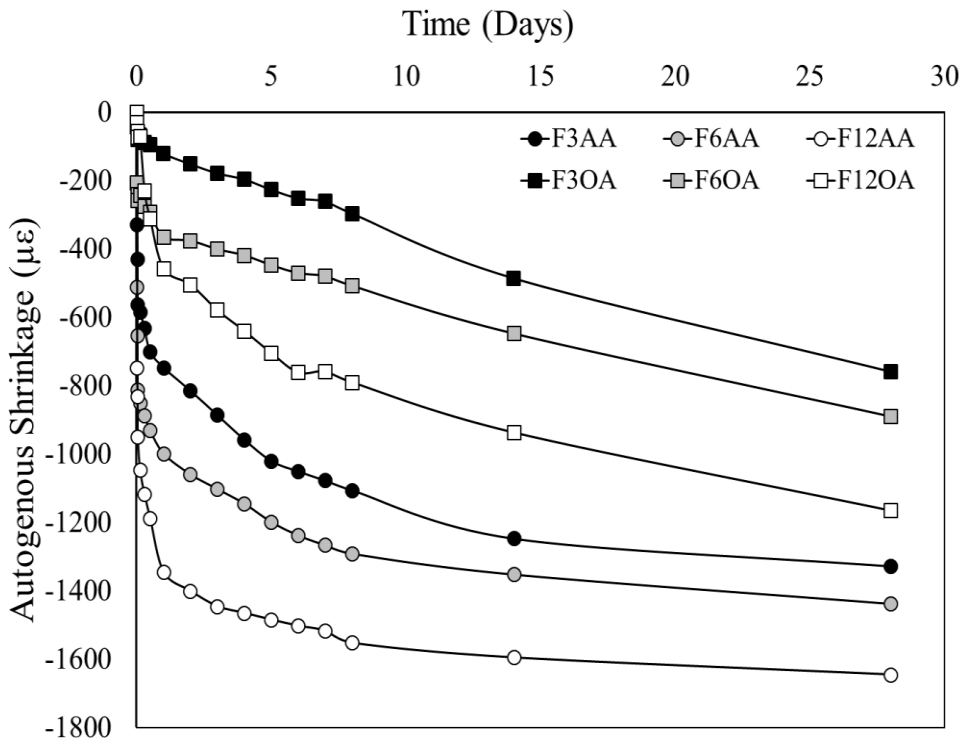

Figure 4.26 Autogenous shrinkage of AAF mortars (ambient and oven cured).

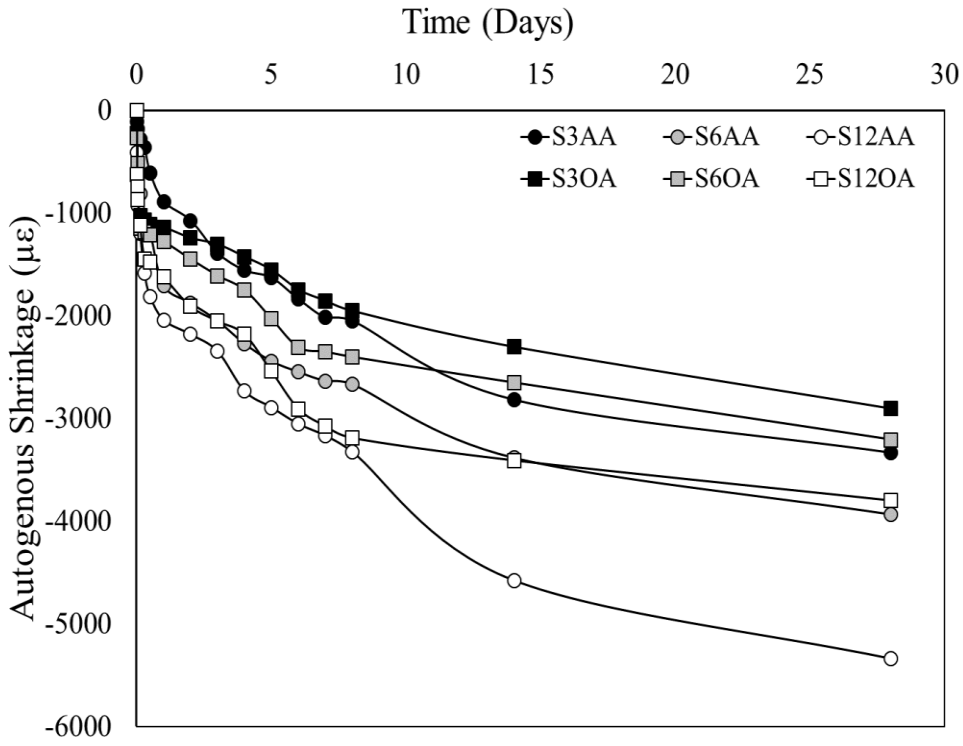

Figure 4.27 Autogenous shrinkage of AAS mortars (ambient and oven cured).

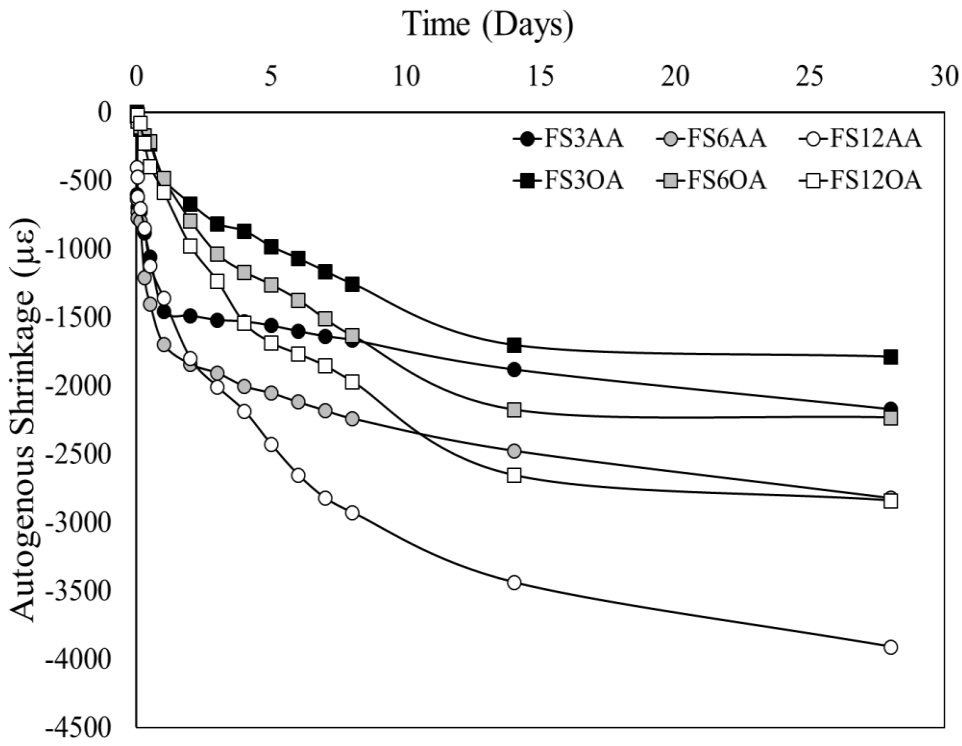

Figure 4.28 Autogenous shrinkage of AAFS mortar specimens (ambient and oven cured).

4.1.7.2 Effect of precursor type

Autogenous shrinkage strains for different mortar specimens activated with 3M, 6M, and 12M (NaOH) concentrations and cured at ambient temperature are plotted in **Figs. 4.30-4.32**. Generally, AAS mortars experienced the highest autogenous shrinkage strains followed by AAFS, and finally, AAF mortars. For example, the autogenous shrinkage strain of ambient cured AAS mortar was 56%, and 144% higher than those of AAFS, and AAF mortars activated with low activator concentrations (3M NaOH), respectively. At oven curing condition, the increase in autogenous shrinkage strains was 25.2%, and 71.8% higher, respectively. For AAMs activated with high activator concentrations (12M), the drying shrinkage strain of AAS mortar was 35.4%, and 217% higher than those experienced by AAFS, and AAF mortars under ambient curing, respectively. The corresponding drying shrinkage under oven curing was 63%, and 275% higher, respectively.

These results give an idea of the much better dimensional stability of AAF mortar compared to AAS and AAFS mortars.

In AAF and AAFS mortars, about 85% of the final shrinkage was experienced within 7 days regardless of activator concentrations, achieving a high degree of dimensional stability afterward. While, in AAS mortars only 60% of final shrinkage was experienced in 7 days, and a high degree of dimensional stability was experienced in 14 days. Generally, AAF and AAS mortars experienced higher autogenous shrinkage compared to that of the OPC mortar (Lee *et al.*, 2014). The following will state some unique characteristics of FA and GGBFS that could account for these results. Fly ash particles have a unique spherical profile, which retains less water compared to GGBFS particles meaning more free water for hydration, thus lower self-desiccation and consequently lower autogenous shrinkage (Tongaroonsri, 2009). Conversely, GGBFS has a strong and rapid pozzolanic action that accelerates the hydration process leading to a dense microstructure and consequently a substantial autogenous shrinkage (Zhao *et al.*, 2017). As the binder hydrates, hydration products form around the binder particles and fill up the water-filled spaces between solid particles. The water in the small capillaries begins exerting hydrostatic tension. As a result, this capillary pressure reduces the distance between the solid mortar particles, forcing mortar to shrink (Chi and Huang, 2013). Hence, GGBFS increase autogenous shrinkage more significantly than FA in AAMs.

The mesoporous volume of AA pastes which is directly related to self-desiccation was also studied by (Lee *et al.*, 2014). The highest mesoporous volume was found in stated that AAS mixtures followed by AAF and finally OPC mixtures. The mixture of FA and GGBFS compensates certain disadvantages of each other: FA slows down the early strength development of AAM but

adding active GGBFS could solve this problem. The inclusion of FA is expected to reduce autogenous shrinkage of AAS leading to a low early cracking risk (Zhao *et al.*, 2017).

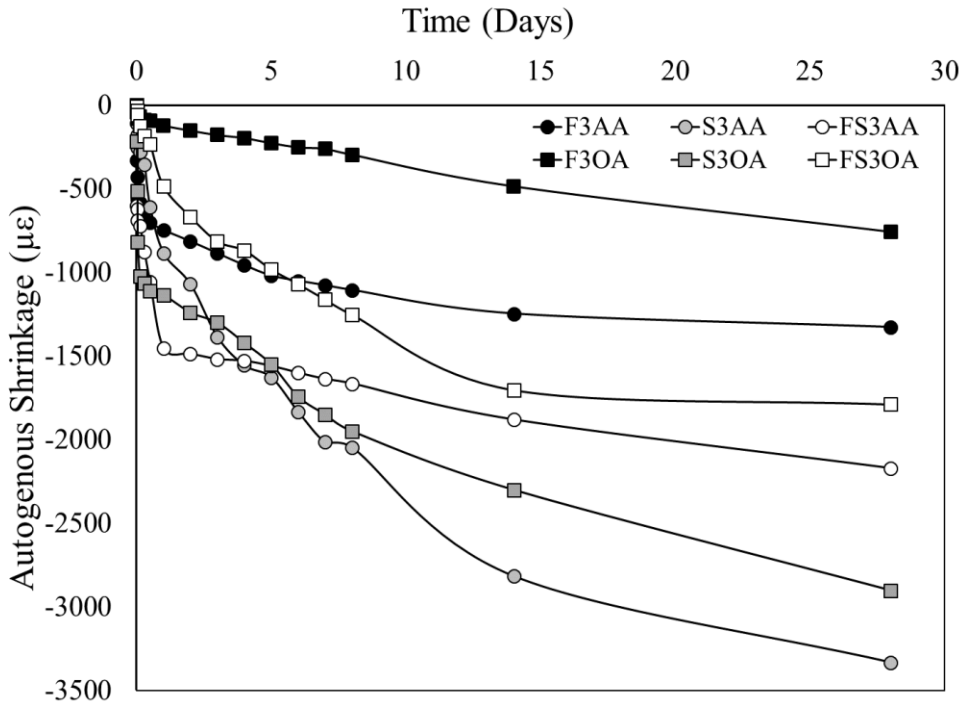

Figure 4.29 Autogenous shrinkage of AAMs activated with 3M NaOH.

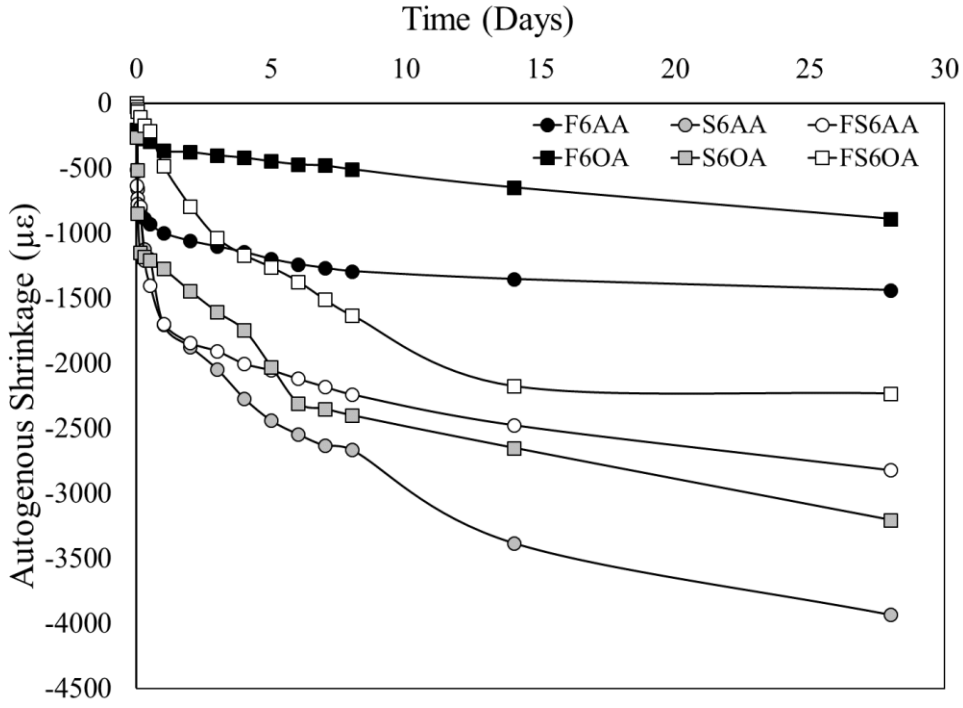

Figure 4.30 Autogenous shrinkage of AAMs activated with 6M NaOH.

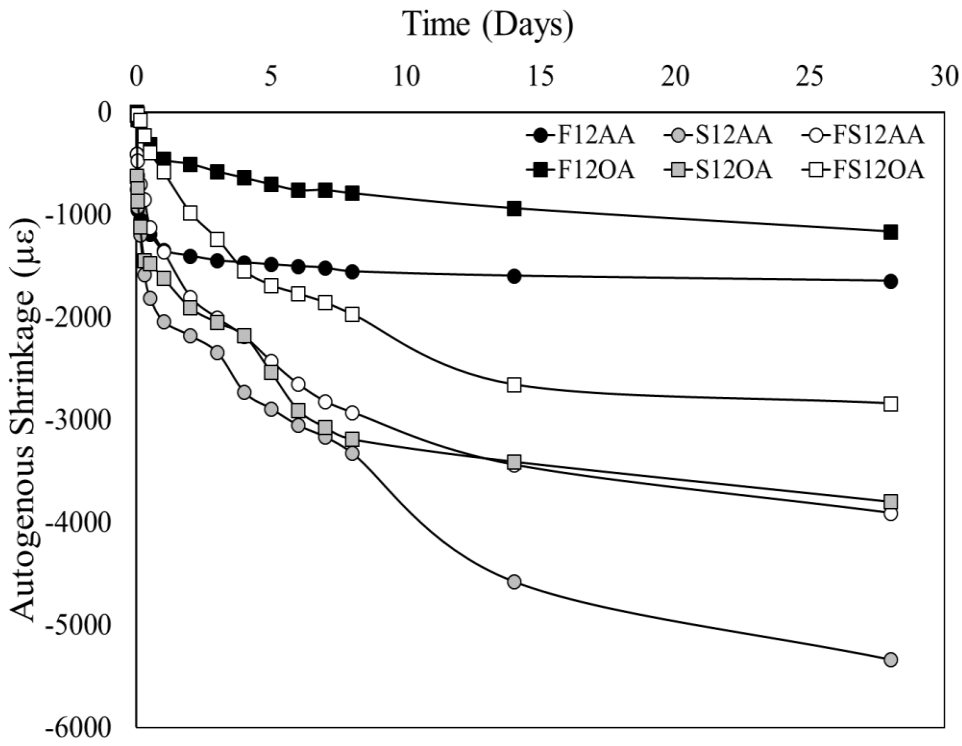

Figure 4.31 Autogenous shrinkage of AAMs activated with 12M NaOH.

4.1.7.3 Effect of curing conditions

Autogenous shrinkage results of AAF, AAS, and AAFS mortars cured at both ambient and oven conditions are shown in **Figs. 4.27-4.29**, respectively. Generally, the autogenous shrinkage strains were reduced in all AAM specimens cured in the oven at 60 °C compared to those cured at ambient temperature. Reduction in autogenous shrinkage strains due to oven curing was slightly more pronounced in AAF mortars and almost equal in AAS and AAFS mortars. For instance, the autogenous shrinkage strains experienced by 3M, 6M, and 12M NaOH activated AAF mortars were reduced by around 46.4, 40.5, and 30% when oven curing is adopted, respectively. The corresponding reductions in AAS mortars were 17.24, 20.58, and 30%, respectively and in AAFS mortars 20.74, 24.8, and 30%, respectively compared to ambient cured specimens. Reductions had increased as NaOH concentrations increased for both AAS and AAFS mortars.

Generally, at higher temperatures curing conditions, the hydration rate and the refinement of pore structure is accelerated. Hence, significant strength development is expected to rise in oven cured specimens providing a much denser matrix and increasing the rigidity of the solid network (Ma and Ye, 2015). Therefore, this higher strength development is expected to mitigate or reduce the maximum shrinkage observed in AAM cured at ambient temperature. All shrinkage results were in accordance with the above argument. However, the influence of higher NaOH concentrations on the shrinkage reductions due to oven curing is not very clear. The autogenous shrinkage of AAMs has been previously reported to be larger than the one found in OPC mortars (Cartwright *et al.*, 2014). In this work, the autogenous shrinkage strains observed in AAMs were significantly higher than the ones experienced by OPC mortars, especially in AAS mortars.

4.1.8 *Conclusion*

In this phase, different properties for two-part alkali activated mortars were investigated including, fresh and hardened properties along with associated shrinkage. The following conclusion can be drawn:

1- Activators with high concentrations possess high viscosity leading to a reduction in the AAM flowability. Reduction in AAM flowability will depend on the physical properties of the precursor. The higher the activator concentrations, the shorter the setting time as a result of accelerating hydration and polymerization reactions.

2- Activator concentration and curing temperature have a significant effect on hydration progress in AAMs regardless of the precursor type. Strength of AAMs depends proportion to added activator concentration at all ages regardless of precursor type.

3- Shrinkage behaviour of AAMs depends on pore size and the stiffness of the microstructure. Pore size distribution is highly affected by precursor type and activator concentration.

4.2 Phase 2: Evaluation for Shrinkage Behaviour of One Part Alkali-Activated Mortars

4.2.1 *Flowability*

Variations in workability for different AAM mixtures with respect to activator type and dosage are presented in **Table 4.2**. Generally, the flow values of AAF mortar mixtures was the highest followed by AAFS, and finally, AAS mortar mixtures regardless of the activator type. For instance, the flowability of AAF mortars activated with 5% $Ca(OH)_2$ was approximately 7.14%, and 12.2% higher than that of the corresponding AAS and AAFA mortars, respectively. AAF mortars flow exceeded the flow table diameter indicating high flow values above 30 cm. These findings support the previous argument regarding the effect of FA particle's spherical shape on the flow of AAF mortars (Umniati *et al.*, 2017; Fernández-Jimenez *et al*., 2006). On the other hand, the flowability of AAS mortars is dominantly affected by the rapid reaction between GGBFS and the alkali activator (Jang *et al*., 2014). $NaHCO_3$ activated mortars showed a slightly higher flowability compared to that of mixtures activated with $Ca(OH)_2$. For instance, the flowability of $NaHCO_3$ AAS mortars was around 5% higher than that of $Ca(OH)_2$ activated ones at 5% activator dosage.

The flow of AAM mixtures slightly decreased as the activator dosage increased regardless of activator type. For example, the flowability of AAS mortars activated with 15% $NaHCO_3$ was 3%, and 5% lower than that of AAS mortars activated with 10%, and 5% $NaHCO_3$, respectively. This can be attributed to the increase in solid and fine materials leading to less free water. This is in agreement with the previous study done by (Nematollahi *et al.*, 2015) on sodium silicate one-part AAMs.

It is clear that the effect of activator percentage on flow values at a specific binder type is little. This is in converse to the previously reported results in two-part AAM mixtures, as the

impact of alkaline activator concentration on the flowability of those mixtures was much more significant. Nevertheless, the recorded flow values of one-part AAM mixtures were higher than those previously reported for two-part AAMs mixtures. This behaviour can be attributed to the much lower viscosity of the water compared to the Na_2SiO_3-NaOH solution used in two-part AAMs. It was reported that fly ash and blast furnace slag one-part AA materials tend to have a thixotropic behaviour, that is, good workability during mixing and vibration (Nematollahi *et al.*, 2017). Authors observed that one-part AA pastes were still workable/flowable into molds for more than an hour after the addition of water.

Table 4.2 Setting times and flow of AAM mixtures.

Mixture	Setting time (min)		Flow (cm)
	Initial	Final	
FL5	292	462	>120
FL10	274	436	>120
FL15	255	409	>120
SL5	160	286	107
SL10	145	261	105
SL15	130	238	102
FSL5	230	362	112
FSL10	218	344	112
FSL15	205	317	110
FN5	282	452	>120
FN10	268	441	>120
FN15	260	420	>120
SN5	172	283	112
SN10	165	269	108
SN15	152	244	106
FSN5	231	365	120
FSN10	218	347	116
FSN15	202	318	114

4.2.2 *Setting time*

The initial and final setting times of AAM mixtures activated with $Ca(OH)_2$ and $NaHCO_3$ are given in **Table 4.2**. In general, initial and final setting times of AAM mixtures were retarded with higher activator dosage. For example, the initial setting time of FL15 mixture was retarded by 19, and 37 minutes compared to that of FL10 and FL5 mixtures, respectively. Moreover, the corresponding retardation in final setting times was 37, and 53 minutes, respectively. $Ca(OH)_2$ activated mixtures tend to set slightly faster than $NaHCO_3$ activated ones in both initial, and final setting phases. For instance, SL5 mixtures approached the initial, and final setting phases 12, and 3 minutes earlier than SN5 mixtures, respectively. Generally, AAS mortars achieved the shortest initial and final setting times followed by AAFS, and finally, AAF mortars. For example, the initial setting was achieved 59, and 110 minutes earlier in SN5 compared to FSN5, and FN5 mixtures, respectively. This faster setting behaviour in GGBFS based mixtures can be attributed to the high CaO content in slag, which in turn increases the hydration reaction rate hence, causing a rapid set as explained in the previous phase.

It is worth mentioning that the previously reported setting behaviour of two-part AAM mixtures in phase 1 **(sec 4.1.2)** was much quicker compared to one-part AAMs mixtures studied in this phase. For instance, the initial setting times of FL5 and FN5 mixtures were retarded by about 138, and 148 minutes compared to 3M Na_2SiO_3-NaOH activated ones, respectively. Furthermore, the corresponding final setting times were retarded by around 176, and 165 minutes, respectively. Generally, the retardation of setting time was the highest in AAS mortars followed by AAFS, and finally, AAF mortar mixtures compared to the corresponding two-part AAM mixtures. These results clearly show that a much faster hydration reaction occurs in Na_2SiO_3-NaOH activated mixtures (two-part AAMs) compared to $Ca(OH)_2$ and $NaHCO_3$ activated mixtures (one-part AAM mixtures). AAS mortars hardened slower when solid activator is used compared

to liquid activators (Yang *et al.*, 2008). Nematollahi *et al.* (2015) reported that the setting time extended when the GGBFS content in a one-part AAM mixture containing fly ash was decreased. The previous arguments were in accordance with the reported setting times in this phase. Unlike two-part AAMs, it should be noted that, to the best of the author knowledge, there are no publications available about the effect of retardants on the setting time of one-part AA materials. This point can be investigated in the future to control the setting time.

4.2.3 *Compressive strength*

4.2.3.1 Effect of activator type and dosage

The compressive strength development of AAM specimens activated with $Ca(OH)_2$ and $NaHCO_3$ at different dosages and cured at both ambient and oven conditions was investigated. **Figure 4.32** shows the compressive strength of AAF mortars activated with both activators. Generally, $NaHCO_3$ activated fly ash mortars achieved a significantly higher 28 days compressive strength compared to $Ca(OH)_2$ activated ones. For instance, the 28 days compressive strength values of 15% $NaHCO_3$ activated fly ash mortars were 80.7% and 18.5% higher than the 15% $Ca(OH)_2$ activated ones under ambient and oven conditions, respectively. The compressive strength of AAF mortars increased as the activator dosage increased under both curing conditions. For instance, as $Ca(OH)_2$ dosage increased from 5% to 10% and 15%, the 28 days compressive strength of ambient cured AAF mortars increased by 39.8%, and 74.1%, respectively. The corresponding compressive strength values of oven cured AAF mortars were increased by 13.4%, and 35.2%, respectively. Similar increase trend at higher activator dosages was observed in $NaHCO_3$ activated fly ash mortars. The effect of activator type and dosage were more pronounced in ambient cured specimens.

However, a very low level of activation was observed in AAF mortar specimens as compressive strength values achieved were relatively very low. AAF mortars specimens activated with 5, 10, and 15% $Ca(OH)_2$ achieved 28 days compressive strength of 0.7-1.25 MPa when cured under ambient condition. The corresponding achieved strength values under oven curing were in the range of 1.7-2.3 MPa suggesting a slightly enhanced activation but were not promising either. Moreover, AAF mortars activated with $NaHCO_3$ achieved approximately similar strength results compared to $Ca(OH)_2$ activated ones, also suggesting a very low level of activation in AAF mortars under both curing conditions. The activation of AAF mortars using $Ca(OH)_2$ or $NaHCO_3$ at the three proposed dosages, was unsuccessful. Yang *et al.* (2008) reported similar results as one-part sodium silicate activated FA mortars did not achieve significant compressive strength at 28 days. SEM analysis carried by authors revealed that AAF mortar's structure contained porous microcracks and amorphous microspheres surrounded by a crust of reaction products. These imperfect microstructures of AAF mortars would be one of the main causes of the poor compressive strength achieved.

Figure 4.33 shows the compressive strength of AAS mortars activated with both activators and cured under ambient and oven temperatures. In general, compressive strength values of AAS mortars increased as activator dosages increased. For instance, the 28 days compressive strength of ambient cured AAS mortars increased by 21.6%, and 37.2%, when $Ca(OH)_2$ dosage increased from 5% to 10% and 15%, respectively. $Ca(OH)_2$ activated slag mortars achieved a slightly higher 28 days compressive strength compared to $NaHCO_3$ activated ones. For instance, the 28 days compressive strength values of 15% $Ca(OH)_2$ activated slag mortars were 26.4%, and 28% higher than that of 15% $NaHCO_3$ activated mortars under ambient and oven conditions, respectively. Typically, higher activator dosages implement an enhanced alkaline environment; hence, the

hydration reaction is expedited and the subsequent formation of sodium aluminosilicate hydrate (N-A-S-H) and calcium aluminosilicate hydrate (C-A-S-H) binder gels is increased (Cho *et al.*, 2017). Therefore, mortar specimens gain stronger microstructure and higher loading resistance.

Figure 4.34 shows the compressive strength of AAFS mortars activated with both activators and cured under ambient and oven temperatures. Similar strength increase trend with higher activator dosages was observed in AAFS mortars. Furthermore, $Ca(OH)_2$ activated FA/slag mortars achieved a higher 28 days compressive strength compared to $NaHCO_3$ activated ones. The activation reaction seems to be influenced by both activator concentration and type. The better strength results observed in $Ca(OH)_2$ activated mortars compared to $NaHCO_3$ activated ones can be attributed to the calcium content in the former which is well known to increase the hydration products and therefore, the strength properties of AAM specimens with the exception of AAF mortars in this case, as the alkali activation of these mortars wasn't successful using both activators. The effect of activator concentration seems to be almost constant under both curing conditions.

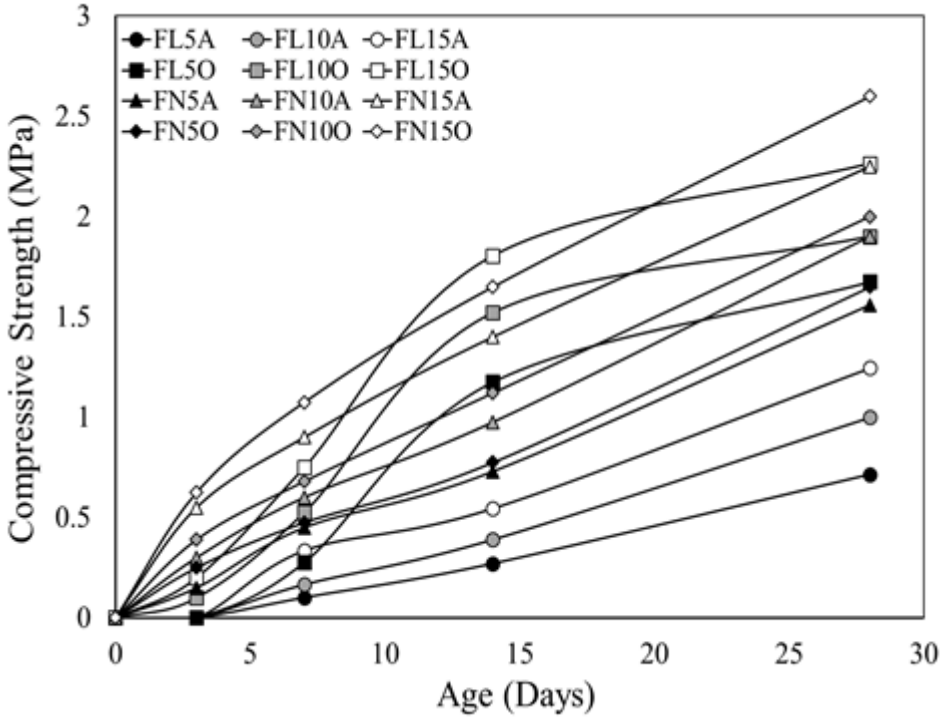

Figure 4.32 Compressive Strength of AAF mortar specimens (ambient and oven cured).

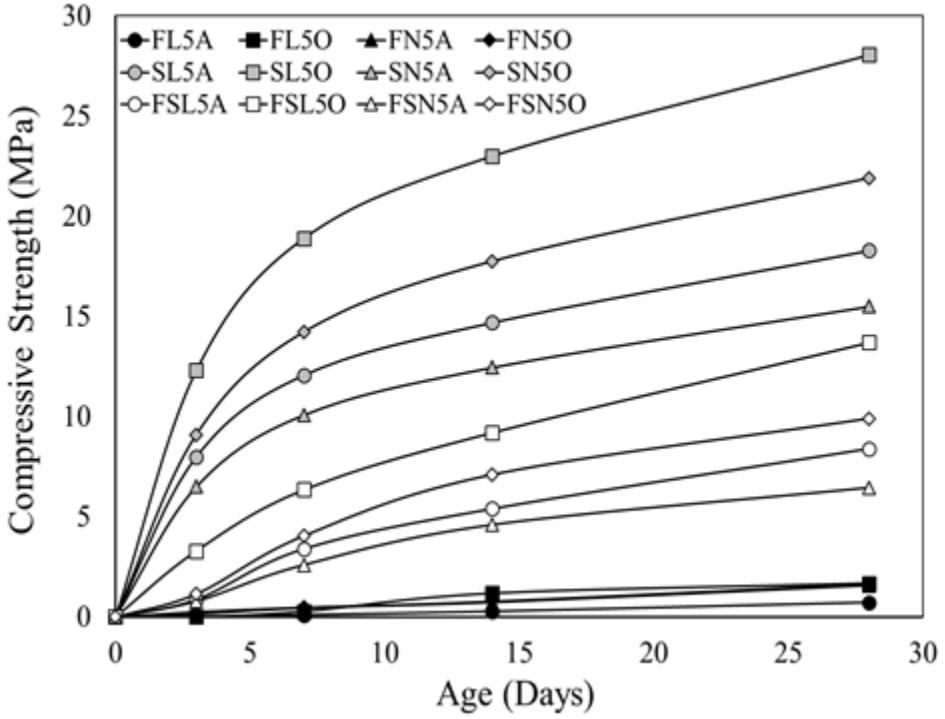

Figure 4.33 Compressive Strength of AAS mortar specimens (ambient and oven cured).

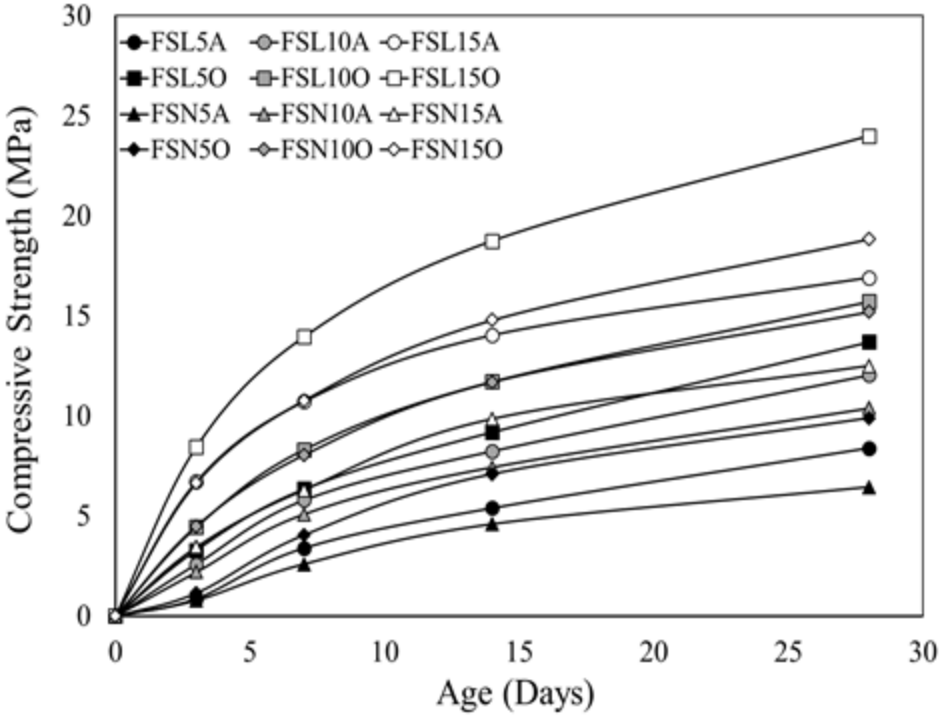

Figure 4.34 Compressive Strength of AAFS mortar specimens (ambient and oven cured).

4.2.3.2 Effect of precursor type and curing condition

The effect of precursor type on compressive strength of AAMs was investigated. Compressive strength values achieved by AAM specimens activated with 5, 10, and 15% $Ca(OH)_2$ or $NaHCO_3$ under both curing conditions are shown in **Figs. 4.35-4.37**. AAM specimens exhibited steady strength improvement between 3 and 28 days. Generally, AAS mortars achieved the highest compressive strength values among all specimens for up to 28 days, followed by AAFS, and finally, AAF mortars. For instance, the 28 days compressive strength of ambient cured AAS mortars was 118%, and 1066% higher than those of AAFS and AAF mortars at low activator dosage of 5% $Ca(OH)_2$, respectively. The corresponding compressive strength of oven cured AAS mortars was 105%, and 1574% higher than those of AAFS and AAF mortars, respectively. A similar trend was observed in $NaHCO_3$ activated mortars. The effect of precursor type was almost similar under both curing conditions excluding AAF mortars. The very high difference between

AAF mortar strength and other AAMs specimens is due to the failure of fly ash activation with both types of activators used.

Furthermore, at a high activator concentration dosage (15% $Ca(OH)_2$), the 28 days compressive strength of ambient cured AAS mortars was 78%, and 1033% higher than those of AAFS and AAF mortars, respectively. The corresponding compressive strength of oven cured AAS mortars was 63%, and 1624% higher than those of AAFS and AAF mortars, respectively. A similar trend was observed in $NaHCO_3$ activated mortars. The effect of precursor type on the compressive strength of AAM specimens was not significantly influenced by the activator concentrations or the curing condition. Two different types of binder gel structures form in AAS and AAF mortars: C-A-S-H (calcium silicate hydrate gel), which is formed mainly in the AAS, and N-A-S-H (sodium aluminosilicate hydrate gel), which is formed mainly in AAF (Van Jaarsveld *et al.*, 2003). The formation of the C-A-S-H gel in AAS mortars seems to be efficiently contributing to the enhancement of mortar specimen's matrix, hence allowing them to sustain more compression. On the other hand, the low level of activation found in $Ca(OH)_2$ and $NaHCO_3$ activated fly ash mortars is not efficiently contributing in the formation of N-A-S-H gels, therefore directly affecting the compressive strength of AAF mortars.

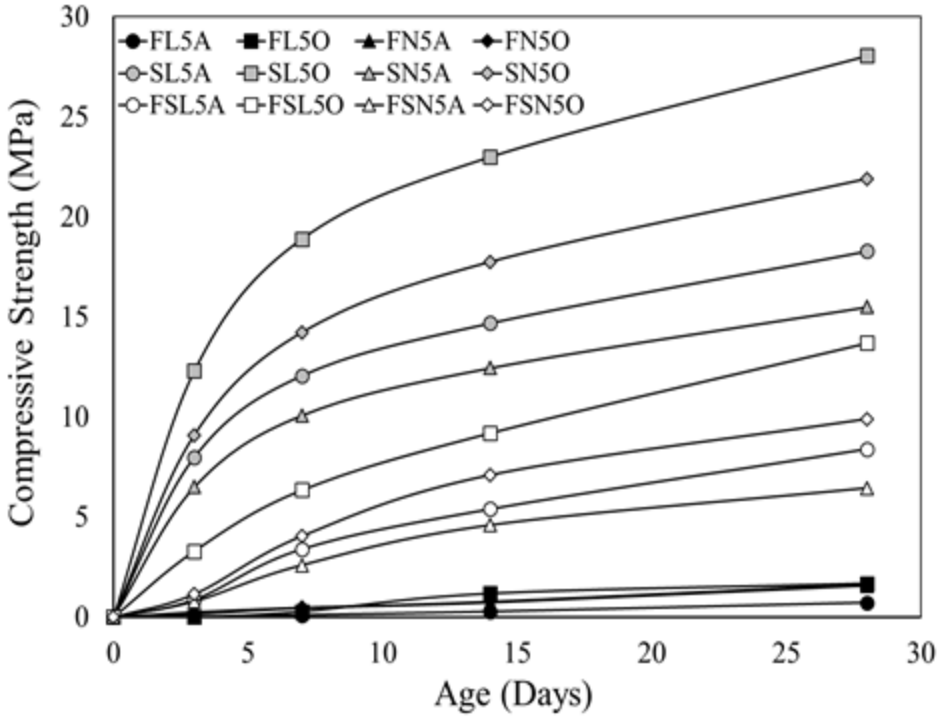

Figure 4.35 Compressive strength of AAM specimens activated with 5% $Ca(OH)_2$ and $NaHCO_3$.

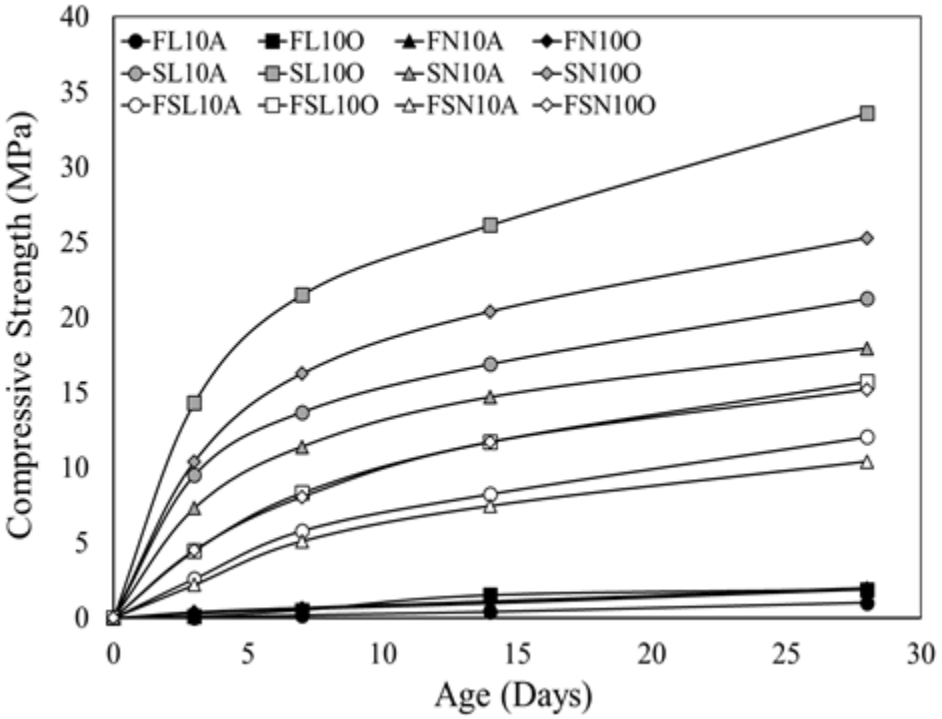

Figure 4.36 Compressive strength of AAM specimens activated with 10% $Ca(OH)_2$ and $NaHCO_3$.

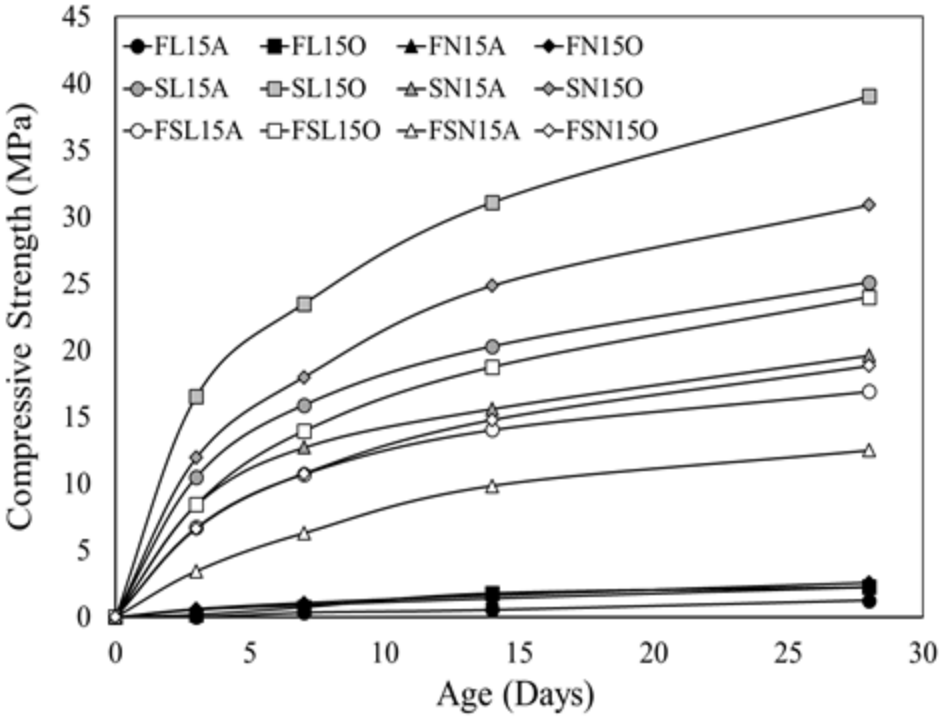

Figure 4.37 Compressive strength of AAM specimens activated with 15% $Ca(OH)_2$ and $NaHCO_3$.

4.2.4 *Heat evolution tests*

4.2.4.1 Effects of precursor type and activator dosage on heat evolution

The effect of precursor type on cumulative heat exhibited by AAF, AAS, and AAFS mortar mixtures activated with 5, 10, and 15% $Ca(OH)_2$ or $NaHCO_3$ were studied at 23 °C as shown in **Figs. 4.38-4.40**. AAS mortars exhibited the largest cumulative heat magnitude followed by AAFS, and finally, AAF mortars. For instance, the cumulative heat released by 15% $Ca(OH)_2$ activated slag mortar was 318, and 1060% more than the ones released by AAFS and AAF mortars, respectively. Similar heat release trend was found in $NaHCO_3$ activated mortars. The very low released heat by AAF mortars supports our previous finding which stated that the activation of fly ash mortars using the proposed $Ca(OH)_2$ or $NaHCO_3$ was not successful.

Previous studies had shown that the formation and polymerization of binder gels are responsible for the released heat (Yao *et al*., 2009*;* Chithiraputhiran and Neithalath, 2013). The

vast difference between the released heat by AAS mortars compared to AAF mortars explains the much higher compressive strength achieved by the former, as it seems that no sufficient binder gels were produced in AAF mortars.

Figures. 4.41-4.43 show the corresponding heat flow of AAF, AAS, and AAFS mortar specimens activated with $Ca(OH)_2$ or $NaHCO_3$ at various dosages. Similar to two-part AAMs, a high short exothermic peak appeared instantly after placing the AAMs in the calorimetry apparatus. This initial peak was designated as the initial wetting and dissolution of precursors solid materials (Provis, 2017), as previously mentioned in two-part AAM results. The initial dissolution heat flow peak in AAF and AAFS specimens was very low compared to AAS mortars. The prolonged heat flow rate is a result of the relatively low level of activation in AAF and AAFS mortars. Although the heat flow and cumulative heat exhibited in AAFS specimens were relatively higher than the ones observed in AAF mortars, the difference is still significant compared to AAS mortars. The heat flow and eventually the cumulative heat released were increasing with higher activator concentration. Increasing the activator dose broadened the heat rate evolution peak. This is primarily due to the accompanied higher degree of hydration reaction with higher activator dose. Higher reaction degree will release high exothermic heat, hence higher heat flow rate and eventually higher cumulative heat.

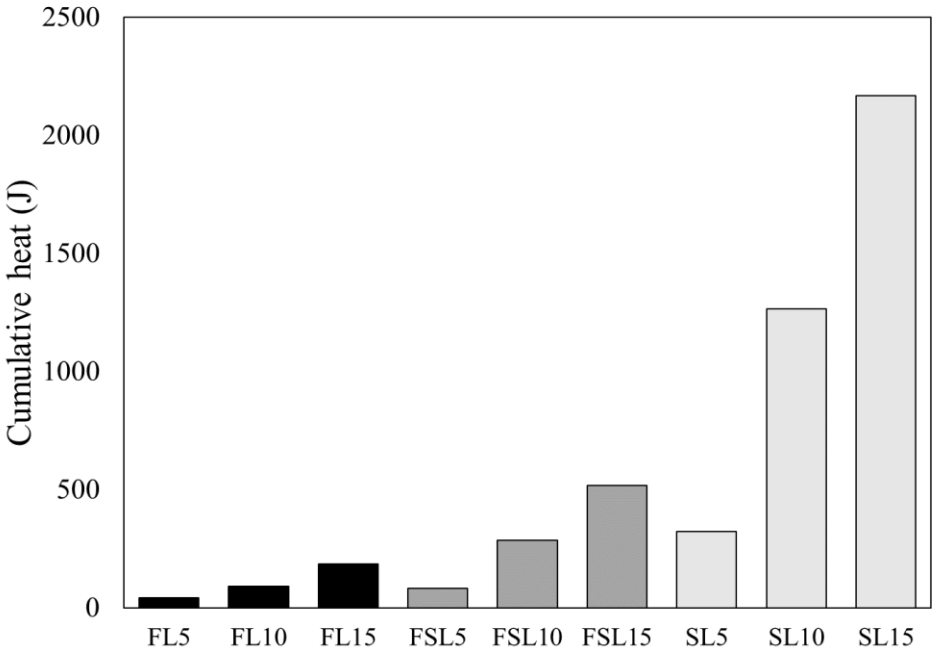

Figure 4.38 Cumulative heat of AAM specimens activated with $Ca(OH)_2$.

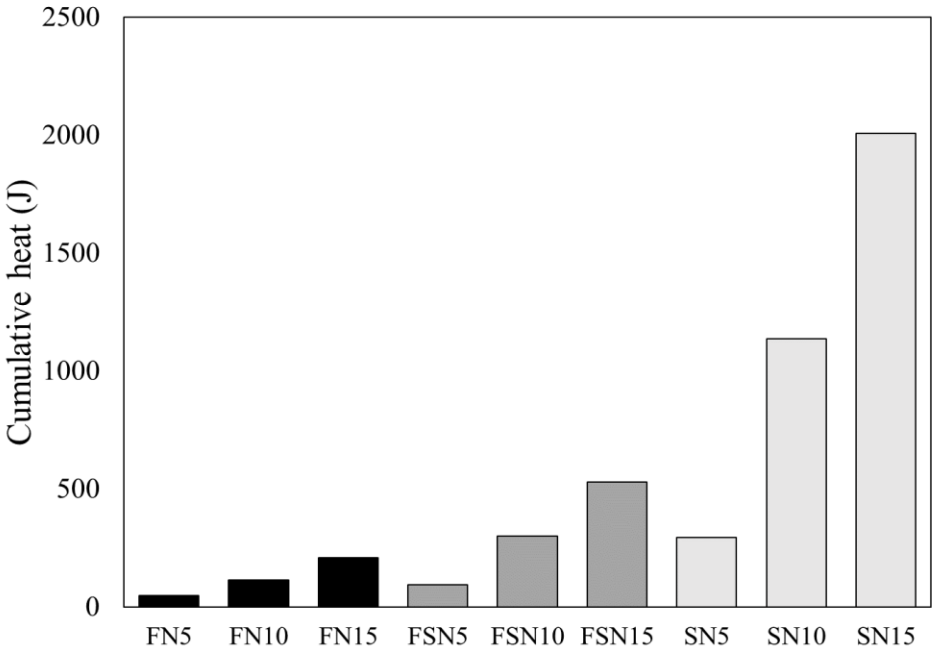

Figure 4.39 Cumulative heat of AAM specimens activated with $NaHCO_3$.

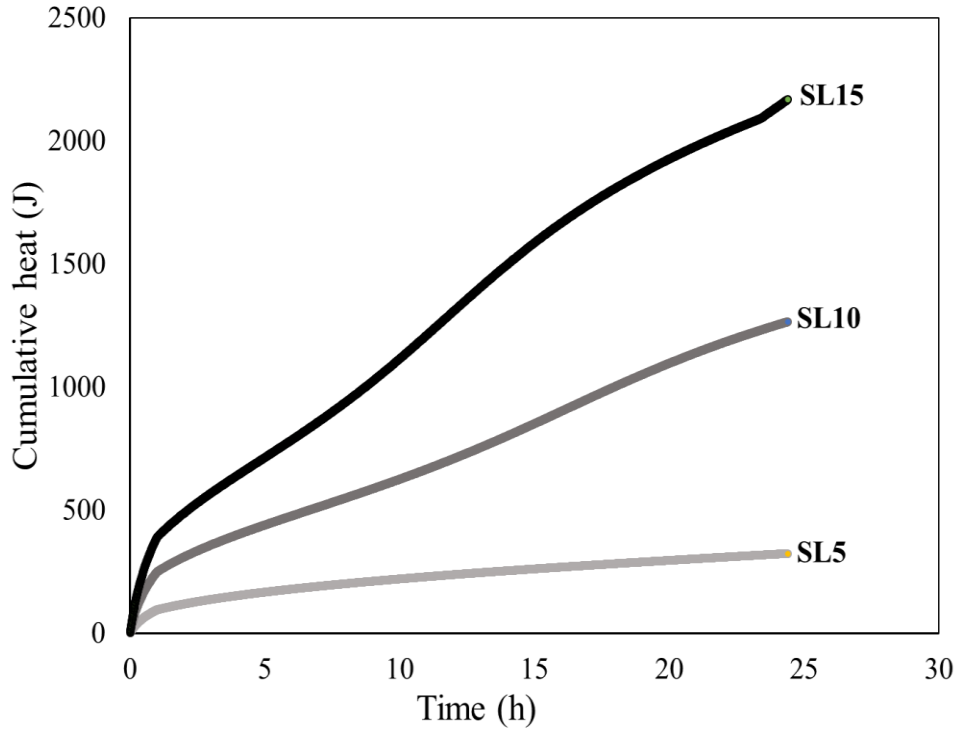

Figure 4.40 Cumulative heat of AAS mortars activated with different $Ca(OH)_2$ dosages.

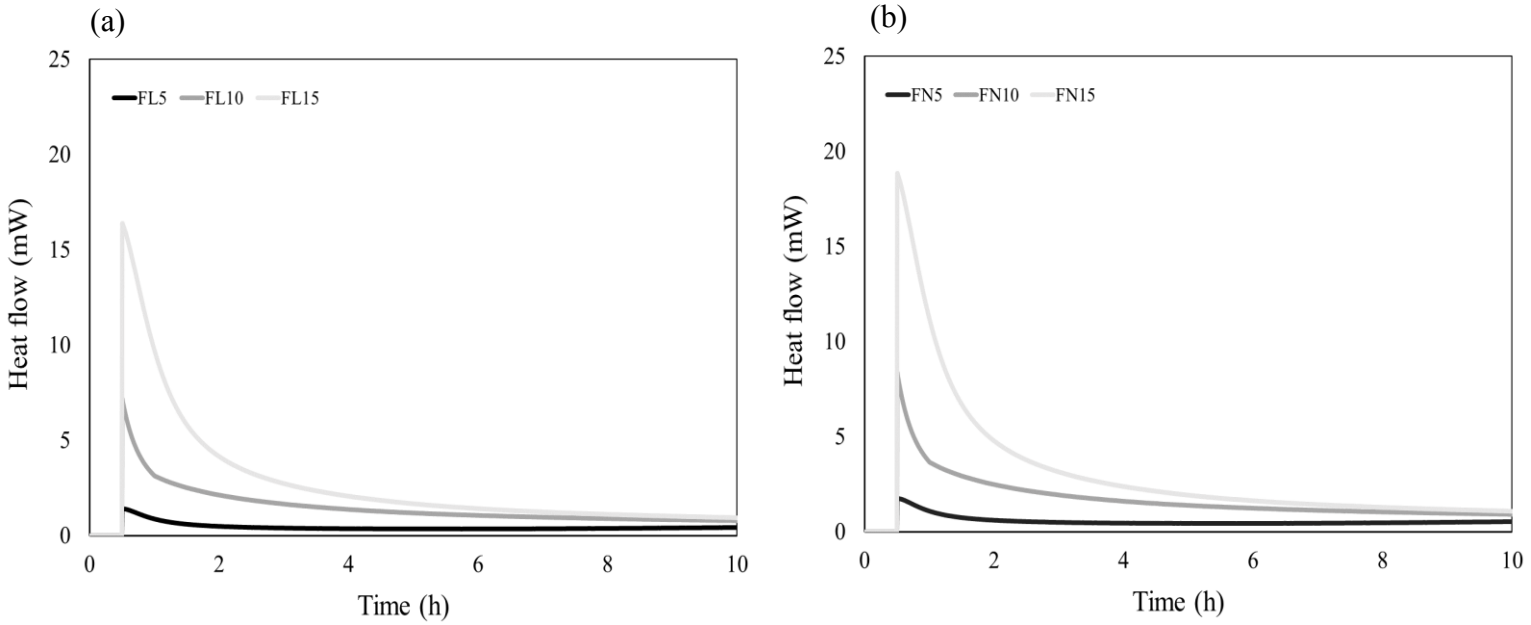

Figure 4.41 Heat flow of AAF mortars activated with $Ca(OH)_2$ and $NaHCO_3$.

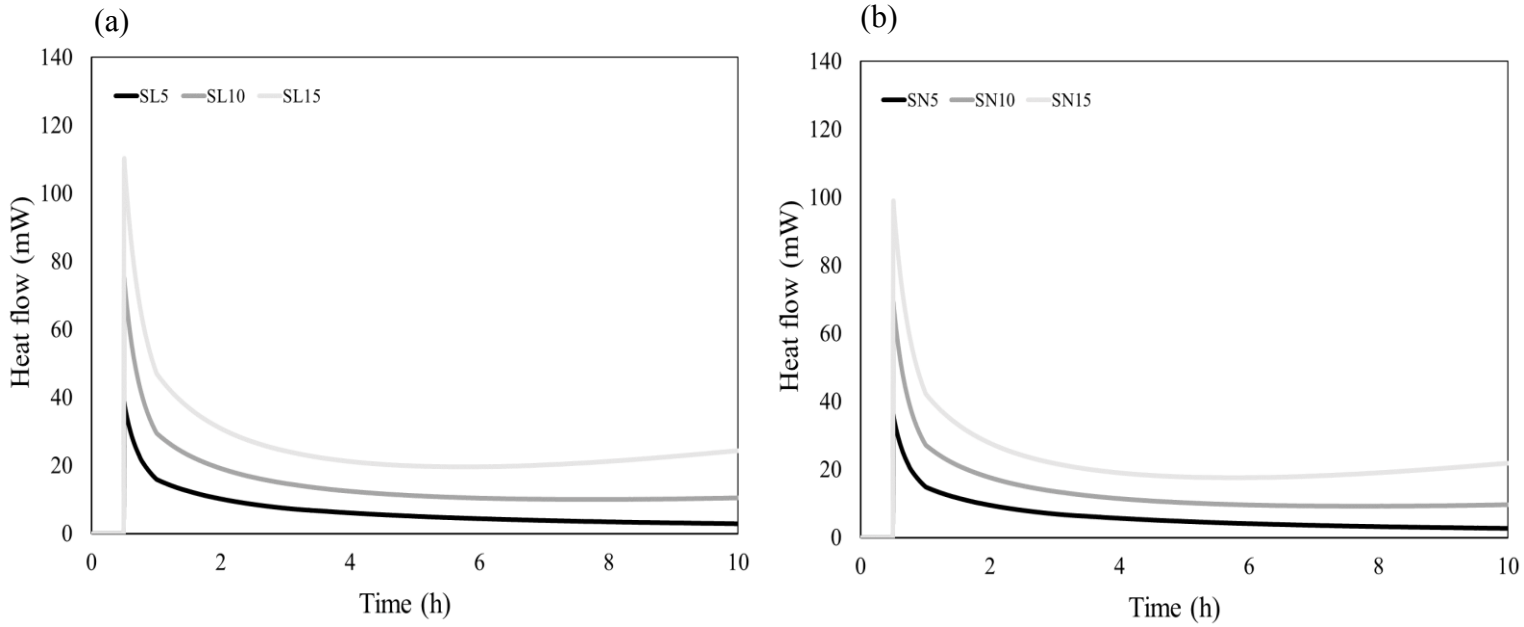

Figure 4.42 Heat flow of AAS mortars activated with $Ca(OH)_2$ and $NaHCO_3$.

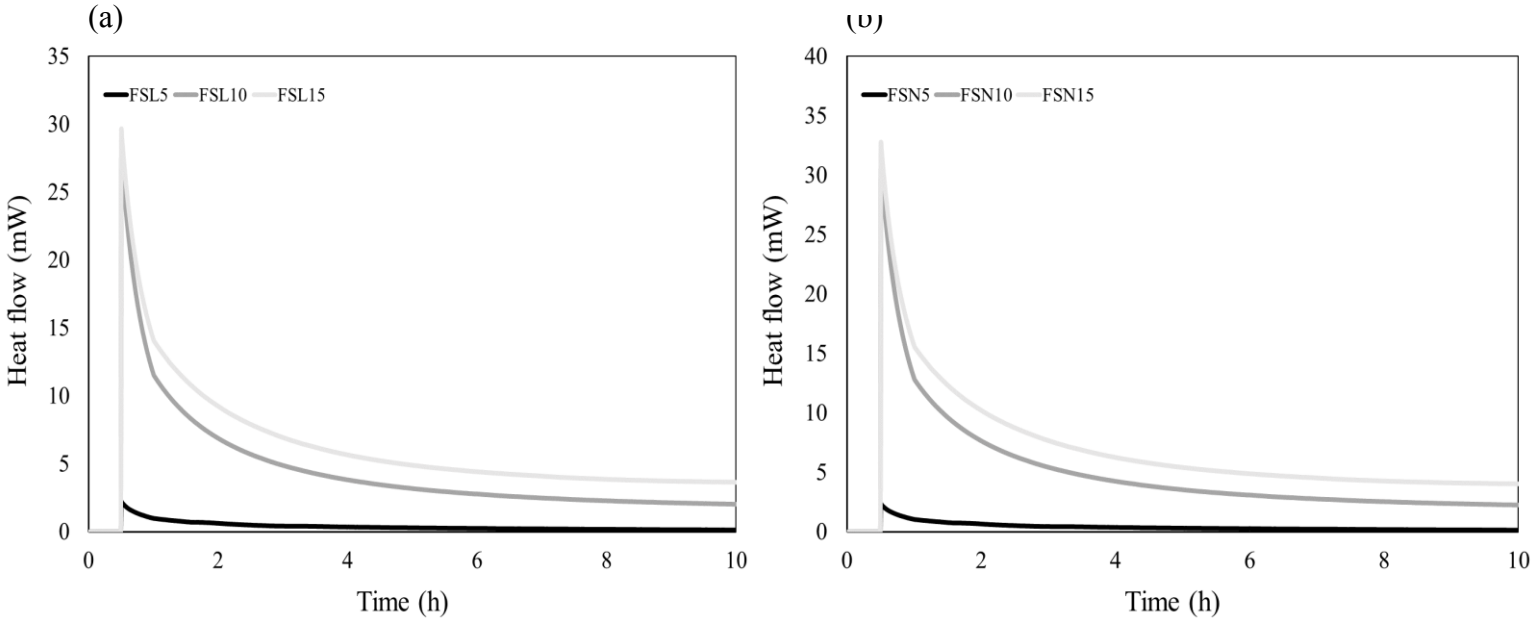

Figure 4.43 Heat flow of AAFS mortars activated with $Ca(OH)_2$ and $NaHCO_3$.

4.2.4.2 Effect of activator type on heat evolution

The effect of activator type on cumulative heat exhibited by AAF, AAFS, and AAS mortars was studied. The effect of $Ca(OH)_2$ and $NaHCO_3$ on the heat flow and heat released during the hydration process of AAM mixtures varied depending on the precursor type. In AAF mortars, the cumulative released heat by 15% $NaHCO_3$ activated mixtures was around 11.3% more than the one released by 15% $Ca(OH)_2$ activated ones. The heat flow was similarly slightly higher in the former compared to the later. Similar observations were found in mortars activated with lower activator dosages. Generally, the larger heat release is a sign of a more intense hydration reaction. These findings support the previously reported compressive strength results, as $NaHCO_3$ fly ash mortars achieved a slightly higher compressive strength compared to $Ca(OH)_2$ activated ones. Overall, heat evolution results indicate the same low degree of hydration in AAF mortars activated with both activators, as the heat evolution pattern was similar.

On the other hand, AAS mortars activated with $Ca(OH)_2$ released slightly larger heat compared to $NaHCO_3$ activated ones. For instance, the cumulative released heat by $Ca(OH)_2$ activated AAS mixtures were 7-10% more than the one released by $NaHCO_3$ activated ones. This minimal difference was reflected in compressive strength results as the achieved strength by $Ca(OH)_2$ activated slag mortars was higher than the one achieved by $NaHCO_3$ activated ones. Similar findings were observed in AAFS mortars.

4.2.5 *Drying Shrinkage*

4.2.5.1 Effect of activator type and concentration

Drying shrinkage experienced by AAS, and AAFS mortars activated with 5, 10, and 15% $Ca(OH)_2$ or $NaHCO_3$ and cured under both conditions are plotted in **Figs. 4.44 and 4.45,** respectively. Around 85% of the total drying shrinkage took place within the first 7 days depending on activator concentrations. In general, the drying shrinkage strains of $Ca(OH)_2$ activated mortars were

relatively higher than those of $NaHCO_3$ activated ones. For example, the drying shrinkage experienced by 15% $Ca(OH)_2$ activated slag mortar was 24.5%, and 16.8% more than the one experienced by 15% $NaHCO_3$ activated mortar under ambient and oven curing temperatures, respectively. Similar higher shrinkage trend was also observed in $Ca(OH)_2$ activated fly ash/slag mortars compared to $NaHCO_3$ activated ones.

Typically, the magnitude and rate of drying shrinkage in AAM specimens increased as activator dosages increased. For instance, the drying shrinkage experienced by 15% $Ca(OH)_2$ activated AAS mortar was 7.5%, and 17.6% more than the ones experienced by 10%, and 5% $Ca(OH)_2$ activated mortars under ambient curing, respectively. The corresponding drying shrinkage under oven curing was 11.2%, and 28.2% higher, respectively. The degree of hydration reaction was reported to increase with higher activator dosages (Atiş *et al*., 2009). Consequently, the higher degree of reaction densifies the mixtures leading to finer pore structure which in turn increase the capillary stresses associated with shrinkage (Thomas *et al*., 2017).

The drying shrinkage strain experienced by ambient cured AAFS mortars activated with 15% $Ca(OH)_2$ was 17%, and 50% higher than the those experienced by 10%, and 5% $Ca(OH)_2$ activated mortars, respectively. The corresponding drying shrinkage strain under oven curing was 30.3%, and 73.3% higher, respectively. Similar drying shrinkage increase trend for higher activator dosages was found in $NaHCO_3$ activated slag and fly ash/slag mortars.

Overall, mortars activated with $NaHCO_3$ experienced lower shrinkage strains compared to $Ca(OH)_2$ activated ones but, on the other hand, achieved lower compressive strength as previously reported. Nevertheless, the cumulative heat released by the hydration reaction in $NaHCO_3$ activated specimens was also lower than the heat released by the $Ca(OH)_2$ activated ones.

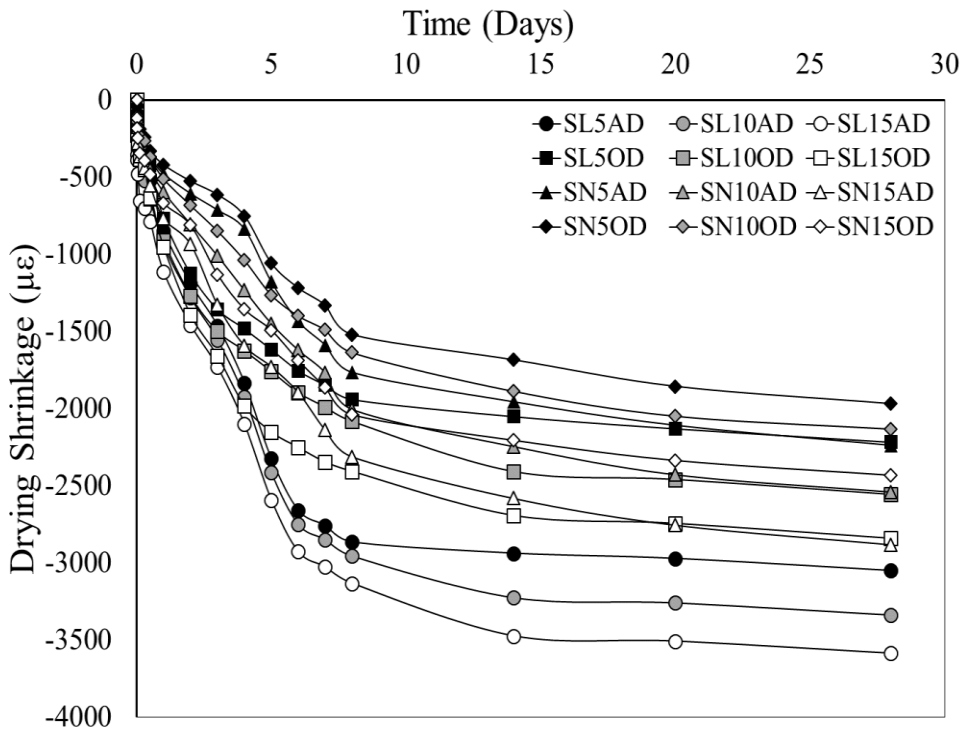

Figure 4.44 Drying shrinkage strains of different AAS mortars (ambient and oven cured).

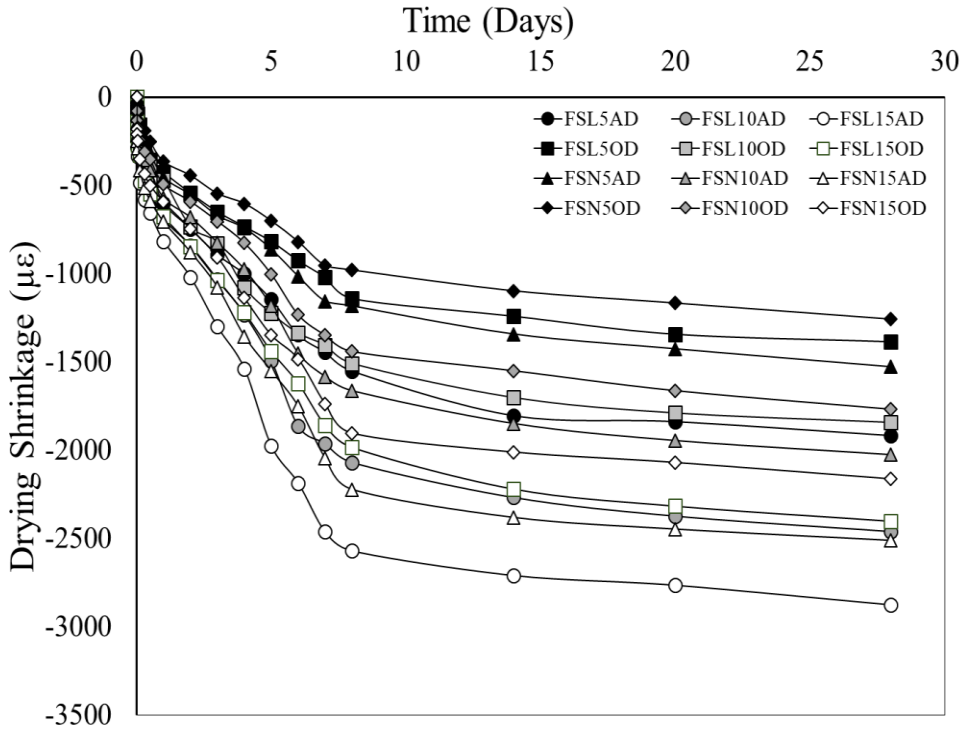

Figure 4.45 Drying shrinkage strains of different AAFS mortars (ambient and oven cured).

4.2.5.2 Effect of precursor type and curing condition

Drying shrinkage of AAS and AAFS mortars activated with different dosages of $Ca(OH)_2$ or $NaHCO_3$ and cured under both ambient and oven conditions are shown in **Figs. 4.46 and 4.47**, respectively. In general, AAS mortars experienced higher drying shrinkage strains compared to AAFS mortars. For instance, the drying shrinkage strain experienced by 5% $Ca(OH)_2$ activated slag mortar was 59.3%, and 60.1% higher than the ones experienced by 5% $Ca(OH)_2$ activated fly ash/slag mortar under ambient and oven curing conditions, respectively. $NaHCO_3$ activated mortars experienced a similar drying shrinkage increase trend. It is clear that the effect of fly ash substitution in AAFS mortars was not influenced by the curing temperature.

Generally, AAS mixtures are well known to experience higher shrinkage strains compared to AAF mixtures because of the higher capillary stresses associated with finer pore structure present in the former. Moreover, the spherical shape of fly ash particles contributes to a coarser porosity structure. As a result, reduction in the surface tension takes place leading to lower drying shrinkage. Hence, the substitution of 50% fly ash in AAFS mortars contributes to reducing the drying shrinkage of AAS mortars.

Drying shrinkage of AAM specimens was significantly reduced under oven curing temperatures. For instance, the drying shrinkage strains experienced by 5, 10, and 15% $Ca(OH)_2$ activated slag mortars oven cured were 27.3, 23.4, and 20.8% lower than the ones experienced under ambient curing temperature, respectively. Furthermore, reductions in drying shrinkage strains of AAFS mortars activated with 5, 10, and 15% $Ca(OH)_2$ due to oven curing were 27.8, 25.12, and 16.5%, respectively. Reductions rates were almost equal in AAS, and AAFS mortars at fixed activator dosages. Reductions were more pronounced in specimens activated with lower activator dosages. A similar reduction trend was found in $NaHCO_3$ activated slag and fly ash/slag mortars.

Curing at elevated temperatures is well known to accelerate the strength development of AAMs resulting in a much denser matrix and hence an increased rigidity of the solid network (Ma and Ye, 2015). This denser and more rigid matrix at early ages implements a higher shrinkage resistance. Significant strength development can be expected in AAMs even when heat-cured for shorter durations (Thomas *et al*., 2017).

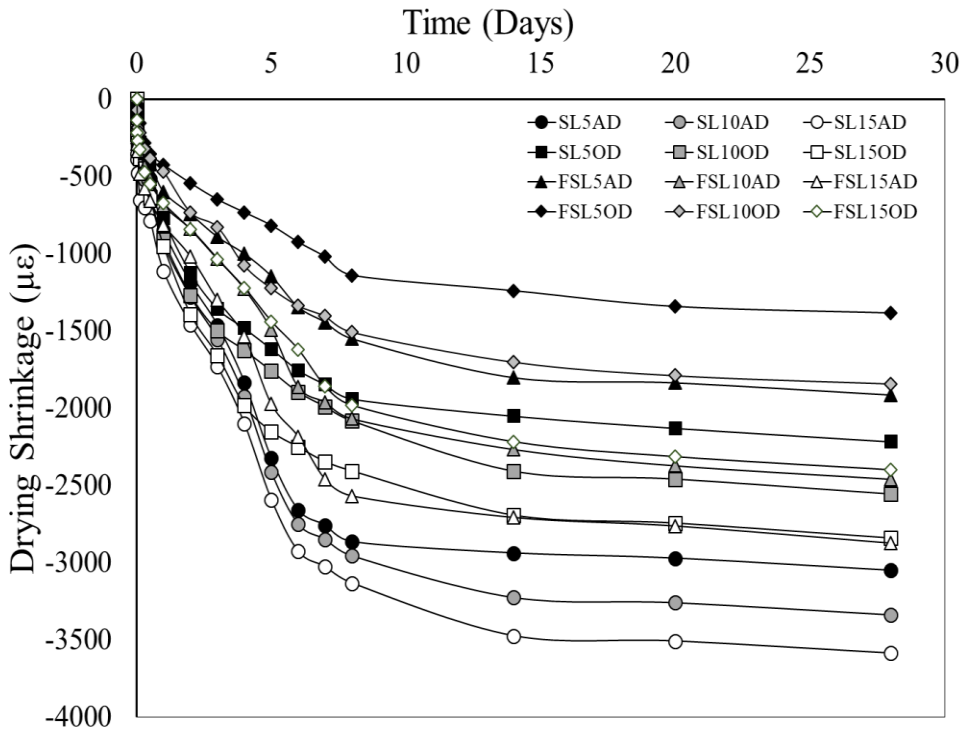

Figure 4.46 Drying shrinkage strains of AAS and AAFS mortars activated with $Ca(OH)_2$ (ambient and oven cured).

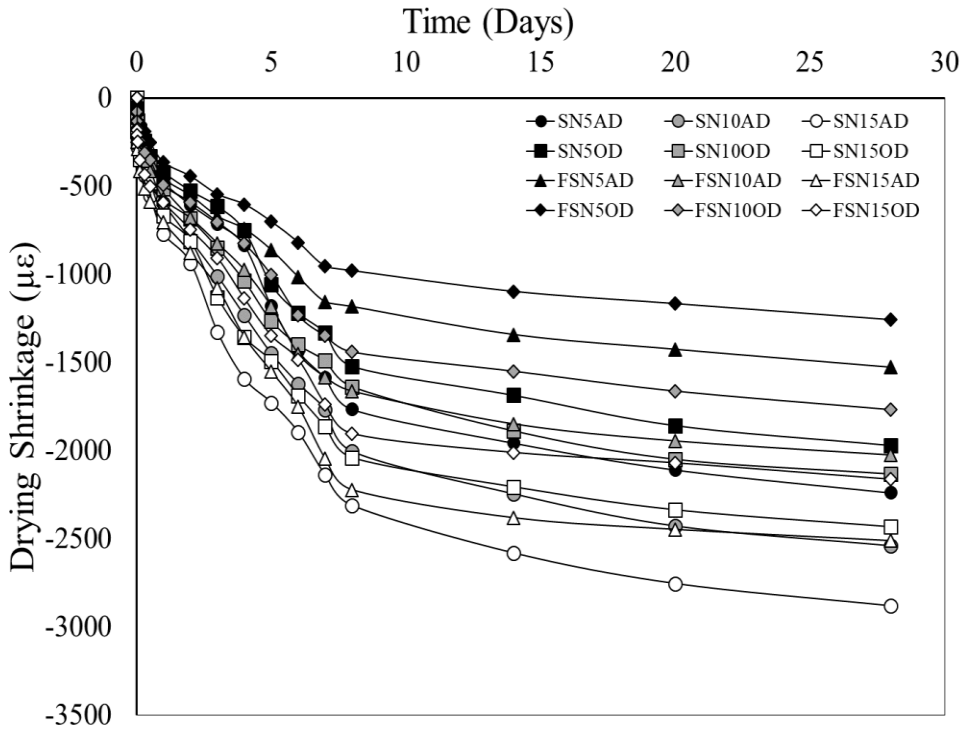

Figure 4.47 Drying shrinkage strains of AAS and AAFS mortars activated with $NaHCO_3$ (ambient and oven cured).

4.2.6 *Mass loss*

4.2.6.1 Effect of mass loss on drying shrinkage of AAMs

Figure 4.48 shows the mass loss with respect to age of AAS mortars activated with 5, 10, and 15% $Ca(OH)_2$ under ambient and oven curing conditions. Typically, mass loss was increasing with age. Oven cured specimens experienced higher mass loss than ambient cured ones. Mass loss was dependent on activator dosage, as specimens activated with higher dosages experienced higher mass loss.

Figures 4.49-4.52 show the curves representing the relationship between drying shrinkage and mass loss for AAS, and AAFS mortars. The slope of the curves represents the length change per unit mass loss. An increase in the slope suggests a finer porosity, while a decrease in slope suggests a coarser porosity. **Figure 4.49** shows the relationship between drying shrinkage and mass loss for ambient cured AAS specimens activated with 5, 10, and 15% $Ca(OH)_2$ and $NaHCO_3$.

Regardless of activator type and dose, AAS mortars curve slopes were similar at early age. This suggests that the pore distribution was not affected at early age. At later age, $NaHCO_3$ activated mortars slope curves kept constant indicating no changes in porosity.

On the other hand, the slope of $Ca(OH)_2$ activated specimens increased indicating a decrease in porosity. At later age, the drying shrinkage in $NaHCO_3$ activated slag mortars showed a slow shrinkage increase rate with the increase in mass loss. This suggests that at later age, the drying shrinkage of $NaHCO_3$ slag mortars was not affected with the increased mass loss. On the other hand, the drying shrinkage per unit mass loss in $Ca(OH)_2$ activated specimens increased significantly, suggesting a further decrease in porosity at later ages. The high reduction in mass loss seen in $Ca(OH)_2$ activated specimens at later age, indicates a major reduction in porosity. Ma *et al*. (2013) suggested that the porosity of AAM specimens is reduced with age.

Figure. 4.50 shows the relationship between mass loss and drying shrinkage in ambient cured AAFS specimens. At the early age, curve slopes were stable indicating no changes in the porosity. While at later age, the curve slopes decreased suggesting an increase in porosity with age. No further significant changes were observed in curve slopes of AAFS specimens. This indicates an almost uniform drying shrinkage per unit mass loss for up to the test end. Regardless of activator dosage, slope changes were similar throughout the test period**.**

Figures. 4.51 and 4.52 show the relationship between drying shrinkage and mass loss in oven cured AAS, and AAFS specimens activated with 5, 10, and 15% $Ca(OH)_2$ and $NaHCO_3$. As seen in **Fig. 4.51**, slope curves changes in oven cured AAS specimens were similar to the ones observed in ambient cured ones. At early age, the slope was constant indicating uniform drying shrinkage per unit mass loss for up to 1.5% mass loss, after which the slope gradient increased indicating a decrease in porosity. No further major changes were observed for up to the test end.

Figure. 4.52 shows the shrinkage per unit mass loss behaviour of AAFS specimens. At early age, drying shrinkage per unit mass loss was constant for up to 3.5% mass loss. The trend was similar to the one observed in AAS specimens but, the shrinkage rate was relatively lower. At later ages, the slope gradient was also increased indicating a decrease in porosity. The decrease in porosity was less pronounced in AAFS specimens, as the slope gradient observed wasn't as steep as the one observed in AAS specimens. Regardless of precursor blend, the drying shrinkage in AAM specimens at later was not affected by the increased mass loss.

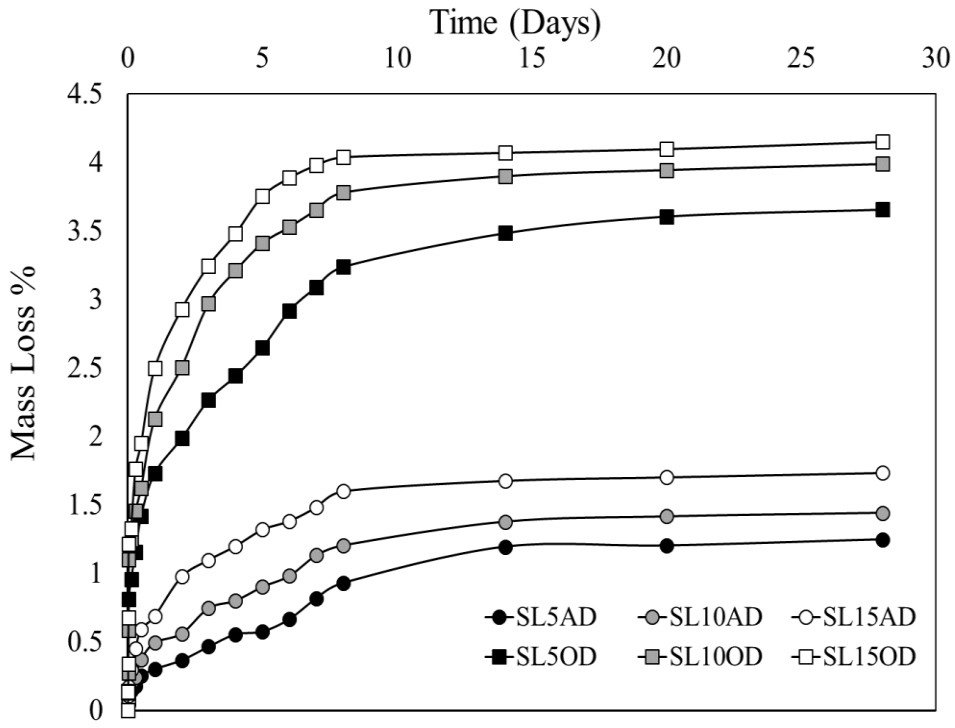

Figure 4.48 Mass loss with age of AAM specimens at oven curing.

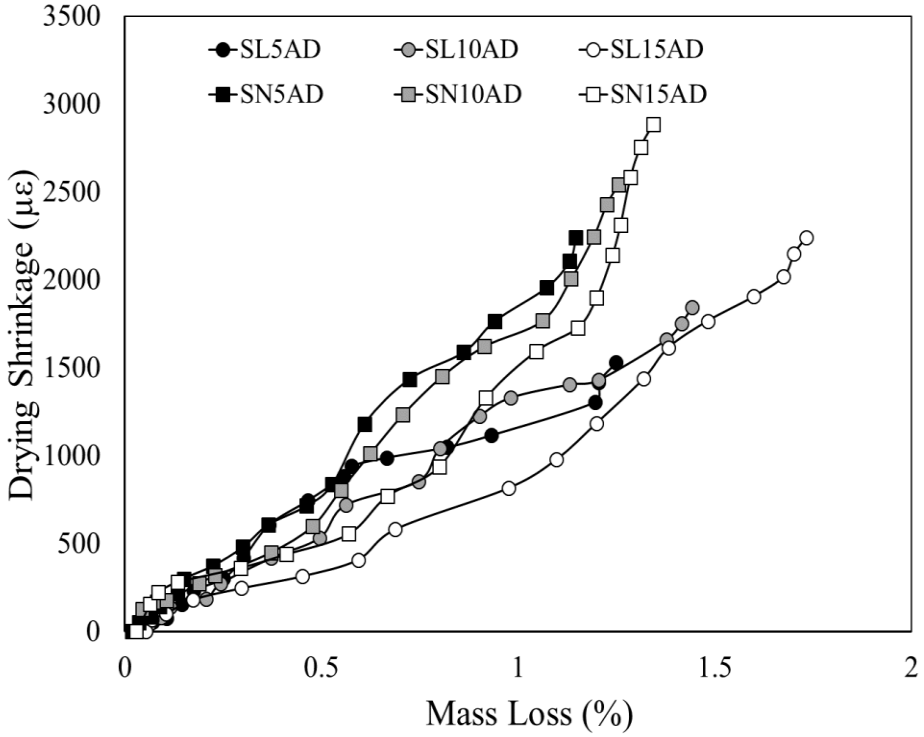

Figure 4.49 Mass loss vs. drying shrinkage for AAS mortars under ambient curing.

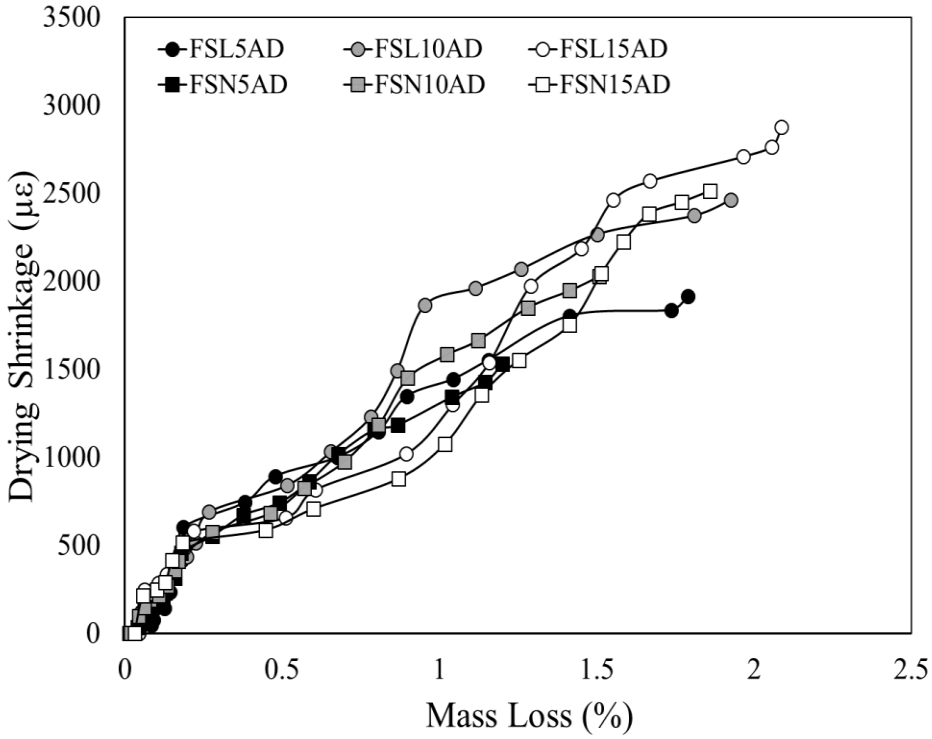

Figure 4.50 Mass loss vs. drying shrinkage for AAFS mortars under ambient curing.

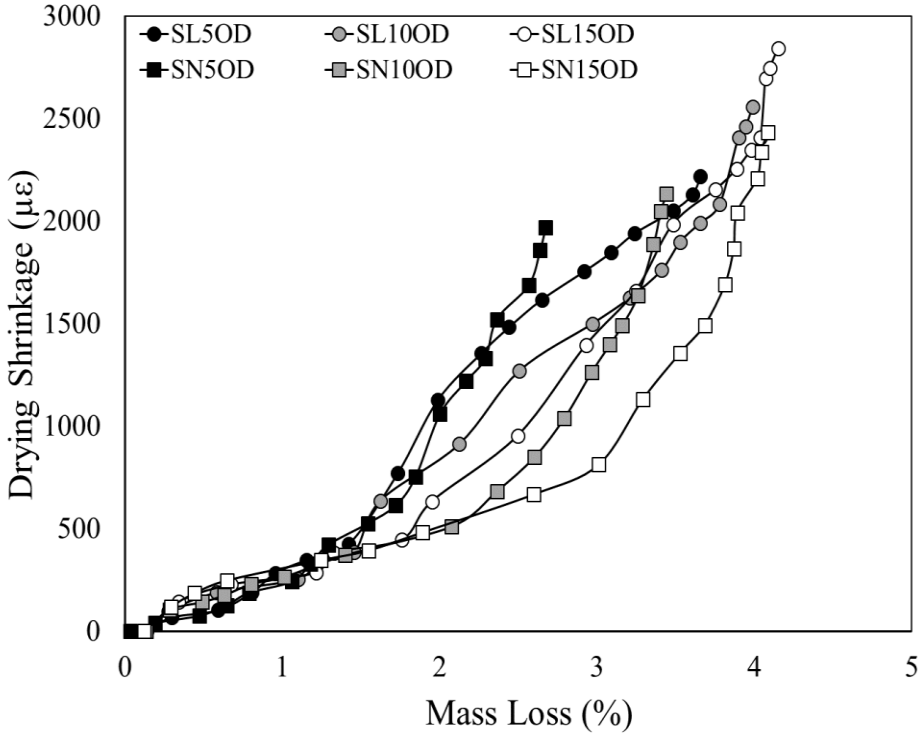

Figure 4.51 Mass loss vs. drying shrinkage for AAS mortars under oven curing.

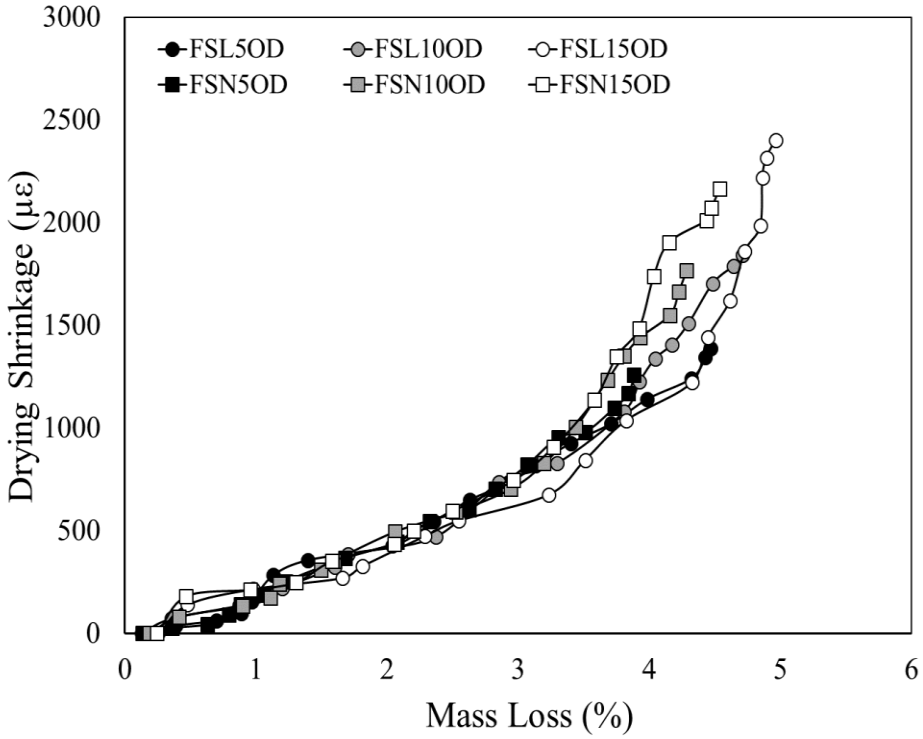

Figure 4.52 Mass loss vs. drying shrinkage for AAFS mortars under oven curing.

4.2.7 *Autogenous shrinkage*

4.2.7.1 Effect of activator type and dosage

Autogenous shrinkage in AAS and AAFS mortars activated with 5, 10, and 15% $Ca(OH)_2$ or $NaHCO_3$ and cured under both ambient and oven conditions are plotted in **Figs. 4.53 and 4.54**. In general, $Ca(OH)_2$ activated mortars experienced higher autogenous shrinkage compared to $NaHCO_3$ activated mortars. For instance, the autogenous shrinkage experienced by AAS mortar activated with 15% $Ca(OH)_2$ was 43%, and 18.4% higher than that experienced by 15% $NaHCO_3$ activated mortars under ambient and oven curing conditions, respectively. A similar trend was observed in AAFS mortar specimens. The effect of activator type on autogenous shrinkage strains of AAS, and AAFS mortars was more pronounced in $NaHCO_3$ activated specimens.

Autogenous shrinkage in AAM specimens increased as activator dosages increased. About 85-90 % of the total autogenous shrinkage was observed in the first 7 days. For example, the autogenous shrinkage strain experienced by 15% $Ca(OH)_2$ activated AAS mortar was 23.5%, and 7.5% more than the ones experienced by 10%, and 5% $Ca(OH)_2$ activated mixtures under ambient curing, respectively. The corresponding autogenous shrinkage strains under oven curing were 28.2%, and 11.2% higher, respectively. AAFS mortars encountered similar higher autogenous shrinkage at higher activator dosages.

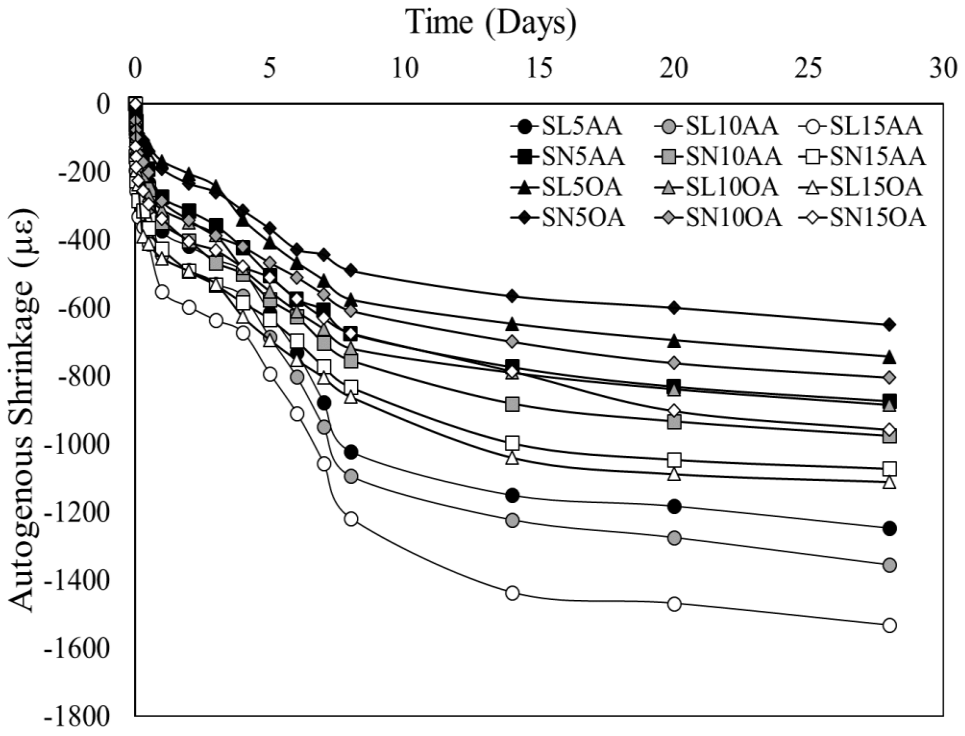

Figure 4.53 Autogenous shrinkage of AAS mortars (ambient and oven cured).

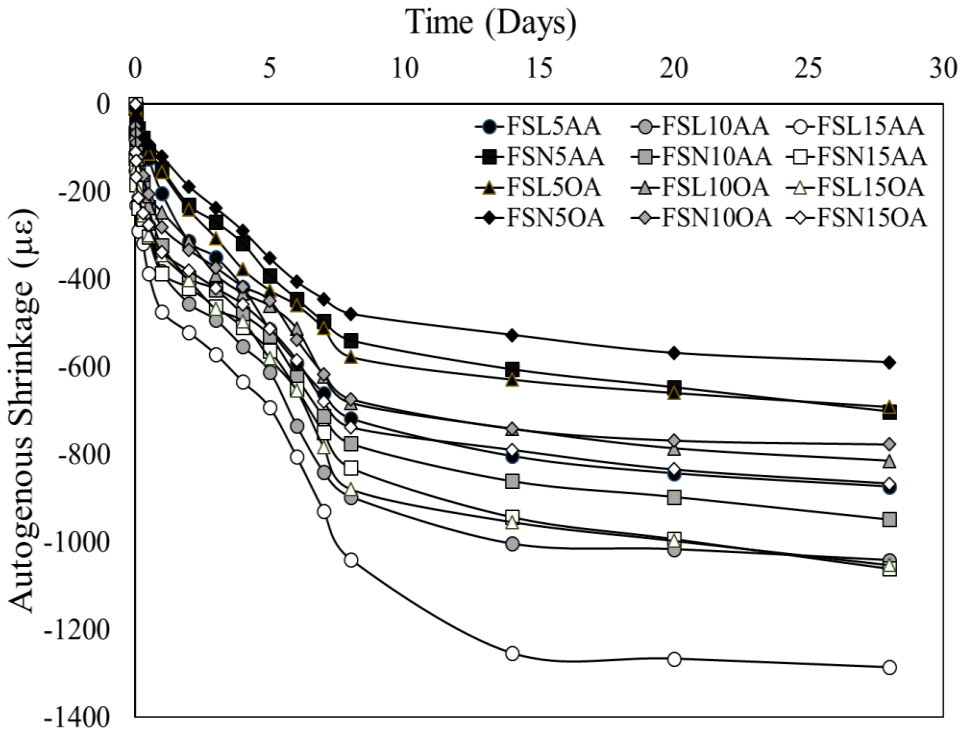

Figure 4.54 Autogenous shrinkage of AAFS mortars (ambient and oven cured).

4.2.7.2 Effect of precursor type and curing condition

Autogenous shrinkage strains of AAS and AAFS specimens activated with different dosages of $Ca(OH)_2$ or $NaHCO_3$ and cured at both conditions are plotted in **Figs. 4.55, and 4.56.** Regardless of curing condition, AAS mortars experienced higher autogenous shrinkage strains compared to AAFS mortars. For instance, the drying shrinkage strain of AAS mortar activated with 15% $Ca(OH)_2$ was 19.1%, and 6% higher than the one experienced in 15% $Ca(OH)_2$ AAFA mortars under ambient and oven curing temperatures, respectively. A similar trend was observed in $NaHCO_3$ activated mortars. The effect of precursor blend on the autogenous shrinkage strains seems to be less pronounced under oven curing temperatures.

Generally, autogenous shrinkage strains were reduced with higher temperature curing (oven) conditions compared to ambience. For instance, the autogenous shrinkage strains experienced by 5, 10, and 15% $Ca(OH)_2$ activated slag mortars were reduced by 40, 34.7, and 27.5%, respectively under oven curing conditions compared to specimens cured at ambience. The corresponding reductions in AAS mortars activated with $NaHCO_3$ were 25.5, 17.5, and 10.7%, respectively.

AAFS mortar specimens activated with 5, 10, and 15% $Ca(OH)_2$ experienced autogenous shrinkage reductions of 21.9, 20.8, and 18.2%, respectively when oven cured compared to specimens ambient cured. The corresponding reductions in AAFS mortars activated with $NaHCO_3$ were 18.4, 18.1, and 15.9%, respectively. Regardless of the precursor type, adopting oven curing conditions reduced the autogenous shrinkage strains in AAM specimens. Reductions were more pronounced in specimens activated with lower activator doses. The observed autogenous shrinkage strain reduction trend was similar to the one reported in drying shrinkage. Higher curing conditions

are expected to increase the rigidity of the mortar matrix, therefore increase the overall shrinkage resistance.

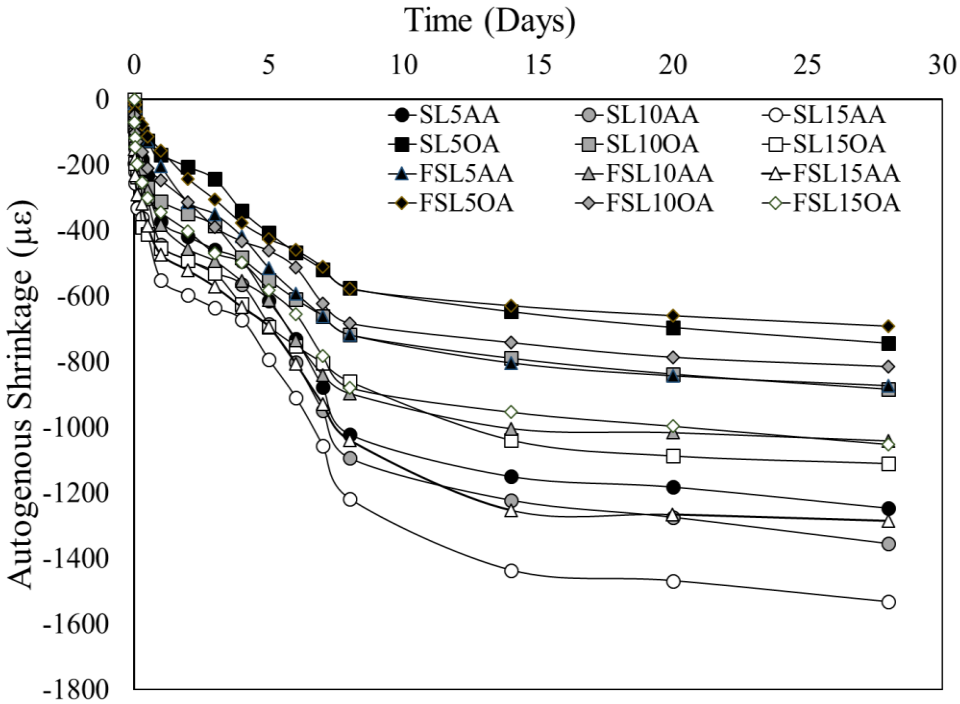

Figure 4.55 Autogenous shrinkage of AAS and AAFS mortars activated with $Ca(OH)_2$ (ambient and oven cured).

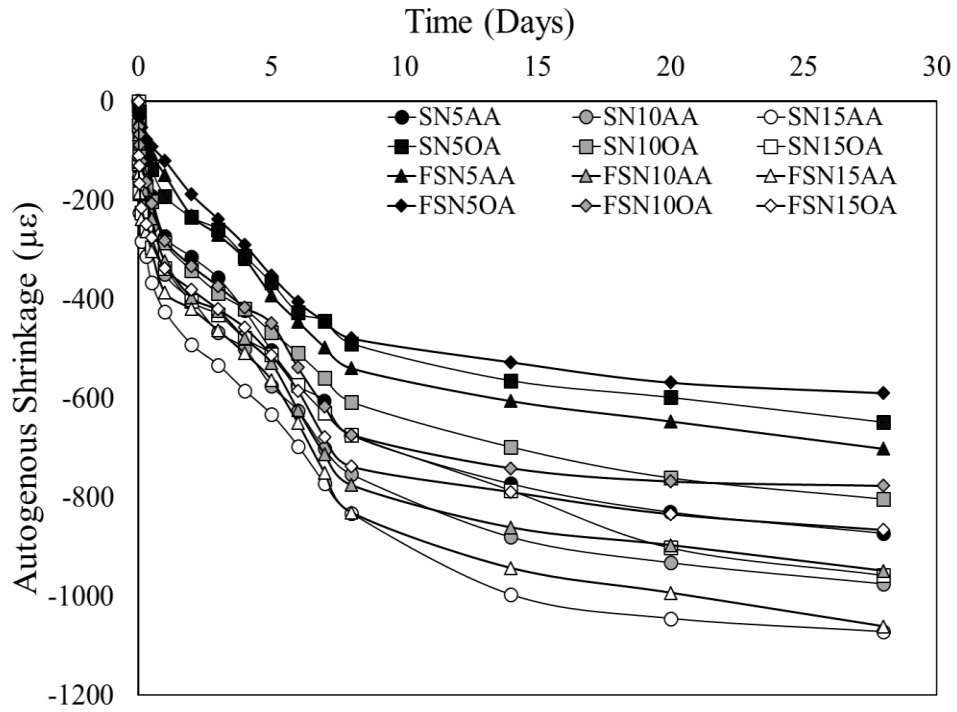

Figure 4.56 Autogenous shrinkage of AAS and AAFS mortars activated with $NaHCO_3$ (ambient and oven cured).

4.2.8 *Conclusion*

In this phase, different properties for one-part alkali activated mortars were investigated including, fresh and hardened properties along with associated shrinkage. The following conclusion can be drawn:

1- Regardless of precursor and activator type, flowability and setting time decreased as the activator dosage increased. AAS mortar specimens showed the lowest flow values followed by AAFS, and finally, AAF mortar specimens. AAS mortars exhibited the quickest setting time followed by AAFS, and finally, AAF mortars. Specimens activated with $NaHCO_3$ exhibited a slightly higher flowability and longer setting compared to specimens activated with $Ca(OH)_2$.

2- The activation of fly ash-based mixtures using neither neat $Ca(OH)_2$ nor $NaHCO_3$ was not successful regardless of the curing condition. The achieved 28 days compressive strength of those mortars was very low. In addition, the activation level in AAFS specimens was not promising also. On the other hand, compressive strength for AAS was enhanced as the curing temperature increased.

3- Calorimetry analysis showed that the heat flow and cumulative heat released by AAF mortars were very low compared to other mortars. The relation between the cumulative heat released and the compressive strength achieved was found to be directly proportional.

4- Regardless of precursor blend, activator type, and curing condition, the magnitude and rate of drying and autogenous shrinkage increased as activator dosages increased. AAS and AAFS specimens activated with $Ca(OH)_2$ exhibited higher shrinkage strains compared $NaHCO_3$ activated ones.

5- The relation between mass loss and drying shrinkage in AAMs showed that, at early ages, the pore distribution in all specimens was not affected by the activator type or dosage. At later age, the drying shrinkage in all specimens was not affected by the increased mass loss. Specimens activated with $Ca(OH)_2$ showed higher shrinkage per unit mass loss compared to the ones activated with $NaHCO_3$.

4.3 Phase 3: Effects of Shrinkage Reducing Admixture on Shrinkage Behaviour of One and Two Part Alkali-Activated Mortars

4.3.1 *Flowability*

The addition of SRA in one-part AAMs was only applied to AAS and AAFS mortar mixtures activated with the proposed activators, as one-part AAF mortar mixtures without SRA failed to establish sufficient strength for compressive strength and shrinkage tests to be accomplished. Hence, these mixtures were neglected. Variations in workability for one-part, and two-part AAS mixtures containing SRA with respect to activator type and dosage are presented in **Table 4.3, and 4.4,** respectively. Generally, the flow values of mortar mixtures slightly increased with the addition of SRA. For instance, the flow values for one-part AAS mortar mixtures containing 1% SRA and activated with 5, 10, and 15% $Ca(OH)_2$ or $NaHCO_3$ were increased by 1-3%, compared to specimens without SRA. When SRA dosage increased to 2%, the increase in flow values was slightly more pronounced. AAFS mortar mixtures achieved fairly similar minor flow increase with the addition of SRA. A Similar trend was observed in two-part AAMs. For instance, the flowability of two-part AAS mortars activated with 3M, 6M, and 12M NaOH concentrations, and containing 1% SRA were increased by 1-3%, compared to AAS mortars without SRA. The corresponding

flow increase in 2% SRA containing AAS mortars was 2-4%, respectively. Two-part AAFS mortars achieved fairly similar minor flow increase with SRA addition.

Typically, the addition of liquid SRA does slightly increase the specific liquid to solid ratio hence, directly influencing the flowability of mortar specimens (Palacios and Puertas, 2005). Bilim *et al*. (2013) stated that SRAs slightly increased the flow values of two-part AAS mortars. These results conform to the findings of this study. Regardless of the mixing mechanism, the increase in flowability due to the addition of SRA was almost equal in all AAS mortar mixtures.

Table 4.3 Setting times and flow of AAMs.

Mixture	Setting time (min)		Flow (cm)
	Initial	Final	
SL5	160	286	107
SL10	145	261	105
SL15	130	238	102
SL5R1	165	295	108
SL10R1	151	276	106
SL15R1	133	251	104
SL5R2	168	301	109
SL10R2	159	280	106
SL15R2	141	262	106
FSL5	430	562	112
FSL10	418	544	112
FSL15	405	517	110
FSL5R1	436	570	113
FSL10R1	424	550	112
FSL15R1	410	521	111
FSL5R2	441	574	114
FSL10R2	430	555	113
FSL15R2	412	524	112

Table 4.3 (Contd'): Setting times and flow of AAMs.

Mixture	Setting time (min)		Flow (cm)
	Initial	Final	
SN5	172	283	112
SN10	165	269	108
SN15	152	244	106
SN5R1	185	292	112
SN10R1	171	278	109
SN15R1	156	253	108
SN5R2	196	310	113
SN10R2	182	289	110
SN15R2	169	270	109
FSN5	431	565	120
FSN10	418	547	116
FSN15	402	518	114
FSN5R1	435	571	>120
FSN10R1	424	555	117
FSN15R1	410	522	116
FSN5R2	441	580	>120
FSN10R2	431	561	119
FSN15R2	414	530	117

4.3.2 *Setting time*

The effect of SRA addition on the initial and final setting time of one-part and two-part AAM mixtures was noted in this study. Variations in setting times of one-part, and two-part AAM mixtures containing SRA with respect to activator type and dosage are presented in **Table 4.3, and 4.4,** respectively. Generally, the addition of SRA admixture retarded both the initial and final setting times of one-part, and two-part AAM mixtures. The retardation effect was more pronounced when the percentage of SRA increased from 1% to 2% (by mass of binder). For

instance, the initial setting times of one-part AAS mortars containing 1% SRA and activated with 5, 10, and 15% $Ca(OH)_2$ were delayed by 3-6 minutes, compared to corresponding mixtures without SRA. When SRA dose increased to 2%, the delay in initial setting was increased to 8-14 minutes, compared to mixtures without SRA. The impact of SRA addition on final setting times of one-part AAS mortars was almost equal. Similar setting delay trend was observed in $NaHCO_3$ activated AAS mortars.

Table 4.4 Setting times and flow of two-part AAMs.

Mixture	Setting time (min)		Flow (cm)
	Initial	Final	
F3	144	286	108
F6	126	254	102
F12	89	186	92
F3R1	150	294	112
F6R1	138	262	104
F12R1	102	196	93
F3R2	155	302	114
F6R2	141	271	105
F12R2	108	204	94
S3	108	171	94
S6	72	114	87
S12	47	76	76
S3R1	120	178	75
S6R1	96	121	88
S12R1	60	84	78
S3R2	131	191	97
S6R2	102	141	89
S12R2	76	93	82
FS3	120	202	101
FS6	104	184	92
FS12	72	112	84
FS3R1	126	222	102
FS6R1	111	191	93
FS12R1	81	132	86
FS3R2	132	224	103
FS6R2	118	202	94
FS12R2	86	144	88

The setting behaviour of two-part AAMs was also retarded with SRA addition. However, the delay in initial and final setting times was more pronounced in two-part AA mortars compared to one-part activated ones. The addition of 1% SRA retarded the initial setting time of AAS mortars activated with 3M, 6M, and 12M NaOH by 12-24 minutes, respectively compared to specimens without SRA. Moreover, increasing the dose of SRA admixture to 2% resulted in further setting retardation. The effect of SRA on setting time of AAFS was almost similar. These results are in accordance with those reported elsewhere (Palacios and Puertas, 2005).

It is worth mentioning that the effect of activator concentration on the setting behaviour of both one-part and two-part AAMs was not altered by the addition of SRA at both dosages adopted in this study.

4.3.3 *Compressive strength*

4.3.3.1 Effect of SRA addition on compressive strength of one-part AAMs

The development of compressive strength for AAS and AAFS mortar specimens, with and without SRA, was studied according to activator type, and curing condition. **Figures 4.57-4.60** show the compressive strength values of 5, 10, and 15% $Ca(OH)_2$ and $NaHCO_3$ activated AAS specimens with and without SRA at both dosages and curing conditions. Generally, the addition of SRA relatively reduced the compressive strength of AAS mortar specimens. For instance, the addition of 1% SRA caused AAS mortar specimens activated with 5, 10, and 15% $Ca(OH)_2$ and cured at the ambient condition to encounter a reduction of 8.72, 5.45, and 9.96% in the 28-day compressive strength, respectively compared to mortar specimens without SRA. The corresponding reductions encountered at oven curing condition were 12.0, 8.0, and 4.0%, respectively. Moreover, the 28-day compressive strength reductions in 2% SRA containing AAS mortars were 22.06, 17.1, and 18.0%, respectively compared to mortar specimens without SRA. The corresponding reductions

encountered at oven curing condition were 19.96, 12.05, and 8.48%, respectively. A Similar strength reduction trend with SRA addition was observed in one-part AAFS mortars.

Nevertheless, the strength reduction trend associated with SRA addition was almost equal in $NaHCO_3$ activated slag mortars. Generally, the compressive strength reductions encountered by AAS mortars specimens might be due to the slightly higher liquid/solid ratio induced by the addition of SRA (Palacios and Puertas, 2007). It is worth mentioning that the effect of activator concentration on the strength behaviour of AAS mortars was not altered by the addition of SRA at both dosages adopted in this study.

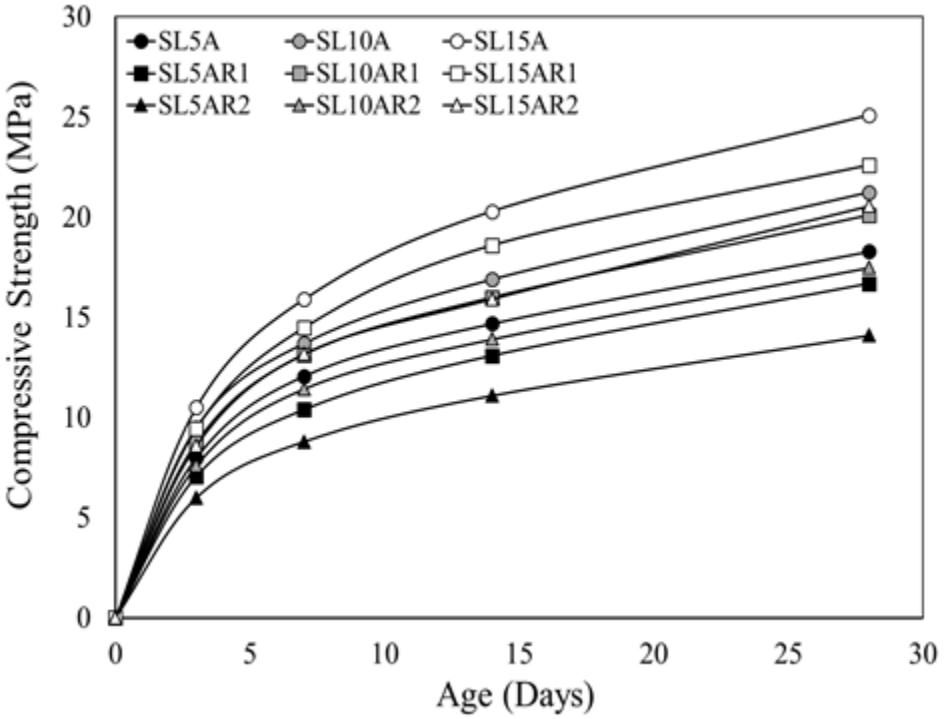

Figure 4.57 Compressive strength of ambient cured AAS mortars activated with $Ca(OH)_2$ with and without SRA.

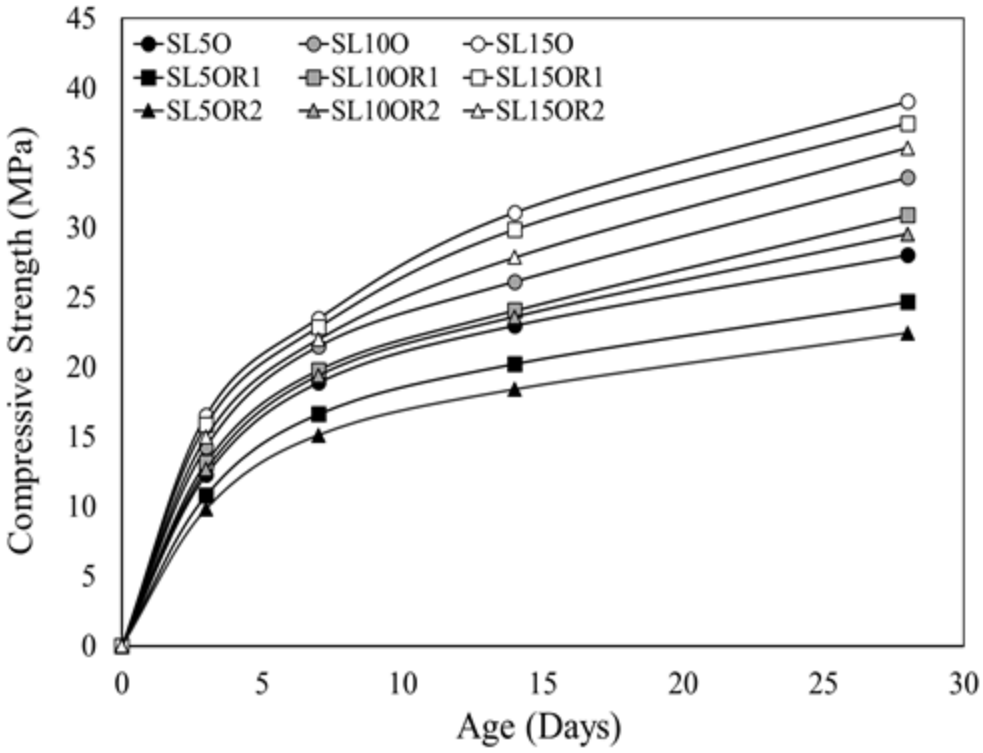

Figure 4.58 Compressive strength of oven cured AAS mortars activated with $Ca(OH)_2$ with and without SRA.

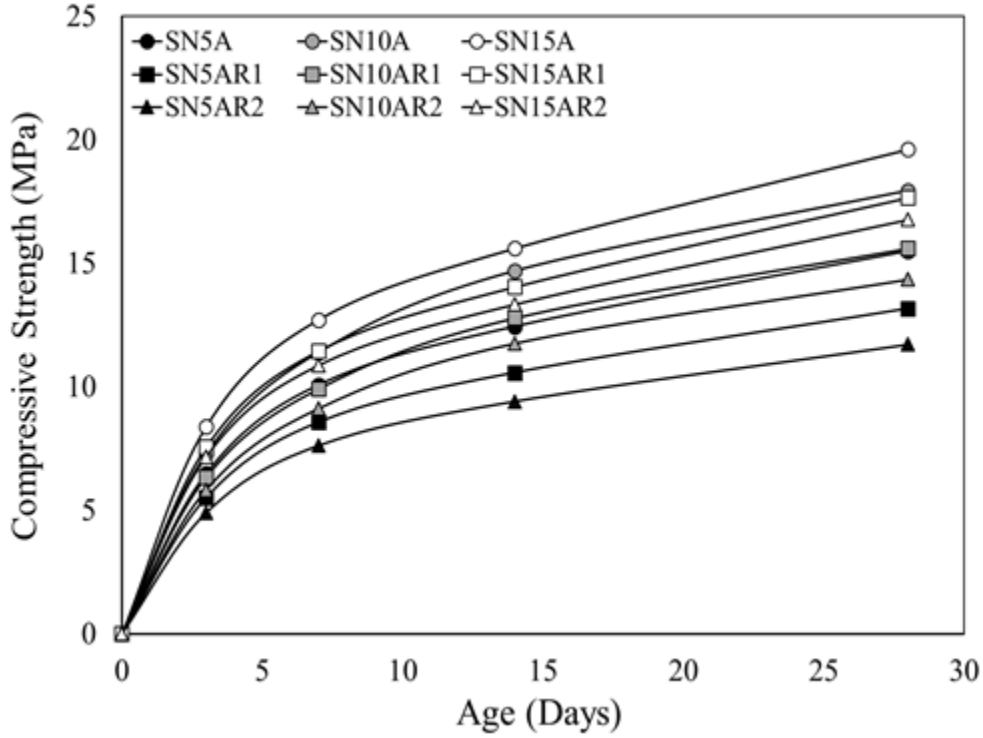

Figure 4.59 Compressive strength of ambient cured AAS mortars activated with $NaHCO_3$ with and without SRA.

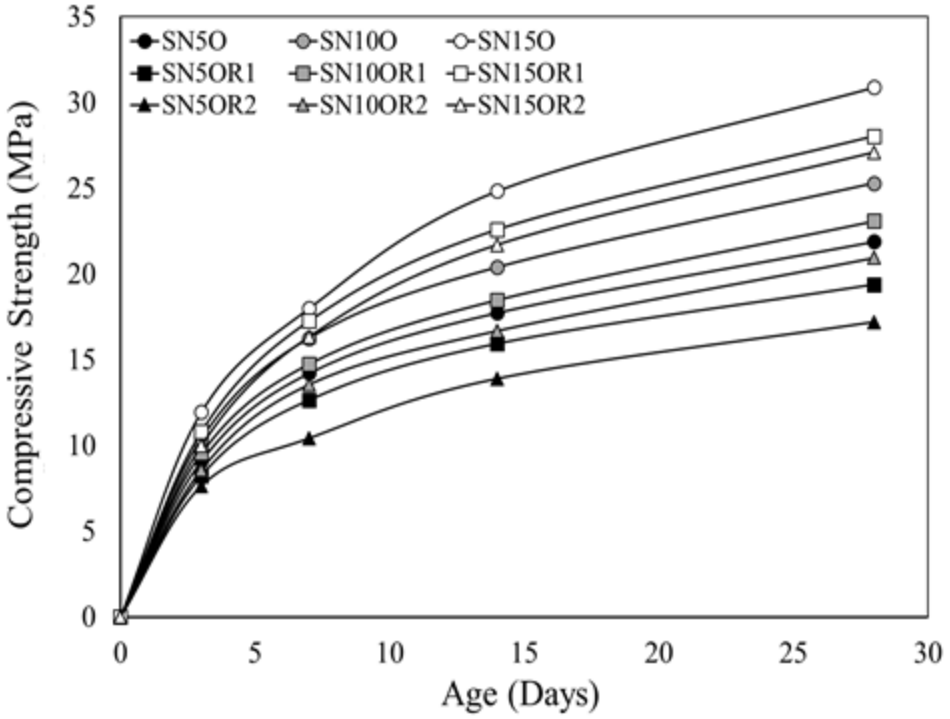

Figure 4.60 Compressive strength of ambient cured AAS mortars activated with $NaHCO_3$ with and without SRA.

4.3.3.2 Effect of SRA addition on compressive strength of two-part AAMs

The development of compressive strength for all AAM specimens, with and without SRA, was studied according to precursor type, curing condition, and age. **Figures 4.61–4.66** show the compressive strength values of AAF, AAS, and AAFS mortars activated with 3M, 6M, and 12M NaOH with and without SRA. Generally, the addition of SRA reduced the compressive strength of mortar specimens. For instance, the addition of 1% SRA admixture caused AAF mortars activated with 3M, 6M, and 12M NaOH to encounter a reduction of 5.88, 11.29, and 9.8% in the 28-day compressive strength values, respectively compared to mortars without SRA. The corresponding reduction percentages for the 2% SRA containing AAF mortars were 11.99, 18.02, and 17.2%, respectively.

Likewise, the addition of 1% SRA admixture caused ambient cured AAS mortars activated with 3M, 6M, and 12M NaOH to encounter a reduction of 9.25, 9.76, and 11.48% in the 28-day compressive strength values, respectively compared to specimens without SRA. The corresponding reductions in the 2% SRA containing AAS mortars were 16.44, 17.35, and 17.8%, respectively. A similar strength decrease trend was observed in AAFS mortars with the addition of SRA. It can be clearly seen that the reduction was even more pronounced when SRA dose increased to 2%. In general, mortar specimens activated with higher activator dosages tend to encounter lower compressive strength reductions due to SRA addition in most cases compared to the ones activated with lower dosages.

Reductions in compressive strength of oven cured AAMs varied in the range of 6.25-17.23% depending on precursor type, activator concentration, and SRA dosage used. Generally, reductions the in compressive strength of oven cured mortars due to the addition of SRA tend to be lower than those observed in ambient cured ones. For example, AAS mortar specimens containing 1% SRA and activated with 3M NaOH encountered compressive strength reductions of 9.25, and 6.81% at ambient, and oven curing temperatures, respectively. It is worth mentioning that the effect of activator concentration on compressive strength was similar in specimens with and without SRA.

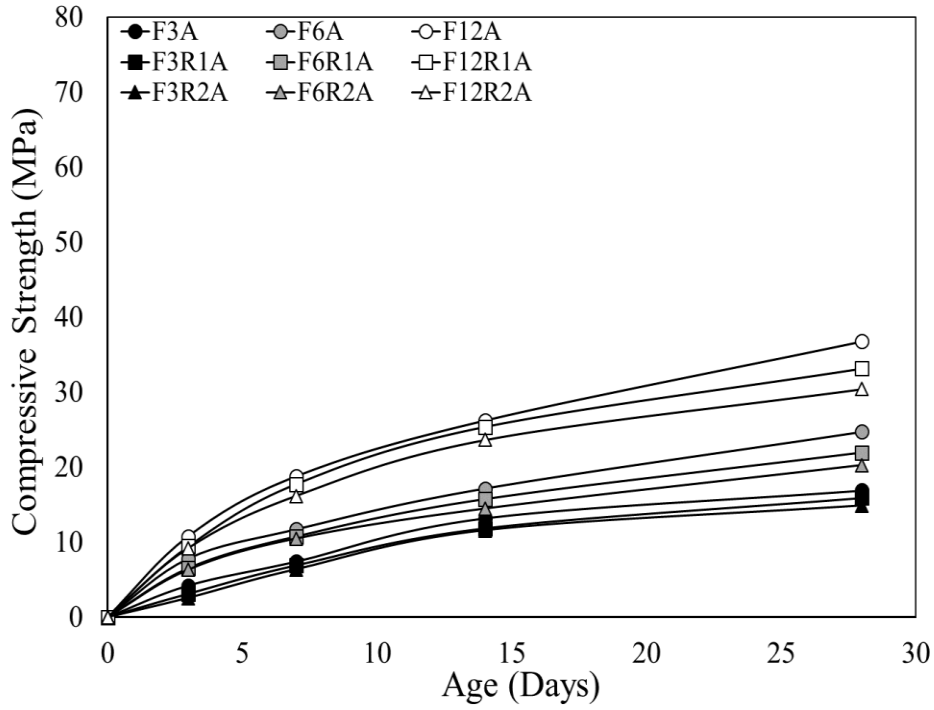

Figure 4.61 Compressive strength of AAF mortars containing 0, 1, and 2% SRA ambient cured.

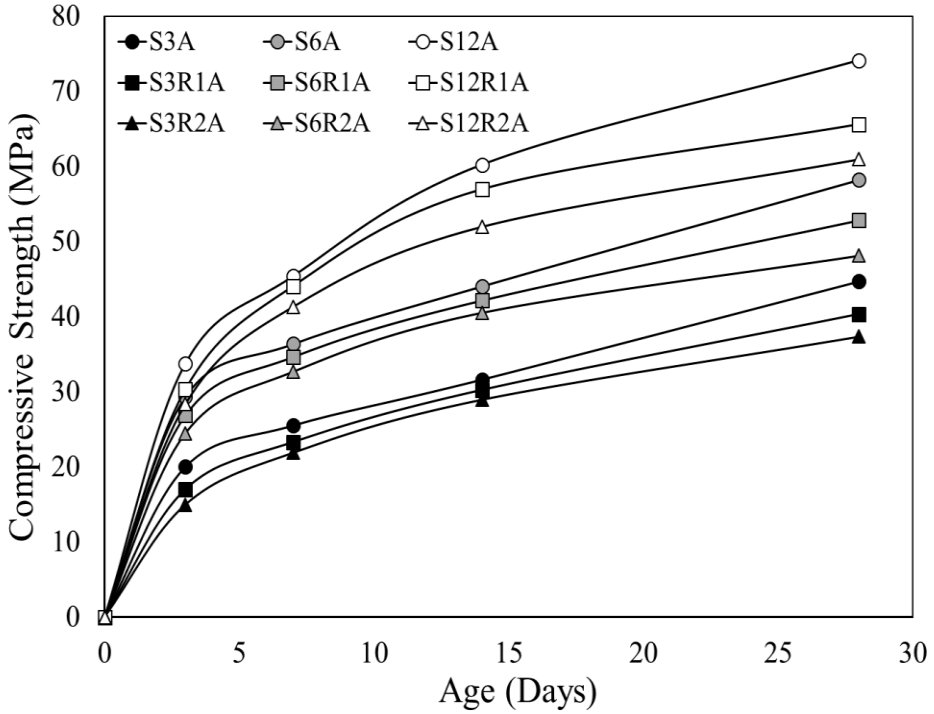

Figure 4.62 Compressive strength of AAS mortars containing 0, 1, and 2% SRA ambient cured.

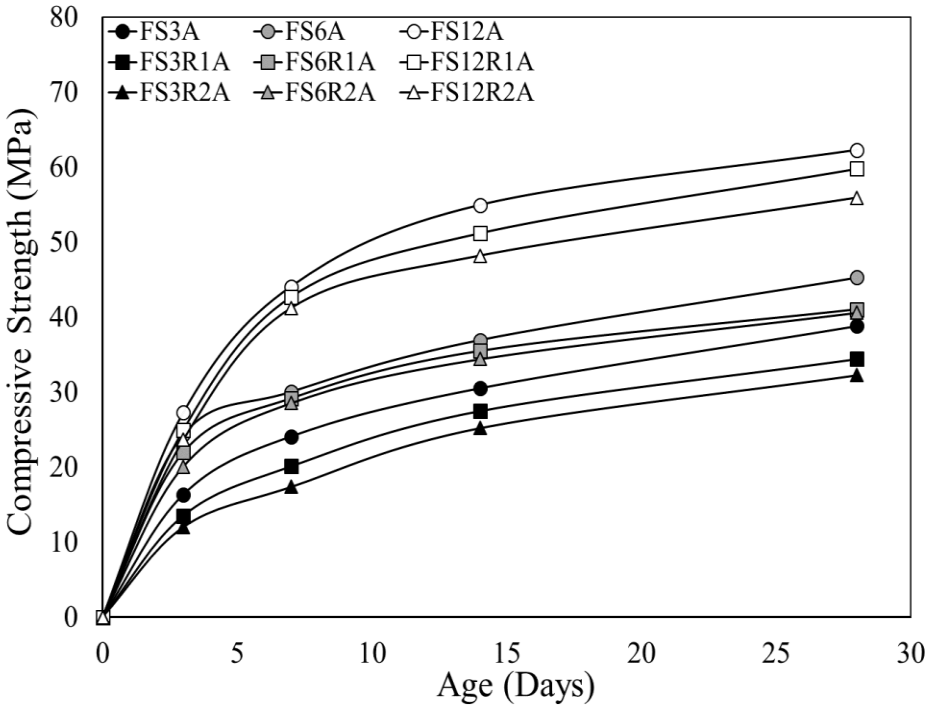

Figure 4.63 Compressive strength of AAFS mortars containing 0, 1, and 2% SRA ambient cured.

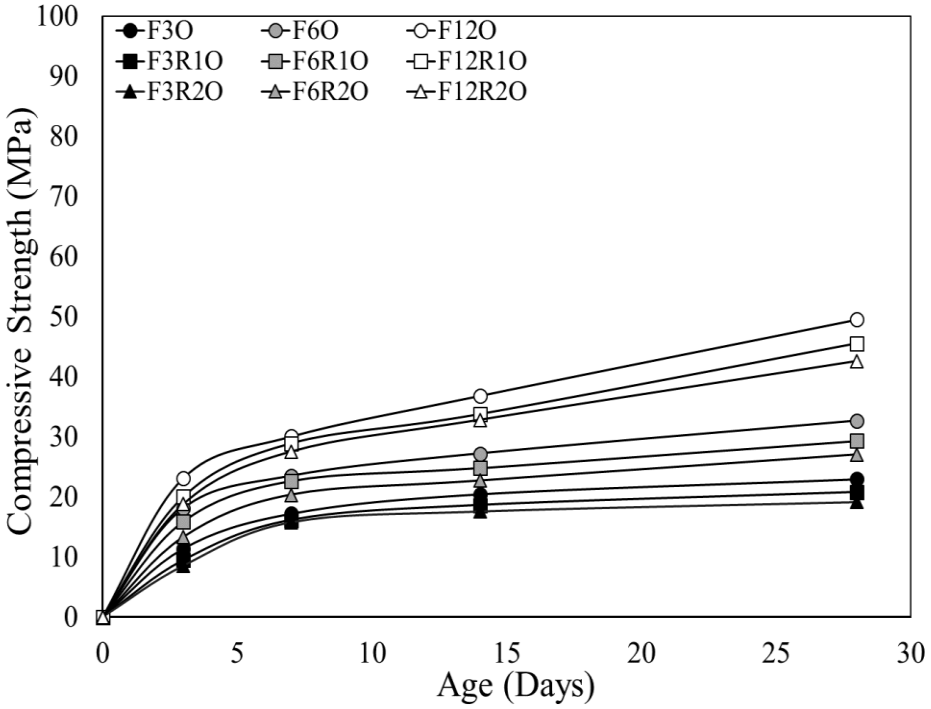

Figure 4.64 Compressive strength of AAF mortars containing 0, 1, and 2% SRA oven cured.

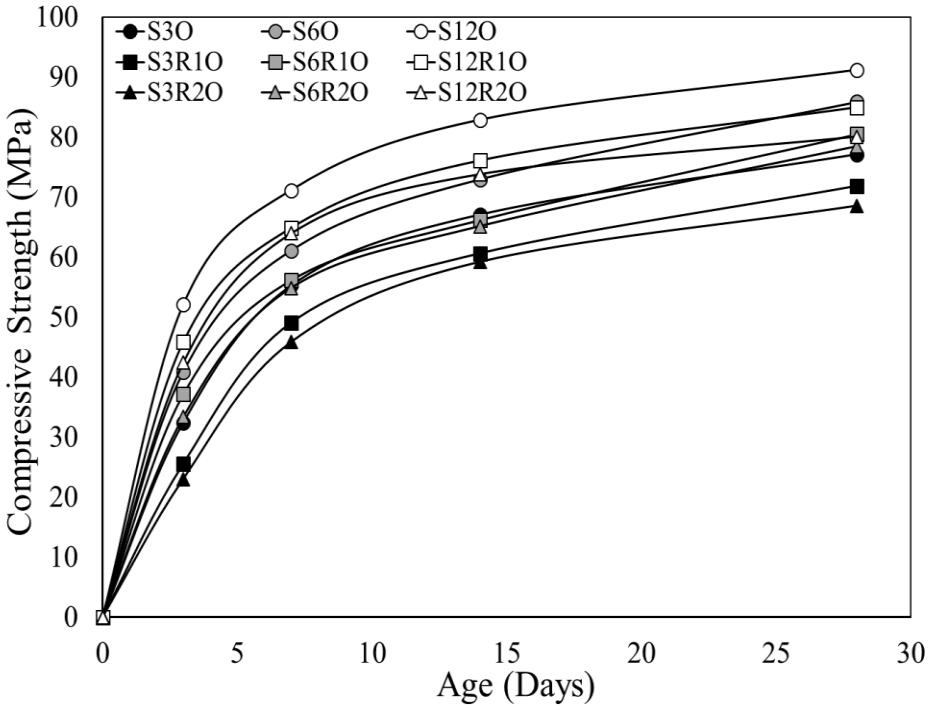

Figure 4.65 Compressive strength of AAS mortars containing 0, 1, and 2% SRA oven cured.

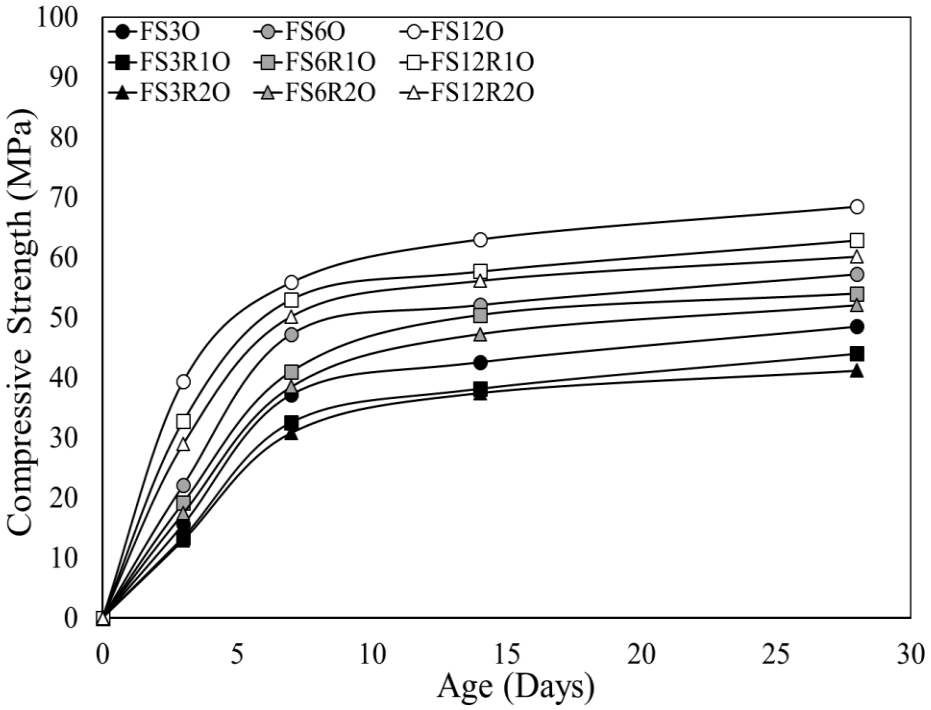

Figure 4.66 Compressive strength of AAFS mortars containing 0, 1, and 2% SRA oven cured.

4.3.4 *Heat evolution tests*

4.3.4.1 Effect of SRA addition on heat evolution of one-part AAMs

The effect of SRA addition on heat flow and cumulative heat of AAS and AAFS mortar mixtures activated with $Ca(OH)_2$ and $NaHCO_3$, were studied at 23 °C as shown in **Figs. 4.67-4.73**. The heat flow was monitored for 48 hours, however, only the first 10 hours are shown on the plot for clarification purposes as the flow rate was almost constant after that. Regardless of the activator type, it can be clearly seen that the addition of SRA reduced the heat flow, and cumulative heat exhibited by AAS and AAFS mortar mixtures. Reductions were more pronounced when SRA dosage increased from 1% to 2%. For instance, the final cumulative heat reductions in AAS mortar mixtures containing 1% SRA and activated with 5, 10, and 15% $Ca(OH)_2$ were 8.8, 5.5, and 3.8%, respectively compared to mortars without SRA. At 2% SRA, the corresponding reductions were 12.5, 10.8, and 7.1%, respectively. A similar cumulative heat reduction trend was observed in AAFS mortars activated with different doses of $Ca(OH)_2$ as shown in **Fig. 4.72**. SRA addition tends to reduce the initial heat flow peak, previously attributed to the initial wetting and dissolution of precursor solid materials (Provis, 2017) as shown in **Figs 4.67 and 4.68**.

Furthermore, cumulative heat reductions in AAS mortar mixtures containing 1% SRA and activated with 5, 10, and 15% $NaHCO_3$ were 22.3, 19.3, and 14.5%, respectively compared to specimens without SRA. While when 2% SRA dosage is used, cumulative heat reductions in AAS mortars increased to 25.9, 23.4, and 18.8%, respectively. Similar heat reduction behaviour was observed in AAFS mortars activated with $NaHCO_3$. In general, reductions in final cumulative heat were more pronounced in mortars activated with $NaHCO_3$ compared to the ones activated with $Ca(OH)_2$ as shown in **Figs. 4.70-4.73.**

Regardless of activator type, reductions in cumulative heat due to SRA addition were affected by the activator dosage. As activator dose increased, lower reductions were observed.

SRA addition induces changes in the chemical reactions occurring during the hydration process and strength development of AAS and AAFS mortars. The addition of SRA seems to retard the degree of hydration reaction in mortar specimens to some extent, as the cumulative heat exhibited by those specimens was dropped. This is also supported by the previously reported reductions in the 28 days compressive strength encountered by AAS and AAFS mortars due to the addition of SRA. The relation between cumulative heat exhibited and compressive strength achieved seem to be directly proportional.

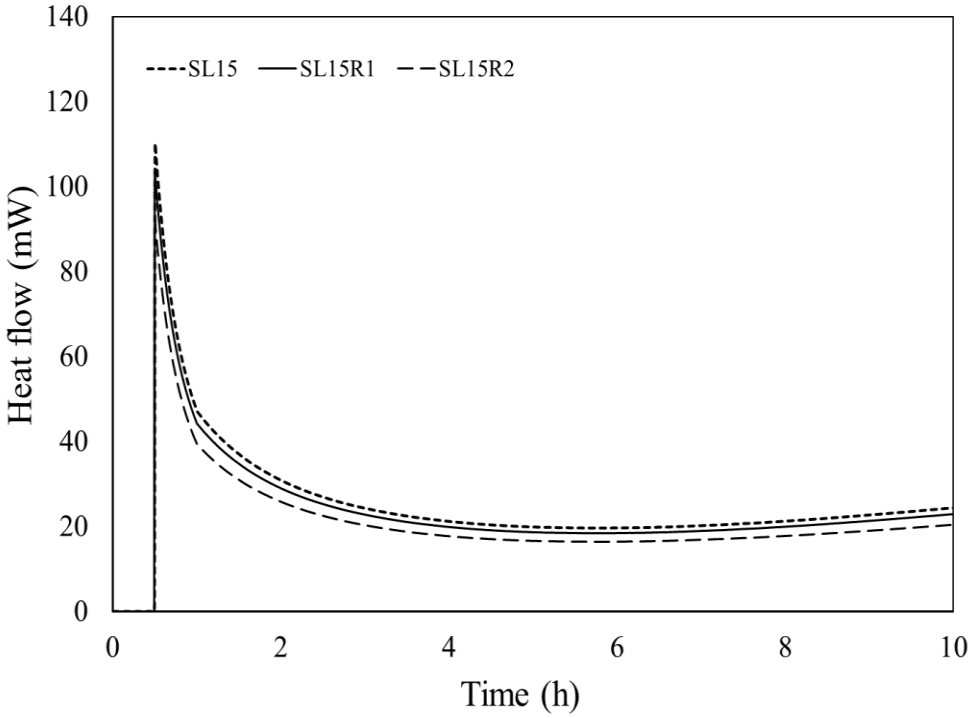

Figure 4.67 Heat flow of AAS mortars activated with 15% $Ca(OH)_2$ with and without SRA.

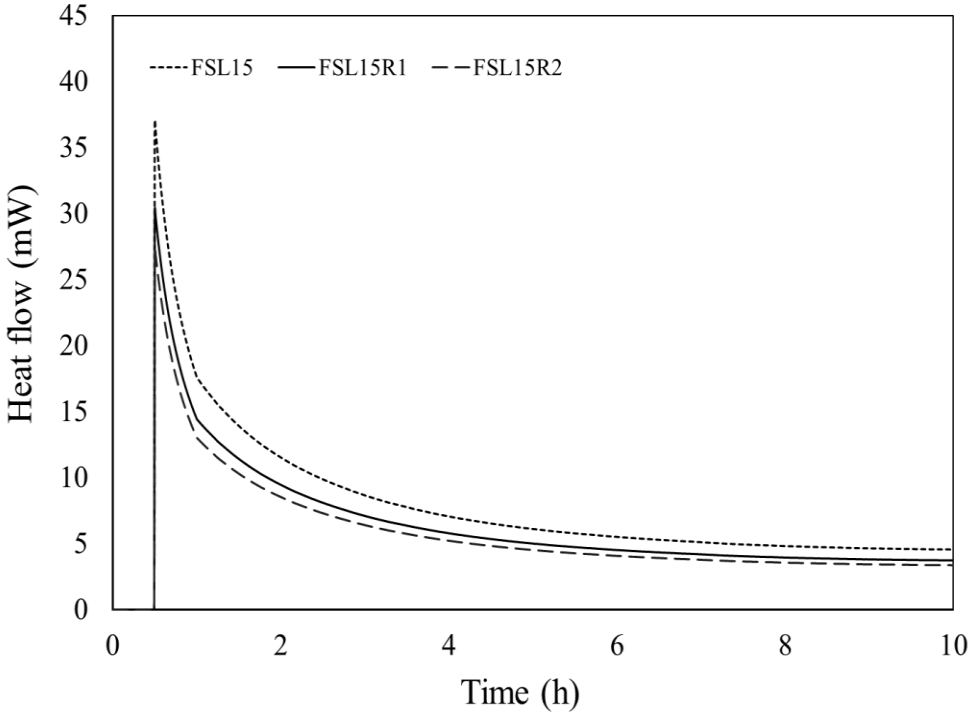

Figure 4.68 Heat flow of AAFS mortars activated with 15% $Ca(OH)_2$ with and without SRA.

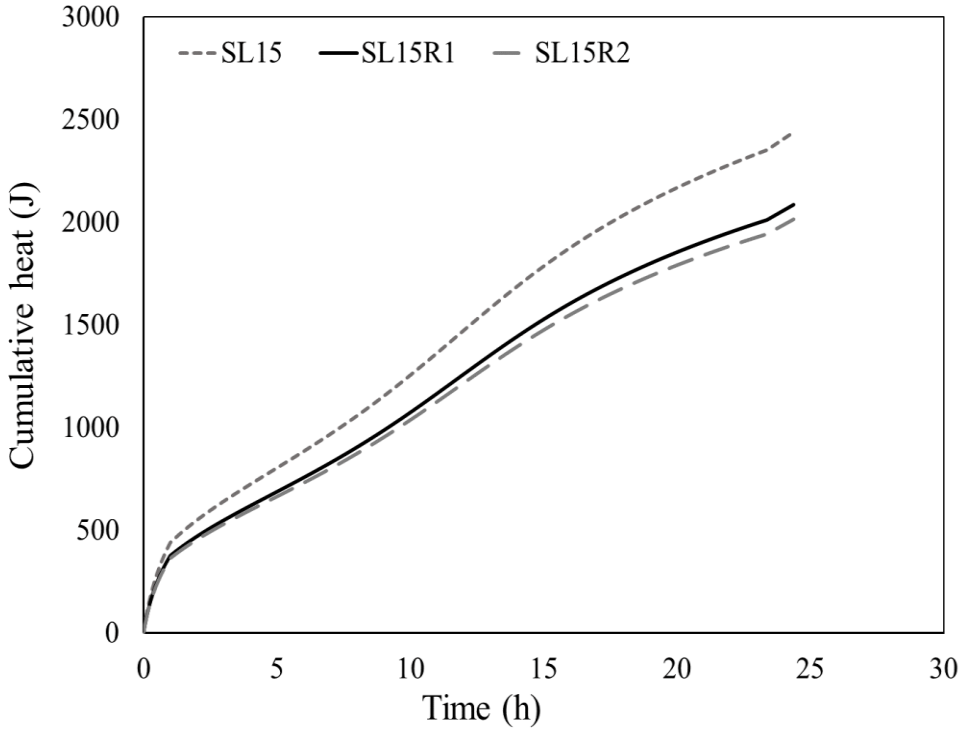

Figure 4.69 Cumulative heat of 15% $Ca(OH)_2$ AAS mortars with and without SRA.

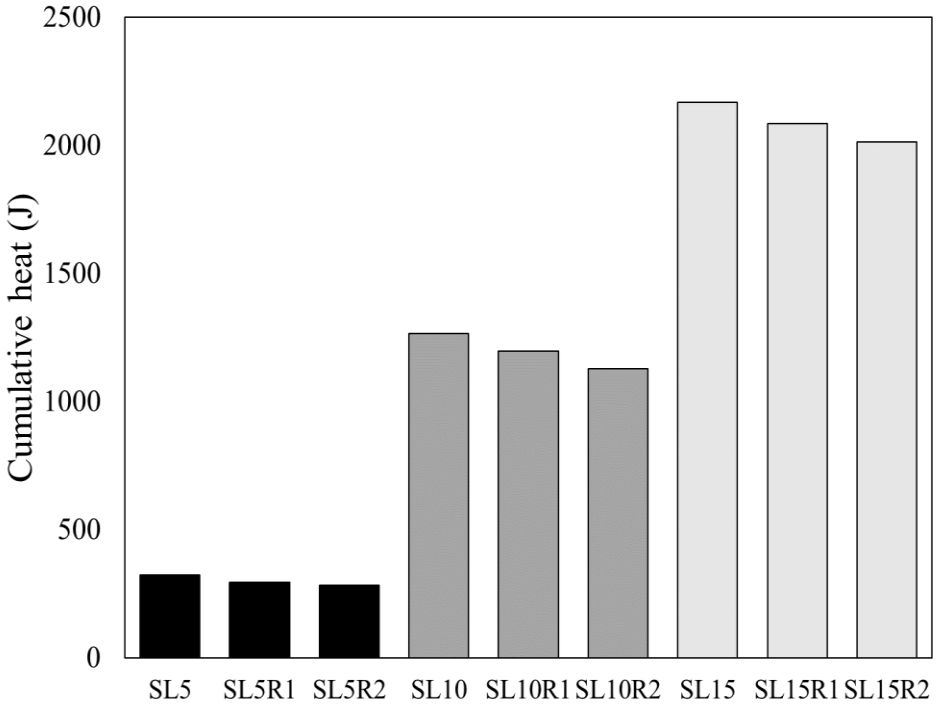

Figure 4.70 Cumulative heat of AAS mortars activated with $Ca(OH)_2$ with and without SRA.

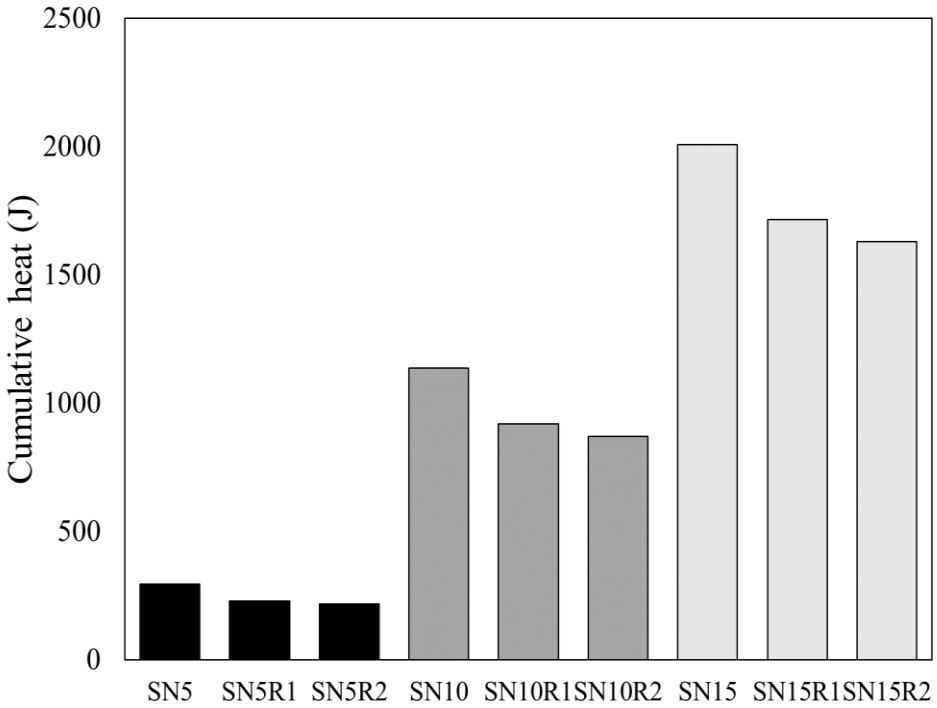

Figure 4.71 Cumulative heat of AAS mortars activated with $NaHCO_3$ with and without SRA.

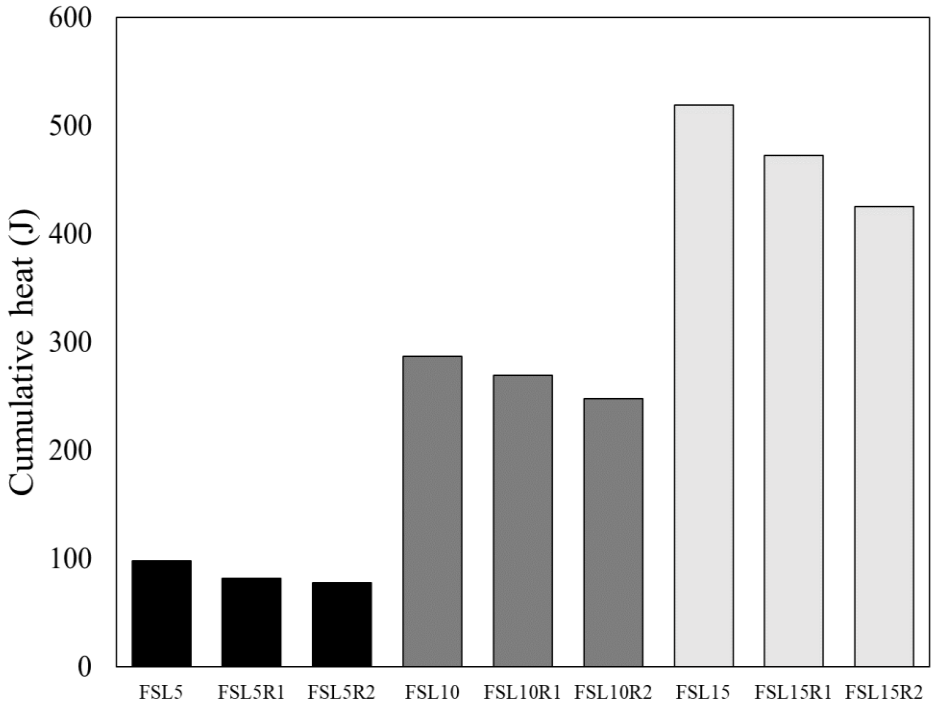

Figure 4.72 Cumulative heat of AAFS mortars activated with $Ca(OH)_2$ with and without SRA.

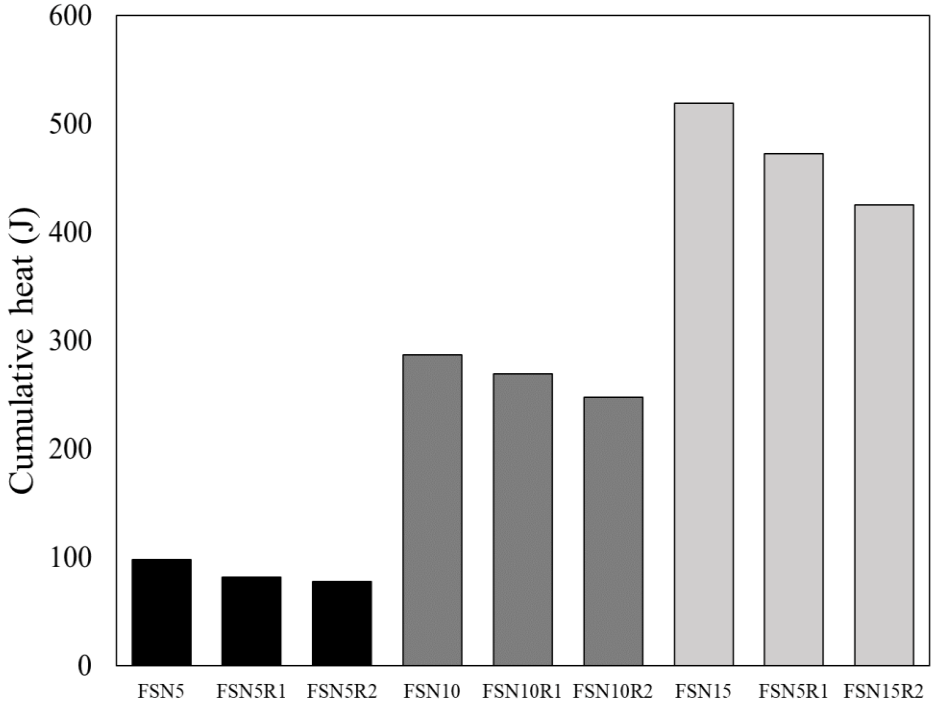

Figure 4.73 Cumulative heat of AAFS mortars activated with $NaHCO_3$ with and without SRA.

4.3.4.2 Effect of SRA on heat evolution of two-part AAMs

The effect of SRA addition on the cumulative heat released by AAF, AAS, and AAFS mortars was studied at 23 °C as shown in **Figs. 4.74-4.75**, respectively. Moreover, the heat flow behavior of AAF, AAS, and AAFS mortars with SRA addition is plotted in **Figs. 4.76-4.77**, respectively. Regardless of the precursor type, it can be clearly seen that the addition of SRA reduced the heat flow peak and the cumulative heat exhibited by the mortar specimens studied. Reductions were more pronounced when SRA dose increased from 1% to 2%. For instance, final cumulative heat reduction experienced by AAF mixtures containing 1% SRA and activated with 3M, 6M, and 12M NaOH were 10.55, 8.13, and 7.06%, respectively, compared to mixtures without SRA. Furthermore, at 2% SRA dosage, reductions were 15.78, 13.27, and 10.24%, respectively. The corresponding reductions in the initial heat flow peak were 17.55, 14.86, and 12.42%, respectively at 1% SRA and 23.48, 19.59, and 14.58%, respectively at 2% SRA.

The final cumulative heat reductions in AAS mixtures containing 1% SRA and activated with 3M, 6M, and 12M NaOH at 48h were 6.36, 4.59, and 2.59% respectively, compared to mixtures without SRA. While, when 2% SRA dose is used, reduction percentages of AAS mixtures increased to 9.86, 7.45, and 5.46%, respectively. The corresponding reductions in the heat flow peak were 10.45, 8.76, and 6%, respectively at 1% SRA and 17.55, 13.42, and 9.59%, respectively at 2% SRA. Furthermore, final cumulative heat reductions in AAFS mixtures containing 1% SRA and activated with 3M, 6M, and 12M NaOH at 48h were 8.11, 6.26, and 4.79%, respectively compared to mixtures without SRA. While, when 2% SRA dose is used, reduction percentages of AAS mixtures increased to 12.60, 9.76, and 6.90%, respectively. The corresponding reductions in the heat flow peak were 14.22, 12.12, and 9.04%, respectively at 1% SRA and 21.73, 17.28, and 12.64%, respectively at 2% SRA. Regardless of SRA dosage and activator concentration, reductions in both heat flow peak, and final cumulative heat where the highest in AAF mortar

mixtures followed by AAFS, and finally, AAS mixtures. The addition of SRA did not show any changes in the heat flow or cumulative heat pattern with time compared to specimens without SRA. The pattern was typical indicating only reductions in the heat flow rates and overall cumulative heat exhibited. This suggests minimal changes in the chemical reactions occurring during the hydration process and strength development of AAM due to the addition of SRA.

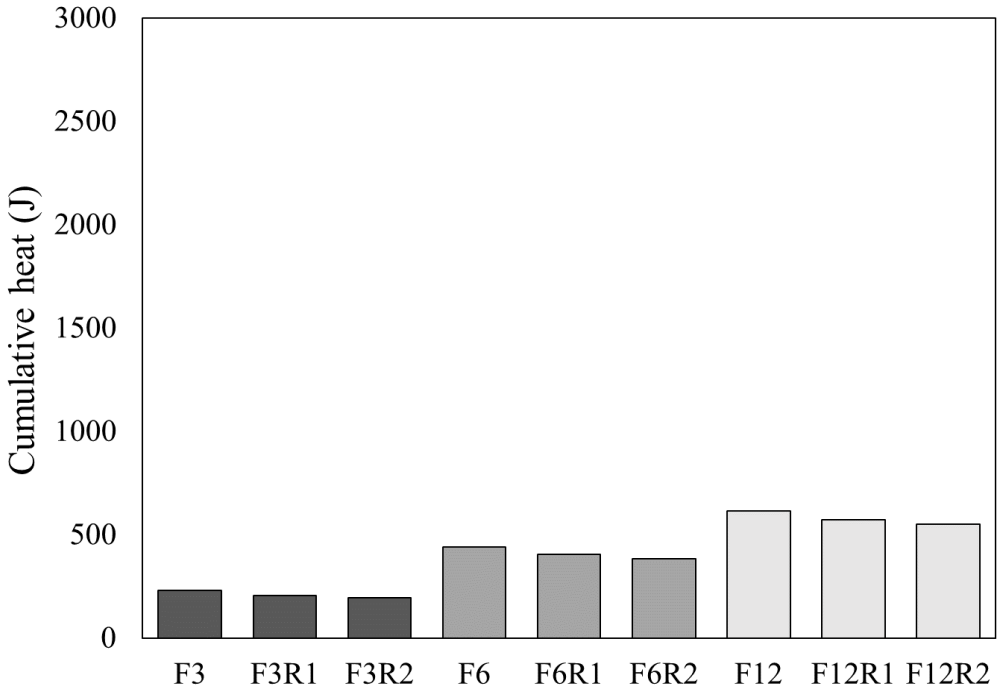

Figure 4.74 Cumulative heat of AAF mortars activated using NaOH of different concentration.

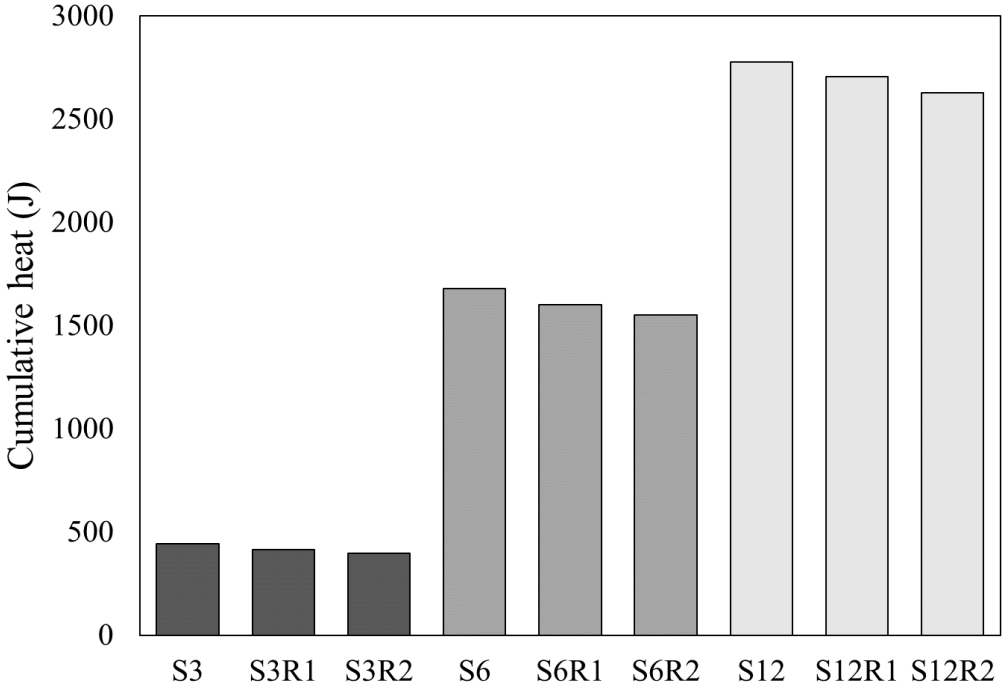

Figure 4.75 Cumulative heat of AAS mortars activated using NaOH of different concentration.

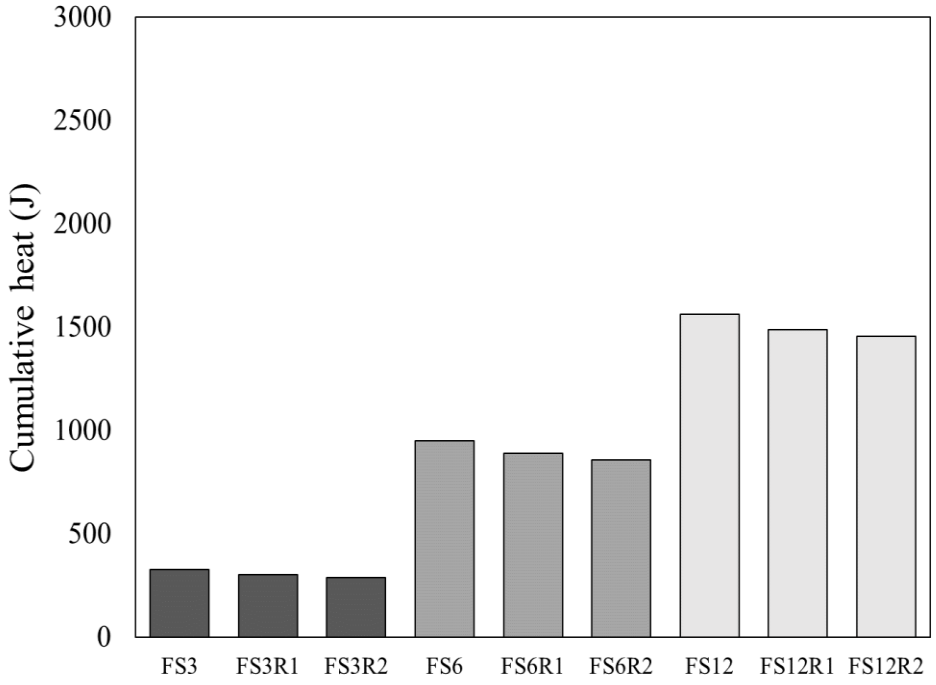

Figure 4.76 Cumulative heat of AAFS mortars activated using NaOH of different concentration.

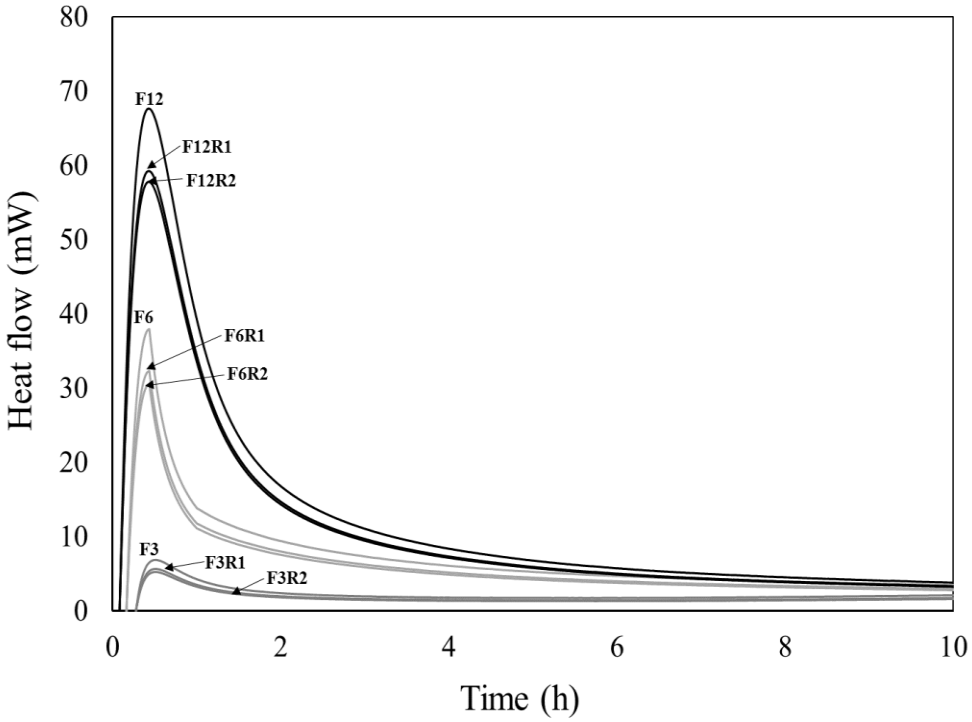

Figure 4.77 Heat flow of different mortars activated with different concentration of NaOH.

4.3.4.3 Effect of heat evolution on compressive strength of two-part AAMs

Figures 4.78-4.81 below show the relationship between cumulative heat exhibited and compressive strength achieved for AAF, AAS, and AAFS mortars tested. The relationship clearly suggested that AAS mixtures had the highest slope gradient followed by AAFS, and finally, AAF mixtures. Regardless of precursor type, the relation between cumulative heat and compressive strength showed slope gradients that were almost linear, with AAS mortars having the steepest gradient. The relationship is directly proportional suggesting that when higher heat is exhibited, higher compressive strength is achieved.

It is well known that the formation and polymerization of binder gels are responsible for the induced cumulative heat (Yao *et al*., 2009; Chithiraputhiran and Neithalath, 2013). AAF mortar is well known to have a low hydration reaction rate at room temperature. On the other hand, AAS mortar is known to have an accelerated hydration reaction because of the high CaO content

compared to fly ash. The polymerization and condensation of geopolymer gels are exothermic and make the main contribution to the exhibited heat (Yao *et al*., 2009). Hence, in AAS mortars the higher exhibited heat can be attributed to the accelerated hydration reaction and high content of CaO. Higher hydration reaction degree with higher CaO content will eventually increase the formation of binder gels. This will cause specimens to achieve higher compressive strength, but also release extra exothermic heat.

Figure 4.78 Cumulative heat and compressive strength relation of AAF mortars.

Figure 4.79 Cumulative heat and compressive strength relation of AAS mortars.

Figure 4.80 Cumulative heat and compressive strength relation of AAFS mortars.

Figure 4.81 Cumulative heat and compressive strength relation of AAF, AAS, and AAFS mortars.

4.3.5 *Drying shrinkage*

4.3.5.1 Effect of SRA on drying shrinkage of one-part AAMs

Previous studies had shown that SRA at various dosages proved successful in reducing shrinkage strains experienced by two-part sodium silicate activated mortars (Palacios and Puertas, 2007). Drying shrinkage strains of AAS mortars activated with 5, 10, and 15% $Ca(OH)_2$ $NaHCO_3$, with and without SRA, are plotted in **Figs. 4.82 -4.85**. Regardless of activator dosage, results indicated reductions in the drying shrinkage strains of AAS mortars with the addition of SRA compared to samples without SRA. Reductions in the final drying shrinkage of ambient cured AAS mortars activated with 5, 10, and 15% $Ca(OH)_2$, caused by the addition of 1% SRA were 12.6, 11.3, and 11%, respectively compared to mortars without SRA. The corresponding reduction percentages in final drying shrinkage, when 2% SRA was used were 30.31, 29.6, and 21.66%, respectively. Moreover, reduction percentages in the final drying shrinkage of ambient cured AAS mortars

activated with 5, 10, and 15% $NaHCO_3$ caused by the addition of 1% SRA were 13.2, 17.25, and 19.8%, respectively compared to mortars without SRA. When 2% SRA was used, reductions were 31, 27.5, and 30.6%, respectively.

On the other hand, reduction percentages in the final drying shrinkage of oven cured AAS mortars activated with 5, 10, and 15% $Ca(OH)_2$, caused by the addition of 1% SRA were 14.7, 11.85, and 9.6%, respectively compared to mortars without SRA. When 2% SRA was used, reductions were 31, 28, and 21.2%, respectively. Reductions in drying shrinkage strains increased with higher SRA dosage. Reductions in drying shrinkage due to SRA addition was almost equal in AAS mortars activated with both activators. Nevertheless, the relationship between shrinkage reduction and compressive strength achieved was inversely proportional. The effect of SRA addition is twofold as specimens which achieved higher shrinkage reductions due to SRA addition encountered higher compressive strength reductions on the other hand. The previously noted reduction in surface tension of water in the porous system prompted by SRA proved efficient in one-part AAMs similar to two-part AA ones.

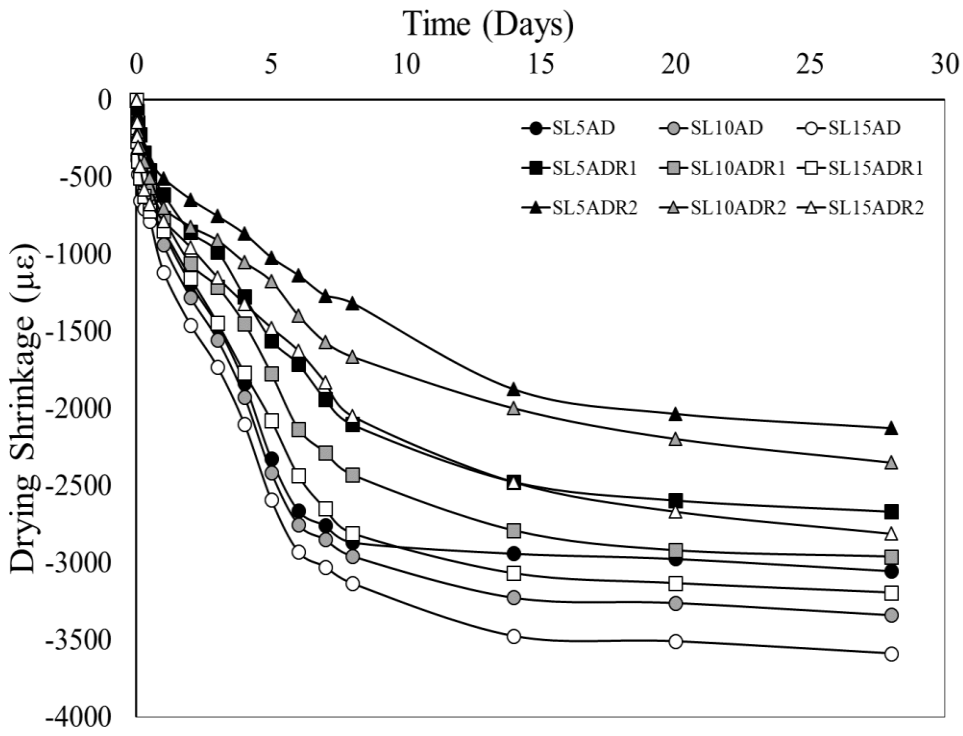

Figure 4.82 Drying shrinkage of AAS mortars activated with $Ca(OH)_2$ containing 0, 1, and 2% SRA (ambient cured).

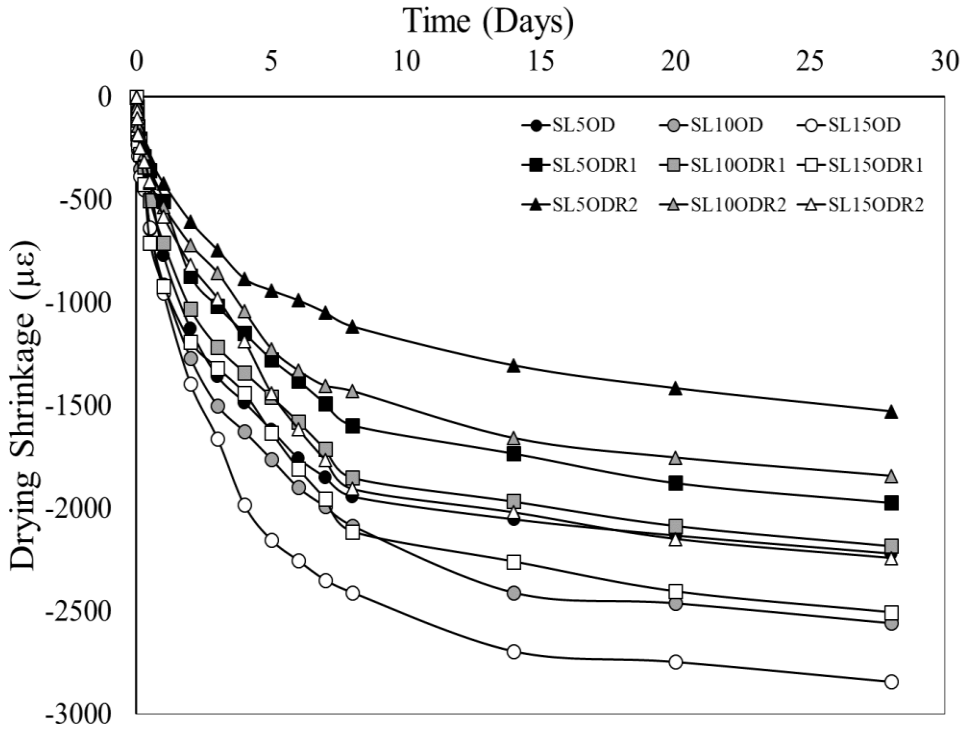

Figure 4.83 Drying shrinkage of AAS mortars activated with $Ca(OH)_2$ containing 0, 1, and 2% SRA (ambient cured).

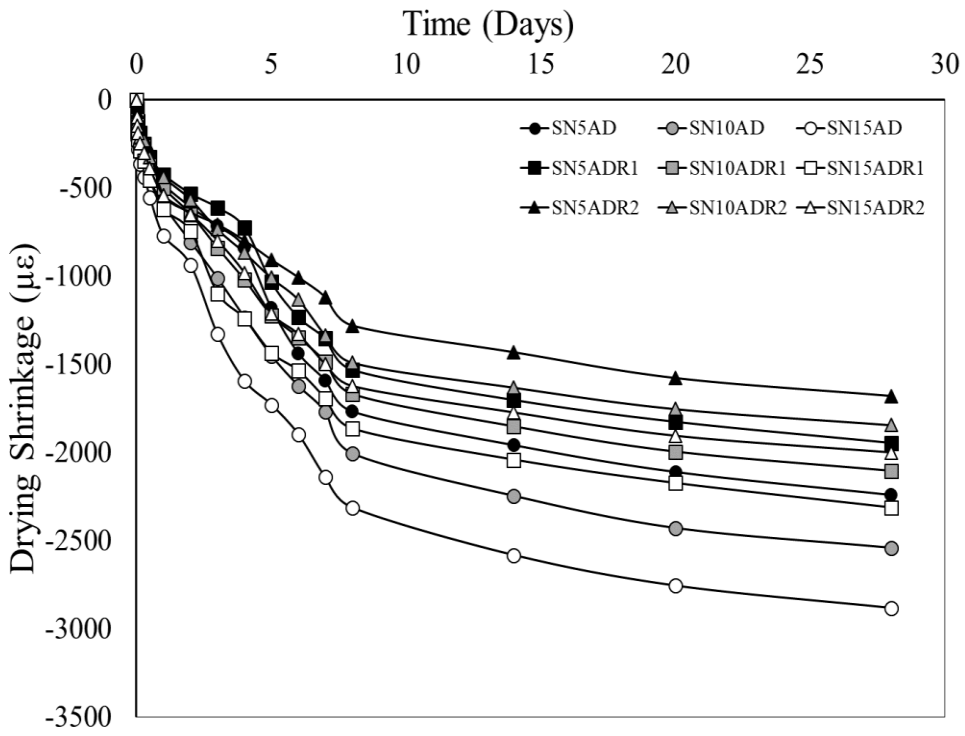

Figure 4.84 Drying shrinkage of AAS mortars activated with $NaHCO_3$ containing 0, 1, and 2% SRA (ambient cured).

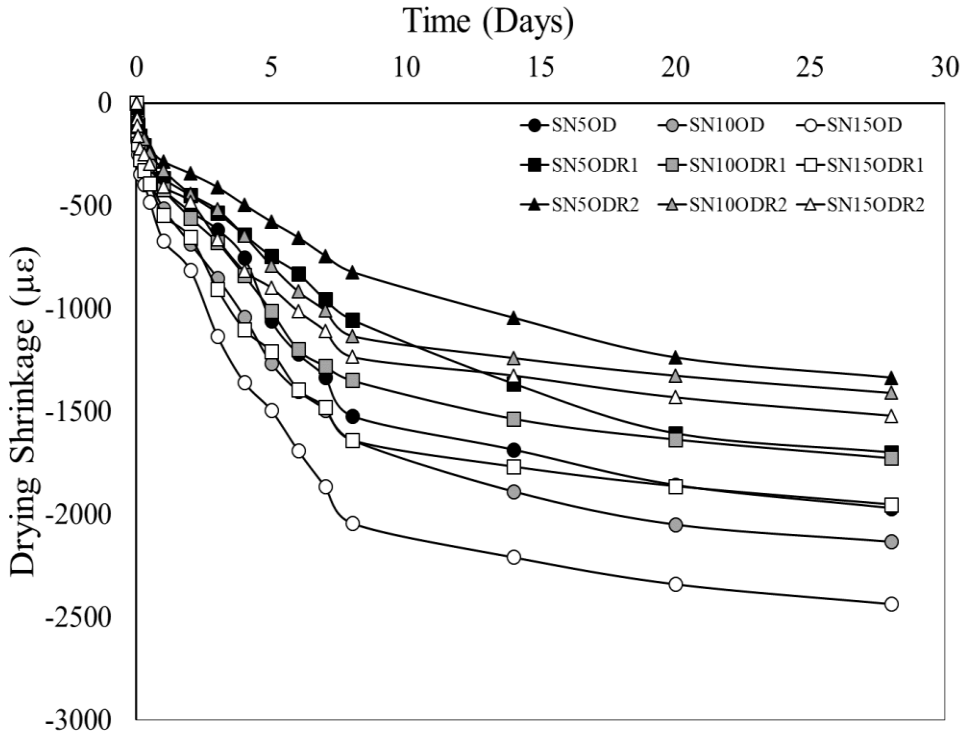

Figure 4.85 Drying shrinkage of AAS mortars activated with $NaHCO_3$ containing 0, 1, and 2% SRA (ambient cured).

4.3.5.2 Effect of SRA on drying shrinkage of two-part AAMs

The effect of SRA addition on the drying shrinkage strains of two-part AAM specimens was studied. Drying shrinkage strains of ambient cured AAF, AAS, and AAFS mortars containing 0, 1, and 2% SRA and activated with 3M, 6M, and 12M (NaOH) concentrations are plotted in **Figs. 4.86-4.91**. Regardless of precursor type and activator concentrations, results indicated reductions in the drying shrinkage of AAMs with the addition of 1% SRA compared to mortars without SRA. Reductions in drying shrinkage were more pronounced when SRA dose was increased to 2%. For instance, reductions in the total drying shrinkage of AAF mortars activated with 3M, 6M, and 12M NaOH, caused by the addition of 1% SRA were 26.79, 16.50, and 25.94%, respectively compared to mortars without SRA. When 2% SRA was used, reductions were 36.71, 26.58, and 35.96%, respectively.

Furthermore, reductions in the total drying shrinkage of AAS mortars activated with 3M, 6M, and 12M NaOH, caused by the addition of 1% SRA were 57.26, 52.35, and 52.39%, respectively compared to mortars without SRA. The corresponding reductions in total drying shrinkage, when 2% SRA was used were 67.06, 65.10, and 65.71%, respectively. Reduction percentages in the total drying shrinkage of AAFS mortars activated with 3M, 6M, and 12M NaOH, caused by the addition of 1% SRA were 55.78, 46.83, and 43.89%, respectively compared to mortars without SRA. The corresponding reduction percentages in total drying shrinkage, when 2% SRA was used were 60.21, 50.82, and 49.27%, respectively. The reduction in the total drying shrinkage was the highest in AAS mortars followed by AAFS, and finally, AAF mortars. This clearly shows the higher response of AAS mortars to SRA compared to AAF mortars, regardless of the activator concentration.

Similar reduction trend was observed in oven cured AAM specimens. Drying shrinkage reductions due to SRA addition were almost equal in oven cured specimens. Reductions also

increased with higher SRA dosages. This states clearly that higher curing temperature did not alter the mechanism of SRA. The beneficial effect of SRA is due to the decrease in the surface tension of water in the porous system prompted by the admixture and the accompanying lower internal stress induced when water evaporates during drying (Palacios and Puertas, 2007). Moreover, Collins and Sanjayan (2000) stated that SRA modified the pore structure by increasing the number of pores having a relatively higher diameter in AAS mortars. Capillary stress is much lower in these pores than in the smaller capillaries prevailing in mortars prepared with zero SRA (Palacios and Puertas, 2007). Moreover, SEM analysis carried by Palacios and Puertas (2007) has shown that the presence of SRA reduces the width and number of shrinkage-generated microcracks. Hence, SRA proved to be a successful mitigation technique for the drying shrinkage of AAMs.

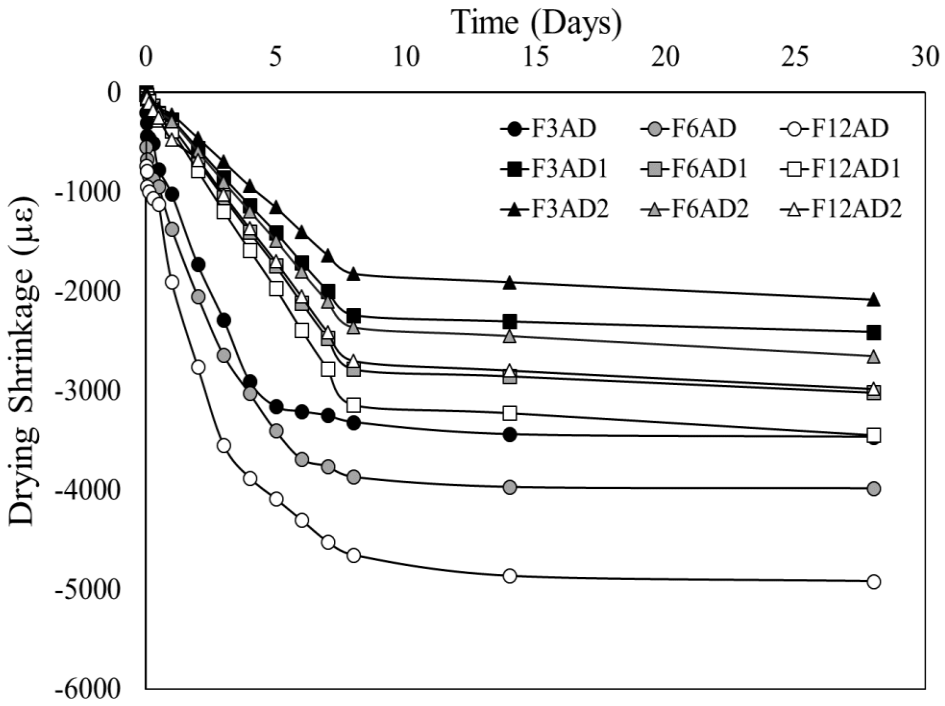

Figure 4.86 Drying shrinkage of AAF mortars containing 0, 1, and 2% SRA (ambient cured).

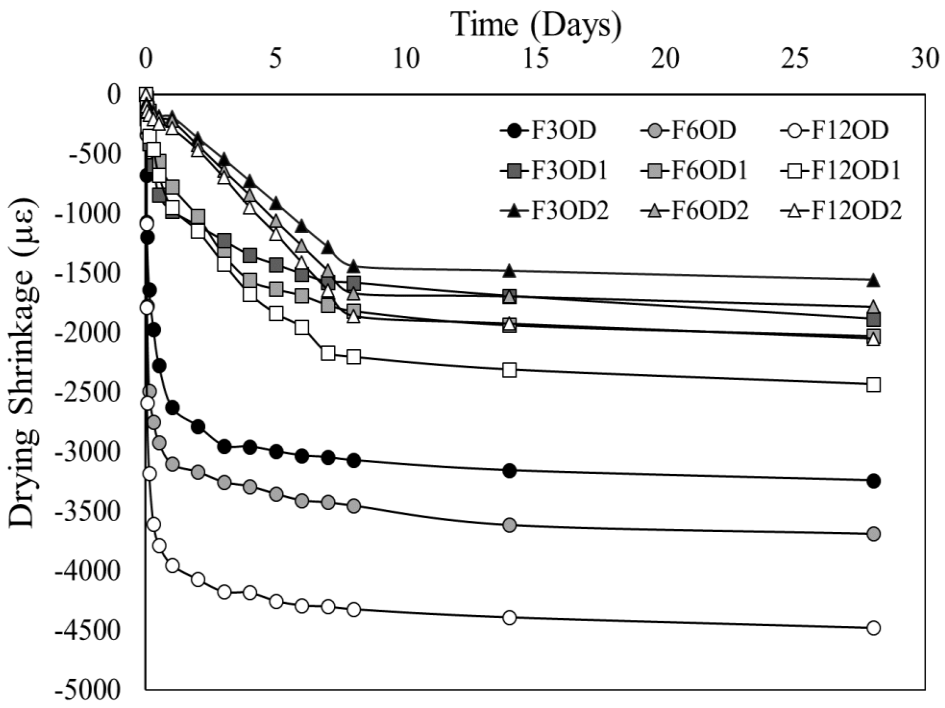

Figure 4.87 Drying shrinkage of AAF mortars containing 0, 1, and 2% SRA (oven cured).

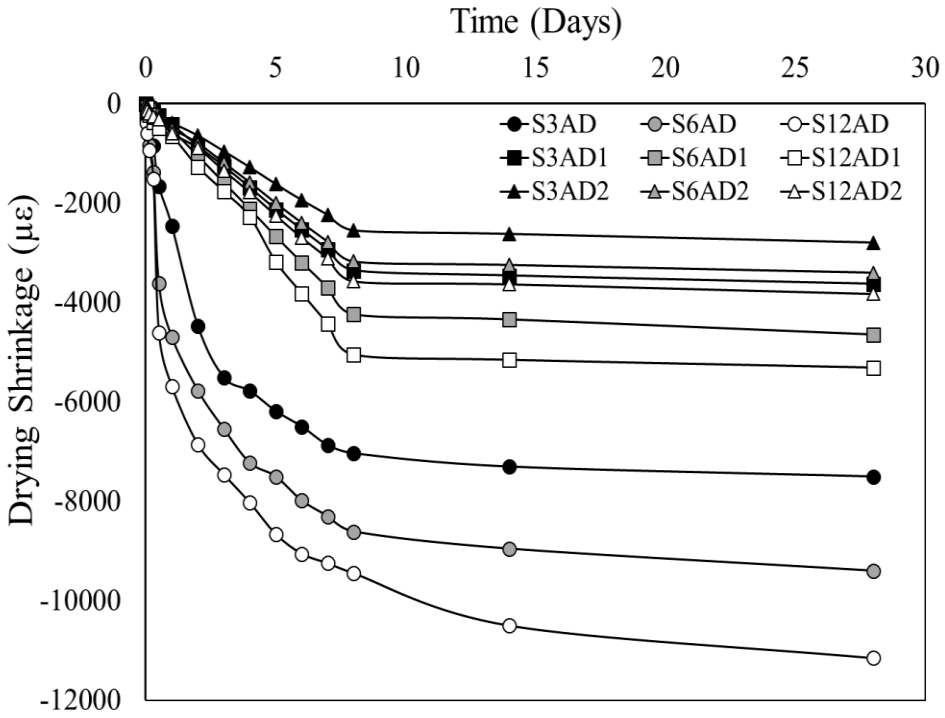

Figure 4.88 Drying shrinkage of AAS mortars containing 0, 1, and 2% SRA (ambient cured).

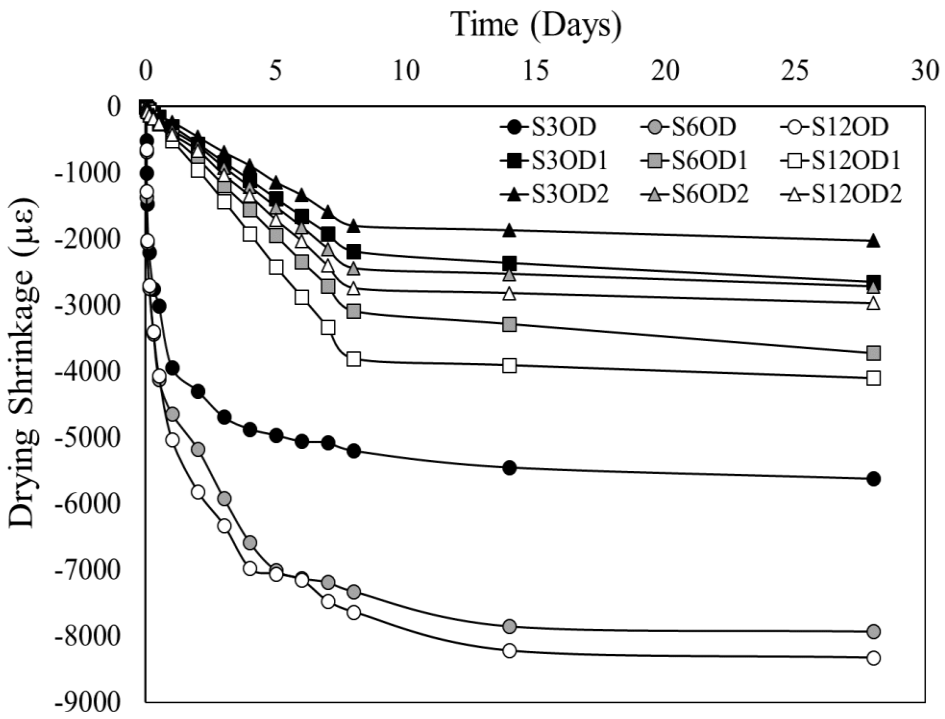

Figure 4.89 Drying shrinkage of AAS mortars containing 0, 1, and 2% SRA (oven cured).

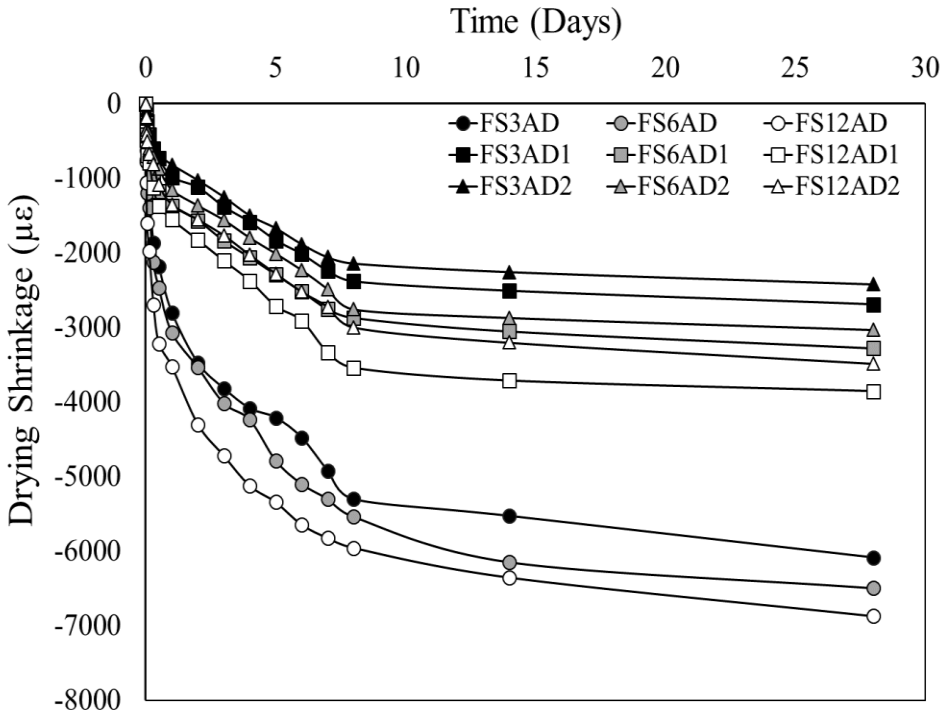

Figure 4.90 Drying shrinkage of AAFS mortars containing 0, 1, and 2% SRA (ambient cured).

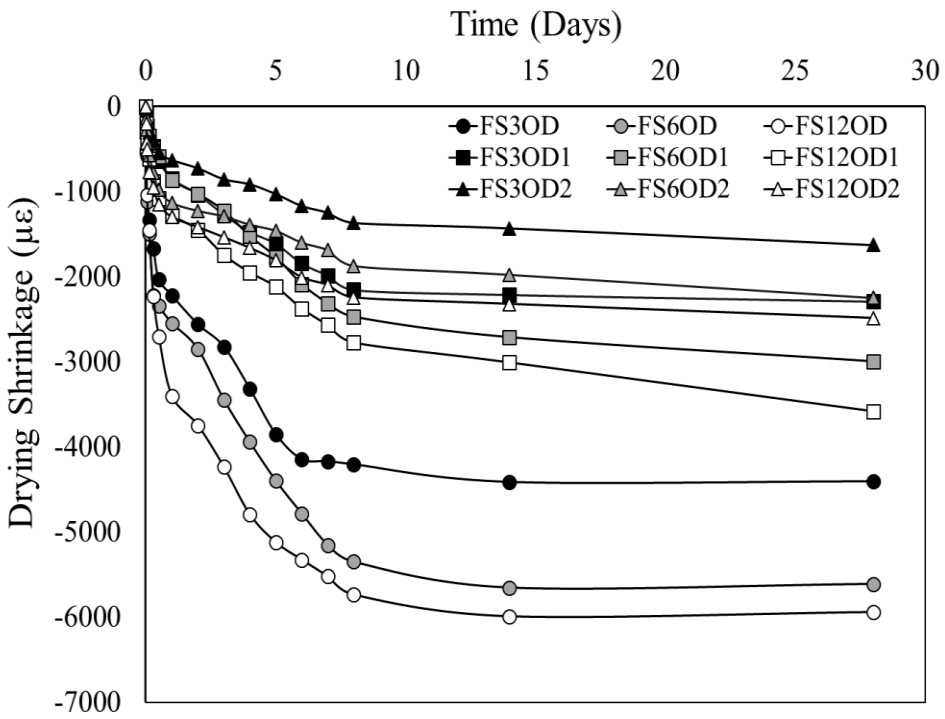

Figure 4.91 Drying shrinkage of AAFS mortars containing 0, 1, and 2% SRA (oven cured).

4.3.6 *Mass loss*

4.3.6.1 Effect of mass loss on drying shrinkage of one-part AAMs containing SRA.

Figures 4.92-4.95 show the curves representing the relationship between drying shrinkage and mass loss of AAS mortars activated with $Ca(OH)_2$ and $NaHCO_3$, containing 0, 1, and 2% SRA, where the abscissa is the mass loss, and the ordinate is drying shrinkage. It is well known that the capillary tensile stress and therefore the magnitude of shrinkage resulting from a unit mass loss, is dependent on the pore radius; hence a change in the curve slope suggests a change in pore distribution (Thomas *et al.*, 2017). An increase in the slope indicates a finer porosity, while a decrease in slope suggests a coarser porosity.

Figures 4.92, and 4.93 show the relationship between drying shrinkage and mass loss of ambient and oven cured AAS mortars activated with $Ca(OH)_2$ containing 0, 1, and 2% SRA.

Generally, the addition of SRA decreased the slope gradient of the curves due to the reduction in shrinkage rates, hence suggesting an increase in the pore size diameter compared to specimens without SRA. Higher SRA dosage of 2% caused further reduction in the curve gradient, indicating a coarser porosity compared to 1% SRA containing mortars. The total measured mass loss of SRA containing AAS mortars was slightly higher than those measured in AAS mortars without SRA. The drying shrinkage per unit mass loss was less in oven cured specimens compared to the ambient cured ones. However, the overall change in drying shrinkage per unit mass loss under oven curing was similar to the one reported under ambient curing. Similar observations were found in $NaHCO_3$ activated mortars under both curing conditions.

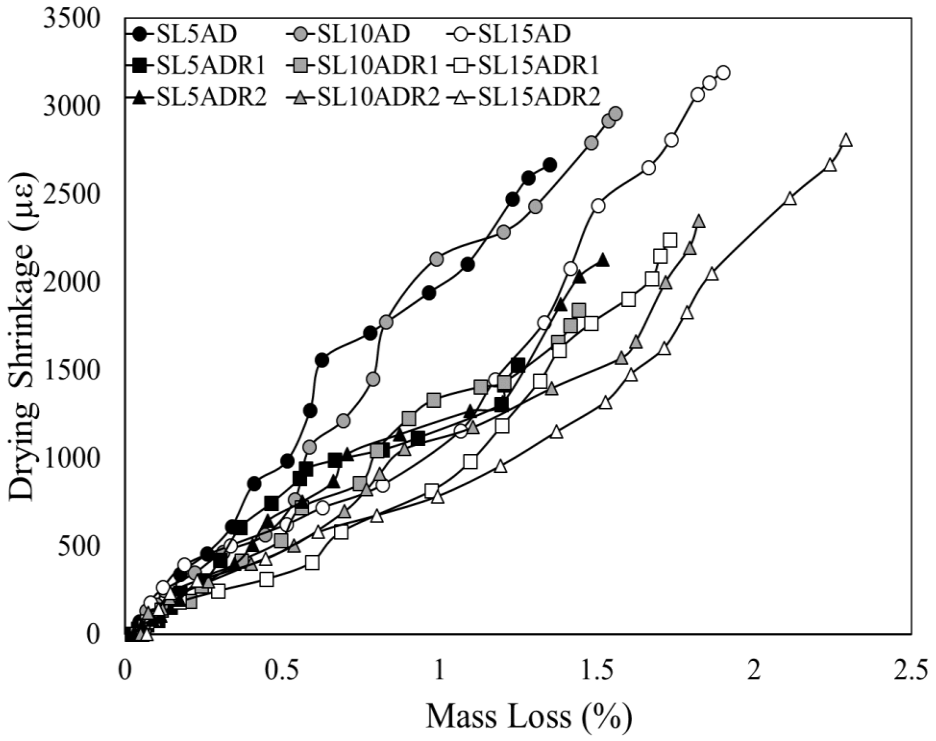

Figure 4.92 Mass loss vs. drying shrinkage of $Ca(OH)_2$ activated slag mortars with and without SRA (ambient cured).

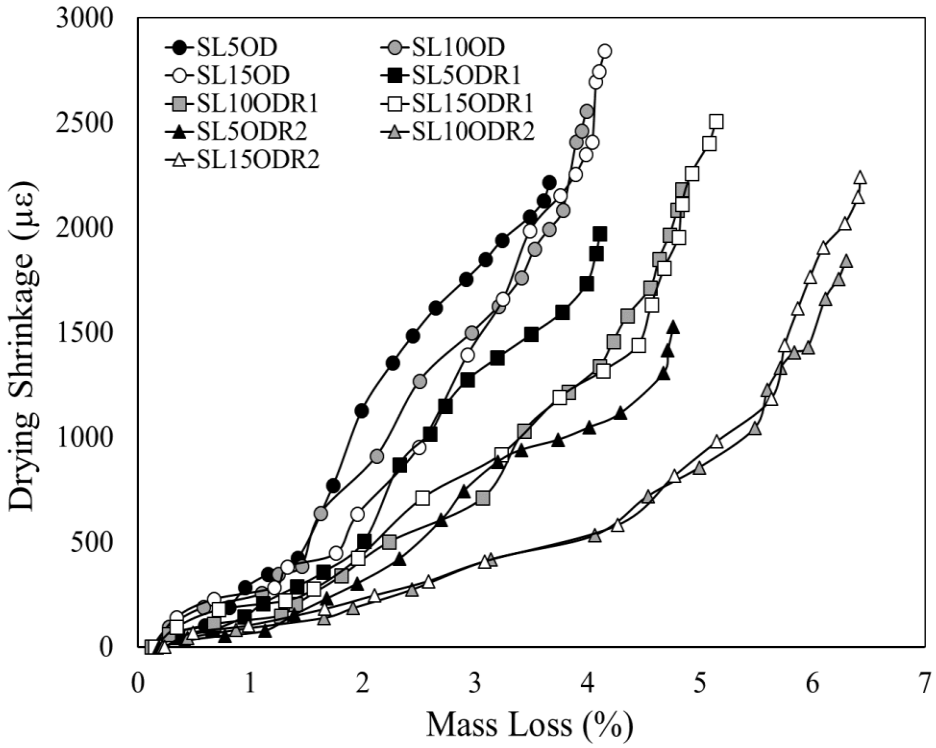

Figure 4.93 Mass loss vs. drying shrinkage of $Ca(OH)_2$ activated slag mortars with and without SRA (oven cured).

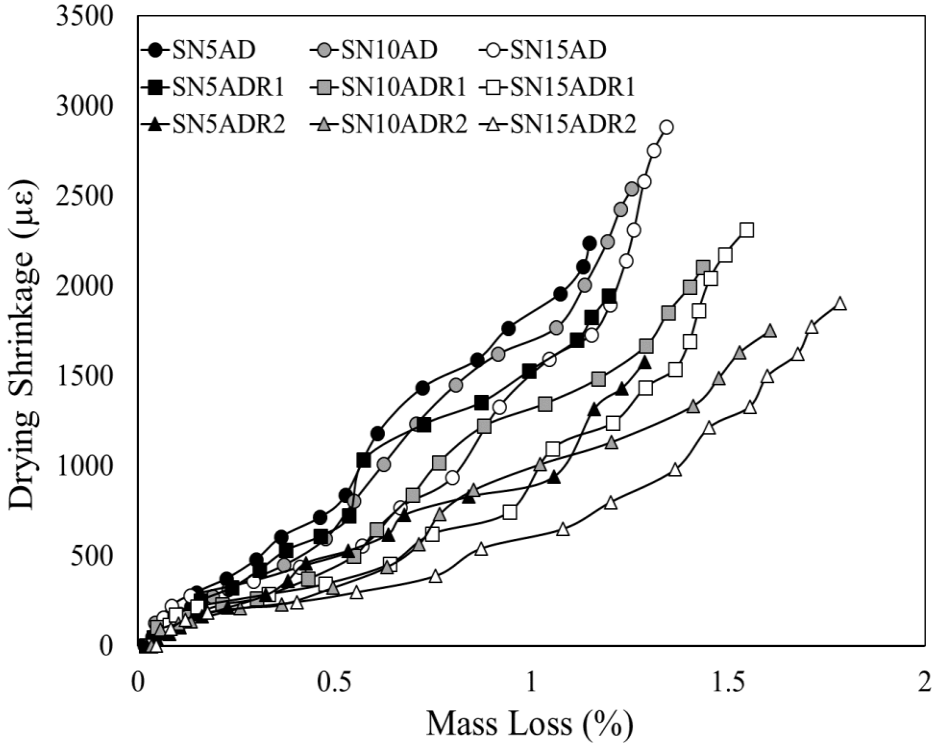

Figure 4.94 Mass loss vs. drying shrinkage of $NaHCO_3$ activated slag mortars with and without SRA (ambient cured).

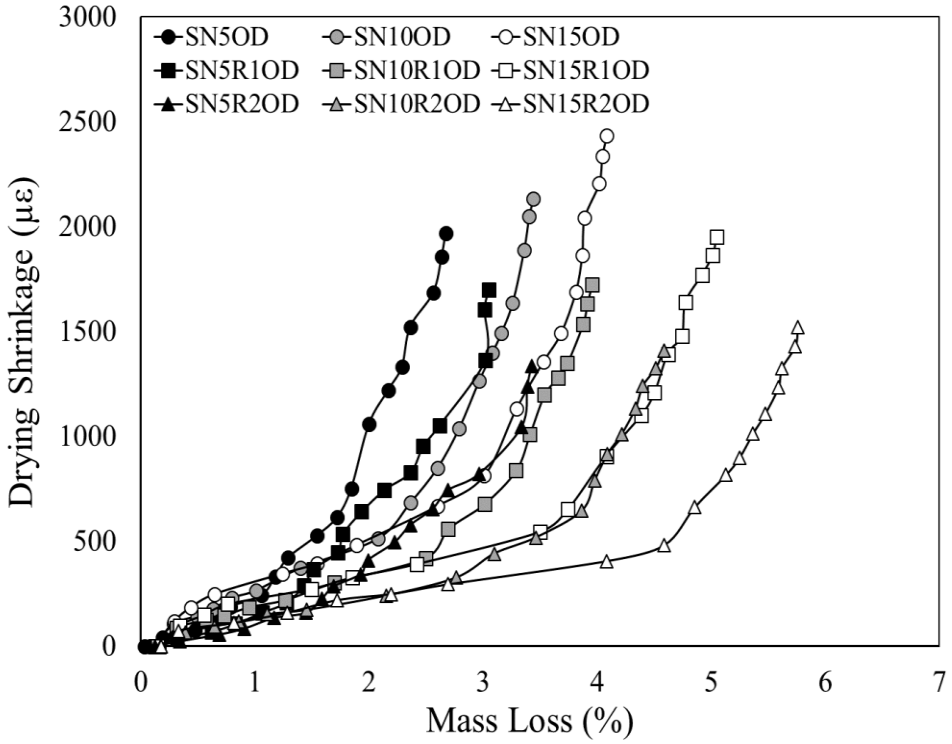

Figure 4.95 Mass loss vs. drying shrinkage of $NaHCO_3$ activated slag mortars with and without SRA (oven cured).

4.3.6.2 Effect of mass loss on drying shrinkage of two-part AAMs containing SRA.

Figures 4.96-4.101 show the curves representing the relationship between drying shrinkage and mass loss for AAF, AAS, and AAFS mortars containing 0, 1, and 2% SRA, where the abscissa is mass loss and the ordinate is drying shrinkage. **Figures 4.96, and 4.97** show the relationship between drying shrinkage and mass loss of ambient and oven cured AAF mortars containing 0, 1, and 2% SRA. Regardless of activator concentrations and SRA dose, the addition of SRA decreased the slope gradient of the curves due to the significant reduction in shrinkage rates, hence suggesting an increase in the pore size diameter compared to specimens without SRA. It can be clearly seen that drying shrinkage seems to be more depended on the mass loss rate when the shrinkage rate was significantly reduced in specimens containing SRA. The mass loss rate does not seem to be

affected with the addition of SRA, although the total measured mass loss of SRA containing specimens was a little bit higher than that recorded in specimens without SRA.

Figures 4.98, and 4.99 show the relationship between drying shrinkage and mass loss of ambient and oven cured AAS mortars containing 0, 1, and 2% SRA. Regardless of activator concentrations, it can be seen that the addition of SRA significantly decreased the slope gradient of the curves due to the significant reduction in shrinkage rates, hence suggesting a coarser porosity compared to specimens without SRA. Regardless of SRA dose, the curve gradient of SRA containing specimens was almost uniform and maintained stability suggesting no changes in pore distribution at later age. The total measured mass loss percentages of SRA specimens were higher than those measured in specimens containing zero SRA. Nevertheless, the observed effects of SRA addition in AAFS specimens were very much similar to the ones found in AAS specimens. Regardless of activator concentration and SRA dose, the curve gradient of 1, and 2% SRA containing specimens was also uniform and maintained stability in its drying shrinkage per unit mass loss.

The drying shrinkage per unit mass loss was less in oven cured specimens compared to the ambient cured ones. Generally, the addition of SRA seems to be regulating the drying shrinkage per unit mass loss by reducing the overall drying shrinkage strains. This is achieved by changing the pore size distribution and increasing the number of pores with a larger diameter, hence reducing the surface tension and capillary tensile stress and therefore the magnitude of shrinkage resulting from a unit mass loss. Increasing the SRA dose to 2% caused further reduction in the curve gradient, suggesting a coarser porosity compared to 1% SRA containing specimens. Regardless of the precursor type, results observed in both 1, and 2% SRA containing specimens were relatively

similar to each other. The overall change in drying shrinkage per unit mass loss at oven curing does not differ from the one reported at ambient curing.

The relation between activator concentration and drying shrinkage per unit mass loss seems to be directly proportional, suggesting an increase in drying shrinkage per unit mass loss with the increase in activator concentration. This relation was not altered by the addition of SRA at both doses and curing conditions.

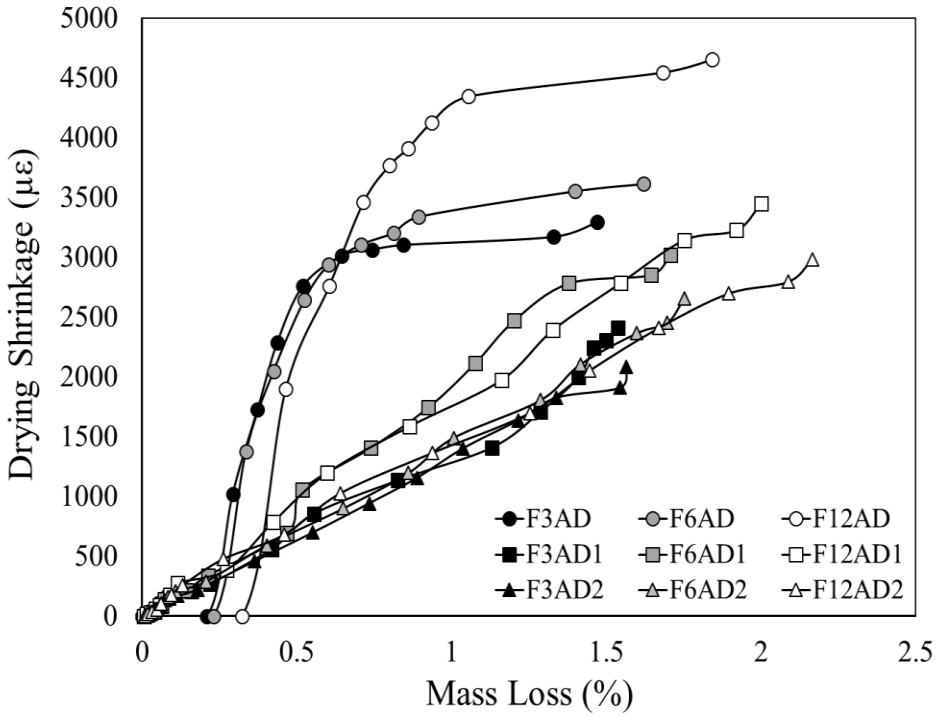

Figure 4.96 Mass loss vs. drying shrinkage of AAF mortars with and without SRA (ambient cured).

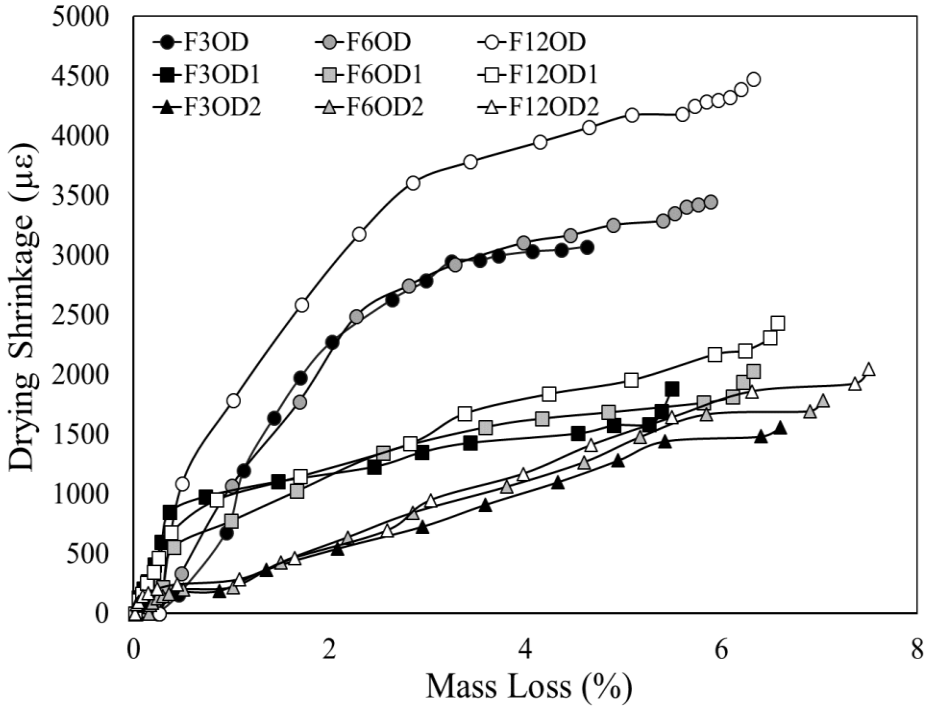

Figure 4.97 Mass loss vs. drying shrinkage of AAF mortars with and without SRA (oven cured).

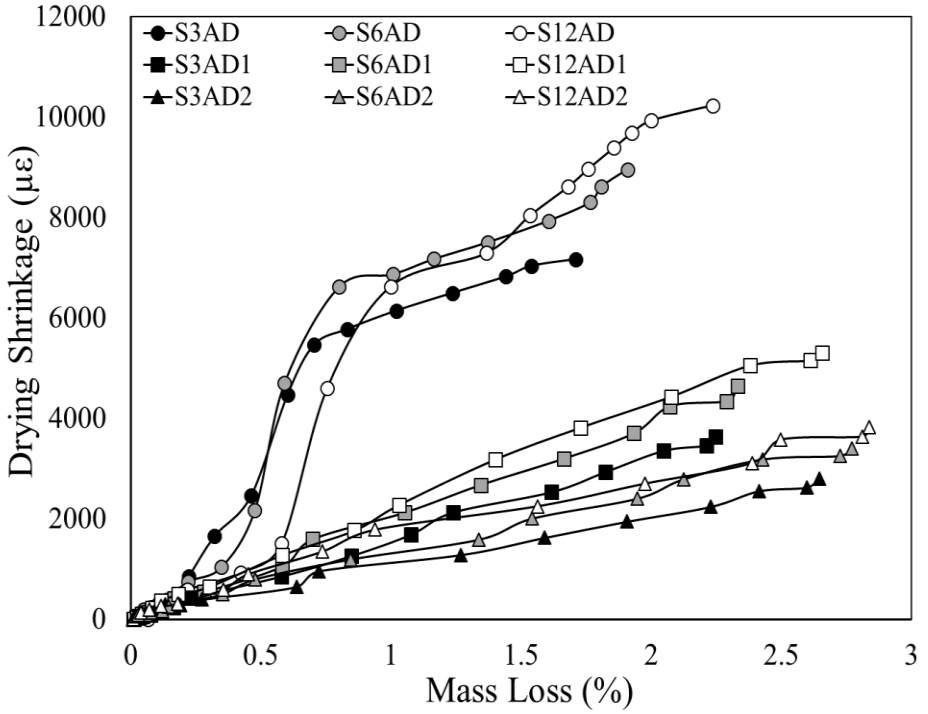

Figure 4.98 Mass loss vs. drying shrinkage of AAS mortars with and without SRA (ambient cured).

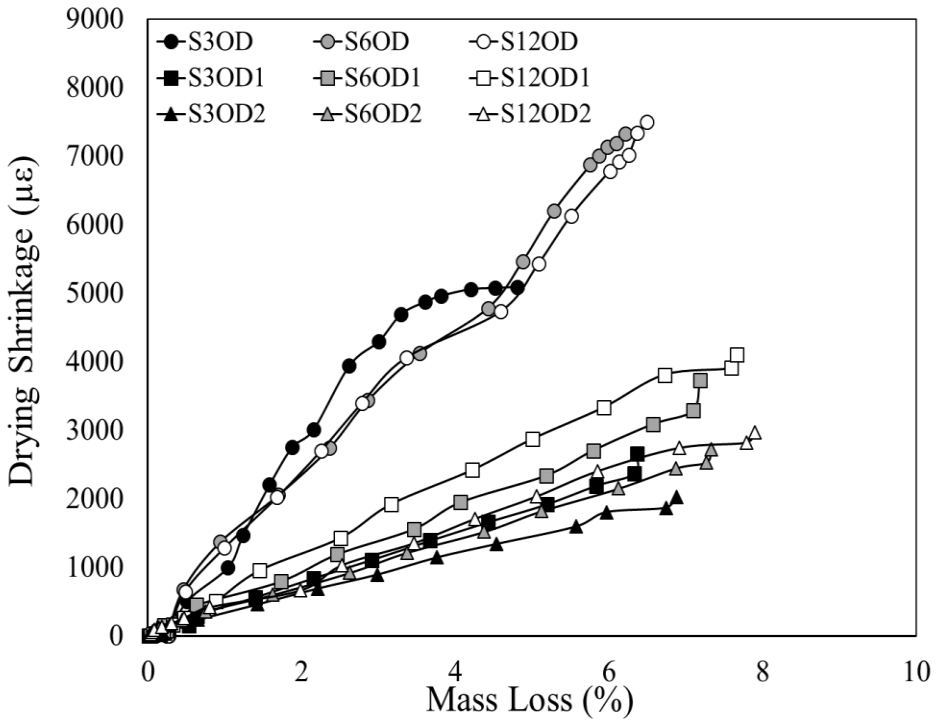

Figure 4.99 Mass loss vs. drying shrinkage of AAS mortars with and without SRA (oven cured).

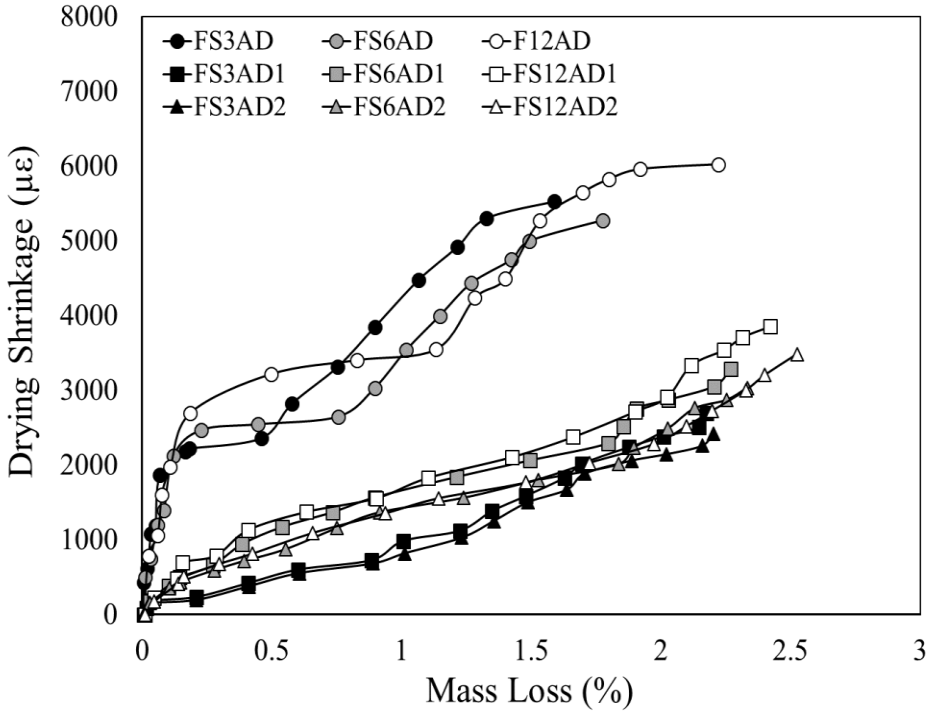

Figure 4.100 Mass loss vs. drying shrinkage of AAFS mortars with and without SRA (ambient cured).

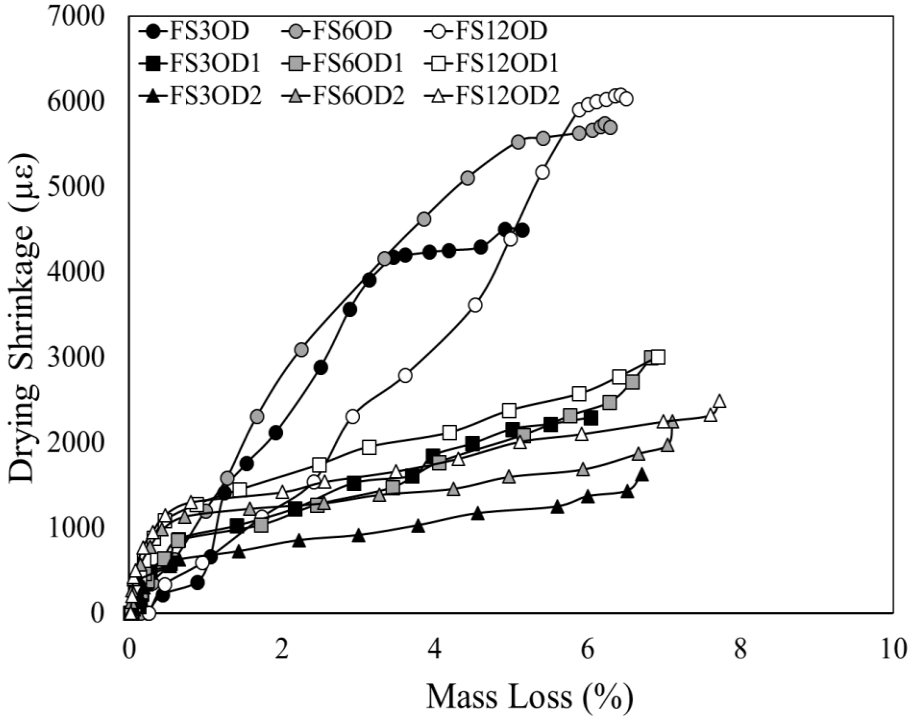

Figure 4.101 Mass loss vs. drying shrinkage of AAS mortars with and without SRA (oven cured).

4.3.7 *Autogenous shrinkage*

4.3.7.1 Effect of SRA addition on the autogenous shrinkage of one-part AAMs.

The effect of SRA addition on the autogenous shrinkage strains of mortar specimens activated with $Ca(OH)_2$ and $NaHCO_3$ was investigated. Autogenous shrinkage strains of AAS mortars activated with 5, 10, and 15% $Ca(OH)_2$ or $NaHCO_3$ at ambient curing conditions, with and without SRA, are plotted in **Figure 4.102 and 4.103**. Results indicated reductions in the autogenous shrinkage strains of AAS specimens with the addition of SRA compared to samples without SRA. For instance, reductions in the final autogenous shrinkage of AAS mortars activated with 5, 10, and 15% $Ca(OH)_2$ caused by the addition of 1% SRA were 18.2, 15.15, and 19.77%, respectively compared to mortars without SRA. The corresponding reductions when 2% SRA was used were 27.4, 25.2, and 28.6%, respectively.

Furthermore, reductions in the final autogenous shrinkage of AAS mortars activated with 5, 10, and 15% $NaHCO_3$ caused by the addition of 1% SRA were 20, 16.5, and 13.97%, respectively compared to mortars without SRA. When 2% SRA was used, reductions in autogenous shrinkage were 30.5, 26.3, and 20.5%, respectively. Reductions in autogenous shrinkage due to the addition of SRA were increasing with higher SRA dosage. Generally, autogenous shrinkage reductions were more pronounced in $NaHCO_3$ activated mortars compared to $Ca(OH)_2$ activated ones. Reductions due to SRA do not seem to be affected by the activator dosages.

Autogenous shrinkage strains of oven cured AAS mortars activated with 5, 10, and 15% $Ca(OH)_2$ or $NaHCO_3$ with and without SRA, are plotted in **Figs 4.104, and 4.105**. Reductions in the final autogenous shrinkage of oven cured AAS mortars activated with 5, 10, and 15% $Ca(OH)_2$, caused by the addition of 1% SRA were 7, 6.7, and 4%, respectively compared to mortars without SRA. The corresponding reduction percentages in total autogenous shrinkage, when 2% SRA was used are 15.8, 15.2, and 13.34%, respectively. Furthermore, reduction percentages in the final autogenous shrinkage of oven cured AAS mortars activated with 5, 10, and 15% $NaHCO_3$ caused by the addition of 1% SRA were 11, 12, and 15.9%, respectively compared to mortars without SRA. When 2% SRA was used, reductions were 18, 19.5, and 22.7%, respectively. Regardless of activator type, shrinkage reduction behavior accomplished by SRA addition seem to be retarded at higher curing temperatures, as autogenous shrinkage reductions were more pronounced in ambiently cured specimens.

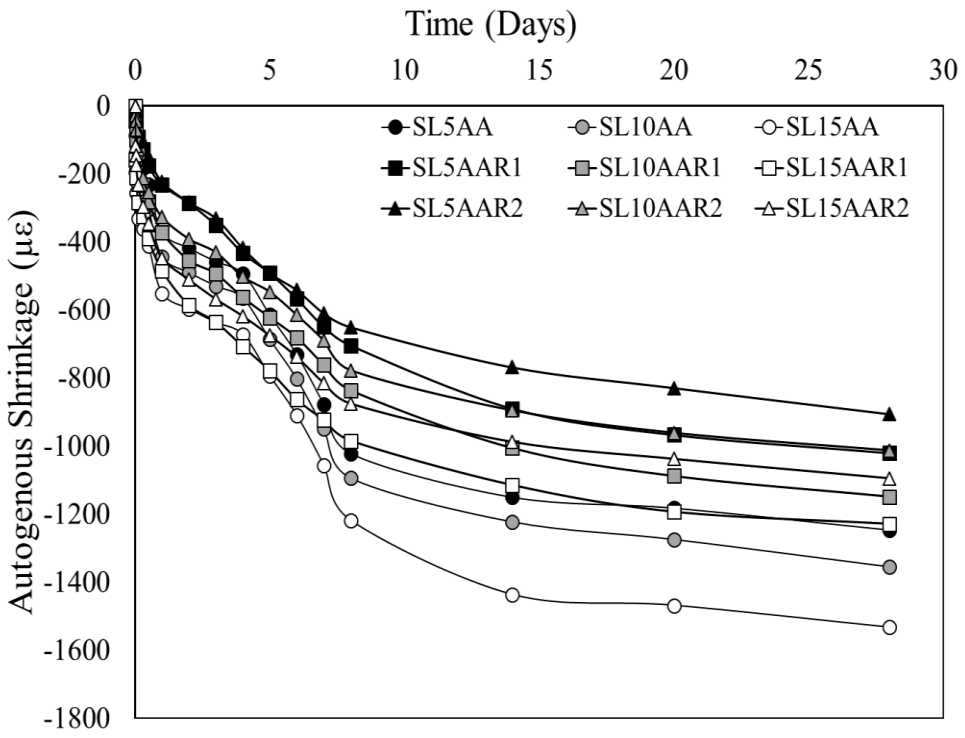

Figure 4.102 Autogenous shrinkage of AAS mortars activated with $Ca(OH)_2$ with and without SRA (ambient cured).

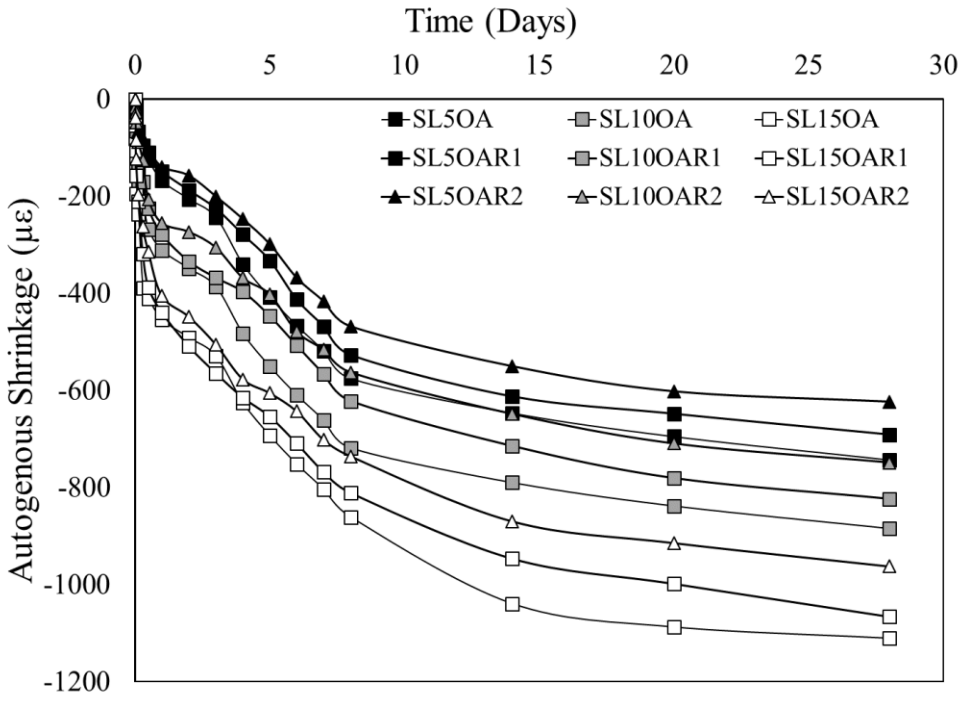

Figure 4.103 Autogenous shrinkage of AAS mortars activated with $Ca(OH)_2$ with and without SRA (oven cured).

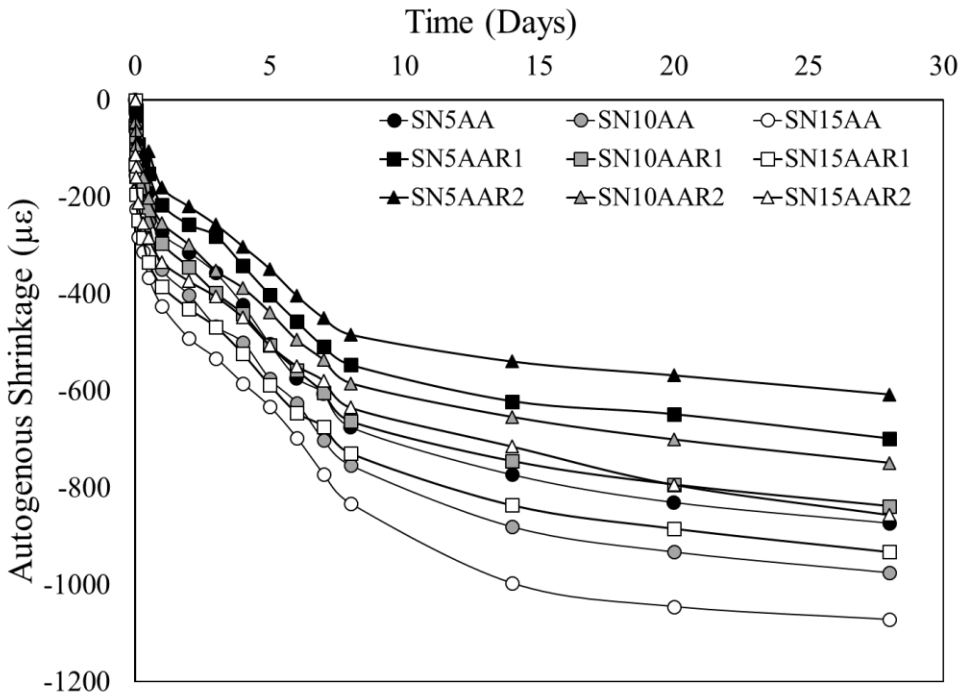

Figure 4.104 Autogenous shrinkage of AAS mortars activated with $NaHCO_3$ with and without SRA (ambient cured).

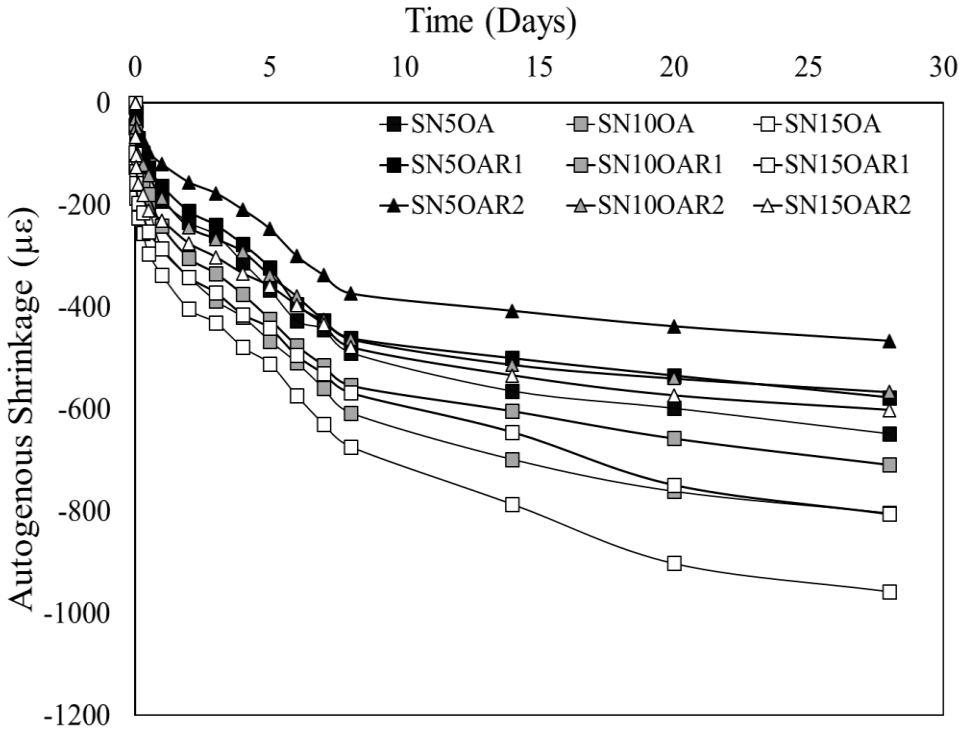

Figure 4.105 Autogenous shrinkage of AAS mortars activated with $NaHCO_3$ with and without SRA (oven cured).

4.3.7.2 Effect of SRA addition on the autogenous shrinkage of two-part alkali-activated mortars.

Autogenous shrinkage strains of AAF, AAS, and AAFS mortars activated with 3M, 6M, and 12M (NaOH) concentrations under both curing conditions, with and without SRA, are plotted in **Figs. 4.106-4.111**. Results indicated reductions in the autogenous shrinkage strains of mortar specimens with the addition of SRA compared to specimens without SRA. For instance, reductions in the total autogenous shrinkage of AAF mortars activated with 3M, 6M, and 12M NaOH, caused by the addition of 1% SRA were 22.25, 11.18, and 12.70%, respectively compared to mortars without SRA. When 2% SRA was used, reductions were 39.87, 31.80, and 27.04%, respectively. Reductions in autogenous shrinkage due to the addition of 2% SRA were much higher compared to when 1% SRA was used. The addition of 1% SRA seems to be insufficient in mitigating the autogenous shrinkage strains in AAF mortars. The response of autogenous shrinkage to SRA addition in terms of total strain reductions was almost similar to the one observed in drying shrinkage.

Moreover, reductions in the total autogenous shrinkage of AAS mortars activated with 3M, 6M, and 12M NaOH caused by the addition of 1% SRA were 60.88, 57.67, and 65.26%, respectively compared to mortars without SRA. When 2% SRA was used, reductions were 66.72, 68.03, and 72.49%, respectively. Autogenous shrinkage reduction response to SRA was much higher in AAS mortars compared to AAF mortars. Moreover, SRA proved its higher ability to reduce autogenous shrinkage strains compared to drying shrinkage strains in AAS mortars. Reduction percentages in the total autogenous shrinkage of AAFS mortars activated with 3M, 6M, and 12M NaOH caused by the addition of 1% SRA were 53.04, 54.59, and 61.47%, respectively compared to mortars without SRA. When 2% SRA was used, reductions were 57.57, 60.92, and 64.12%, respectively.

The response of oven cured AAMs in terms of autogenous shrinkage reduction was almost similar in AAS and AAFS mortars. The effect of SRA in reducing the autogenous shrinkage in AAF mortars seems to be negatively affected by the higher curing temperature. Two main developments are responsible for the useful effect of the SRA in reducing autogenous shrinkage; firstly, surface tension reduction of water in the porous system and the smaller internal stress when water evaporates; secondly, porous structure redistribution caused, because admixture addition increases the percentage of pores with larger diameter, which in turn exhibit a capillary stress much lower than pores with small diameter that prevail in mortars without admixture (Palacios and Puertas, 2007). Regardless of precursor type, the relation between activator concentration and autogenous shrinkage is directly proportional, suggesting an increase in autogenous shrinkage with the increase in activator concentration. This relation was not affected by the addition of SRA at both doses. It is important to mention that other factors affecting the fresh and hardened properties of AAM should be taken into consideration before deciding which SRA dose is optimum.

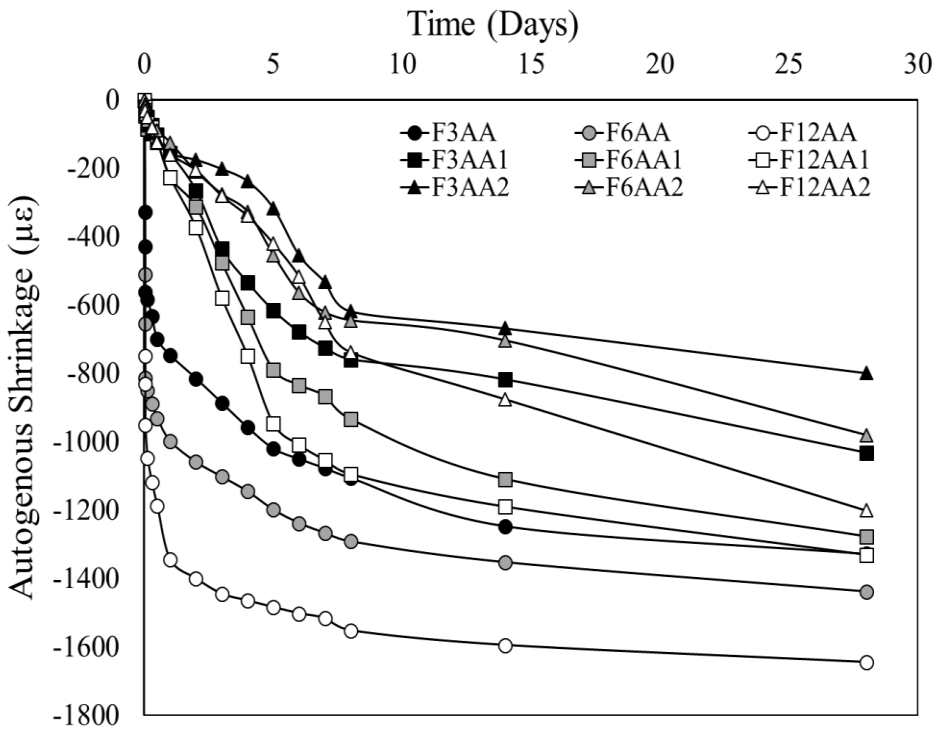

Figure 4.106 Autogenous shrinkage of two-part AAF mortars with and without SRA (ambient cured).

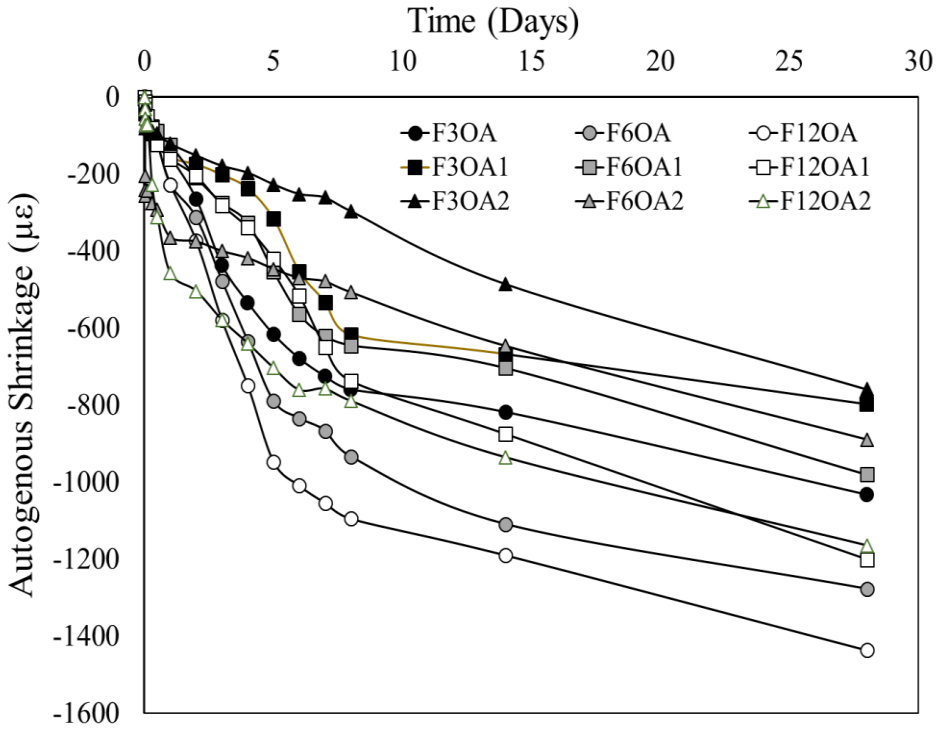

Figure 4.107 Autogenous shrinkage of two-part AAF mortars with and without SRA (oven cured).

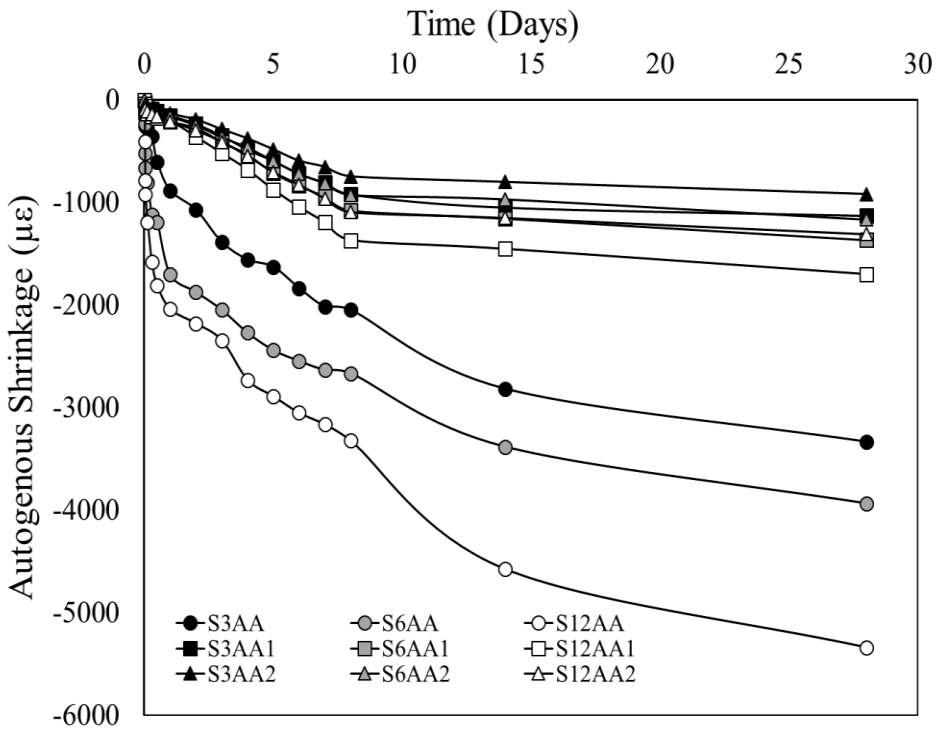

Figure 4.108 Autogenous shrinkage of two-part AAS mortars with and without SRA (ambient cured).

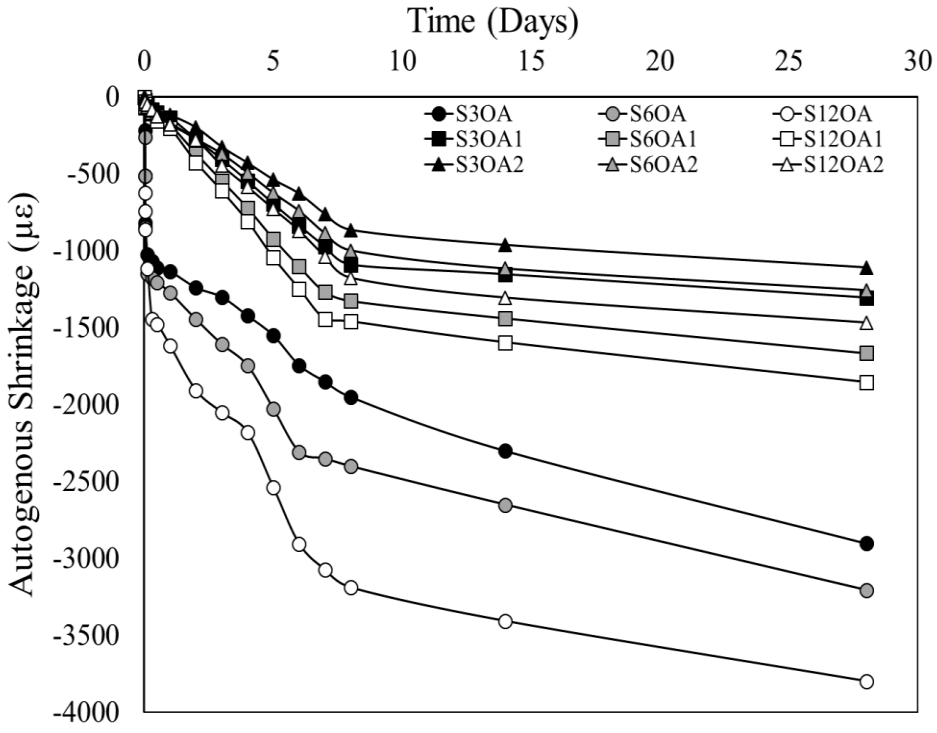

Figure 4.109 Autogenous shrinkage of two-part AAS mortars with and without SRA (oven cured).

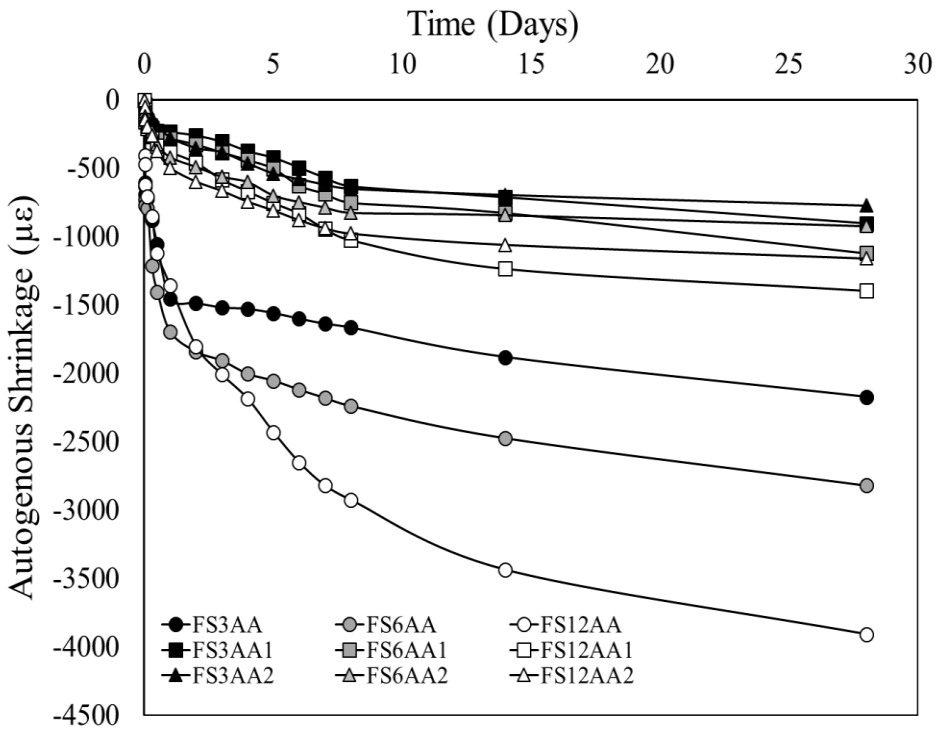

Figure 4.110 Autogenous shrinkage of two-part AAFS mortars with and without SRA (ambient cured).

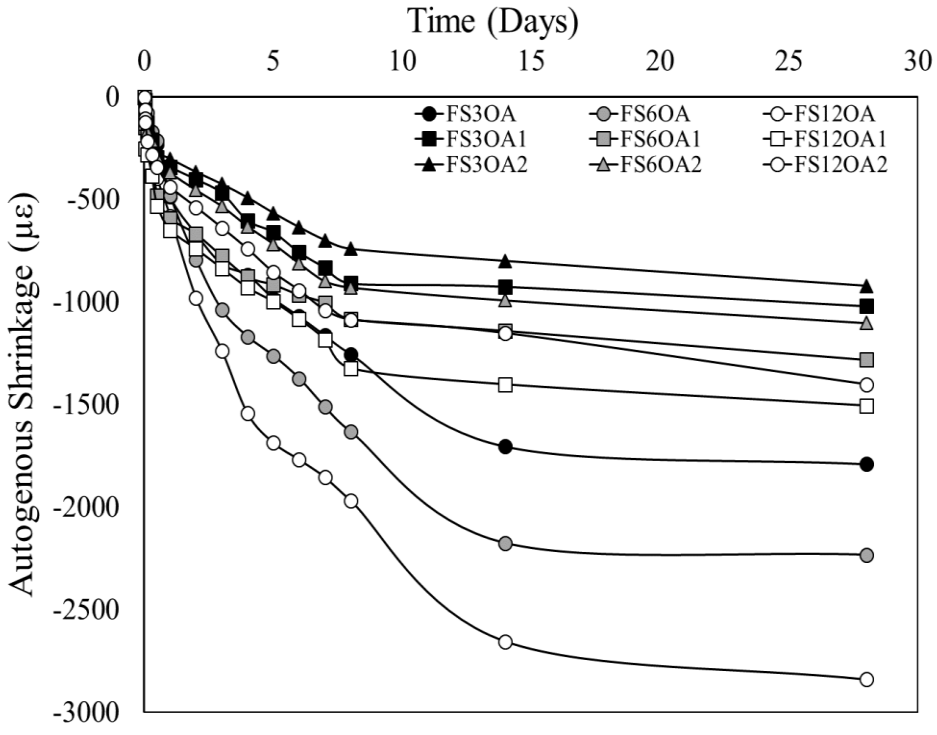

Figure 4.111 Autogenous shrinkage of two-part AAFS mortars with and without SRA (oven cured).

4.3.8 *Conclusion*

Generally, SRAs slightly increased the flowability in both one-part and two-part AAM mixtures tested. On the other hand, both the initial and final settings were retarded. When SRA dose increased from 1% to 2%, flowability increased and setting times were further retarded.

Regardless of precursor type and activator concentrations, the addition of SRA reduced the overall compressive strength of AAMs. Reductions were higher when SRA dose increased from 1 to 2%. Reductions in one-part and two-part AAMs varied between 5.88-20% depending on precursor type, activator concentration, and SRA dosage. Oven cured specimens experienced lower reductions compared to ambient cured ones.

Calorimetry analysis showed that the addition of SRA did decrease both, the heat flow rate and the cumulative heat exhibited by both one-part and two-part AAMs. Reductions in cumulative heat released ranged between 2.59-15.79% depending on SRA dose, precursor type, and activator concentration. However, reductions were more pronounced in two-part AAMs. Regardless of the mixing condition, AAF mortars experienced the highest heat reductions due to SRA addition followed by AAFS, and finally, AAS mortars. The reductions in heat flow and cumulative heat values are a result of the slightly retarded hydration reaction caused by SRA addition.

The addition of SRA significantly reduced the drying and autogenous shrinkage of both one-part and two-part AAM specimens. Typically, reductions were more pronounced when SRA dose was increased from 1 to 2%. However, reductions were much more pronounced in two-part AAMs compared to one-part AA ones. Reductions in drying and autogenous shrinkage strains of two-part AAMs reached up to 67.08% and 72.49%, respectively. On the other hand, the highest autogenous and drying shrinkage reductions recorded in one-part AAMs were 30% and 32%, respectively. The main mechanism of SRA that is responsible for the beneficial shrinkage

reductions in AAMs is proposed to be the reduction in surface tension of pore water prompted by the admixture.

Mass loss vs. drying shrinkage curves showed that the shrinkage induced per unit mass loss was significantly decreased with the use of SRA at different doses in both one-part and two-part AAMs. It is well known that the capillary tensile stress and therefore the magnitude of shrinkage resulting from a unit mass loss, is dependent on the pore radius, hence a change in the curve slope gradient suggests a change in pore distribution. The addition of SRA caused an almost uniform and stable slope gradient suggesting minimal changes in the pore distribution.

5

CHAPTER

Conclusions and Future Work

5.1 Conclusions

This thesis presents a wide study and review on the shrinkage behavior of one-part and two-part AAF, AAFS, and AAS mortars activated with several types of alkali activators and cured under ambient and oven temperatures. Moreover, fresh and hardened properties of the prepared AAMs were also evaluated. Shrinkage reducing admixtures were utilized as a mitigation technique in an attempt to reduce the shrinkage strains experienced by AAM specimens. The following is a brief conclusion of the reported results.

Highly concentrated activators tend to reduce the flowability of AAMs in all cases. The reduction was also dependent on the physical properties of the precursor. One-part AAMs showed better flow properties compared to two-part AA ones. This was mainly attributed to the high viscosity of liquid activators used in the latter. AAF mortars exhibited the highest flow rates followed by AAFS, and finally, AAS mortars under both production methods. This was attributed to the spherical shape of fly ash particles which possess a much larger specific surface area compared to slag particles. The setting behavior of AAMs was significantly accelerated with the use of higher activator concentrations under both production methods. This was attributed to the facilitation of a higher alkaline environment which in turn led to a faster degree of hydration reaction and

ultimately quicker set. The initial and final setting behaviour was shorter in two-part AAMs compared to one-part AA ones. This was attributed the better precursor dissolution ability of liquid activator solutions utilized in two-part AAMs. AAS mortars exhibited the quickest settings followed by AAFS, and finally, AAF mortars. The shorter setting time behaviour observed in AAS mortars can be ascribed to the higher calcium oxide (CaO) content found in slag. Higher CaO content was found to accelerate the hydration reaction, and hardening process of AAMs.

The relationship between activator concentration and compressive strength of AAMs was directly proportional regardless of the mixing conditions. Higher activator concentrations increase the solubility of amorphous silica and alumina present in precursors. Therefore, resulting in an enhanced formation of sodium aluminosilicate hydrate (N-A-S-H) and calcium aluminosilicate hydrate (C-A-S-H) binder. Higher strength properties were achieved in two-part AAMs compared to one-part AA ones. This was mainly due to many factors including, the alkalinity of different activators used and their ability in dissolving the precursor material and initiating a strong polymerization reaction. AAS mortars achieved the highest compressive strength values followed by AAFS, and finally, AAF mortars. This was attributed to the CaO content which is the main component in slag. The higher calcium content accelerated the hardening and strength development in AAS mortars compared to other mortars. Oven cured mortars achieved higher compressive strength values compared to ambient cured ones under both production principles. The activation of one-part AAF mortars was not successful using $Ca(OH)_2$ or $NaHCO_3$ under both curing conditions, as the achieved compressive strength values of those specimens was very poor.

The heat flow and cumulative heat released were higher in two-part AAMs compared to one-part AA ones. The relation between the released heat and compressive strength of AAMs was directly proportional, as mortars releasing the highest heat, achieved the highest compressive

strength values. Generally, the heat flow and cumulative heat released by AAS mortars were the highest followed by AAFS, and finally, AAF mortars. The higher formation and polymerization of binder gels in AAS mortars are accounted responsible for the high cumulative heat release. Furthermore, the heat flow and cumulative released heat were increasing with higher activator concentrations regardless of the production principles. The analysis confirmed the suggested unsuccessful activation of AAF mortars by the aid of $Ca(OH)_2$ or $NaHCO_3$, as the heat flow and cumulative heat released by those specimens were very low. The initial heat of hydration flow peaks observed in AAMs was very similar to the one found in OPC mortars.

The experienced autogenous and drying shrinkage strains were significantly lower in one-part AAMs compared to two-part AA ones. Generally, shrinkage strains increased with higher activator concentrations. The finer pore size distribution along with the higher surface tension of the pore solution found in AAS mortars dominates the capillary stress formation. Reduction in porosity would cause more shrinkage occurring due to the extra-capillary stress induced. AAS mortars experienced the highest shrinkage strains followed by AAFS, and finally, AAF mortars. The effect of using slag in AAMs is twofold, on one hand, it gives the highest compressive strength through the high CaO content and hence, the higher level of hydration reaction. On the other hand, it achieved the highest autogenous and drying shrinkage strains.

Adopting oven curing at 60°C, did increase the compressive strength of one-part and two-part AAMs for up to 73% and decrease the drying, and autogenous shrinkage strains for up to 28%, and 47%, respectively. However, the problem of practicality and higher energy consumption remains a matter of question, as higher temperature curing can be cost hectic or impossible to achieve in cast in-situ concrete applications but can rather be achieved in precast applications. It

is worth mentioning that the shrinkage stains experienced by one-part and two-part AAMs were higher than the ones normally observed in OPC mortars.

The relation between mass loss and drying shrinkage in one-part and two-part AAMs showed that at the early age, the pore distribution in all mortar specimens was not affected by the activator type or concentration. Furthermore, at later age, the shrinkage behavior was not affected by the increased mass loss. AAS mortars showed higher drying shrinkage per unit mass loss compared to AAFS, and AAF mortars.

The addition of SRA in an attempt to control the shrinkage behaviour of one-part and two-part AAMs proved a success. However, compressive strength was slightly reduced due to SRA addition under both production principles. Compressive strength reductions observed in one-part and two-part AAMs varied between 5.88-20% depending on precursor type, activator concentration, and SRA dosage. Oven cured specimens experienced lower strength reductions compared to ambient cured ones. The addition of SRA slightly decreased both the heat flow and cumulative heat released by one-part and two-part AAMs. However, reductions were more pronounced in two-part AAMs. The reductions in heat flow and cumulative heat values are a result of the slightly retarded hydration reaction caused by SRA addition.

The addition of SRA significantly reduced the drying and autogenous shrinkage of both one-part and two-part AAM specimens. The shrinkage mitigation effect of SRA was more pronounced in two-part AAMs compared to one-part AA ones. Moreover, the mitigation effect increased with higher SRA dosage. Generally, AAS mortars responded the best to the shrinkage mitigation mechanism of SRA followed by AAFS, and finally, AAF mortars. The main mechanism of SRA that is responsible for the beneficial shrinkage reductions in AAMs is proposed to be the reduction in surface tension of pore water prompted by the admixture.

5.2 Future Work

It is worth considering further investigations on the following main points:

- Porosity and microstructure testing to better understand the structure of the polymerization products in one and two part AABs. This will enhance the evaluation of the proposed production methods under the parameters specified in this work.
- Testing several activators in the production of one part AABs. This will help in identifying the most sustainable and promising activator type.
- Optimizing the much practical one part AAB mixtures compared to the two part activated ones, so that similar mechanical properties could be achieved in the former compared to the later.
- Testing and evaluating other types of shrinkage mitigation techniques in order to find the most efficient and economical one.

References

Altan, E., & Erdoğan, S. T. (2012). Alkali activation of a slag at ambient and elevated temperatures. *Cement and Concrete Composites,* 34(2), 131-139.

Atiş, C. D., Bilim, C., Çelik, Ö., & Karahan, O. (2009). Influence of activator on the strength and drying shrinkage of alkali-activated slag mortar. *Construction and Building Materials*, 23(1), 548-555.

Bakharev, T., Sanjayan, J. G., & Cheng, Y. B. (1999). Alkali activation of Australian slag cements. *Cement and Concrete Research*, 29(1), 113-120.

Bakharev, T., Sanjayan, J. G., & Cheng, Y. B. (1999). Effect of elevated temperature curing on properties of alkali-activated slag concrete. *Cement and Concrete Research*, 29(10), 1619-1625.

Bakharev, T., Sanjayan, J. G., & Cheng, Y. B. (2000). Effect of admixtures on properties of alkali-activated slag concrete. *Cement and Concrete Research*, 30(9), 1367-1374.

Bakharev, T., Sanjayan, J. G., & Cheng, Y. B. (2001). Resistance of alkali-activated slag concrete to carbonation. *Cement and Concrete Research*, 31(9), 1277-1283.

Balczar, I., Korim, T., & Dobradi, A. (2015). Correlation of strength to apparent porosity of geopolymers–Understanding through variations of setting time. *Construction and Building Materials*, 93, 983-988.

Barbosa, V. F., MacKenzie, K. J., & Thaumaturgo, C. (2000). Synthesis and characterisation of materials based on inorganic polymers of alumina and silica: sodium polysialate polymers. *International Journal of Inorganic Materials*, 2(4), 309-317.

Bentz, D. P., & Weiss, W. J. (2011). *Internal curing: a 2010 state-of-the-art review*. Gaithersburg, Maryland: US Department of Commerce, National Institute of Standards and Technology.

Berke, N. S., Li, L., Hicks, M. C., & Bae, J. (2003). Improving concrete performance with shrinkage-reducing admixtures. *Special Publication*, 217, 37-50.

Bilim, C., Karahan, O., Atiş, C. D., & Ilkentapar, S. (2013). Influence of admixtures on the properties of alkali-activated slag mortars subjected to different curing conditions. *Materials & Design*, 44, 540-547.

Brough, A. R., & Atkinson, A. (2002). Sodium silicate-based, alkali-activated slag mortars: Part I. Strength, hydration and microstructure. *Cement and Concrete Research*, 32(6), 865-879.

C. Heidrich, Slag- not a dirty word, Geopolymer 2002: *International Geopolymer Conference: Turn Potential into Profit*, Melbourne, Australia, 2002.

Cartwright, C., Rajabipour, F., & Radlińska, A. (2014). Shrinkage characteristics of alkali-activated slag cements. *Journal of Materials in Civil Engineering*, 27(7), B4014007.

Chareerat, T., Lee-Anansaksiri, A., & Chindaprasirt, P. (2006, May). Synthesis of High Calcium Fly Ash and Calcined Kaoline Geopolymer Mortar. *In International Conference on Pozzolan, Concrete and Geopolymer* (pp. 24-25).

Chen, W., & Brouwers, H. J. H. (2007). The hydration of slag, part 1: reaction models for alkali-activated slag. *Journal of Materials Science*, 42(2), 428-443.

Chi, M., & Huang, R. (2013). Binding mechanism and properties of alkali-activated fly ash/slag

Chindaprasirt, P., Chareerat, T., & Sirivivatnanon, V. (2007). Workability and strength of coarse high calcium fly ash geopolymer. *Cement and Concrete Composites*, 29(3), 224-229.

Chindaprasirt, P., Chareerat, T., Hatanaka, S., & Cao, T. (2010). High-strength geopolymer using fine high-calcium fly ash. *Journal of Materials in Civil Engineering*, 23(3), 264-270.

Chithiraputhiran, S., & Neithalath, N. (2013). Isothermal reaction kinetics and temperature dependence of alkali activation of slag, fly ash and their blends. *Construction and Building Materials*, 45, 233-242.

Cho, Y. K., Yoo, S. W., Jung, S. H., Lee, K. M., & Kwon, S. J. (2017). Effect of Na_2O content, SiO_2/Na_2O molar ratio, and curing conditions on the compressive strength of FA-based geopolymer. *Construction and Building Materials*, 145, 253-260.

Christy, C. F., & Tensing, D. (2011). Greener building material with fly ash. *Asian Journal of Civil Engineering*, 12(1), 87-105.

Cincotto, M. A., Melo, A. A., & Repette, W. L. (2003, May). Effect of different activators type and dosages and relation to autogenous shrinkage of activated blast furnace slag cement. *In Proceedings of the 11th International Congress on the Chemistry of Cement*, Durban, South Africa (Vol. 1878-1888).

Collins, F., & Sanjayan, J. G. (2000). Effect of pore size distribution on drying shrinking of alkali-activated slag concrete. *Cement and Concrete Research*, 30(9), 1401-1406.

Davidovits, J. (1994, October). Properties of geopolymer cements. *In First international conference on alkaline cements and concretes* (Vol. 1, pp. 131-149). Kiev State Technical University, Ukraine: Scientific Research Institute on Binders and Materials.

Deir, E., Gebregziabiher, B. S., & Peethamparan, S. (2014). Influence of starting material on the early age hydration kinetics, microstructure and composition of binding gel in alkali activated binder systems. *Cement and Concrete Composites*, 48, 108-117.

Doležal, J., Škvára, F., Svoboda, P., Šulc, R., Kopecký, L., Pawlasová, S., & Dvořáček, K. (2006). Concrete based on fly ash geopolymers. *Proceedings of 16th Intern. Baustofftagung IBAUSIL*.

Douglas, E., & Brandstetr, J. (1990). A preliminary study on the alkali activation of ground granulated blast-furnace slag. *Cement and Concrete Research*, 20(5), 746-756.

Duxson, P., Provis, J. L., Lukey, G. C., & Van Deventer, J. S. (2007). The role of inorganic polymer technology in the development of 'green concrete'. *Cement and Concrete Research*, 37(12), 1590-1597.

Farris, A. (2017, May). *Coal.* Retrieved from http://energybc.ca/coal.html

Feng, D., Tan, H., & Van Deventer, J. S. J. (2004). Ultrasound enhanced geopolymerisation. *Journal of Materials Science*, 39(2), 571-580.

Fernández-Jimenez, A. M., Palomo, A., & Lopez-Hombrados, C. (2006). Engineering properties of alkali-activated fly ash concrete. *ACI Materials Journal*, 103(2), 106.

Fernández-Jiménez, A., & Puertas, F. (2002). The alkali–silica reaction in alkali-activated granulated slag mortars with reactive aggregate. *Cement and Concrete Research*, 32(7), 1019-1024

Fernández-Jiménez, A., Palomo, A., & Criado, M. (2005). Microstructure development of alkali-activated fly ash cement: a descriptive model. *Cement and Concrete Research*, 35(6), 1204-1209.

García-Lodeiro, I., Palomo, A., & Fernández-Jiménez, A. (2007). Alkali–aggregate reaction in activated fly ash systems. *Cement and Concrete Research*, 37(2), 175-183.

Garcia-Lodeiro, I., Palomo, A., & Fernández-Jiménez, A. (2015). An overview of the chemistry of alkali-activated cement-based binders. *In Handbook of Alkali-Activated Cements, Mortars and Concretes* (pp. 19-47).

Gebregziabiher, B. S., Thomas, R. J., & Peethamparan, S. (2016). Temperature and activator effect on early-age reaction kinetics of alkali-activated slag binders. *Construction and Building Materials*, 113, 783-793.

Görhan, G., & Kürklü, G. (2014). The influence of the NaOH solution on the properties of the fly ash-based geopolymer mortar cured at different temperatures. *Composites Part B: Engineering*, 58, 371-377.

Gourley, J. T. (2003, October). Geopolymers; opportunities for environmentally friendly construction materials. *In Materials 2003 Conference: Adaptive Materials for a Modern Society,* Sydney, Institute of Materials Engineering Australia.

Guerrieri, M., Sanjayan, J., & Collins, F. (2010). Residual strength properties of sodium silicate alkali activated slag paste exposed to elevated temperatures. *Materials and Structures*, 43(6), 765-773.

Guo, X., Shi, H., & Dick, W. A. (2010). Compressive strength and microstructural characteristics of class C fly ash geopolymer. *Cement and Concrete Composites*, 32(2), 142-147.

Heah, C. Y., Kamarudin, H., Al Bakri, A. M., Binhussain, M., Luqman, M., Nizar, I. K., & Liew, Y. M. (2011). Effect of curing profile on kaolin-based geopolymers. *Physics Procedia*, 22, 305-311.

Heidrich, C., Sanjayan, J., Berndt, M. L., Foster, S., & Sagoe-Crentsil, K. (2015). Pathways and barriers for acceptance and usage of geopolymer concrete in mainstream construction. *Proceedings of the 2015 World of Coal Ash (WOCA),* Nashville, TN, USA.

Holt, E. E. (2001). Early age autogenous shrinkage of concrete. Espoo, Finland: *Technical Research Centre of Finland.*

Ismail, I., Bernal, S. A., Provis, J. L., San Nicolas, R., Brice, D. G., Kilcullen, A. R., & van Deventer, J. S. (2013). Influence of fly ash on the water and chloride permeability of alkali-activated slag mortars and concretes. *Construction and Building Materials*, 48, 1187-1201.

Jang, J. G., Lee, N. K., & Lee, H. K. (2014). Fresh and hardened properties of alkali-activated fly ash/slag pastes with superplasticizers. *Construction and Building Materials*, 50, 169-176.

Janz, M. (2000). Moisture transport and fixation in porous materials at high moisture levels. *Division of Building Materials*, LTH, Lund University.

Kani, E. N., & Allahverdi, A. (2009). Effects of curing time and temperature on strength development of inorganic polymeric binder based on natural pozzolan. *Journal of Materials Science*, 44(12), 3088-3097.

Khale, D., & Chaudhary, R. (2007). Mechanism of geopolymerisation and factors influencing its development: a review. *Journal of Materials Science*, 42(3), 729-746.

Kim, M. S., Jun, Y., Lee, C., & Oh, J. E. (2013). Use of CaO as an activator for producing a price-competitive non-cement structural binder using ground granulated blast furnace slag. *Cement and Concrete Research*, 54, 208-214.

Kovtun, M., Kearsley, E. P., & Shekhovtsova, J. (2015). Dry powder alkali-activated slag cements. *Advances in Cement Research*, 27(8), 447-456.

Kumar, S., Kumar, R., & Mehrotra, S. P. (2010). Influence of granulated blast furnace slag on the reaction, structure and properties of fly ash based geopolymer. *Journal of Materials Science*, 45(3), 607-615.

Lee, N. K., & Lee, H. K. (2013). Setting and mechanical properties of alkali-activated fly ash/slag concrete manufactured at room temperature. *Construction and Building Materials*, 47, 1201-1209.

Lee, N. K., Jang, J. G., & Lee, H. K. (2014). Shrinkage characteristics of alkali-activated fly ash/slag paste and mortar at early ages. *Cement and Concrete Composites*, 53, 239-248.

Lee, W. K. W., & Van Deventer, J. S. J. (2002). The effect of ionic contaminants on the early-age properties of alkali-activated fly ash-based cements. *Cement and Concrete Research*, 32(4), 577-584.

Li, C., Sun, H., & Li, L. (2010). A review: The comparison between alkali-activated slag (Si+ Ca) and metakaolin (Si+ Al) cements. *Cement and Concrete Research*, 40(9), 1341-1349.

Li, Z., & Liu, S. (2007). Influence of slag as additive on compressive strength of fly ash-based geopolymer. *Journal of Materials in Civil Engineering*, 19(6), 470-474.

Luga, E., Atis, C. D., Karahan, O., Ilkentapar, S., & Gorur, E. B. (2017). Strength properties of slag/fly ash blends activated with sodium metasilicate. *GRADEVINAR*, 69(3), 199-205.

Ma, Y., & Ye, G. (2015). The shrinkage of alkali activated fly ash. *Cement and Concrete Research*, 68, 75-82.

Ma, Y., Hu, J., & Ye, G. (2013). The pore structure and permeability of alkali activated fly ash. *Fuel*, 104, 771-780.

McDonald, M., & Thompson, J. L. (2006). Sodium silicate a binder for the 21st century. *National silicates and PQ Corporation of Industrial Chemicals Division*.

Mishra, A., Choudhary, D., Jain, N., Kumar, M., Sharda, N., & Dutt, D. (2008). Effect of concentration of alkaline liquid and curing time on strength and water absorption of geopolymer concrete. *ARPN Journal of Engineering and Applied Sciences*, 3(1), 14-18.

Nath, P., & Sarker, P. K. (2014). Effect of GGBFS on setting, workability and early strength properties of fly ash geopolymer concrete cured in ambient condition. *Construction and Building Materials*, 66, 163-171

Nematollahi, B., Sanjayan, J., & Shaikh, F. U. A. (2015). Synthesis of heat and ambient cured one-part geopolymer mixes with different grades of sodium silicate. *Ceramics International*, 41 (4), 5696-5704.

Nematollahi, B., Sanjayan, J., Qiu, J., & Yang, E. H. (2017). Micromechanics-based investigation of a sustainable ambient temperature cured one-part strain hardening geopolymer composite. *Construction and Building Materials*, 131, 552-563.

Neto, A. A. M., Cincotto, M. A., & Repette, W. (2008). Drying and autogenous shrinkage of pastes and mortars with activated slag cement. *Cement and Concrete Research*, 38(4), 565-574.

Oh, J. E., Monteiro, P. J., Jun, S. S., Choi, S., & Clark, S. M. (2010). The evolution of strength and crystalline phases for alkali-activated ground blast furnace slag and fly ash-based geopolymers. *Cement and Concrete Research*, 40(2), 189-196.

Pacheco-Torgal, F., Castro-Gomes, J., & Jalali, S. (2008). Alkali-activated binders: a review. Part 2. About materials and binders manufacture. *Construction and Building Materials*, 22(7), 1315-1322.

Palacios, M., & Puertas, F. (2005). Effect of superplasticizer and shrinkage-reducing admixtures on alkali-activated slag pastes and mortars. *Cement and Concrete Research*, 35(7), 1358-1367.

Palacios, M., & Puertas, F. (2007). Effect of shrinkage-reducing admixtures on the properties of alkali-activated slag mortars and pastes. *Cement and Concrete Research*, 37(5), 691-702.

Palomo, A., Grutzeck, M. W., & Blanco, M. T. (1999). Alkali-activated fly ashes: a cement for the future. *Cement and concrete research*, 29(8), 1323-1329.

Pangdaeng, S., Phoo-ngernkham, T., Sata, V., & Chindaprasirt, P. (2014). Influence of curing conditions on properties of high calcium fly ash geopolymer containing Portland cement as additive. *Materials & Design*, 53, 269-274.

Provis, J. L. (2017). Alkali-activated materials. Cement and Concrete Research.

Provis, J. L., & Bernal, S. A. (2014). Geopolymers and related alkali-activated materials. *Annual Review of Materials Research*, 44, 299-327.

Provis, J. L., & Van Deventer, J. S. J. (Eds.). (2009). Geopolymers: structures, processing, properties and industrial applications. *Elsevier.*

Provis, J. L., Duxson, P., Kavalerova, E., Krivenko, P. V., Pan, Z., Puertas, F., & van Deventer, J. S. (2014). Historical aspects and overview. *In Alkali activated materials (pp. 11-57). Springer*, Dordrecht.

Provis, J. L., Palomo, A., & Shi, C. (2015). Advances in understanding alkali-activated materials. *Cement and Concrete Research*, 78, 110-125.

Puertas, F., Martínez-Ramírez, S., Alonso, S., & Vazquez, T. (2000). Alkali-activated fly ash/slag cements: strength behaviour and hydration products. *Cement and Concrete Research*, 30(10), 1625-1632.

Puertas, F., Palacios, M., & Vázquez, T. (2006). Carbonation process of alkali-activated slag mortars. *Journal of Materials Science*, 41(10), 3071-3082.

Rangan, B. V. (2008). Fly ash-based geopolymer concrete.

Rashad, A. M. (2013). Properties of alkali-activated fly ash concrete blended with slag. Iran J *Mater Sci Eng*, 10(1), 57-64.

Ravikumar, D., & Neithalath, N. (2012). Reaction kinetics in sodium silicate powder and liquid activated slag binders evaluated using isothermal calorimetry. *Thermochimica acta*, 546, 32-43.

Shen, W., Wang, Y., Zhang, T., Zhou, M., Li, J., & Cui, X. (2011). Magnesia modification of alkali-activated slag fly ash cement. *Journal of Wuhan University of Technology--Materials Science Edition*, 26(1), 121-125.

Shi, C., & Day, R. L. (1999). Early strength development and hydration of alkali-activated blast furnace slag/fly ash blends. *Advances in Cement Research*, 11(4), 189-196.

Sindhunata,, Van Deventer, J. S. J., Lukey, G. C., & Xu, H. (2006). Effect of curing temperature and silicate concentration on fly-ash-based geopolymerization. *Industrial & Engineering Chemistry Research*, 45(10), 3559-3568

Song, S., & Jennings, H. M. (1999). Pore solution chemistry of alkali-activated ground granulated blast-furnace slag. *Cement and Concrete Research*, 29(2), 159-170.

Sumajouw, D. M. J., Hardjito, D., Wallah, S. E., & Rangan, B. V. (2007). Fly ash-based geopolymer concrete: study of slender reinforced columns. *Journal of Materials Science*, 42(9), 3124-3130.

Sun, Z., & Vollpracht, A. (2017). Isothermal calorimetry and in-situ XRD study of the NaOH activated fly ash, metakaolin and slag. *Cement and Concrete Research.*

Temuujin, J., van Riessen, A., & MacKenzie, K. J. D. (2010). Preparation and characterisation of fly ash based geopolymer mortars. *Construction and Building Materials*, 24(10), 1906-1910.

Thomas, R. J., Lezama, D., & Peethamparan, S. (2017). On drying shrinkage in alkali-activated concrete: Improving dimensional stability by aging or heat-curing. *Cement and Concrete Research*, 91, 13-23.

Tongaroonsri, S. (2009). Prediction of autogenous shrinkage, drying shrinkage and shrinkage cracking in concrete (Doctoral dissertation, School of Civil Engineering and Technology, Sirindhorn International Institute of Technology, Thammasat University).

Umniati, B., Risdanareni, P. and Zein, F (2017). Workability enhancement of geopolymer concrete through the use of retarder. *AIP Conference Proceedings*, Volume 1887, Issue 1, pp. 020033/1 – 020033/9.

Van Deventer, J. S., Provis, J. L., & Duxson, P. (2012). Technical and commercial progress in the adoption of geopolymer cement. *Minerals Engineering*, 29, 89-104.

Van Jaarsveld, J. G. S., Van Deventer, J. S. J., & Lukey, G. C. (2003). The characterisation of source materials in fly ash-based geopolymers. *Materials Letters*, 57(7), 1272-1280.

Van Jaarsveld, J., & Van Deventer, J. S. J. (1999). Effect of the alkali metal activator on the properties of fly ash-based geopolymers. *Industrial & Engineering Chemistry Research*, 38(10), 3932-3941.

Wallah, S.E., Rangan, B.V., "Low Calcium Fly Ash Based Geopolymer Concrete: Long Term Properties", *Research Report GC2, Faculty of Engineering, Curtin University of Technology, Perth, Australia,* pp. 01-97, 2006.

Wang, S. D., Scrivener, K. L., & Pratt, P. L. (1994). Factors affecting the strength of alkali-activated slag. Cement and Concrete Research, 24(6), 1033-1043.

Xie, J., Yin, J., Chen, J., & Xu, J. (2009, October). Study on the geopolymer based on fly ash and slag. In *Energy and Environment Technology, 2009. ICEET'09. International Conference on* (Vol. 3, pp. 578-581). IEEE.

Xie, Z., & Xi, Y. (2001). Hardening mechanisms of an alkaline-activated class F fly ash. *Cement and Concrete Research*, 31(9), 1245-1249.

Xu, H., Van Deventer, J. S. J., Roszak, S., & Leszczynski, J. (2004). Ab initio study of dissolution reactions of five- membered aluminosilicate framework rings. *International Journal of Quantum Chemistry*, 96(4), 365-373.

Yang, K. H., & Song, J. K. (2009). Workability loss and compressive strength development of cementless mortars activated by combination of sodium silicate and sodium hydroxide. *Journal of Materials in Civil Engineering*, 21(3), 119-127.

Yang, K. H., Song, J. K., & Song, K. I. (2013). Assessment of CO2 reduction of alkali-activated concrete. *Journal of Cleaner Production*, 39, 265-272.

Yang, K. H., Song, J. K., Ashour, A. F., & Lee, E. T. (2008). Properties of cementless mortars activated by sodium silicate. *Construction and Building Materials*, 22(9), 1981-1989.

Yao, X., Zhang, Z., Zhu, H., & Chen, Y. (2009). Geopolymerization process of alkali–metakaolinite characterized by isothermal calorimetry. *Thermochimica Acta*, 493(1), 49-54.

Ye, H., & Radlińska, A. (2016). Shrinkage mechanisms of alkali-activated slag. *Cement and Concrete Research*, 88, 126-135.

Ye, H., Cartwright, C., Rajabipour, F., & Radlińska, A. (2017). Understanding the drying shrinkage performance of alkali-activated slag mortars. *Cement and Concrete Composites*, 76, 13-24.

Yip, C. K. B. (2004). The role of calcium in geopolymerisation (Doctoral dissertation, University of Melbourne, Department of Chemical and Biomolecular Engineering).

Zhao, Y., Gong, J., & Zhao, S. (2017). Experimental study on shrinkage of HPC containing fly ash and ground granulated blast-furnace slag. *Construction and Building Materials*, 155, 145-153.